PB85-137388

Continued Research in Mesoscale Air Pollution Simulation Modeling. Volume 7 Mathematical Modeling of Urban Aerosol Dynamics

Systems Applications, Inc., San Rafael, CA

Prepared for

Environmental Sciences Research Lab.
Research Triangle Park, NC

Dec 84

U.S. Department of Commerce
National Technical Information Service
NTIS

EPA-600/3-84-095c
December 1984

PB85-137388

CONTINUED RESEARCH IN MESOSCALE AIR POLLUTION SIMULATION MODELING

VOLUME VII -- Mathematical Modeling of Urban Aerosol Dynamics

by

T.N. Jerskey and L.E. Reid

Systems Applications, Incorporated
101 Lucas Valley Road
San Rafael, California 94903

J.H. Seinfeld and F. Gelbard

California Institute of Technology
Pasadena, California 91125

Contract No. 68-02-2216

Project Officer

Kenneth L. Demerjian
Meteorology and Assessment Division
Environmental Sciences Research Laboratory
Research Triangle Park, North Carolina 27711

ENVIRONMENTAL SCIENCES RESEARCH LABORATORY
OFFICE OF RESEARCH AND DEVELOPMENT
U.S. ENVIRONMENTAL PROTECTION AGENCY
RESEARCH TRIANGLE PARK, NORTH CAROLINA 27711

REPRODUCED BY
NATIONAL TECHNICAL
INFORMATION SERVICE
U.S. DEPARTMENT OF COMMERCE
SPRINGFIELD, VA. 22161

TECHNICAL REPORT DATA

(Please read Instructions on the reverse before completing)

1. REPORT NO. EPA-600/3-84-095c	2.	3. RECIPIENT'S ACCESSION NO. PB85 137388
4. TITLE AND SUBTITLE CONTINUED RESEARCH IN MESOSCALE AIR POLLUTION SIMULATION MODELING Volume VII -- Mathematical Modeling of Urban Aerosol Dynamics		5. REPORT DATE December 1984
		6. PERFORMING ORGANIZATION CODE
7. AUTHOR(S) T.N. Jerskey, J.H. Seinfeld, F. Gelbard, and L.E. Reid		8. PERFORMING ORGANIZATION REPORT NO.
9. PERFORMING ORGANIZATION NAME AND ADDRESS Systems Applications, Inc. 101 Lucas Valley Road San Rafael, CA 94903		10. PROGRAM ELEMENT NO. CDWA1A/02-2260 (FY-84)
		11. CONTRACT/GRANT NO. Contract No. 68-02-2216
12. SPONSORING AGENCY NAME AND ADDRESS Environmental Sciences Research Laboratory-RTP, NC Office of Research and Development U.S. Environmental Protection Agency Research Triangle Park, NC 27711		13. TYPE OF REPORT AND PERIOD COVERED Final (10/79-7/82)
		14. SPONSORING AGENCY CODE EPA/600/09
15. SUPPLEMENTARY NOTES		

16. ABSTRACT

A simplified model of the dynamics of photochemical aerosols is developed, and initial applications are presented. The model, which can be incorporated in or coupled to a photochemical air quality simulation model, takes into consideration the emissions of particles with diameters of 0.01 to 1.0 micrometer and their growth in this size range by the formation of secondary aerosol. The formation of particulate matter is assumed to occur in two stages--condensable material first forms in the gas phase and then diffuses to the particles. A pseudo-steady-state is assumed in which the rate of formation of condensable material in the gas phase is set equal to the rate at which condensation occurs on particles. Model simulations are presented for a batch system both with and without sources of primary aerosol and for a trajectory system. Model simulations and smog chamber experiments are in qualitative agreement.

17. KEY WORDS AND DOCUMENT ANALYSIS

a. DESCRIPTORS	b. IDENTIFIERS/OPEN ENDED TERMS	c. COSATI Field/Group

18. DISTRIBUTION STATEMENT RELEASE TO PUBLIC	19. SECURITY CLASS *(This Report)* UNCLASSIFIED	21. NO. OF PAGES 203
	20. SECURITY CLASS *(This page)* UNCLASSIFIED	22. PRICE

EPA Form 2220-1 (9-73)

NOTICE

This document has been reviewed in accordance with U.S. Environmental Protection Agency policy and approved for publication. Mention of trade names or commercial products does not constitute endorsement or recommendation for use.

ABSTRACT

A simplified model of the dynamics of photochemical aerosols is developed, and initial applications are presented. The model, which can be incorporated in or coupled to a photochemical air quality simulation model, takes into consideration the emissions of particles with diameters of 0.01 μm to 1.0 μm and their growth in this size range by the formation of secondary aerosol. The formation of very small particles by homogeneous nucleation and their subsequent growth is treated as a boundary condition on the particle size distribution function at a diameter of 0.01 μm. Although coagulation is not included in the model, methods were studied for obtaining solutions to the coagulation equation with computational efficiency.

In the aerosol model, the formation of particulate matter is assumed to occur in two stages--condensable material first forms in the gas phase and then diffuses to the particles. A pseudo-steady-state is assumed in which the rate of formation of condensable material in the gas phase is set equal to the rate at which condensation occurs on particles. Calculations are presented that justify this assumption for secondary aerosol production rates and particle concentrations typical of moderate smog conditions in the Los Angeles Basin. Estimates are made of the rate of formation of sulfuric acid droplets by homogeneous nucleation as a function of the aerosol number density, the rate of production of condensable material, and the relative humidity.

Model simulations are presented for a batch system (with constant rates of aerosol production) both with and without sources of primary aerosol and for a trajectory system. Model simulations and smog chamber experiments are in qualitative agreement.

CONTENTS

ABSTRACT iii

LIST OF ILLUSTRATIONS vii

LIST OF TABLES xii

I PROSPECTS FOR DYNAMIC MODELING OF AIR POLLUTION AEROSOLS. . 1

- A. Introduction. 1
- B. Status of Aerosol Emission Inventories. 4
- C. Data Available for Validation 5
- D. Ultimate Uses of an Aerosol Model 10
- E. Outline of the Remainder of the Report. 10

II BASIC EQUATIONS OF AN AEROSOL MODEL 11

- A. General Dynamic Equation for the Size-Composition Distribution Function 11
- B. Equation for the Mean Size Distribution Function. . . . 17

III APPLICATION OF THE GENERAL EQUATIONS TO PHOTOCHEMICAL AEROSOLS. 20

- A. Model for Condensational Growth of Aerosols 22
- B. Expressions for the Rate of Growth of Aerosol Particles 24
  - 1. Theoretical Growth Laws 25
  - 2. Empirical Growth Laws 27
- C. Components of the Model 31
  - 1. Pseudo-Steady-State Model of Condensable Gaseous Species 32
  - 2. Formation of Condensable Species 41
  - 3. Sources of Primary Aerosol 44
  - 4. Flux of Small Particles into the Size Range $D_p > D_{p_{min}}$. 49
- D. Solution of the Equation Governing $\bar{n}_0(D_p,t)$ 57
- E. Properties of the Model 58

Preceding page blank

IV SIZE DISTRIBUTION SOLUTIONS 60

A. Size Distribution Dynamics in a Batch System. 61

1. Effect of Production of Sub-0.01 μm Particles . . . 61
2. Effect of Primary Aerosol Sources 70
3. Comparison of Batch System Simulations with Smog Chamber Data 100
4. Reductions in the Resolution of $\bar{n}_0(D_p,t)$. 104

B. Size Distribution Dynamics Along a Trajectory 109

1. Effects of the Boundary Condition $\bar{n}_0(0.01,t)$ and of Very Small Particles on the Volume Distribution. 110
2. The Effect of Varying Source and Background Distributions 130
3. The Effect on the Predicted Volume Distribution of Varying the Ratio of Primary to Secondary Volume. 142
4. The Sensitivity of the Predicted Size Distribution to the Auto Exhaust Distribution 148

V NUMERICAL SOLUTION OF THE COAGOLATION EQUATION. 150

A. Introduction. 151

B. Scaling of the Equations. 153

C. Orthorgonal Collocation 155

D. Numerical Implementation of the Method for Special Cases 158

1. Finite Domain Error 162
2. Numerical Results 164

E. Summary 175

VI CONCLUSIONS AND RECOMMENDATIONS 177

REFERENCES 181

ILLUSTRATIONS

1. Classification of Aerosol Particles 22

2. Aerosol Number Distributions as a Function of Time. . . . 36

3. Normalized Particle Volume Distributions Used for Primary Aerosols in This Study. 46

4. Measured and Fitted Volume Distribution for Auto Organic Aerosols. 48

5a. Initial Volume Distribution for Runs With No Primary Aerosol: $\sigma = 0.50$, $\mu = -1.80$ 63

5b. Volume Distribution After Three Hours for Case with No Primary Aerosol and $n(0.01) = 10^4$. 64

5c. Volume Distribution After Seven Hours for Case with No Primary Aerosol and $n(0.01) = 10^4$. 65

6a. Volume Distribution After Three Hours for Case with No Primary Aerosol and $n(0.01) = 600/I(0.01)$. 68

6b. Volume Distribution After Seven Hours for Case with No Primary Aerosol and $n(0.01) = 600/I(0.01)$. 69

7a. The Volume Distribution After One Hour of Simulation in Run 1. 73

7b. The Volume Distribution After Three Hours of Simulation in Run 1. 74

7c. The Volume Distribution After Seven Hours of Simulation in Run 1. 75

8a. The Volume Distribution After Seven Hours of Simulation with $S_0 = 600\ cm^{-3}min^{-1}$ 79

8b. The Volume Distribution After Seven Hours of Simulation with $S_0 = 10\ cm^{-3}min^{-1}$ 80

8c. The Volume Distribution After Seven Hours of Simulation with $S_0 = 6 \times 10^5\ cm^{-3}min^{-1}$ 81

9. The Growth of Particles in the Batch Systems of Runs 4 and 6 84

10a. The Volume Distribution Predicted After a Seven-Hour Simulation With a 60/40 Split of Primary and Secondary Mass 85

10b. The Volume Distribution Predicted After a Seven-Hour Simulation With a 20/80 Split of Primary and Secondary Aerosol. 86

11a. The Source-Normalized Volume Distribution for $\mu = -1.802$, $\sigma = 0.65$ 87

11b. The Source-Normalized Volume Distribution for $\mu = -1.802$, $\sigma = 0.20$ 88

11c. The Source-Normalized Volume Distribution for $\mu = -3.19$, $\sigma = 0.362$ 89

12a. Volume Distribution After One Hour of Simulation in Run 6 90

12b. Volume Distribution After Three Hours of Simulation in Run 6 91

12c. Volume Distribution After Seven Hours of Simulation in Run 6 92

13a. Volume Distribution After One Hour of Simulation in Run 7 93

13b. Volume Distribution After Three Hours of Simulation in Run 7 94

13c. Volume Distribution After Seven Hours of Simulation in Run 7 95

14a. Volume Distribution After One Hour of Simulation in Run 8 96

14b. Volume Distribution After Three Hours of Simulation in Run 8 97

14c. Volume Distribution After Seven Hours of Simulation in Run 8 98

15. Chemistry and Aerosol Concentration Data for Calspan Run No. 14 102

16. Chemistry and Aerosol Concentration for Calspan Run No. 15, a Xylene-NO-Filtered Air System. 103

17a. Initial Number Distribution for Calspan Run 14 105

17b. Initial Number Distribution for Calspan Run 15 106

18. Predicted and Measured Aerosol Size Distribution for Calspan Run 14 107

19. Predicted and Measured Aerosol Size Distribution for Calspan Run 15 108

20. The Volume Distribution After Seven Hours of Simulation with $n(D_p,t)$ Originally Defined at 11 Particle Diameters. 110

21. The Volume Distribution After Seven Hours of Simulation with $n(D_p,t)$ Originally Defined at 26 Particle Diameters. 111

22. The Volume Distribution After Seven Hours of Simulation with $n(D_p,t)$ Originally Defined at 50 Particle Diameters. 112

23. Seven-Hour Air Parcel Trajectory in the Los Angeles Basin on 30 September 1969 113

24. The Number Distributions After Seven Hours of Simulation with $n(0.01) = 10^4\ \mathrm{cm}^{-3}\mu\mathrm{m}^{-1}$ and $n(0.01) = 10^6\ \mathrm{cm}^{-3}\mu\mathrm{m}^{-1}$ . . 121

25a. The Volume Distribution After One Hour of Simulation in Run 1 122

25b. The Volume Distribution After Four Hours of Simulation in Run 1 123

25c. The Volume Distribution After Seven Hours of Simulation in Run 1 124

26a. The Volume Distribution After One Hour of Simulation in Run 2 125

26b. The Volume Distribution After Four Hours of Simulation in Run 2 126

26c. The Volume Distribution After Seven Hours of Simulation in Run 2 127

27. The Volume Distribution After Seven Hours of Simulation Without the Lead Emissions 129

28. The Number Distributions After Seven Hours of Simulation in Runs 1, 4, 5, and 6. 131

29a. The Volume Distribution After One Hour of Simulation in Run 5 132

29b. The Volume Distribution After Three Hours of Simulation in Run 5 133

29c. The Volume Distribution After Seven Hours of Simulation in Run 5 134

30a. The Volume Distribution After One Hour of Simulation in Run 6 136

30b. The Volume Distribution After Three Hours of Simulation in Run 6 137

30c. The Volume Distribution After Seven Hours of Simulation in Run 6 138

31a. The Volume Distribution After One Hour of Simulation in Run 12. 139

31b. The Volume Distribution After Three Hours of Simulation in Run 12. 140

31c. The Volume Distribution After Seven Hours of Simulation in Run 12. 141

32a. The Volume Distribution After Seven Hours of Simulation in Run 5 143

32b. The Volume Distribution After Seven Hours of Simulation in Run 10. 144

33a. The Volume Distribution After Seven Hours of Simulation in Run 1 145

33b. The Volume Distribution After Seven Hours of Simulation in Run 8 146

33c. The Volume Distribution After Seven Hours of Simulation in Run 9 147

34. Comparison of Analytical and Numerical Solutions for Case 1 167

35. Comparison of Analytical and Numerical Solutions for Case 2 168

36. Comparison of Analytical and Numerical Solutions for Case 3 169

37. Comparison of Analytical and Numerical Solutions for Case 4 170

38. Comparison of Analytical and Numerical Data for Case 5 174

TABLES

1 Levels of Detail Required for Primary Aerosol Emission Inventories 5

2 Sources of Data for an Aerosol Emission Inventory. 6

3 Methods for Measuring Aerosol Properties 7

4 Thermodynamic Data for Some Organic Acids. 30

5 Values of S and γx Calculated from Heisler's (1975) Rate Parameters. 30

6 Estimated Rates of Conversion of H_2SO_4 Vapor to Aerosol by Homogeneous Nucleation and Heterogeneous Condensation 37

7 Pseudo-First-Order Rate Constants for Conversion of SO_2 to Sulfate in Los Angeles 42

8 Source Breakdown of CO, SO_2, and Particulate Emissions in Los Angeles in 1973 45

9 Homogeneous Nucleation Rates for Sulfuric Acid Droplets 52

10 The Growth of Particles Associated with $D_{P_{max}}$. 67

11 Simulations in a Batch System. 71

12 Approximate Surface Mean Diameters 79

13 Variations with Time of Parameters Characterizing the Aerosol Size Distribution. 83

14 Data Used in Trajectory Simulations. 114

15 Conditions for Trajectory Simulations. 116

16 Values of Various Parameters Characterizing the Aerosol Distribution After Seven Hours of Simulations. . . 118

17 Surface Area Mean Diameters Calculated From Eq. (71) . . . 128

18 Sensitivity of Predicted Volume Distributions to Automobile Lead and Organic Distribution 149

19 Previous Work on the Numerical Solutions of the Coagulation Equation. 160

20 Weighted Residual Weight Functions. 161

21 Error Introduced by Using a Finite Volume Domain (0-10) For $\beta = \beta_0$ and $n(v,0) = 4ve^{-2v}$. 163

22 Error Introduced by Using a Finite Volume Domain (0-10) for $\beta = \beta_0(u+v)$ and $n(v,0) = 4ve^{-2v}$ 165

23 Finite Domain Error for Cases 1-4 166

24 Finite Domain Error for Case 5. 173

I PROSPECTS FOR DYNAMIC MODELING OF AIR POLLUTION AEROSOLS

A. INTRODUCTION

Urban air pollution consists of both gaseous and particulate components. To obtain a thorough understanding of the relationship between primary pollutant emissions and atmospheric concentrations it is necessary to study the behavior of both gaseous and particulate species. Previous efforts directed to the simulation of air pollution have largely been confined to gaseous species (or to primary aerosols, which behave dynamically as inert gases). Although the total mass of pollutants in particulate form in an urban atmosphere may be small compared with that of pollutants in gaseous form, aerosols play a key role in visibility degradation and human health effects. In this report we formulate a mathematical model for air pollution aerosol dynamics and apply the model to the aerosol in photochemical smog.

In the last several years a great deal has been learned about air pollution aerosols (Whitby et al., 1972; Husar et al., 1972; Willeke et al., 1974; Hidy et al., 1975; Willeke and Whitby, 1975). Although our knowledge is still far from complete, there is general agreement on the nature of urban aerosol size distributions and their interpretation (Willeke and Whitby, 1975). (See Figure 1 for a classification of particles.) For example, atmospheric aerosol size distributions are almost always bimodal in surface or volume. The mode in the 0.1 to 1.0 μm diameter size range has been termed by Whitby the "Accumulation Mode" because aerosol particles which grow into this range from smaller sizes by coagulation or condensation tend to remain in this size range. The Coarse Particle Mode for diameters exceeding 1 to 2 μm results from mechanically produced aerosols and has very little interaction with the Accumulation Mode. In the presence of fresh combustion aerosols, a third mode, on the order of 0.01 μm diameter, termed the "Transient Nuclei Mode", is found. From the point of view of air pollution studies, the Accumulation and Transient Nuclei Modes are of most interest, because of their role in visibility limitation and possible health effects. In this study, therefore, we confine our attention to aerosoles of diameter smaller than about 1 μm.

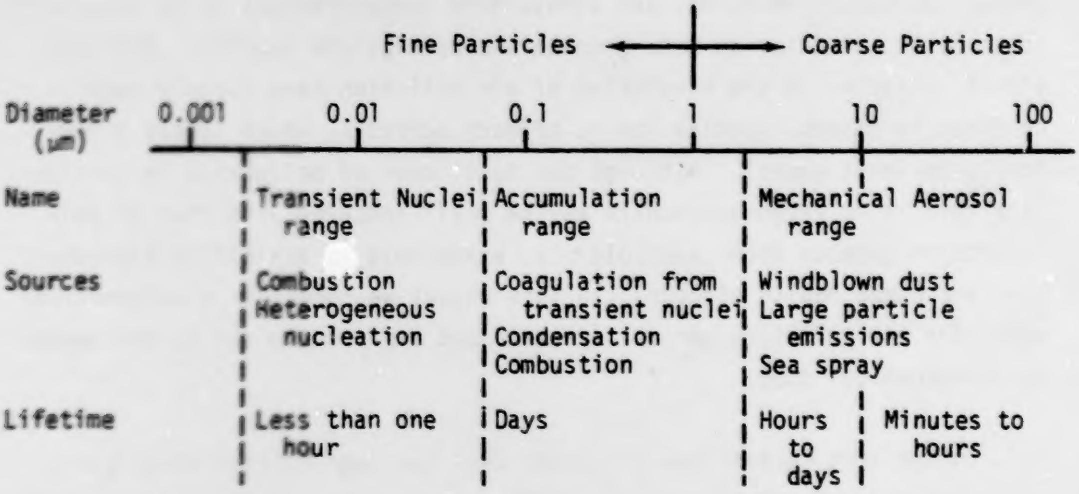

Name	Transient Nuclei range	Accumulation range	Mechanical Aerosol range	
Sources	Combustion Heterogeneous nucleation	Coagulation from transient nuclei Condensation Combustion	Windblown dust Large particle emissions Sea spray	
Lifetime	Less than one hour	Days	Hours to days	Minutes to hours

Source: Adapted from Willeke and Whitby (1975).

FIGURE 1. CLASSIFICATION OF AEROSOL PARTICLES

It has been established that the principal growth mechanism for photochemical aerosols in the Accumulation Mode is gas-to-particle conversion (Husar, et al., 1972, 1976; Gartrell and Friedlander, 1975; Hidy et al., 1975). The major secondary species in photochemical aerosols have been identified as sulfates, nitrates and particulate organic species (Hidy et al., 1975; Grosjean and Friedlander, 1975). The chemistry through which SO_2, NO_x and hydrocarbons are converted to particulate species is not completely understood at present. Consequently, we have chosen to represent the chemistry of the gas-to-particle conversion process here in a simple manner that relies on experimentally measured rates of conversion of precursors to aerosol species. The lack of understanding of the detailed chemical processes also precludes us from predicting the size-dependent chemical composition of the aerosol. We concentrate here, therefore, on predicting size distribution changes only. Clearly, a future goal is to be able to predict both size and composition distributions for the aerosol.

The qualitative picture of photochemical aerosol that has evolved is that primary aerosol provides the surface upon which secondary species condense, so that eventually the volume of secondary aerosol substantially exceeds that of the original primary aerosol (Hidy et al., 1975). Even though the aerosol volume from gas-to-particle conversion exceeds that of the primary aerosol, the size distribution of the primary aerosol has been found to influence considerably the ultimate size distribution of the total aerosol (Miller and Levy, 1976). Therefore, an aerosol emissions inventory, including size distribution of primary aerosols, is required for an urban aerosol model. Particulate emissions from sources are generally less well characterized than are gaseous emissions. When reported, they are usually specified in terms of the total mass of emissions per unit time. Size distributions of primary particulate emissions are seldom reported. Suffice it to say that development of primary aerosol emission inventories for major urban areas, stratified with respect to chemical composition and particle size if possible, represents an important need, particularly if prediction of aerosol behavior is anticipated. In our subsequent development it will be assumed that the data on the size distributions of primary aerosol emissions are available or can be estimated.

Validation of the aerosol model we will develop requires size distribution data for ambient aerosol. Very little of such data exist at present. Only in a few special studies have size distribution measurements been obtained (Willeke et al., 1974; Hidy et al., 1975). Consequently, data are not available for direct comparison with our predictions. Nevertheless, it will be possible to compare the qualitative features of the predicted size distributions with those observed in Los Angeles.

The general dynamic equations governing the size and chemical composition distribution of an aerosol undergoing coagulation, homogeneous nucleation, heterogeneous nucleation (or condensation), advection, and turbulent diffusion were derived by Chu and Seinfeld (1975). These equations were applied to the growth of an aerosol population consisting of two-component droplets as a first approximation to actual atmospheric growth by gas-to-particle conversion. Jerskey and Seinfeld (1976) considered in some detail each of the physical and chemical processes involved in air pollution aerosol behavior and assessed the relative importance of each to urban aerosol dynamics. Several of the relevant conclusions from that study are summarized here.

B. STATUS OF AEROSOL EMISSION INVENTORIES

The level of detail required in an aerosol emission inventory used as input to a model depends on the level of detail of the model's description of aerosol properties. An aerosol emission inventory is concerned only with primary aerosol, as secondary aerosol is, of course, the result of gas-to-particle conversion in the atmosphere. The various levels of detail required for aerosol emission inventories are summarized in Table 1 corresponding to the level of detail in the model for which the inventory is compiled.

TABLE 1. LEVELS OF DETAIL REQUIRED FOR PRIMARY AEROSOL EMISSION INVENTORIES

Level of Detail of Aerosol Properties Described in Model	Level of Detail Required for Primary Emission Inventory
Total aerosol mass concentration as a function of location and time	Total aerosol mass emitted from each source as a function of location and time
Aerosol mass concentration as a function of particle size, location, and time	Aerosol mass as a function of particle size emitted from each source as a function of location and time
Aerosol chemical composition as a function of particle size, location, and time	Mass emissions by chemical composition and particle size from each source as a function of location and time

Particulate emissions from sources are generally less well characterized than are gaseous emissions. When reported, they are usually specified in terms of the total mass of emissions per unit time. Size distributions of particulate emissions are seldom reported. The chemical composition of particulate emissions may be known from the process producing the emissions. Table 2 indicates some sources of data for a primary aerosol emission inventory. We note that natural sources, such as sea spray and soil dust, must also be considered.

We choose not to enter into a detailed discussion of available aerosol emission data here. Suffice it to say that development of priamry aerosol emission inventories for major urban areas, stratified with respect to chemical conposition and particle size if possible, represents an important need, particularly if aerosol modeling is anticipated.

C. DATA AVAILABLE FOR VALIDATION

Table 1 suggests three possible levels of detail in aerosol modeling. The validation of a model involves the comparison of predictions to measurements from the atmosphere or a laboratory system such as a smog chamber.

TABLE 2. SOURCES OF DATA FOR AN AEROSOL EMISSION INVENTORY

Emission Source	Chemical Composition	Size Distribution
Motor Vehicles	Miller et al. (1972)	Whitby et al. (1969)
	Gangley and Springer (1974)	Gartrell and Friedlander (1975)
	Hirschler et al. (1957)	Gangley and Springer (1974)
	Cahill and Feeney (1974)	Cahill and Feeney (1974)
	Gatz (1974)	Ter Haar (1972)
		Ter Haar and Stephens (1971)
		White and Husar (1976)
Power plants	Miller et al. (1972)	
	Gatz (1974)	
Sea	Miller et al. (1972)	Gartrell and Friedlander (1975)
		Woodcock (1953)
Soil	Gatz (1974)	Gartrell and Friedlander (1975)
	Miller et al. (1972)	

A number of methods are available for measuring the characteristics of aerosols. Methods exist for measuring the number or mass of particles in a given size range or for determining the chemical composition. Some measurement methods operate in situ, but most methods require removal of the aerosol from the air. Before discussing the development of aerosol models, we review briefly the methods of measuring aerosol properties, in order to assess the nature of the data available for validation of an aerosol model.

The most commonly measured property of aerosols is the total mass per unit volume (see Table 3). The most direct total mass measurement involves collection of the aerosol on a filter. Chemical analysis of the deposited aerosol can also be performed. Filter measurements require continued deposition for a time period long enough to obtain a sample sufficient for weighing or chemical analysis. Necessary time periods range from a few minutes to several hours, depending on the particulate loading in the air and the sensitivity of the method of analysis. Table 3 summarizes other common total mass measurement techniques, as well as total number concentration and size distribution measurement techniques. Mass concentration methods are most sensitive to larger particles because they contribute most of the mass, whereas counting methods are most sensitive to small particles, which contribute most of the number.

No method is capable of measuring an aerosol property over the entire range of particle sizes. Therefore, to obtain information over the range of particle sizes one must employ several methods simultaneously (see, for example, Whitby et al., 1972).

Validation of the model we discuss in this report requires size distribution data for both the aerosol sources and the ambient aerosol. Very little data of these types exist. Present federal air quality standards for particulates are stated in terms of the total mass of particulate. Partly for this reason, most available data, such as those from the Aerosol Characterization Experiment (ACHEX)(Hidy et al., 1975), were obtained with high-volume filters. Although these data are useful for measuring the total mass and the integrated chemical composition of an aerosol, they cannot be used in the model discussed herein without some assumption about the size distribution of particles. Only in a few special studies were size distribution measurements obtained. For example, dichotomous sampling data are available for the St. Louis area (Demerjian, 1976).

TABLE 3. METHODS FOR MEASURING AEROSOL PROPERTIES

Property Measured	Method	Comments
Mass per unit volume of air	Filtration	Aerosol is collected on a filter. Mass can be determined by differential weight or attenuation of beta radiation. Beta radiation intensity is proportional to the area density of collected aerosol. Beta radiation attenuation can be automated and used to monitor particulate mass in stack gases.
	Piezoelectric microbalance (Sem and Borgos, 1973; Cadle, 1975)	Aerosol is deposited on a vibrating crystal, and decrease in vibrational frequency can be related to mass deposition on the crystal. The method is highly sensitive but suffers from loss of particles from the vibrating crystal.
	Integrating nephelometer	The flux of light scattered by both molecules and particles over approximately 180° is integrated to obtain b_{scat}. The degree of light scattering by a particle depends on its size, shape, and index of refraction, but not directly on the mass or volume of the particle. Approximately 90 percent of measured scattering is from particles between 0.15 and 1.5 μm in diameter (Whitby and Cantrell, 1975). b_{scat} is then related to the total particle mass (Charlson et al., 1968).
Number concentration	Condensation nuclei counter	Expanding a chamber saturated with water vapor causes water to condense on the particles. The droplets are measured optically by light transmission or light scattering. Particles as small as 2 nm in diameter can be detected. Usually employed to obtain number concentration of particles less than 0.1 μm diameter, which is difficult to obtain by other methods.
	Electrical integral sensor	Particles are charged and collected, and the current produced by the collected particles is measured. Sensitive to particles as small as 0.01 μm diameter.

TABLE 3. (Concluded)

Property Measured	Method	Comments
Size distribution	Optical particle counter	Individual particles are counted by light scattering, with resolution up to 15 discrete size ranges between 0.3 and 10 μm diameter.
	Impactor	Particles are collected on stages in a device wherein particle inertia is used to deposit particles on plates around which the air must flow. The smallest particle collected depends on the geometry of the impactor and the velocity of the gas stream. Impactors are available with up to 10 stages that collect particles from 0.5 to 10 μm diameter. Cut-off diameters between stages are not sharp, and depend on the size distribution of the aerosol being sampled (Ludwig, 1968). An after-filter is used to collect particles that escape collection on the impactor stages. Impactors for particles below 0.5 μm in diameter are still in the stage of research and development.
	Electrical aerosol analyzer	Measures number of particles as a function of diameter by charging the aerosol with unipolar gaseous ions and measuring the mobility of the charged particles. Sensitive to particles from 0.006 to 1 μm diameter. Size range is usually divided into 10 subranges. The surface area and volume of the aerosol can be determined in a subrange. Its sensitivity to small particles makes the electrical aerosol analyzer the best available method for photochemical aerosols. Accuracy depends on the efficiency of charging, because the charges on the particles are counted (Liu and Pui, 1975). Errors arise for larger particles from inaccurate size classification.

Although the data needed to exercise and validate a mathematical model for air pollution aerosols are not at present routinely available, it is important that work on the development of such a model be instituted if a model is to be available when the appropriate data are obtained.

D. ULTIMATE USES OF AN AEROSOL MODEL

As mentioned above, present federal ambient air quality standards for suspended particulate matter are stated in terms of total mass concentration. The State of California has promulgated a visibility standard, that the visibility should not be less than 10 miles on a day when the relative humidity is below 70 percent. It is likely that particulate standards based on size or chemical composition will be enacted in the future, particularly after relationships between health effects and particulate properties are elucidated (Shannon et al., 1974). To assess effects such as visibility degradation it will be necessary to predict the quantity of aerosol in various size ranges, particularly the 0.1 to 1 μm diameter range. These uses are the motivation for our development of a model capable of predicting aerosol size distributions. Because routine measurement of aerosol chemical composition as a function of size is perhaps several years away, in the present study we do not proceed to that point in modeling.

E. OUTLINE OF THE REMAINDER OF THE REPORT

The remainder of this report is devoted to the description of the model developed, and to preliminary implementation of that model. In Chapter II we develop the basic equations of the model and in Chapter III we discuss the application of the equations to photochemical aerosols. Chapter IV presents the results of preliminary applications of the model. In Chapter V we consider the description of coagulation processes. Chapter VI contains a summary of our work and recommendations for further research.

II BASIC EQUATIONS OF AN AEROSOL MODEL

In this chapter we develop the basic equations of an aerosol model. First, we present the equations governing the size and chemical composition distribution of an aerosol. Then, based on these equations, we develop equations for the total mean number concentration and the total mean volume concentration. It is useful at this point to discuss the terminology used in the description of particulate formation and growth, since we refer to other works that employ this terminology. Homogeneous nucleation refers to any process by which a particle is formed spontaneously from vapor molecules. If the new particle formed consists of a single chemical species, then the process can be referred to as homomolecular nucleation. If the particle is formed from two or more species, such as sulfuric acid and water for example, the process is called heteromolecular nucleation. In this work when we discuss homogeneous nucleation, we are really concerned with heteromolecular nucleation. The general process of incorporation of vapor molecules in an existing particle is referred to as heterogeneous nucleation or condensation. If only a single chemical species condenses on a particle, the process may also be referred to as heterogeneous-homomolecular nucleation. Finally, when several species are condensing the process can be called heterogeneous-heteromolecular nucleation.

A. GENERAL DYNAMIC EQUATION FOR THE SIZE-COMPOSITION DISTRIBUTION FUNCTION

Let us assume that the aerosol is composed of liquid droplets of M chemical species. We let c_i denote the concentration of species i in a droplet, $i = 1,2, \ldots, M$, and v denote the volume of the particle. We then define $n(v,c_1,\ldots,c_M,\underset{\sim}{r},t)$ as the size-composition distribution function, such that $n\,dv\,dc_1 \cdot\cdot\cdot dc_M$ is the number of particles per unit volume of atmosphere at location $\underset{\sim}{r}$ at time t of volume v to v+dv and of composition c_i to c_i+dc_i (moles l^{-1}) of species i, i = 1, 2, ..., M. The total particle number density (cm^{-3}) at location $\underset{\sim}{r}$ at time t is

$$N(\underset{\sim}{r},t) = \int_0^\infty \cdots \int_0^\infty n(v,c_1,\ \ldots,\ c_M,\underset{\sim}{r},t)dv\ dc_1 \cdots dc_M \quad . \tag{1}$$

The distribution of particles by particle volume ($\mu m^{-3}cm^{-3}$) is defined by $n_0(v,\underset{\sim}{r},t)$ and given by

$$n_0(v,\underset{\sim}{r},t) = \int_0^\infty \cdots \int_0^\infty n(v,c_1,\ \ldots,\ c_M,\underset{\sim}{r},t)dc_1 \cdots dc_M \quad . \tag{2}$$

In addition, the total aerosol volume per unit volume of atmosphere (μm^3cm^{-3}) at location $\underset{\sim}{r}$ and time t is

$$V(\underset{\sim}{r},t) = \int_0^\infty vn_0(v,\underset{\sim}{r},t)dv \quad . \tag{3}$$

We now present the general equation governing the size-composition distribution function $n(v,c_1,\ \ldots,\ c_M,\underset{\sim}{r},t)$. This equation includes the effects of coagulation, heteromolecular nucleation, heterogeneous nucleation, aerosol-phase chemical reaction, and advection and diffusion processes. First, we consider the equation governing the spatially homogeneous form of n, $n(v,c_1,\ \ldots,\ c_M,t)$. Therefore, for the moment we neglect any processes that alter the spatial distribution of aerosol. We define $S_0(v,c_1,\ \ldots,\ c_M,t)$ as the rate of formation of particles of volume v and composition $c_1,\ \ldots,\ c_M$ by heteromolecular nucleation and $S_1(v,c_1,\ \ldots,\ c_M,t)$ as the rate of introduction of particles from sources. Then the equation governing $n(v,c_1,\ \ldots,\ c_M,t)$ is

$$
\begin{aligned}
&\frac{\partial n(v,c_1,\ldots,c_M,t)}{\partial t} + \frac{\partial}{\partial v}\Big[F_v(v,c_1,\ldots,c_M,t)n\Big] + \sum_{i=1}^{M}\frac{\partial}{\partial c_i}\Big[F_i(v,c_1,\ldots,c_M,t)n\Big] \\
&\quad = \frac{1}{2}\int_0^{v}\int_0^{c_1}\cdots\int_0^{c_M}\beta(v-\tilde{v},\tilde{v})\,n(v-\tilde{v},c_1-\tilde{c}_1,\ldots,c_M-\tilde{c}_M,t) \\
&\qquad \cdot n(\tilde{v},\tilde{c}_1,\ldots,\tilde{c}_M,t)\,d\tilde{c}_1\cdots d\tilde{c}_M\,d\tilde{v} \qquad\qquad (4) \\
&\qquad - \int_0^{\infty}\cdots\int_0^{\infty}\beta(v,\tilde{v})\,n(v,c_1,\ldots,c_M,t)\,n(\tilde{v},\tilde{c}_1,\ldots,\tilde{c}_M,t)\,d\tilde{c}_1\cdots d\tilde{c}_M\,d\tilde{v} \\
&\qquad + S_0(v,c_1,\ldots,c_M,t) + S_1(v,c_1,\ldots,c_M,t) \quad ,
\end{aligned}
$$

where $F_v = dv/dt$, $F_i = dc_i/dt$, and $\beta(v,\tilde{v})$ is the coagulation constant for particles of volume v and $\tilde{v}$. (We assume that the coagulation rate between particles of volumes v and $\tilde{v}$ is not influenced by the compositions of the two particles.)

Let us now consider the specification of F_v and F_i. We let $R_i(c_1,\ldots,c_M)$ be the rate of production of species i in a particle by aerosol-phase chemical reaction. We also define $q_i(v,c_1,\ldots,c_M,n_1,\ldots n_M,t)$ as the rate of input of species i (moles sec^{-1}) into a particle from the gas phase, where $n_1,\ldots,n_M$ are the gas phase concentrations of species 1 to M. By considering each particle as a homogeneous chemical reactor, we obtain

$$\frac{dc_i}{dt} = \frac{q_i}{v} - \frac{c_i}{v}\left(\sum_{j=1}^{M} q_j\bar{v}_j\right) + R_i \quad , \tag{5}$$

$$\frac{dv}{dt} = \sum_{j=1}^{M} q_j\bar{v}_j \quad , \tag{6}$$

where volume change resulting from chemical reaction has been neglected. In the absence of heterogeneous chemical reaction,

$$\frac{dc_i}{dt} = \frac{q_i}{v} - \frac{c_i}{v} \sum_{j=1}^{M} q_j \bar{v}_j \quad , \tag{7}$$

$$\frac{dv}{dt} = \sum_{j=1}^{M} q_j \bar{v}_j \quad , \tag{8}$$

and changes in composition and volume result only from heterogeneous nucleation of vapor molecules.

If we consider the processes that alter the spatial distribution of aerosol, we can develop the full equation governing $n(v, c_1, \ldots, c_M, \underline{r}, t)$. To account for advection by the fluid velocity, $u(\underline{r},t)$, we must add the term $\nabla_{\underline{r}} \cdot \underline{u}n$ to the left side of Eq. (4). Brownian diffusion is represented by a term $\mathcal{D}\nabla_{\underline{r}}^2 n$ added to the right side of Eq. (4), and settling is included through the addition of the term $-\underline{u}_s \cdot \nabla n$ to the left side of Eq. (4). When the fluid is turbulent, the fluid velocity $\underline{u}$ contains random components. In addition, the vapor concentrations, $\eta_1, \ldots, \eta_M$, are random functions in a turbulent field. Consequently, n is itself a random function. In developing the conservation equation for n in a turbulent flow field, we follow the usual procedure of decomposing the turbulent variables into mean and random components, $\underline{u} = \bar{\underline{u}} + \underline{u}'$, $\eta_i = \bar{\eta}_i + \eta_i'$, and $n = \bar{n} + n'$. Because F_v and F_i depend in general on the η_i, these two functions must be expressed as $\bar{F}_v + F_v'$ and $\bar{F}_i + F_i'$

We wish to obtain an equation governing $\bar{n}$. The desired equation can be obtained in the usual manner by substituting $\underline{u}$, $\underline{\eta}$, and n into Eq. (4) (with the additional terms discussed in the preceding paragraph included), and then taking the mean value of the resulting equation. During this operation a number of new dependent variables emerge that represent mean values of the products of two fluctuating quantities, $\overline{\underline{u}'n'}$, $\overline{F_v'n'}$, and $\overline{n'n'}$.

The first of these is simply the turbulent flux of the number density distribution and can be expressed in the customary manner in terms of a turbulent eddy diffusivity, K_{ii}, as

$$\overline{u_i' n'} = -K_{ii} \frac{\partial \bar{n}}{\partial r_i} \quad . \tag{9}$$

Seinfeld and Ramabhadran (1975) showed that the terms $\overline{F_v' n'}$, and, consequently, $\overline{F_i' n'}$, are not expected to be important in urban-scale situations. Also, we do not anticipate that the contribution to the mean coagulation rate will be influenced by the correlation $\overline{n'n'}$ in situations of interest here.

Thus, the full general dynamic equation governing the mean size-composition distribution function is

$$\frac{\partial \bar{n}}{\partial t} + \sum_{i=1}^{3} \frac{\partial}{\partial r_i} (\bar{u}_i \bar{n}) + \frac{\partial}{\partial v}\left(\bar{F}_v \bar{n}\right) + \sum_{i=1}^{M} \frac{\partial}{\partial c_i}\left(\bar{F}_i \bar{n}\right) - u_s \frac{\partial \bar{n}}{\partial r_3}$$

$$= \sum_{i=1}^{3} \left[\frac{\partial}{\partial r_i} (K_{ii} + D) \frac{\partial \bar{n}}{\partial r_i}\right]$$

$$+ \frac{1}{2} \int_0^{v} \int_0^{c_1} \cdots \int_0^{c_M} \beta(v - \tilde{v}, \tilde{v}) \bar{n}(v - \tilde{v}, c_1 - \tilde{c}_1, \ldots, c_M - \tilde{c}_M, \underline{r}, t)$$

$$\cdot \bar{n}(\tilde{v}, \tilde{c}_1, \ldots, \tilde{c}_M, \underline{r}, t) d\tilde{c}_1 \cdots d\tilde{c}_M \, d\tilde{v} \tag{10}$$

$$- \int_0^{\infty} \cdots \int_0^{\infty} \beta(v, \tilde{v}) \bar{n}(v, c_1, \ldots, c_M, \underline{r}, t) \bar{n}(\tilde{v}, \tilde{c}_1, \ldots, \tilde{c}_M, \underline{r}, t)$$

$$\cdot d\tilde{c}_1 \cdots d\tilde{c}_M \, d\tilde{v}$$

$$+ S_0(v, c_1, \ldots, c_M, \underline{r}, t) + S_1(v, c_1, \ldots, c_M, \underline{r}, t) \quad .$$

Whereas the physical processes that can affect the dynamics of gaseous species are limited to those that alter concentrations in a unit volume of air through atmospheric transport, as we can see from Eq. (10), those that influence particle behavior are much more diverse.

Equation (10) has been derived on the basis of the particle volume v as the independent variable defining particle size. For purposes of application it is often easier to deal with particle diameter D_p. To do so we consider the size-composition distribution function $\bar{n}(D_p, c_1, \ldots, c_M, \underline{r}, t)$. The full general dynamic equation governing $\bar{n}(D_p, c_1, \ldots, c_M, \underline{r}, t)$ is

$$
\begin{aligned}
&\frac{\partial n}{\partial t} + \sum_{i=1}^{3} \frac{\partial}{\partial r_i}(\bar{u}_i \bar{n}) + \frac{\partial}{\partial D_p}\left(\bar{F}_{D_p} \bar{n}\right) + \sum_{i=1}^{M} \frac{\partial}{\partial c_i}(\bar{F}_i \bar{n}) - u_s \frac{\partial \bar{n}}{\partial r_3} \\
&\quad = \sum_{i=1}^{3} \frac{\partial}{\partial r_i}\left[(K_{ii} + \mathcal{D}) \frac{\partial \bar{n}}{\partial r_i}\right] \\
&\quad + \int_0^{D_p/2^{1/3}} \int_0^{c_1} \cdots \int_0^{c_M} \beta\left[\left(D_p^3 - \bar{D}_p^3\right)^{1/3}, \bar{D}_p\right] \\
&\qquad \cdot \bar{n}\left[\left(D_p^3 - \bar{D}_p^3\right)^{1/3}, c_1 - \bar{c}_1, \ldots, c_M - \bar{c}_M, \underline{r}, t\right] \\
&\qquad \cdot \bar{n}\left(\bar{D}_p, \bar{c}_1, \ldots, \bar{c}_M, \underline{r}, t\right) \frac{D_p^2}{\left(D_p^3 - \bar{D}_p^3\right)^{2/3}}\, d\bar{D}_p\, d\bar{c}_1 \cdots d\bar{c}_M \\
&\qquad - \int_0^{\infty} \cdots \int_0^{\infty} \beta(D_p, \bar{D}_p) \bar{n}(D_p, c_1, \ldots, c_M, \underline{r}, t) \\
&\quad - \cdot \bar{n}(\bar{D}_p, \bar{c}_1, \ldots, \bar{c}_M, \underline{r}, t)\, d\bar{c}_1 \cdots d\bar{c}_M\, d\bar{D}_p \\
&\qquad + S_0(D_p, c_1, \ldots, c_M, t) + S_1(D_p, c_1, \ldots, c_M, \underline{r}, t) \quad ,
\end{aligned}
\tag{11}
$$

where $\bar{F}_{D_p} = dD_p/dt$. It can be noted that $K_{ii} >> \mathcal{D}$, so that Brownian diffusion can be neglected relative to turbulent diffusion.

B. EQUATION FOR THE MEAN SIZE DISTRIBUTION FUNCTION

With the appropriate boundary conditions, Eq. (11) constitutes a general model capable of describing the dynamic behavior of an air pollution aerosol. It is clear, however, that without considerable simplification, it is not practical to attempt to solve Eq. (11) on a grid with spatial resolution comparable to existing gas phase models. Furthermore, the size-composition distribution function, $\bar{n}(D_p,c_1, \ldots, c_M,\underset{\sim}{r},t)$, which is the fundamental description of the aerosol population, includes more detail than virtually any data currently available for model validation. Thus, it is necessary, at least for initial modeling studies, to consider certain integral properties of the size and composition distribution that can be calculated more easily and that conform to available data. Because of the great importance of the size distribution and because of the general lack of chemical composition data, the obvious property to consider is the mean size distribution function [see Eq. (2)]:

$$\bar{n}_0(D_p,\underset{\sim}{r},t) = \int_0^\infty \cdots \int_0^\infty \bar{n}(D_p,c_1, \ldots, c_M,\underset{\sim}{r},t)dc_1 \cdots dc_M \quad . \tag{12}$$

Equation (11) can be integrated with respect to c_1 to c_M to produce the equation governing $\bar{n}_0(D_p,\underset{\sim}{r},t)$,

$$\begin{aligned} &\frac{\partial \bar{n}_0}{\partial t} + \sum_{i=1}^{3} \frac{\partial}{\partial r_i}(\bar{u}_i\bar{n}_0) + \int_0^\infty \cdots \int_0^\infty \frac{\partial}{\partial D_p}\left(\bar{F}_{D_p}\bar{n}\right)dc_1 \cdots dc_M \\ &\quad + \int_0^\infty \cdots \int_0^\infty \sum_{i=1}^{M} \frac{\partial}{\partial c_i}(\bar{F}_i\bar{n})dc_1 \cdots dc_M - u_s \frac{\partial \bar{n}_0}{\partial r_3} \\ &= \sum_{i=1}^{3} \frac{\partial}{\partial r_i}\left(K_{ii}\frac{\partial \bar{n}_0}{\partial r_i}\right) + \int_0^{D_p/2^{1/3}} \beta\left[\left(D_p^3 - \tilde{D}_p^3\right)^{1/3},\tilde{D}_p\right] \end{aligned} \tag{13}$$

$$\cdot\bar{n}_0\left[\left(D_p^3 - \bar{D}_p^3\right)^{1/3}, \underline{r}, t\right]\bar{n}_0(\bar{D}_p, \underline{r}, t)\,\frac{D_p^2}{\left(D_p^3 - \bar{D}_p^3\right)^{2/3}}\,d\bar{D}_p$$

$$- \int_0^\infty \beta(D_p, \bar{D}_p)\bar{n}_0(D_p, \underline{r}, t)\bar{n}_0(\bar{D}_p, \underline{r}, t)d\bar{D}_p$$

$$+ S_0'(D_p, t) + S_1'(D_p, \underline{r}, t) \quad , \qquad (13)$$

where

$$S_0'(D_p, t) = \int_0^\infty \cdots \int_0^\infty S_0(D_p, c_1, \ldots, c_M, t)dc_1 \cdots dc_M \quad , \qquad (14)$$

$$S_1'(D_p, \underline{r}, t) = \int_0^\infty \cdots \int_0^\infty S_1(D_p, c_1, \ldots, c_M, \underline{r}, t)dc_1 \cdots dc_M \quad . \qquad (15)$$

The fourth term on the left-hand side of Eq. (13) can be shown to be zero for any reasonably defined $\bar{n}$ ($\bar{n}$ should approach zero as the concentration of any one species goes to zero or infinity). Hence we can write

$$\frac{\partial}{\partial D_p}\left[\bar{I}_0(D_p, \underline{r}, t)\bar{n}_0(D_p, \underline{r}, t)\right] = \int_0^\infty \cdots \int_0^\infty \frac{\partial}{\partial D_p}\left(\bar{F}_{D_p}\bar{n}\right)dc_1 \cdots dc_M \quad . \qquad (16)$$

Physically $\bar{I}_0 = dD_p/dt$, the rate of change of diameter of all particles of diameter D_p, regardless of their individual compositions. Of course, to compute $\bar{I}_0(D_p, \underline{r}, t)$ requires knowledge of the detailed compositions through Eq. (16). Clearly, this calculation should be avoided if the model is based on $\bar{n}_0(D_p, \underline{r}, t)$. It is desirable to use a growth law $\bar{I}_0$ that can be expressed in terms of the particle diameter and the concentrations of gaseous condensing species only.

Using Eq. (16) in Eq. (12), we obtain the form of the model for $\bar{n}_0(D_p,\underline{r},t)$,

$$\frac{\partial \bar{n}_0}{\partial t} + \sum_{i=1}^{3} \frac{\partial}{\partial r_i}(\bar{u}_i \bar{n}_0) + \frac{\partial}{\partial D_p}(\bar{I}_0 \bar{n}_0) - u_s \frac{\partial \bar{n}_0}{\partial r_3}$$

$$= \sum_{i=1}^{3} \frac{\partial}{\partial r_i}\left(K_{ii} \frac{\partial \bar{n}_0}{\partial r_i}\right) + \int_0^{D_p/2^{1/3}} \beta\left[\left(D_p^3 - \bar{D}_p^3\right)^{1/3}, \bar{D}_p\right]$$

$$\cdot \bar{n}_0\left[\left(D_p^3 - \bar{D}_p^3\right)^{1/3}, \underline{r}, t\right] \bar{n}_0(\bar{D}_p, \underline{r}, t) \frac{D_p^2}{\left(D_p^3 - \bar{D}_p^3\right)^{2/3}} \, d\bar{D}_p \qquad (17)$$

$$- \int_0^{\infty} \beta(D_p, \bar{D}_p) \bar{n}_0(D_p, \underline{r}, t) \bar{n}_0(\bar{D}_p, \underline{r}, t) d\bar{D}_p + S_0'(D_p, t) + S_1'(D_p, \underline{r}, t) \quad .$$

For a spatially homogeneous aerosol $\bar{n}_0 = \bar{n}_0(D_p,t)$ and Eq. (17) becomes

$$\frac{\partial \bar{n}_0}{\partial t} + \frac{\partial}{\partial D_p}\left[\bar{I}_0(D_p,t)\bar{n}_0\right]$$

$$= \int_0^{D_p/2^{1/3}} \beta\left[\left(D_p^3 - \bar{D}_p^3\right)^{1/3}, \bar{D}_p\right] \bar{n}_0\left[\left(D_p^3 - \bar{D}_p^3\right)^{1/3}, t\right]$$

$$\cdot \bar{n}_0(\bar{D}_p, t) \frac{D_p^2 \, d\bar{D}_p}{\left(D_p^3 - \bar{D}_p^3\right)^{2/3}} - \int_0^{\infty} \beta(D_p, \bar{D}_p) \bar{n}_0(D_p, t) \bar{n}_0(\bar{D}_p, t) d\bar{D}_p \qquad (18)$$

$$+ S_0'(D_p, t) + S_1(D_p, t) \quad .$$

III APPLICATION OF THE GENERAL EQUATIONS TO PHOTOCHEMICAL AEROSOLS

The objective of this study is to develop a model capable of describing the size distribution of air pollution aerosols. In the remainder of this work we consider the application of the general model developed in the preceding chapter to aerosols in photochemical air pollution. The general model is described by Eq. (17) or Eq. (18), depending on the spatial homogeneity of the system. For the purposes of this initial study we do not consider atmospheric transport processes. Clearly, the critical issues at this stage of aerosol model development involve the physics and chemistry of particle formation and growth. Once these phenomena are understood, advection, turbulent diffusion, and sedimentation can be accounted for in developing a full urban-scale model.

The processes influencing the dynamics of photochemical aerosols are as follows: Primary aerosols are emitted and provide surface area for the gas-to-particle conversion. The gas-to-particle conversion process may involve gas phase chemical reaction to produce a condensable species that transfers to particles by diffusion, or it may involve the diffusion of gaseous pollutants to particles followed by chemical transformation within the particle. The mechanism that seems to be most consistent with the observed chemical nature of secondary aerosol species is that of gas phase chemical reaction to produce species that subsequently transfer to particles by diffusion (Liepeles et al., 1973; Hidy et al., 1975; O'Brien et al., 1975a,b;Schuetzle et al., 1975; Grosjean, 1977), although there is not complete accord with this view (Novakov et al., 1976). Once a condensable species is produced, it may nucleate homogeneously to produce very small particles or transfer to an existing particle. The very small particles, once formed, may then coagulate with other particles in the system or grow by accretion of more vapor molecules. Because the heterogeneous coagulation coefficient between particles of diameters 0.01 μm and 0.2 μm is one or two orders of magnitude higher than that between two 0.01 μm diameter particles, most of the nuclei, whether primary or secondary in origin, coagulate with the Accumulation Mode rather than grow continously in size (Willeke and Whitby, 1975). The quantity of mass added to the Accumulation Mode by coagulation with nuclei can be estimated to be small (Jerskey and Seinfeld, 1976). For example, Miller et al. (1976) reported photochemical aerosol dynamics resulting from irradiation of automobile exhaust. During the first 10 minutes of the irradiation, new aerosol surface formed in the sub-0.1 μm size range by homogeneous nucleation. After 40 minutes aerosols in the nucleating size region had disappeared from the distribution. It was estimated by Miller et al. (1976) that at 40 minutes the maximum rate of transfer of aerosol volume from the 0.05 μm mode to the >0.1 μm mode was about 8 $\mu m^3 cm^{-3} hr^{-1}$, whereas the observed volumetric growth rate during this period was about 200 $\mu m^3 cm^{-3} hr^{-1}$. Thus, apart from the initial irradiation period of inconsequential volume growth by nucleation, condensation was found to be the predominant mechanism of photochemical aerosol formation.

As a result of these observations we will assume that secondary gaseous species will tend to transfer directly to existing particles in the Accumulation Mode rather than to nucleate homogeneously. We do not expect that this assumption will introduce much error in calculated volumetric conversion rates. Therefore, we will neglect the effect of coagulation on $\bar{n}_0$. In the vicinity of sources, coagulation can be expected to be an important influence on the size distribution of primary emissions. The neglect of coagulation in the near-source region can be expected to be a source of error. Also, we will neglect coagulation of primary aerosol in the sub-0.1 μm range with those in the Accumulation Mode, another possible source of error.

A. MODEL FOR CONDENSATIONAL GROWTH OF AEROSOLS

The basic model for the spatially homogeneous mean size distribution function is

$$\frac{\partial \bar{n}_0}{\partial t} + \frac{\partial}{\partial D_p}\left[\bar{I}_0(D_p,t)\bar{n}_0\right] = S_0'(D_p,t) + S_1'(D_p,t) \qquad (19)$$

where the coagulation term in Eq. (18) has been neglected. Growth by heterogeneous condensation is represented by $\bar{I}_0(D_p,t)(\mu m\ min^{-1})$, $S_1'(D_p,t)$ represents the rate of change of the size distribution as a result of fresh particle emissions from sources ($cm^{-3}\mu m^{-1}min^{-1}$), and $S_0'(D_p,t)$ represents the contribution from homogeneous nucleation ($cm^{-3}\mu m^{-1}min^{-1}$).

It is inconvenient to attempt to solve Eq. (19) over the diameter range $D_p \geq 0$. It is considerably easier to consider a size range $D_p \geq D_{p_{min}}$, where $D_{p_{min}}$ is chosen as the lower limit of the size range in which heterogeneous condensation is expected to be important. The choice of $D_{p_{min}}$ is arbitrary--particles are continuously being formed by nucleation, emitted from sources, and growing by coagulation and condensation over the complete range of diameters from molecular sizes up. The classification shown earlier in Figure 1 has been suggested by Willeke and Whitby (1975) for representing the origins and lifetimes of three ranges of particle sizes in the atmosphere.

Our objective is to concentrate on the accumulation range, as defined in Figure 1, and not to attempt to describe the dynamics of the transient nuclei. If we call the smallest size $D_{p_{min}}$, and consider only $D_p > D_{p_{min}}$, Eq. (19) becomes

$$\frac{\partial \bar{n}_0}{\partial t} + \frac{\partial}{\partial D_p}\left[\bar{I}_0(D_p,t)\bar{n}_0\right] = S_1'(D_p,t) \quad \text{for } D_p > D_{p_{min}} \quad , \tag{20}$$

where $S_1'(D_p,t)$ represents all particle sources for which $D_p > D_{p_{min}}$. If $D_{p_{min}}$ is chosen large enough, S_1' represents sources of primary aerosol, and the influx from the transient nuclei range can be represented by the boundary condition at $D_p = D_{p_{min}}$.

The initial condition for Eq. (20) is the initial size distribution,

$$\bar{n}_0(D_p,0) = \bar{n}_0^0(D_p) \quad . \tag{21}$$

The boundary condition at $D_p = D_{p_{min}}$ can be expressed in either of two ways. The size distribution at $D_p = D_{p_{min}}$, $g(t)$, can be specified,

$$\bar{n}_0(D_{p_{min}},t) = g(t) \quad , \tag{22a}$$

or the flux of particles at $D_{p_{min}}$, $S_0(t)$ ($cm^{-3}sec^{-1}$), can be specified,

$$\bar{n}_0(D_{p_{min}},t) = \frac{S_0(t)}{\bar{I}_0(D_{p_{min}},t)} \quad . \tag{22b}$$

The choice of boundary condition depends on the processes responsible for providing particles of diameter $D_{p_{min}}$. For this study, $D_{p_{min}}$ was selected as 0.01 μm.

B. EXPRESSIONS FOR THE RATE OF GROWTH OF AEROSOL PARTICLES

The function $\bar{I}_0(D_p,t)$ describes the rate of growth of a particle of diameter D_p as a result of heterogeneous condensation and chemical reaction processes. The precise mechanisms by which secondary species are incorporated into photochemical aerosols have not been elucidated although available evidence seems to indicate that the rate-determining step is conversion of precursors (SO_2, NO_x, HC) to condensable species followed then by vapor phase diffusion to the particle (Schuetzle et al., 1975; O'Brien et al., 1975ab; Grosjean, 1977, Heisler and Friedlander, 1977). We therefore assume $\bar{I}_0$ to represent the rate of growth of a particle by diffusional transfer of gaseous species to the surface of a multicomponent liquid droplets.

A general expression for the growth by diffusion of a particle consisting of M species over the full range of Knudsen numbers ($Kn = 2\lambda/D_p$, λ being the mean free path of the background gas)is

$$\frac{dD_p}{dt} = \frac{2\pi D_p^{-1}}{\rho_L RT_\infty} \sum_{i=1}^{M} \frac{M_i \mathcal{D}_i p_{i_s}(T_\infty)}{1 + \ell Kn} \left[S_i - \gamma_i x_i \exp\left(\frac{4\bar{\sigma} V_{L_i}}{RT_\infty D_p} \right) \right] , \qquad (23)$$

where

$$\ell = \frac{1.333 + 0.71\ Kn^{-1}}{1 + Kn^{-1}} . \qquad (24)$$

In Eq. (23), ρ_L denotes the density of the droplet, and M_i, $\mathcal{D}_i$, and $p_{i_s}(T_\infty)$ denote the molecular weight, diffusivity, and vapor pressure at T_∞ of species i, respectively, T_∞ is the ambient temperature, S_i is the saturation ratio of species i $[\rho_i/p_{i_s}(T_\infty)]$, $\gamma_i x_i$ is the product of the activity coefficient and mole fraction of species i in the droplet, $\bar{\sigma}$ is the surface tension of the droplet, and V_{L_i} is the specific volume of species i in the droplet.

1. Theoretical Growth Laws

The simplest theoretical expression for the growth of a particle occurs for heterogeneous-homomolecular nucleation, i.e., condensation of one species on a droplet composed of several species. In this case, Eq. (23) becomes

$$\frac{dD_p}{dt} = \frac{4\sigma D_p^{-1}}{\rho_L RT_\infty}\left(\frac{M\mathcal{D}p_s(T_\infty)}{1 + \ell Kn}\right)\left[S - \gamma x \exp\left(\frac{4\sigma V_L}{RT_\infty D_p}\right)\right] . \qquad (25)$$

The equilibrium vapor pressure of a species over very small droplets is larger than that over larger droplets. Because of this phenomenon (the Kelvin effect), for a fixed nonzero γx, particles below a critical diameter will not grow. The critical diameter can be obtained by equating the terms in parenthesis in Eq. (25) and rearranging. Thus, $dD_p/dt = 0$ when

$$D_p^{crit} = \frac{4\sigma V_L}{RT_\infty}\left(\ell n \frac{S}{\gamma x}\right)^{-1} . \qquad (26)$$

It is evident that when heterogeneous-homomolecular nucleation occurs on soluble, as opposed to insoluble, particles, the nucleation barrier represented by Eq. (26) is reduced by the solution effect (in which the vapor pressure of the condensing species is lower over a solution than in its pure state).* Growth ceases when Eq. (26) is satisfied, resulting, for example, from increase of the mole fraction S.

The heterogeneous-homomolecular growth of a soluble particle was first analyzed by Köhler (1926), who determined the equilibrium size of droplets as a function of the mass of the salt nucleus and the saturation ratio of water vapor. Fletcher (1958), Byers (1965), and Mason (1971) considered the heterogeneous-homomolecular nucleation of water on spherical particles. Chu and Seinfeld (1975) considered the heterogeneous-homomolecular nucleation of organic acids on particles of sea salt and on lead and organics emitted by automobiles.

Heterogeneous-bimolecular nucleation refers to the condensation of two species on an existing particle. Of systems of this type, by far the most attention has been given to the sulfuric acid-water system. The heterogeneous nucleation of H_2SO_4 and H_2O was studied by Stauffer et al. (1973), Nair and Vohra (1975), Takahashi et al. (1975), Hamill (1975), and Hamill et al. (1975). In the last three studies it was assumed that, because the gas-phase concentration of H_2O is much higher than that of H_2SO_4, growth is limited by the rate of diffusion of H_2SO_4 to the droplet. Recently, Middleton et al. (1976) made use of such models to develop a kinetic model for the growth of sulfate aerosol.

All the growth expressions discussed above and all the theoretical studies of which we are aware consider the condensation of at most two species. Furthermore, all these growth expressions involve knowledge of the composition of the particles. For these reasons, none of these can be applied to photochemical smog without simplification.

---

* Hamill et al. (1975) note that the nucleation barrier can also be reduced for insoluble particles by decreasing the surface energy due to a change in shape or size of the droplet formed. For deliquescent substances, such as NaCl, a particle can participate in the nucleation process in both ways. At relative humidities above 76 percent, NaCl absorbs water vapor to become a solution droplet. Below 76 percent relative humidity, the NaCl crystal acts as an insoluble particle during the nucleation process.

2. Empirical Growth Laws

In a recent experimental study, Heisler (1975) deduced empirical growth laws from data on particle growth rates. Equation (23) was used as the basis for the analysis of the data. Assuming that the mole fraction of each species i in a droplet remains constant in time and that the saturation ratio S_i remains constant and near unity, Heisler expanded the exponential in Eq. (23) to yield the growth law

$$\frac{dv}{dt} = \sum_{i=1}^{M} \frac{A_i}{1 + \ell Kn}\left(D_p - D_{p_i}^{*}\right) \quad , \tag{27}$$

where

$$A_i = \frac{2\pi \mathcal{D}_i M_i p_{i_s}(T_\infty)(S_i - \gamma_i x_i)}{\rho_L R T_\infty} \tag{28}$$

$$D_{p_i}^{*} = \frac{4\bar{\sigma} V_{L_i}}{RT_\infty\left[(S_i/\gamma_i x_i) - 1\right]} \quad . \tag{29}$$

The growth law in Eq. (27), when A_i and Dp_i^* are constant [as assumed by Heisler (1975)], represents a fundamental difference from Eq. (23).

Equation (27) predicts that as long as $D_p > D_{p_i}^*$ a particle will grow, whereas the more general form in Eq. (23) predicts that growth ceases when the partial pressure of species i equals its vapor pressure, or when

$$S_i = \gamma_i x_i \exp\left(\frac{4\bar{\sigma} V_{L_i}}{RT_\infty D_p}\right) \quad . \tag{30}$$

If $x_i << 1$, and $S_i \approx 1$, then an equilibrium size is not reached and a law similar to Eq. (27) is obtained. The two possible growth laws give rise to the basic question of whether particle composition changes with time must be considered in formulating a growth law. Ideally, this question would be resolved by a comparison of predictions with observations.

Heisler (1975) employed Eq. (27) with $M = 2$ to analyze his growth data. The data were plotted in the form $(1 + \ell Kn)(dv/dt)$ versus D_p, and were found to conform basically to Eq. (27) for $M = 2$. A minimum particle size for growth of about 0.25 μm diameter was determined. Good agreement with the data was found when $A_1 t_f = 0.236\ \mu m^2$, $D_{p_1}^* = 0.055$ μm, $A_2 t_f = 0.581\ \mu m^2$, and $D_{p_2}^* = 0.24$ μm, where t_f represents the time of duration of the experiment.* The two condensing species represented only an approximation to the real situation. We estimated the saturation ratio, S_i, and the activity of the condensing species, $\gamma_i x_i$, associated with the empirical growth parameters calculated by Heisler (1975). Because Heisler applied Eq. (27) to situations in which the secondary aerosol was organic, we considered organic acids that might be formed from cyclic olefin precursors. Thermodynamic data for octanoic, capric, and lauric acid that are necessary to compute growth rates by Eq. (27)

---

*Heisler (1975) adjusted the growth parameters to fit the submicron aerosol volume distribution measured at Pomona, California, between 1200 and 1400 PST on October 24, 1972.

are listed in Table 4. Vapor pressures for these compounds at atmospheric temperatures have not been measured, so we extrapolated from data tabulated in the Handbook of Chemistry and Physics, 46th Edition, using the Clausius-Clapeyron equation,

$$\ln p_s = \frac{a}{T} + b \quad , \tag{31}$$

where a and b are determined by a least-squares fit of the tabulated vapor pressures.

The saturation ratio, S_i, can be expressed in terms of the thermodynamic parameters and A_i and D_{p_i} by solving for S_i from Eqs. (28) and (29). Hence,

$$S_i = \frac{\rho_L R T_\infty A_i}{2\pi D_i M_i p_{i_s}(T_\infty)} \left[1 - \left(1 + \frac{4\sigma \bar{V}_L}{R T_\infty D_{p_i}^*} \right)^{-1} \right]^{-1} \quad . \tag{32}$$

Similarly, the activity can be determined from

$$\gamma_i x_i = S_i \left(1 + \frac{4\sigma \bar{V}_L}{R T_\infty D_{p_i}^*} \right)^{-1} \quad . \tag{33}$$

If we assume a growth time, t_f, of 5 hours, Heisler's values of A_1 and A_2 are 1.3×10^{-5} $\mu m^2 sec^{-1}$ and 3.2×10^{-5} $\mu m^2 sec^{-1}$. We used these values of A_1 and A_2, Heisler's values of $D_{p_1}^*$ and $D_{p_2}^*$, and data from Table 4 in Eqs. (32) and (33) to calculate S_i and $\gamma_i x_i$ for the three organic acids listed in Table 4. The results are presented in Table 5.

The parameters calculated by Heisler (1975) imply that growth of the aerosol occurs at extremely low partial pressures and that the activity of the condensed species is very low. The magnitude of γx suggests that with multicomponent growth either the activities of the

TABLE 4. THERMODYNAMIC DATA FOR SOME ORGANIC ACIDS

Parameter	Value	Comments
σ	26.25 dynes cm^{-1}	Surface tensions of organic acids range from 25.5 to 27.25 dynes cm^{-1} (Dreisbach, 1959).
ρ_L	0.94 g cm^{-3}	Densities of organic acids range from 0.939 to 0.957 (Dreisbach, 1959)
D	0.07 $cm^2 sec^{-1}$	Estimate

Acid	Structure	Molecular Weights	Vapor Pressure at 25°C* (dynes cm^{-2})
Octanoic	$CH_3(CH_2)_6COOH$	144	11.9
Capric	$CH_3(CH_2)_8COOH$	172	0.67
Lauric	$CH_3(CH_2)_{10}COOH$	200	1.82

---

* Extrapolated from data in Handbook of Chemistry and Physics, 46th Edition, pp. D-114, D-117, D-118.

TABLE 5. VALUES OF S AND γx CALCULATED FROM HEISLER'S (1975) RATE PARAMETERS

Acid	S_1	$\gamma_1 x_1$	S_2	$\gamma_2 x_2$
Octanoic	3.85×10^{-5}	3.45×10^{-5}	3.80×10^{-4}	3.70×10^{-4}
Capric	4.89×10^{-4}	4.29×10^{-4}	4.76×10^{-3}	4.61×10^{-3}
Lauric -	1.36×10^{-4}	1.17×10^{-4}	1.30×10^{-3}	1.25×10^{-3}

condensed species are extremely low in the aerosol droplet or some process occurs in or on the particles to convert the condensed material to some other substance. The magnitude of S suggests that either the production of condensable species does not occur continuously or the rate of condensation is much greater than the rate of production of the condensable species. If the latter is correct, then it may be reasonable to assume that the condensable species are present at steady-state concentrations and that the rate of formation of secondary aerosol is equal to the rate of production of condensable species. We show subsequently that this is a good approximation for sulfuric acid vapor. Heisler's results suggest that the steady-state approximation may also be valid for the condensable organics.

While the growth equation [Eq. (27)] and the empirical growth parameters applied by Heisler (1975) are of interest for understanding particle growth in the atmosphere, their appropriateness for application in a dynamic aerosol model is questionable. The magnitudes of S and γx calculated above suggest that the growth of aerosol is limited by the rate of production of condensable species in the gas phase. Based on this conclusion, the empirical growth equation is of little value for predictive aerosol modeling because the empirical parameters have not been related to the gas phase chemistry. Another link is required between the gas phase chemistry and the aerosol composition. In the next section we suggest such a link and illustrate its use in an aerosol model.

C. COMPONENTS OF THE MODEL

In this section we develop each of the inputs necessary for the general model of Eqs. (20) to (22). First, we draw on the results of the previous section to suggest a pseudo-steady-state model for the dynamics of condensing species, wherein the rate of growth is controlled by the rate of production of condensable species in the gas phase. Next, we develop compact means of representing the rate of formation of condensable species. Finally, we consider the two sources of fresh particles, primary emissions and homogeneous nucleation.

1. Pseudo-Steady-State Model of Condensable Gaseous Species

The gas-to-particle conversion process in photochemical smog is not completely understood. Primary species, such as SO_2 and NO, may be absorbed directly and converted to secondary species in the particle. Secondary species, formed first in the gas phase, transfer to the particulate phase by diffusion or homogeneous nucleation. Identification of secondary particulate species indicates that these species, if formed in the gas phase, have low vapor pressures and will transfer rapidly to particles. If we denote primary gaseous pollutant i by P_i, secondary gaseous species i by C_i^g, and secondary particulate species i by C_i^p, then the overall gas-to-particle conversion process can be depicted as

$$\begin{tikzcd}
 & C_i^g \arrow[dr, "2"] & \\
P_i \arrow[ur, "1"] \arrow[rr, "3"'] & & C_i^p
\end{tikzcd} .$$

Path 1 represents the gas-phase conversion of primary pollutant species i to condensable species i, and Path 2 represents the transfer of i to the particulate phase by homogeneous nucleation and heterogeneous condensation. The direct absorption of P_i into a particle followed by conversion to C_i^p within the particle is depicted by Path 3.

If $[P_i]$ denoted the concentration of P_i, then a local conservation equation for $[P_i]$ is

$$\frac{d[P_i]}{dt} = -R_{1i} - R_{3i} , \qquad (34)$$

where R_{1i} and R_{3i} represent the rates of depletion of P_i by gas-phase conversion and direct transport to aerosols, respectively. If $[C_i^g]$ represents the concentration of C_i^g, the corresponding local conservation equation for C_i^g is

$$\frac{d[C_i^g]}{dt} = R_{1i} - R_{2i}^c - R_{2i}^n \quad , \qquad (35)$$

where R_{2i}^c and R_{2i}^n denote the rates of depletion of C_i^g by heterogeneous condensation and homogeneous nucleation, respectively. Clearly,

$$\frac{d[C_i^p]}{dt} = R_{2i}^c + R_{2i}^n + R_{3i} \quad . \qquad (36)$$

The rate R_{1i} depends on gas-phase chemical processes and is discussed subsequently for SO_2, NO_x, and primary organic species. The rate of conversion of a condensable species C_i^g to the particulate phase by heterogeneous condensation is given by

$$R_{2i}^c = \left(\frac{\pi}{2}\right) V_{L_i}^{-1} \int_{D_{p_{min}}}^{\infty} D_p^2 \left(\frac{dD_p}{dt}\right) \bar{n}_0(D_p,t)\, dD_p \qquad (37)$$

where V_{L_i} is the molar volume of species C_i^p in the condensed phase and where $dD_p/dt = \bar{I}_0$ is the rate of growth of a particle of diameter D_p by condensation.

A generalized theory for the formation of multicomponent droplets by homogeneous nucleation does not exist. A theory for binary systems has been developed and applied to the sulfuric acid-water system in several studies (Reiss, 1950; Doyle, 1961; Mirabel and Katz, 1974; Kiang and Stauffer, 1973; Stauffer, et al., 1973; Nair and Vohra, 1975; Takahashi et al., 1975; Hamill, 1975). The rate of formation, j, of a nucleus composed of M molecules is given by $J = J_0 \exp(-\Delta G^*/RT)$, where ΔG^* is the free energy of formation of that nucleus and J_0 is a function that depends on M and on the properties of the species and their vapor concentrations. The loss of molecules of condensable material as a result of homogeneous nucleation is then

$$R_{2i}^{n} = \int_{D^{+}_{p_{min}}}^{\infty} M(D_p) J_o \exp(-\Delta G^{*}/RT) \, dD_p \quad , \tag{38}$$

where $M(D_p)$ is the number of molecules of condensable material in a particle of diameter D_p, and $D^{+}_{p_{min}}$ is the minimum particle diameter for which homogeneous nucleation will occur (a function of the vapor pressure of the condensable species).

From Eq. (37) and Eq. (38), it can be seen that the rate at which condensation occurs depends explicitly on the aerosol size distribution present, whereas the rate of homogeneous nucleation does not. The relative magnitudes of R_{2i}^{c} and R_{2i}^{n} depend on the total number of particles on which condensation can occur,

$$N = \int_{D_{p_{min}}}^{\infty} \bar{n}_o(D_p, t) \, dD_p \quad . \tag{39}$$

For the sake of simplicity we will represent each of the rates R_{1i}, R_{2i}, and R_{3i} as first order, i.e. $R_{1i} = k_{1i}[P_i]$, $R_{2i}^{c} = k_{2i}^{c}[C_i^g]$, $R_{2i}^{n} = k_{2i}^{n}[C_i^g]$, and $R_{3i} = k_{3i}[P_i]$. First-order representation of R_{1i} and R_{3i} is an approximation that, in the absence of detailed chemical information, should be expected to be adequate.

Because of the low vapor pressure of C_i^g, we anticipate that the rate of conversion, R_{2i}, by either condensation or nucleation, will be rapid. If, in fact, this step is rapid enough so that $k_{2i} >> k_{1i}$, where $k_{2i} = k_{2i}^{c} + k_{2i}^{n}$, then C_i^g will effectively be in a pseudo-steady-state for which

$$R_{1i} = R_{2i}^{c} + R_{2i}^{n} \quad . \tag{40}$$

In such a case, the conversion of P_i to C_i^g is the rate-determining step in gas-to-particle conversion via the gas-phase route.

It is necessary, therefore, to establish whether the steady-state approximation of Eq. (40) is valid for typical secondary species. If so, we then wish to estimate which of the two routes, homogeneous nucleation or heterogeneous condensation, generally predominates in the urban atmosphere. Let us consider the H_2SO_4-H_2O system. First we wish to investigate the relative magnitudes of the rate constants, k_{1i} and k_{2i}, where i refers now to the SO_2/H_2SO_4 system. To obtain as conservative an estimate as possible, we will compare k_{1i} and k_{2i}^c. If it can be established that $k_{2i}^c >> k_{1i}$, then the steady state approximation for gaseous sulfuric acid can be deemed valid regardless of the importance of homogeneous nucleation. The first-order rate constant for heterogeneous condensation can be expressed as follows (since the H_2SO_4 aerosol-phase vapor pressure is neglected, this represents the maximum value of k_{2i}^c):

$$k_{2i}^{c} = 2\pi \mathcal{D}_{H_2SO_4} \int_{D_{p_{min}}}^{\infty} \frac{D_p \bar{n}_0(D_p,t)}{1+\ell Kn} \, dD_p \quad , \tag{41}$$

where $\mathcal{D}_{H_2SO_4}$, the molecular diffusivity of H_2SO_4 in air at S.T.P., equals 0.054 $cm^2 sec^{-1}$ (Reif, 1965). To estimate typical values of k_{2i}^c it is necessary, from Eq. (41), to select a size distribution $\bar{n}_0(D_p,t)$. Using the size distributions shown in Figure 2 representing the "base case" trajectory calculation to be described subsequently, the values of k_{2i}^c calculated for each of the seven hours of simulation are given in Table 6. Calculated values of k_{2i}^c range from 21 to 74 min^{-1}. Typical first-order rate constants for conversion of SO_2 to H_2SO_4 range from 0.01 hr^{-1} ($1.7 \times 10^{-4} min^{-1}$)

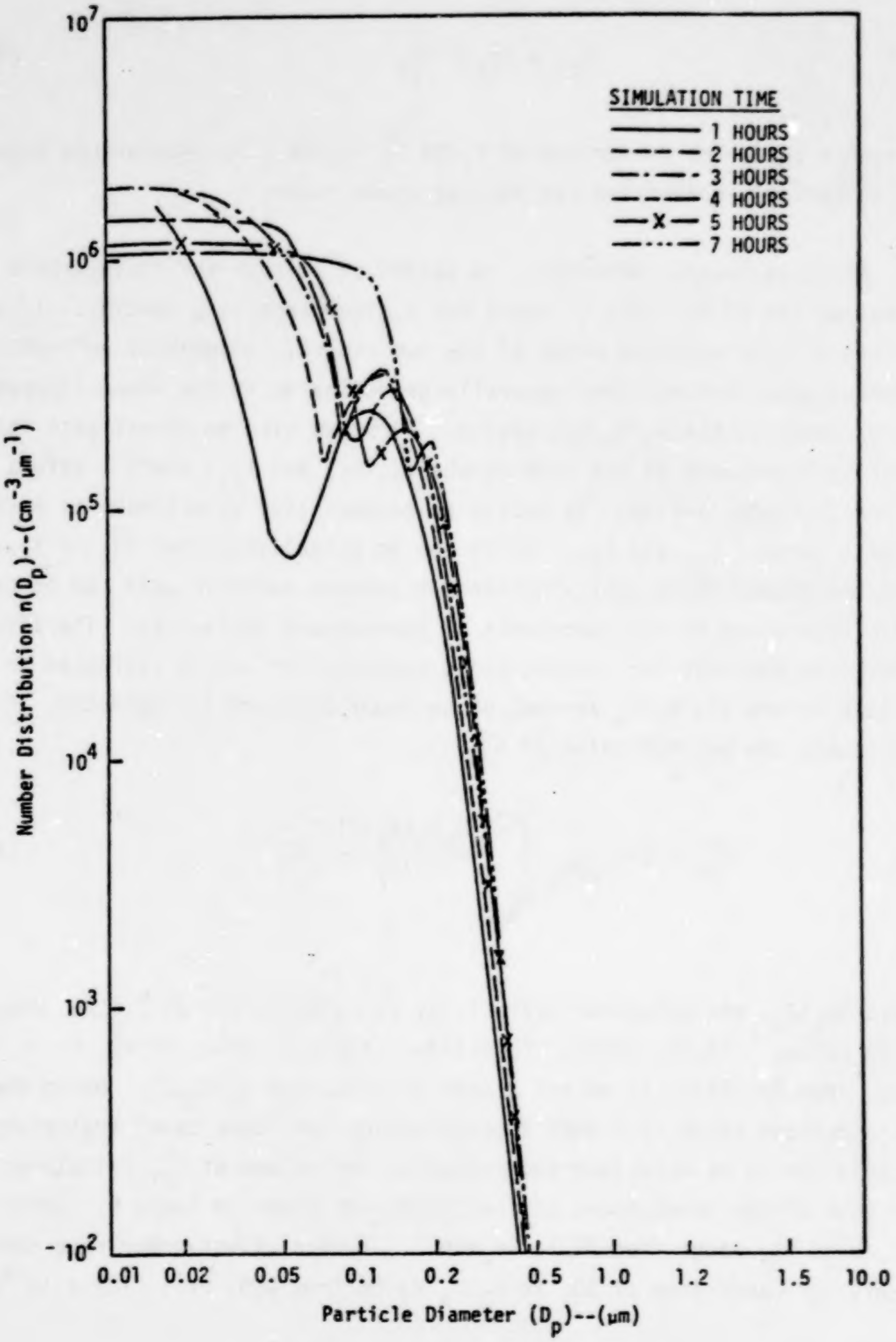

FIGURE 2. AEROSOL NUMBER DISTRIBUTIONS AS A FUNCTION OF TIME. Data derived from the base case trajectory simulation described in Chapter IV.

TABLE 6. ESTIMATED RATES OF PRODUCTION OF SUB-0.01 μm PARTICLES BY HOMOGENEOUS NUCLEATION AT VARIOUS RELATIVE HUMIDITIES

				Relative Humidity							
				10 percent*		50 percent			90 percent		
Time (hours)	Rate Constant for Condensation of Sulfate on Existing Droplets (k_{21}^{S}) (min^{-1})	SO$_2$ Concentration (ppb)	Average H$_2$SO$_4$ Concentration (ppb)	Particle Diameter (μm)	Nucleation Rate (cm^{-3}sec^{-1})	Particle Diameter (μm)	Nucleation Rate (cm^{-3}sec^{-1})	Mass Rate (g cm^{-3}sec^{-1})	Particle Diameter (μm)	Nucleation Rate (cm^{-3}sec^{-1})	Mass Rate (g cm^{-3}sec^{-1})
1	21	21	1.2×10^{-3}	--	1.3×10^{-31}	1.5×10^{-3}	2.7×10^{-5}	7.3×10^{-26}	1.2×10^{-3}	9.3×10^{2}	1.3×10^{-18}
2	36	46	1.5×10^{-3}	--	9.4×10^{-30}	1.4×10^{-3}	3.4×10^{-4}	8.5×10^{-25}	1.2×10^{-3}	3.8×10^{3}	5.2×10^{-18}
3	44	56	1.5×10^{-3}	--	9.4×10^{-30}	1.4×10^{-3}	3.4×10^{-4}	8.5×10^{-25}	1.2×10^{-3}	3.8×10^{3}	5.2×10^{-18}
4	41	31	9.1×10^{-4}	--	1.8×10^{-34}	1.6×10^{-3}	4.6×10^{-7}	1.4×10^{-27}	1.3×10^{-3}	1.0×10^{2}	1.6×10^{-19}
5	39	36	1.1×10^{-3}	--	1.4×10^{-32}	1.6×10^{-3}	7.0×10^{-6}	2.0×10^{-26}	1.3×10^{-3}	4.5×10^{2}	7.0×10^{-17}
6	46	30	7.8×10^{-4}	--	7.5×10^{-36}	1.6×10^{-3}	6.0×10^{-8}	1.9×10^{-28}	1.4×10^{-3}	35	5.9×10^{-20}
7	74	28	4.5×10^{-4}	--	3.6×10^{-41}	1.7×10^{-3}	1.4×10^{-11}	5.3×10^{-32}	1.4×10^{-3}	0.46	8.4×10^{-22}

---

*Insufficient data available to calculate diameter or mass.

to 0.1 hr^{-1} ($1.7\times10^{-3}min^{-1}$), corresponding to "clean air" and "polluted air" rates. Hence, the criterion that $k_{2i} >> k_{1i}$ for pseudo-steady-state conditions of the condensable species is met for typical urban conditions.

Having established the validity of the pseudo-steady-state approximation for gaseous condensable species, we now wish to estimate which of the two routes, homogeneous nucleation or heterogeneous condensation, generally predominates in the urban atmosphere. Of those in photochemical air pollution, the H_2SO_4-H_2O system represents that which is probably most prone to homogeneous nucleation. Thus, an estimate of the rates of homogeneous nucleation and heterogeneous condensation in that system provides a liberal estimate of the importance of homogeneous nucleation in general.

The pseudo-steady-state assumption implies that the gas phase sulfuric acid concentration is given by

$$[H_2SO_4] = \frac{k_{1i}}{k_{2i}} [SO_2] \quad , \tag{42}$$

where $k_{2i} = k_{2i}^c + k_{2i}^n$. We now wish to compare the relative magnitudes of k_{2i}^c and k_{2i}^n, or, equivalently, R_{2i}^c and R_{2i}^n. Table 6 presents the average conversion rate (in g H_2SO_4 $cm^{-3}sec^{-1}$) for heterogeneous condensation (column 5) and homogeneous nucleation (columns 10 and 13 for relative humidities of 50 and 90 percent) for the base case size distributions of Figure 2 and the SO_2 and H_2SO_4 concentrations given. The maximum condensation rate was calculated as follows.

The growth by diffusion of a droplet consisting of M species can be expressed as

$$\bar{I}_0(D_p,t) = \sum_{i=1}^{M} \frac{B_i D_p^{-1}}{1+\ell Kn} \left[p_i - p_{i_0}(D_p, c_1, \ldots, c_M) \right] \quad . \tag{43}$$

The only term in Eq. (43) that depends on the composition of the particle is the vapor pressure p_{i_0} (assuming that ρ_L is not a function of composition). If $p_{i_0} = 0$, the maximum rate of diffusion of species i is obtained. (The case $p_{i_0} = 0$ is obtained in the case of irreversible conversion of species i to another species in the particle.)

It would be desirable to obtain an expression for $\bar{I}_0$ that is independent of particle composition. Clearly, such an expression would represent only an approximation because of the dependence of p_{i_0} on composition. We take the course here of estimating the maximum rate of growth of the particle by setting $p_{i_0} = 0$. We therefore replace $\bar{I}_0$ in Eq. (43) with the maximum condensation rate,

$$\bar{I}_0^{max}(D_p,t) = \sum_{i=1}^{M} \frac{B_i D_p^{-1} p_i}{1+\ell Kn} \quad . \qquad (44)$$

Homogeneous nucleation rates were calculated from Eq. (38) and the results of Takahashi et al. (1975). We have carried out the analysis for the H_2SO_4-H_2O system, which is not only the most widely studied with respect to homogeneous nucleation but also perhaps the atmospheric system most susceptible to homogeneous nucleation. We conclude, therefore, that homogeneous nucleation is generally several orders of magnitude less important in removing condensable species than is heterogeneous condensation under typical urban atmospheric conditions. Thus, Eq. (40) becomes

$$R_{1i} = R_{2i}^{c} \quad . \qquad (45)$$

The rate of transfer of C_i^g to the particulate phase by heterogeneous condensation is given by Eq. (37) with

$$\frac{dD_p}{dt} = \bar{I}^{max}_{0_i} = \frac{B_i D_p^{-1} p_i}{1+\ell Kn} , \tag{46}$$

where p_i denotes the partial pressure of C_i^g. Combining Eqs. (37), (45), (46), we obtain the following expression for the steady-state partial pressure of C_i^g,

$$p_i = \frac{2V_{L_i} R_{1i}}{\pi B_i} \left[\int_{D_{p_{min}}}^{\infty} \frac{D_p \bar{n}_0(D_p,t)}{1+\ell Kn} \, dD_p \right]^{-1} . \tag{47}$$

Once R_{1i} has been determined, Eq. (47) can be used to compute p_i. Knowing p_i, we can then evaluate $\bar{I}_0^{max}$ from Eq. (44) as

$$\bar{I}_0^{max} (D_p,t) = \sum_{i=1}^{M} \frac{2V_{L_i} R_{1i} D_p^{-1}}{\pi(1+\ell Kn)} \left[\int_{D_{p_{min}}}^{\infty} \frac{D_p \bar{n}_0(D_p,t)}{1+\ell Kn} \, dD_p \right]^{-1} . \tag{48}$$

Finally, we can use $\bar{I}_0^{max}$ in Eq. (20) to obtain the equation governing $\bar{n}_0(D_p,t)$,

$$\frac{\partial \bar{n}_0}{\partial t} + \frac{\frac{\partial}{\partial D_p}\left[\left(\sum_{i=1}^{M} \frac{2V_{L_i} R_{1i} D_p^{-1}}{\pi(1+\ell Kn)} \right) \bar{n}_0(D_p,t) \right]}{\int_{D_{p_{min}}}^{\infty} \frac{D_p \bar{n}_0(D_p,t)}{1+\ell Kn} \, dD_p} = S(D_p,t) . \tag{49}$$

A property of this model is that the particle composition for secondary species is independent of particle size. Each species transfers to the aerosol phase at a rate dependent only on its ambient partial pressure and the size of the particle. The fraction of total aerosol mass composed of sulfate, nitrate, or organic material in any given size range varies because of the size distributions of the initial aerosol and that emitted from sources. The overall rate of increase of particle volume depends only on the rate of conversion of primary gaseous species to condensable species. Particles of different sizes grow at different rates because of the dependence of growth rate on particle size through Eq.(48).

2. Formation of Condensable Species

In this study we have chosen to concentrate on three classes of secondary aerosol: sulfates, nitrates and organics. The formation of these species is not completely understood at present, and we have chosen not to attempt to study detailed chemical mechanisms in this work. Our object is to represent the rate-determining processes in as concise a manner as possible while at the same time retaining as much chemical reality as possible.

a. Conversion of SO_2 to Sulfate

The conversion of SO_2 to sulfate is a highly complex process that may involve both homogeneous and heterogeneous paths (Castleman, 1974; Calvert, 1974; Hidy and Burton, 1975; Sander and Seinfeld, 1976). In this work we assume that the conversion of SO_2 to sulfate may be represented by a process first order in SO_2 concentration, i.e. $R_{11} = k_{11}[SO_2]$. Reported values of k_{11} under laboratory and ambient conditions are numerous. Since in our applied studies we consider the Los Angeles atmosphere, we will employ a value of k_{11} derived from the data of Roberts and Friedlander (1975) for SO_2 to sulfate conversion in the Los Angeles atmosphere (see Table 7).

TABLE 7. PSEUDO-FIRST-ORDER RATE CONSTANTS FOR CONVERSION OF SO_2 TO SULFATE IN LOS ANGELES

Date (1973)	Time of Arrival of Air Parcel at Pasadena (PST)	k_{SO_4} (percent per hour)	Starting Location
July 10	1300	1.2	El Segundo
	1400	3.0	El Segundo
	1500	9.0	El Segundo
	1600	13.0	El Segundo
July 25	1400	12.8	Alamitos Bay
	1500	8.2	El Segundo
	1600	8.8	El Segundo
July 26	1200	4.3	Alamitos Bay
	1300	5.6	Alamitos Bay
	1400	7.6	Alamitos Bay
	1500	4.7	Alamitos Bay

Source: Roberts and Friedlander (1975).

b. Conversion of NO_x to Nitrate

The conversion of NO_x to particulate nitrate is not well understood at present. Attempts to correlate particulate nitrate formation with other atmospheric variables have largely been unsuccessful (Hidy et al., 1975; Clark et al., 1976). For the purpose of this study we will assume merely that $R_{12} = k_{12}[NO_2]$. Values of k_{12} can be inferred from the data of Clark et al. (1976) for nitrate formation under simulated photochemical smog conditions.

c. Conversion of Hydrocarbons to Particulate Organics

The formation and identification of organic aerosol has received a substantial amount of attention (Cukor et al., 1972; Ciaccio et al., 1974; Grosjean, 1975, 1977; O'Brien et al., 1975ab; Appel et al., 1976; Schuetzle et al., 1973, 1975). There seems to be general agreement, at least for olefinic species, that the rate-determining step for organic aerosol formation is the reaction with ozone (Liepeles et al., 1973; O'Brien et al., 1975ab; Grosjean, 1977). Therefore, we express the rate of formation of organic aerosol as $R_{13} = \alpha k_{13}[NMHC][O_3]$, where [NMHC] is the total non-methane hydrocarbons, and a is the fraction of [NMHC] that are aerosol precursors. The value k_{13} is taken as the rate constant for the reaction of cyclohexene with O_3, namely 0.25 ppm^{-1} min^{-1} (Japar et al., 1974).

d. Physical Properties

The only physical property needed to complete $\bar{I}_0^{max}$ are the molar volumes V_{L_i} of the particulate species. From the ACHEX study, Hidy et al. (1975) reported that the average mass ratio of compounds to ions for both nitrates and sulfates was about 1.3. They estimated that the average ratio of the mass of organic compounds to that of elemental carbon in the aerosol was about 1.4, and also that over half of the organic aerosol was composed of compounds with carbon numbers greater than 6. Furthermore, O'Brien et al. (1975 ab) obtained the empirical formula $C_{10}H_{20}O_4$-ONO for an aerosol formed in the laboratory from a mixture of 1,6-heptadiene, NO_2, and ozone. Hence, assuming a 10-carbon-atom organic compound, we estimate the average molecular weight of the organic condensable species to be 160. The densities associated with each compound were assumed to be 1.77 g cm^{-3} (ammonium sulfate), 1.73 g cm^{-3} (ammonium nitrate), and 0.94 g cm^{-3} (organics).

3. Sources of Primary Aerosol

The term $S(D_p,t)$ in Eq. (20) accounts for the rate of introduction of fresh particles with $D_p > D_{p_{min}}$ from primary sources. In this study primary sources will be assumed to fall into one of three categories: auto lead, auto organics, and other primary aerosols. In addition, it is necessary to specify a primary background aerosol. The source breakdown of particulate emissions in Los Angeles County in 1973 is given in Table 8. There are several studies in which size distributions of automotive aerosols have been reported (Miller et al., 1976; White and Husar, 1976). It has been shown that where similar driving conditions and adequate exhaust dilution are employed in the laboratory, the size and concentration of the laboratory aerosols are similar to those measured along roadways (Miller et al., 1976). For this study we will employ the auto lead and organic aerosol size distributions reported by White and Husar (1976) in Figure 3. The volume distributions shown in Figure 3 are similar in nature to those reported by Miller et al. (1976) for primary automobile aerosol that was allowed to stand in a chamber prior to irradiation. The coagulation that occurred in the chamber was sufficient to bring the mode in the volume distribution close to 0.1 μm diameter. Thus, by using distributions that include the effect of early coagulation, we should minimize errors due to our neglect of coagulation in the dynamics of $\bar{n}_0$.

To represent the automotive distributions as well as those of other sources (for which size distributions are not available) we use the

TABLE 8. SOURCE BREAKDOWN OF CO, SO_2, AND PARTICULATE EMISSIONS IN LOS ANGELES IN 1973

Source	Percentage Contribution of Total Emissions		
	Carbon Monoxide	Oxides of Sulfur	Particulates
Gasoline-Powered Motor Vehicles	97.1	8.2	30.8
Other Transportation	--	4.1	19.3
Combustion of Fuels	--	48.0	26.9
Petroleum Operations	--	15.1	--
Other Industrial Operations	--	8.2	11.5
Sulfur Recovery Operations	--	16.4	--
Organic Solvent Operations	--	--	11.5
Other	2.9	--	--

Note: Total emissions: carbon monoxide--7300 tons/day; oxides of sulfur--365 tons/day; particulates--130 tons/day.

Adapted from Birakos (1974).

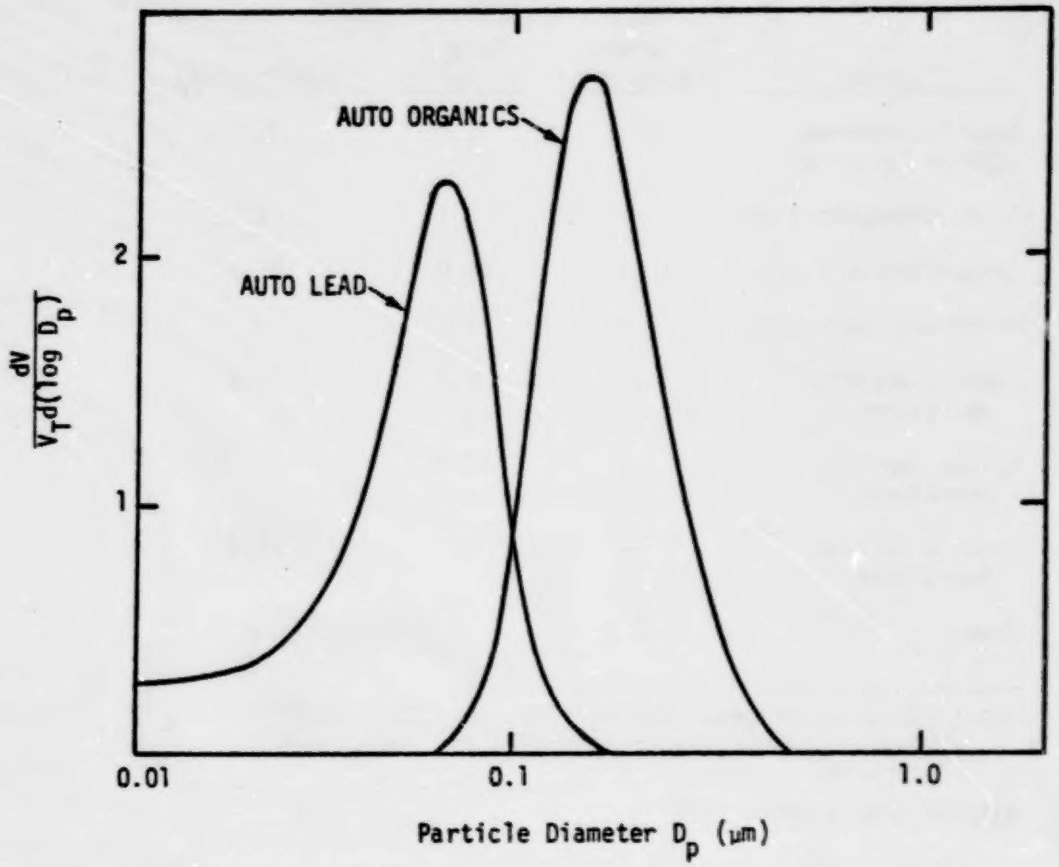

Source: White and Husar (1976).

FIGURE 3. NORMALIZED PARTICLE VOLUME DISTRIBUTIONS USED FOR PRIMARY AEROSOLS IN THIS STUDY.

log-normal distribution of particle volume,

$$\frac{dV}{V_T d(\log D_p)} = \frac{(\log e)^{-1}}{\sqrt{2\pi}\,\sigma} \exp\left[- \frac{(\ln D_p - \mu)^2}{2\sigma^2} \right] \quad . \qquad (50)$$

As shown in Figure 4, Eq. (50) provides a good fit to the auto organic size distribution for $\mu = -1.802$ and $\sigma = 0.362$.

The source distribution used in the aerosol model is determined from the equation

$$S_i'(D_p,t) = \sum_j \alpha_j' s_j(D_p) h_j(t) \quad , \qquad (51)$$

where α_j' is the fraction of the mass of particles emitted that becomes airborne, and $s_j(D_p)$ is the size distribution function for a unit mass of emissions from source $j(\mu m^{-1} cm^{-3} g^{-1})$ with a mass emission rate $h_j(t)$ $(g\ cm^{-3} sec^{-1})$. (Note that the sources are assumed to be volume sources.)

The volume source distribution given by Eq. (50) and Figure 3 can be converted to the normalized size distribution function by

$$s(D_p) = \frac{6}{\pi} (\ln 10)^{-1} \rho^{-1} D_p^{-4} \frac{dV}{V_T d(\log D_p)} \quad . \qquad (52)$$

where ρ denotes the density of the aerosol.

We performed two types of simulations (described in Chapter IV) that required specification of the rate of volume density emissions of primary aerosol. In the batch system, the primary particle emission rate was chosen as 15 $\mu m^3 cm^{-3} min^{-1}$. For the trajectory simulations, particulate emission rates were estimated from known SO_2 and CO emission

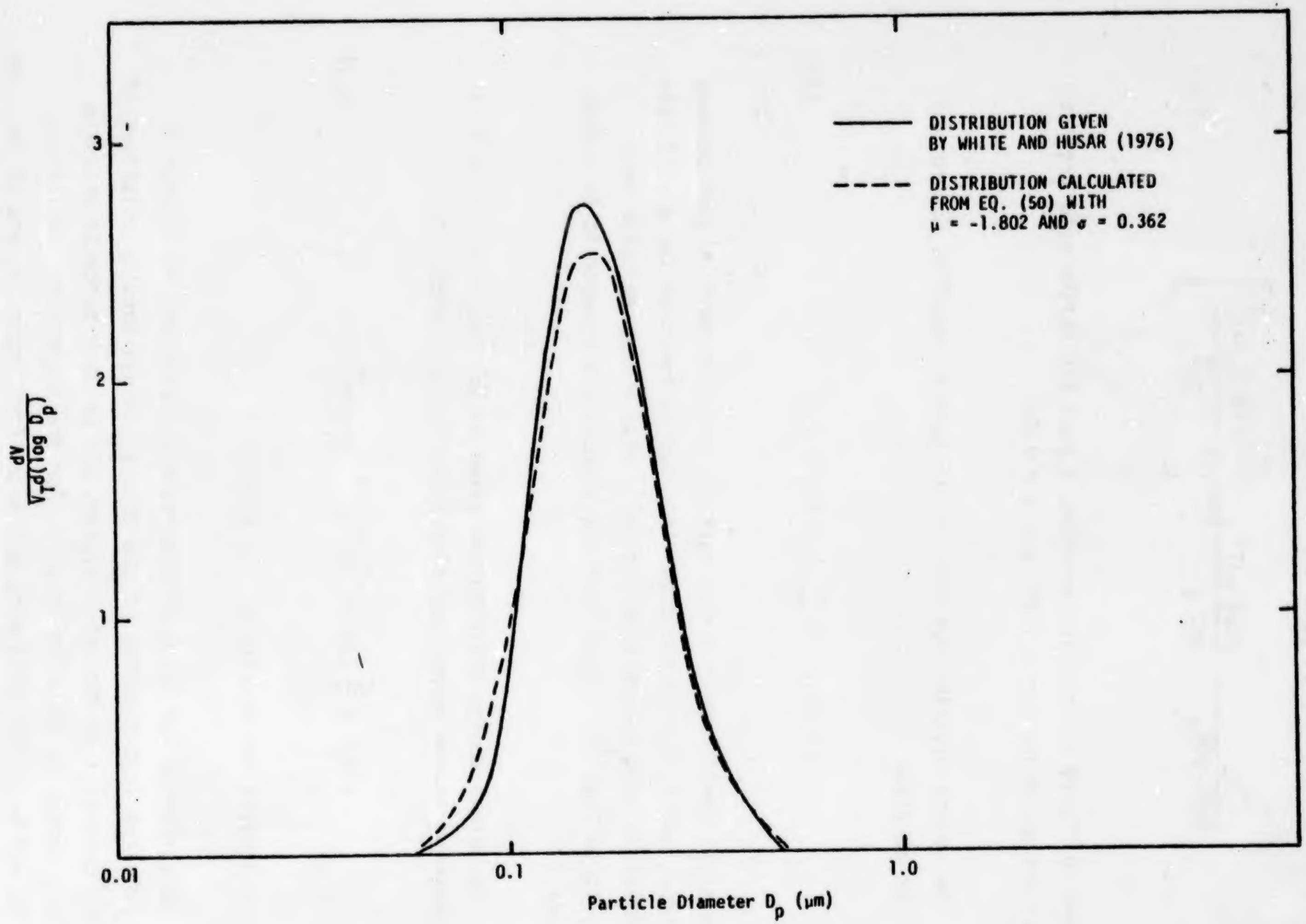

FIGURE 4. MEASURED AND FITTED VOLUME DISTRIBUTIONS FOR AUTO ORGANIC AEROSOL

rates. Particulate emission rates can be calculated from the known ratios of particulate to SO_2 emissions from stationary sources and particulate to CO emissions from mobile sources. These rates are summarized in Table 8. It was assumed that one half of the emissions from gasoline-powered motor vehicles was lead aerosol and one half organic aerosol. Furthermore, we assumed that α', the fraction of the mass of particles emitted that becomes airborne [Eq. (51)], equals 0.43 for lead and 1.0 for other emissions (Huntzicker et al., 1975).

4. Flux of Small Particles into the Size Range $D_p > D_{p_{min}}$

In the model we consider the size range $D_p > D_{p_{min}}$, which necessitates the specification of either the size distribution function at $D_{p_{min}}$, [g(t) in Eq. (22a)], or the particle flux at $D_{p_{min}}$ [$S_0(t)$ in Eq. (22b)]. Our intention in considering only the region $D_p > D_{p_{min}}$ is to avoid the necessity of accounting in detail for all the processes influencing the transient nuclei, such as homogeneous nucleation and coagulation. Nevertheless, these processes lead to a flux of particles into the range $D_p > D_{p_{min}}$ that must be specified as a boundary condition.* As noted, we selected $D_{p_{min}} = 0.01$ μm. In this section we consider the dynamics of sub-0.01 μm particles. A detailed consideration would entail calculations of growth rates including nucleation, condensation, and coagulation. We attempt here to estimate the relative importance of these processes to the number and volume of particles in the sub-0.01 μm range. The objective is to specify the boundary condition at $D_{p_{min}}$.

---

* In addition, particles of diameter $D_p < D_{p_{min}}$ can coagulate with particles of diameter $D_p > D_{p_{min}}$. We do not account for this interaction in the present formulation of the model because the total aerosol volume added to the accumulation range ($0.1 < D_p < 1.0$ μm) by coagulation can be shown to be small compared to the volume added by other processes.

We discuss briefly here the dynamics of the transient nuclei. The primary mechanism for gas-to-particle conversion has been assumed to be by the formation of condensable products of homogeneous gas phase reactions. Such products, e.g. sulfuric acid, can combine with other condensable molecules to form new particles or to condense on preexisting particles (heterogeneous condensation). The relative importance of each mechanism depends on the thermodynamic properties of the condensing molecules, the rate at which they are being produced, and the quantity of preexisting aerosol. The processes are shown in the following diagram.

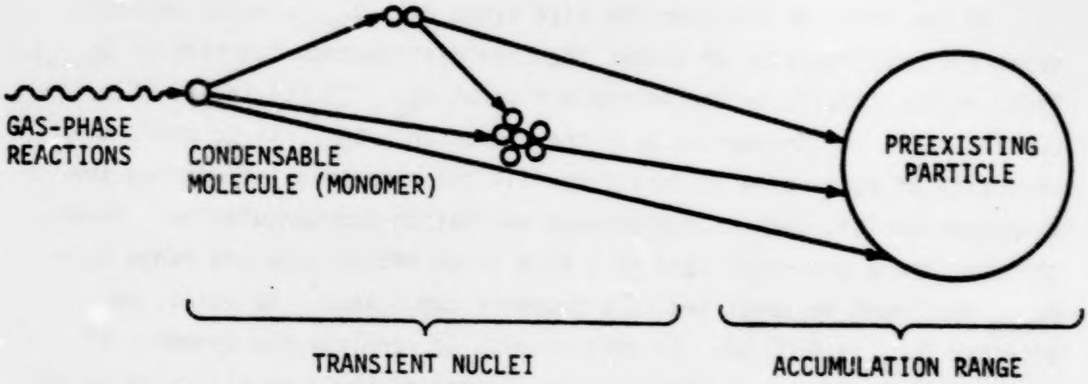

In the atmosphere new particle formation (homogeneous nucleation) and heterogeneous condensation occur simultaneously. To study the dynamics of the transient nuclei mode one must consider the simultaneous processes depicted above. We recall that in developing the pseudo-steady-state model for the condensable species we neglected the transient nuclei dynamics because the total aerosol volume contained within the transient nuclei mode at any time is small. In developing the boundary condition at the upper end of the transient nuclei spectrum we must consider all the processes influencing the transient nuclei.

Classic homogeneous nucleation theory is concerned with the rate of formation of stable nuclei of condensable molecules in the absence of preexisting aerosol. The size and composition of a stable nucleus are determined by the thermodynamic properties of the species involved. The sulfuric acid/water system has been rather thoroughly studied from the standpoint of homogeneous nucleation. For example, Table 9 presents the results of Doyle (1961) and Takahashi et al. (1975) for homogeneous nucleation rates in the H_2SO_4/H_2O system for H_2SO_4 partial pressures ranging from 1.3×10^{-4} to 0.13 ppb and relative humidities of 10, 50, and 90 percent.

At partial pressures of H_2SO_4 below 0.01 ppb (4×10^{-14}g cm^{-3}) the rate of removal of H_2SO_4 vapor by homogeneous nucleation is very slow compared with typical rates of oxidation of SO_2 except at very high relative humidities. (Assuming a 10 percent per hour conversion of 0.1 ppm SO_2 the SO_2 oxidation rate is 10^{-15} g cm^{-3}sec^{-1}.) Even at relative humidities of 50 percent, however, the rate at which nuclei form at partial pressures of H_2SO_4 above 3×10^{-3} ppb is very high. Hence, over a range of partial pressures of sulfuric acid vapor and a range of relative humidities, the rate of removal of H_2SO_4 vapor by homogeneous nucleation is very slow and yet the number of droplets produced is very large. Thus these droplets are very small, normally consisting of fewer than 50 molecules of sulfuric acid. As indicated in column 5 of Table 9, sulfuric acid represents only 20 to 37 percent of the molecules in these droplets--the remaining molecules are water.

Previously we showed (Table 6) that homogeneous nucleation is negligible compared to heterogeneous condensation as a source of aerosol volume. Our calculation of the size distribution dynamics in the accumulation regime requires a particle flux at the lower end of the region, in this case chosen as 0.01μm particles, including homogeneous nucleation and coagulation as well as condensation of particles on aerosol in the super-0.01 μm regime. Such an analysis has not been carried out in general. As we noted before, classical homogeneous nucleation theory does not take into account

TABLE 9. HOMOGENEOUS NUCLEATION RATES FOR SULFURIC ACID DROPLETS

Partial Pressure of H_2SO_4 (ppb)	Relative Humidity (percent)	Nucleation Rate ($cm^{-3}sec^{-1}$)	Molecules per Nucleus	Mole Fraction of H_2SO_4	Homogeneous Nucleation Rate ($g\ cm^{-3}sec^{-1}$)
0.13	10	1.1×10^{2}	25	0.37	2.2×10^{-19}
	50*	6.8×10^{9}	11	0.32	1.7×10^{-11}
	50	2.9×10^{9}	10	0.31	2.1×10^{-12}
	90	1.5×10^{12}	7	0.30	7.3×10^{-10}
1.3×10^{-2}	10	2.3×10^{-11}	80	0.31	1.3×10^{-31}
	50*	8.3×10^{5}	18	0.28	3.6×10^{-15}
	50	1.5×10^{5}	18	0.28	1.8×10^{-16}
	90	7.2×10^{8}	11	0.26	5.1×10^{-13}
1.3×10^{-3}	10	4.6×10^{-29}	--	--	--
	50*	7.8×10^{-3}	41	0.25	8.1×10^{-23}
	50	8.4×10^{-4}	40	0.25	2.1×10^{-24}
	90	6.2×10^{3}	21	0.22	7.7×10^{-18}
1.3×10^{-4}	10	9.4×10^{-52}	--	--	--
	50*	1.5×10^{-20}	118	0.22	4.6×10^{-40}
	50	7.9×10^{-20}	110	0.21	5.0×10^{-40}
	90	3.7×10^{-5}	45	0.20	9.4×10^{-26}

Source: Data marked * from Doyle (1961), all other data from Takahashi et al. (1975).

coagulation between growing clusters or between growing clusters and pre-existing aerosol. A detailed analysis of the transient nuclei mode is beyond the scope of this report. Nevertheless, we wish to develop briefly the elements of such an analysis, the specific object being the prediction of the flux of particule at the lower limit of the accumulation range, e.g., 0.01 μm.

We define

N_j = concentration of particulates containing j monomers (cm^{-3}), j = 1, 2, ..., (the monomer is defined as one molecule of the condensable species, such as sulfuric acid),

ρ_{ij} = coagulation coefficient between particles containing i and j monomers. Since these particles are characterized by Kn >> 1, β_{ij} is given by the free molecule formula,

R = rate of production of monomer molecules by gas phase chemical reaction ($cm^2 sec^{-1}$),

$$\beta_{ij} = \left(\frac{3}{4\pi}\right)^{1/6} \left(\frac{6kT}{\rho}\right)^{1/2} \left(\frac{1}{v_i} + \frac{1}{v_j}\right)^{1/2} \left(v_i^{1/3} + v_j^{1/3}\right)^2 \quad (cm^3 sec^{-1})$$

$\mathcal{D}_j$ = Brownian (or molecular) diffusivity of a particle containing j monomer units ($cm^2 sec^{-1}$),

γ_j = rate of evaporation of monomer from a particle containing j monomer units (sec^{-1}).

A dynamic balance on monomer yields

$$\frac{dN_1}{dt} = R - \beta_{11} N_1^2 - N_1 \sum_{j=2}^{K} \beta_{1j} N_j + \sum_{j=2}^{K} \gamma_j N_j - 2\pi \mathcal{D}_1 I N_1 \quad , \qquad (53)$$

where

$$I = \int_{Kv_1}^{\infty} \frac{D_p \bar{n}_0(D_p,t)}{1 + \ell Kn} \, dD_p \quad . \tag{54}$$

Thus, the last term on the right in Eq. (53) accounts for loss of monomer due to heterogeneous condensation on aerosol in the accumulation range. (The diameter corresponding to Kv_1 is 0.01 μm.)

It is likely that a pseudo-steady-state approximation can be invoked with respect to the monomer, as assumed previously, i.e.

$$0 = R - \beta_{11}N_1^2 - N_1 \sum_{j=2}^{K} \beta_{1j}N_j + \sum_{j=2}^{K} \gamma_j N_j - 2\pi \mathcal{D}_1 I N_1 \quad . \tag{55}$$

The dynamic balance for clusters is

$$\frac{dN_j}{dt} = \frac{1}{2} \sum_{\ell=1}^{j-1} \beta_{j-\ell,\ell} N_{j-\ell} N_\ell - N_j \sum_{\ell=1}^{K} \beta_{j\ell} N_\ell + \gamma_{j+1} N_{j+1} - \gamma_j N_j - 2\pi \mathcal{D}_j I N_j$$

$$j = 2, 3, \ldots, K \tag{56}$$

If a pseudo-steady-state approximation is invoked for N_j, the right hand side of Eq. (56) may be set equal to zero. The quantity of interest is the net flux ($cm^{-3}sec^{-1}$) of particles of size K, dN_K/dt. As we noted, this problem has not been solved, in part because the coefficients γ_j are not generally available.

A solution to a special case of the set Eqs. (55) and (56) under the assumption of steady staste has been obtained by McMurry (1977). For sufficiently high concentrations of condensable molecules, rates of molecular collisions with clusters or with freexisting aerosol should exceed rates of evaporation. Also, collisions among clusters can be neglected relative to collisions between clusters and monomer. Under these circumstances, Eqs. (55) and (56) become

$$0 = R - \beta_{11}N_1^2 - N_1 \sum_{j=2}^{K} \beta_{1j}N_j - 2\pi D_1 I N_1 \quad , \tag{57}$$

and

$$0 = \beta_{1,j-1}N_1 N_{j-1} - \beta_{1j}N_1 N_j - 2\pi D_j I N_j \quad . \tag{58}$$

If we define

$$\tilde{N}_j = \frac{\beta_{11}N_j}{2\pi D_1 I} \qquad L = \frac{(2\pi D_1 I)^2}{\beta_{11}R} \qquad c_j = \frac{\beta_{1j}}{\beta_{11}} \qquad \mu_j = \frac{D_j}{D_1}$$

then Eqs. (57) and (58) can be written in dimensionless form as

$$1 = L\tilde{N}_1^2 + L\tilde{N}_1 \sum_{j=2}^{K} c_j \tilde{N}_j + L\tilde{N}_1 \tag{59}$$

and

$$0 = c_{j-1}\tilde{N}_{j-1}\tilde{N}_1 - c_j \tilde{N}_j \tilde{N}_1 - \mu_j \tilde{N}_j \quad . \tag{60}$$

The dimensionless cluster concentration can be obtained in terms of the dimensionless monomer concentration from

$$\frac{\tilde{N}_j}{\tilde{N}_{j-1}} = \frac{c_{j-1}\tilde{N}_1}{c_j \tilde{N}_1 + \mu_j} \tag{61}$$

which, upon successive substitution, yields

$$\frac{\tilde{N}_j}{\tilde{N}_1} = \prod_{\ell=2}^{j} \frac{c_{\ell-1}\tilde{N}_1}{c_\ell \tilde{N}_1 + \mu_\ell} \quad . \qquad (62)$$

The rate of formation of particles of size K is then $G(K) = \beta_{1,K-1}N_1N_{K-1}$, which in dimensionless terms can be expressed as

$$\frac{G(K)}{R} = c_{K-1}\, L\, \tilde{N}_{K-1}\tilde{N}_1 \quad . \qquad (63)$$

Since $\tilde{N}_{K-1}$ depends only on $\tilde{N}_1$, and $\tilde{N}_1$ depends only on L, G(K)/R is a function only of L at a certain value of K. The parameter L is a measure of the ratio of the rate at which monomer molecules collide with pre-existing aerosol to the rate at which they collide with themselves. Note that L can be calculated from a knowledge of the rate R of products of condensable molecules and the available aerosol surface area in the accumulation range.

Using Eq. (63), McMurry (1977) has calculated G as a function of D_p for the following conditions:* $R = 1.43 \times 10^{7}$ cm^{-3}sec^{-1}, aerosol surface area = 5×10^{-6} cm^2/cm^3, aerosol density = 1.46 g cm^{-3}, and monomer volume = 2.1×10^{-22} cm^3. These values correspond to sulfuric acid/water aerosol at 30 percent relative humidity. McMurry (1977) predicted that G(0.01 μm) = 10^2 cm^{-3}sec^{-1}. Subsequently, we will employ this rate as the lower bound on the particle flux at 0.01 μm since it does not, of course, include the effect of primary particle sources.

---

* In McMurry's (1977) calculation $\mu_j = j^{-1/2}$, and $2\pi D_1 I$ was approximated by the corresponding free molecule regime expression.

D. SOLUTION OF THE EQUATION GOVERNING $\bar{n}_0(D_p,t)$

The basic model, given by Eqs. (20) to (22), is a first-order, hyperbolic partial differential equation, which may be solved numerically by the method of characteristics (Lapidus, 1962). We rewrite Eq. (20) as

$$\frac{\partial \bar{n}_0}{\partial t} + \bar{I}_0 \frac{\partial \bar{n}_0}{\partial D_p} = S_1'(D_p,t) - \bar{n}_0 \frac{\partial \bar{I}_0}{\partial D_p} \quad . \tag{64}$$

Along any characteristic curve given by

$$\frac{dD_p}{dt} = \bar{I}_0(D_p,t) \quad , \tag{65}$$

Eq. (64) reduces to

$$\frac{d\bar{n}_0}{dt} = S_1' - \bar{n}_0 \frac{d\bar{I}_0}{dD_p} \quad . \tag{66}$$

Using Eq. (41), and noting that

$$\beta(t) = \int_{D_{p_0}}^{\infty} \frac{2\pi D_p}{1 + \ell Kn} \bar{n}_0(D_p,t)dD_p \tag{67}$$

is independent of D_p, we obtain an explicit solution of Eq. (65)

$$\int_{t_0}^{t} 4\beta(t)^{-1} \sum_i R_i^+ \, dt' = \frac{1}{2}\left(D_p^2 - D_{p_0}^2\right) + 5.33\,\lambda^2 \ln\left(\frac{1 + D_p/2\lambda}{1 + D_{p_0}/2\lambda}\right)$$
$$+ 1.42\left[\lambda\left(D_p - D_{p_0}\right) - 2\lambda^2 \ln\left(\frac{1 + D_p/2\lambda}{1 + D_{p_0}/2\lambda}\right)\right] \quad . \qquad (68)$$

Equation (68) gives the characteristic curve in terms of D_p at any t corresponding to D_{p_0} at t_0.

We note that Eqs. (66) and (68) are coupled through $\beta(t)$, so that they must be solved simultaneously in the numerical solution along each characteristic curve.

In finite-difference form, Eq. (66) becomes

$$\bar{n}_0\left(D_{p_{new}}\right) - \bar{n}_0\left(D_{p_{old}}\right) = S_1'\left(D_{p_{old}}, t\right) \Delta t - \frac{1}{2}\left[\bar{n}_0\left(D_{p_{new}}\right)\right.$$
$$\left. + \bar{n}_0\left(D_{p_{old}}\right)\right]\left(\frac{\partial \bar{I}_0}{\partial D_p}\right)_{D_{p_{old}}} \Delta t \quad . \qquad (69)$$

E. PROPERTIES OF THE MODEL

Based on the results of this chapter we can summarize some of the properties of the model developed here.

Because coagulation has not yet been included in the model, we expect the model to predict number concentrations larger than those that actually occur. Furthermore, when typical formation rates of droplets by homogeneous nucleation are included in the model the predicted number density should also be too large. The volume distributions should also reflect the excessive number of particles because excessive growth would occur on the small particles due to their large number density.

A property of the model developed here is that the particle composition for secondary species is independent of particle size. Each species is assumed to transfer to particles at a rate dependent only on its ambient partial pressure and on the size of the particle. Of course, the fraction of total aerosol mass composed of sulfate, nitrate, or organic material in any given size range varies because of the size distributions of the initial aerosol and that emitted from primary sources.

Because particle composition has been neglected, an equilibrium particle size is not approached. However, as the number of particles and the aerosol surface area increase, the integral in Eq. (67), which normalizes the rate of growth, also increases. Thus, at a constant rate of formation of condensable material, the rate of growth of a given particle will decrease as the total surface area increases.

IV SIZE DISTRIBUTION SOLUTIONS

This chapter describes the application of the model developed in Chapters II and III to the growth of photochemical aerosol in a batch system and in an air parcel along a wind trajectory in Los Angeles. The main purpose of the application was to gain an understanding of the properties of the model and to determine its sensitivity to changes in various parameters.

In the batch system constant rates of production of primary and secondary aerosol were assumed. In the trajectory system emissions and production rates of secondary aerosol precursors were determined by the conditions along the trajectory. The secondary aerosol production rate was determined by interpolating measured pollutant concentrations along the trajectory and employing the approximate reaction rates discussed in Chapter III.

The model developed does not account for the effect of particle composition on particle growth. The overall rate of increase of particle volume depends on the rate of conversion of gaseous species to aerosol precursors. Particles of different sizes grow at different rates because of the dependence of the growth rate on particle surface area. The batch and trajectory systems differ in that the rates of emission of primary aerosol and the rates of conversion of gases to aerosol are different.

In studies in which we examined the effect of changes in the size distribution of the primary aerosol, we varied μ and σ in Eq. (50). By changing-the source distribution in this way, we did not change the total volume of particles emitted, although the number of particles emitted did change. (This approach, in which volume is conserved rather than number, is more reasonable for sensitivity studies because in most common measurement methods the volume of aerosol is the quantity determined.)

A. SIZE DISTRIBUTION DYNAMICS IN A BATCH SYSTEM

We considered a batch system in which an initial charge of aerosol grows by gas-to-particle conversion with and without particle sources. In this system we assumed that the rate of conversion of gaseous species to aerosol precursors was constant.

Our objectives in applying the aerosol model to simulate a batch system were

> To examine the effect of production of sub-0.01 μm particles.
> To examine the effect of primary aerosol source strength and size distribution.

Thus, our main concern was to gain an understanding of the properties of the model and the effects of changes in various parameters of the model on the dynamics of the predicted size distributions.

1. Effect of Production of Sub-0.01 μm Particles

A hypothetical system analogous to that which might exist in a smog chamber consists of an initial aerosol charge that grows by gas-to-particle conversion, accompanied by the formation of sub-0.01 μm particles by homogeneous nucleation. Because coagulation and wall losses are not explicitly accounted for, such a system is an idealization of the processes that would occur in an actual smog chamber.

In this hypothetical system, the initial aerosol was assumed to have a volume concentration of 20 $\mu m^3 cm^{-3}$ and the volume distribution shown in Figure 5a. The distribution in Figure 5a is given by Eq. (50) with $\mu = -1.8$ and $\sigma = 0.5$. The rate of production of secondary aerosol was assumed to be 0.42 $\mu m^3 cm^{-3} min^{-1}$, a rate that leads to a total aerosol volume increase after 7 hours of approximately 10 times the initial volume. To study the effect of the rate of production of sub-0.01 μm particles on the size distribution dynamics, we considered two cases of the boundary condition, Eq. (22b): Case (1)--$S_0(t) = 100$ $cm^3 min^{-1}$, and Case (2)--$S_0(t) = 600$ $cm^3 min^{-1}$. Case (1) represents a situation in which there is very little production of small particles by homogeneous nucleation. The production rate in Case (2) is roughly the rate at which sub-0.01 μm particles are added by automobile lead emissions.

a. Case (1)

The normalized volume distributions at t = 0, 3, and 7 hours are shown in Figures 5a, b, and c. The location of the maximum in the volume distribution, initially at D_p slightly less that 0.17 μm, reached 0.19 μm after three hours and 0.22 μm after seven hours. After seven hours of growth the magnitude of the peak in the volume distribution had increased by a factor of five from its initial value. Furthermore, there was considerable narrowing of the distribution. Let us consider the behavior exhibited in Figure 5. From Eq. (50), the normalized volume distribution can be expressed in terms of $\bar{n}_0 (D_p,t)$ by

$$\frac{dV}{V_T d \log D_p} = \frac{\pi}{6} \ell n \; 10 \left(\frac{\rho}{m}\right) D_p^4 \; \bar{n}_0(D_p,t) \quad . \tag{70}$$

Upon differentiating with respect to D_p, we obtain

$$\frac{\partial}{\partial D_p}\left(\frac{dV}{V_T d \log D_p}\right) = \frac{\pi}{6} \ell n \; 10 \left(\frac{\rho}{m}\right)\left[\bar{n}_0(D_p,t) 4 D_p^3 + D_p^4 \frac{\partial \bar{n}_0}{\partial D_p}\right] \quad . \tag{71}$$

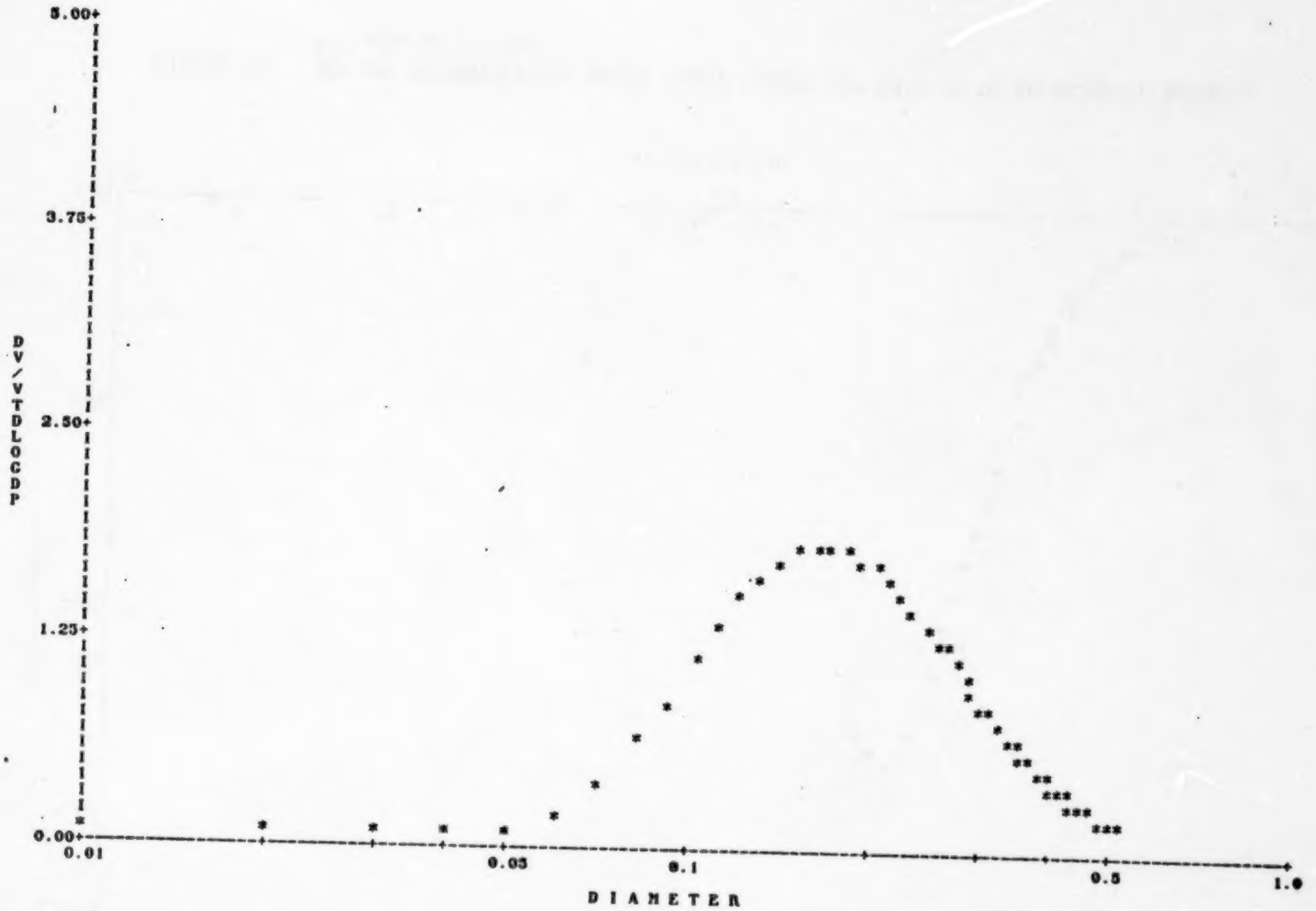

FIGURE 5a. INITIAL VOLUME DISTRIBUTION FOR RUNS WITH NO PRIMARY AEROSOL: $\sigma = 0.50$, $\mu = -1.80$

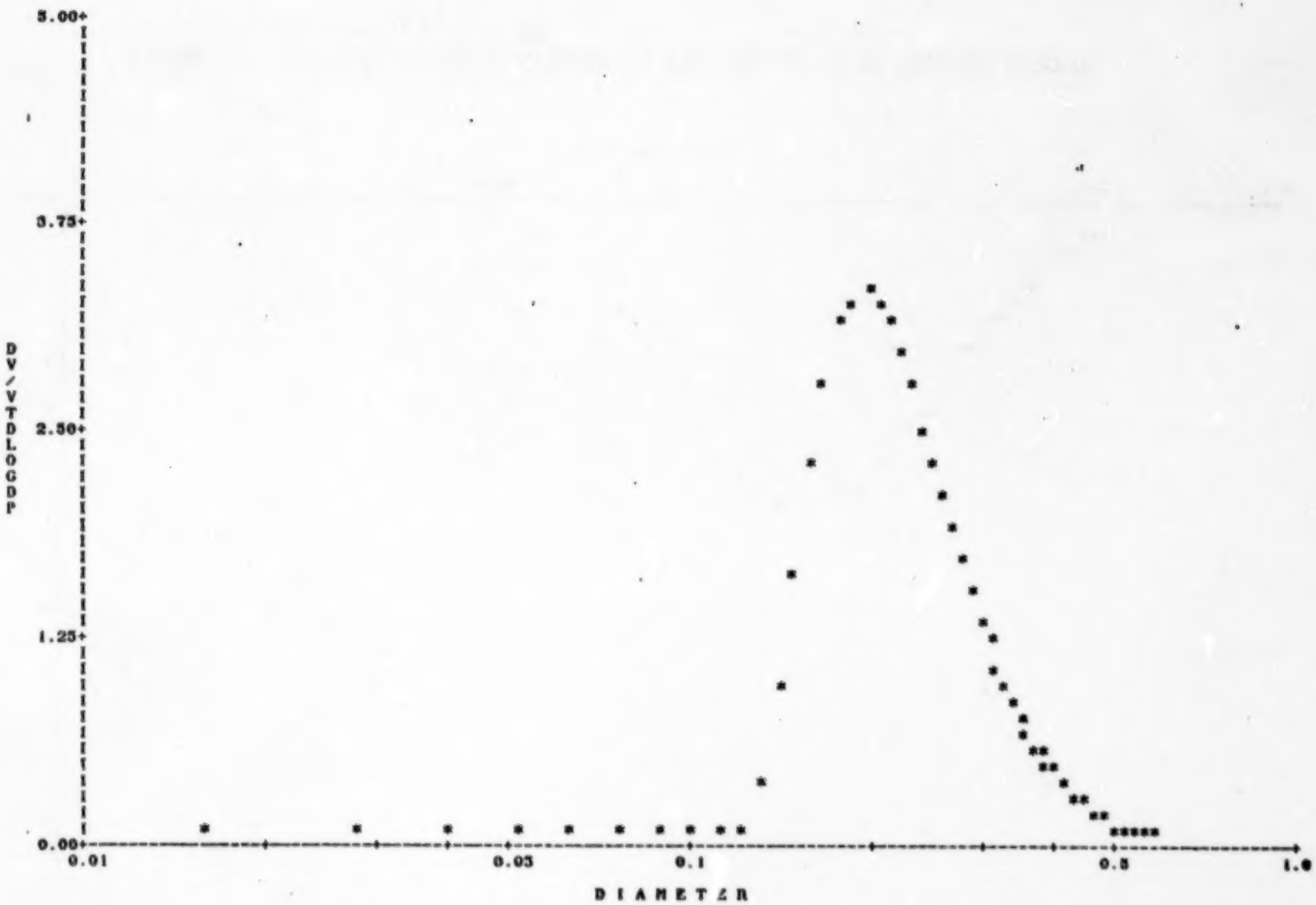

FIGURE 5b. VOLUME DISTRIBUTION AFTER THREE HOURS FOR CASE WITH NO PRIMARY AEROSOL AND $n(0.01) = 10^4$

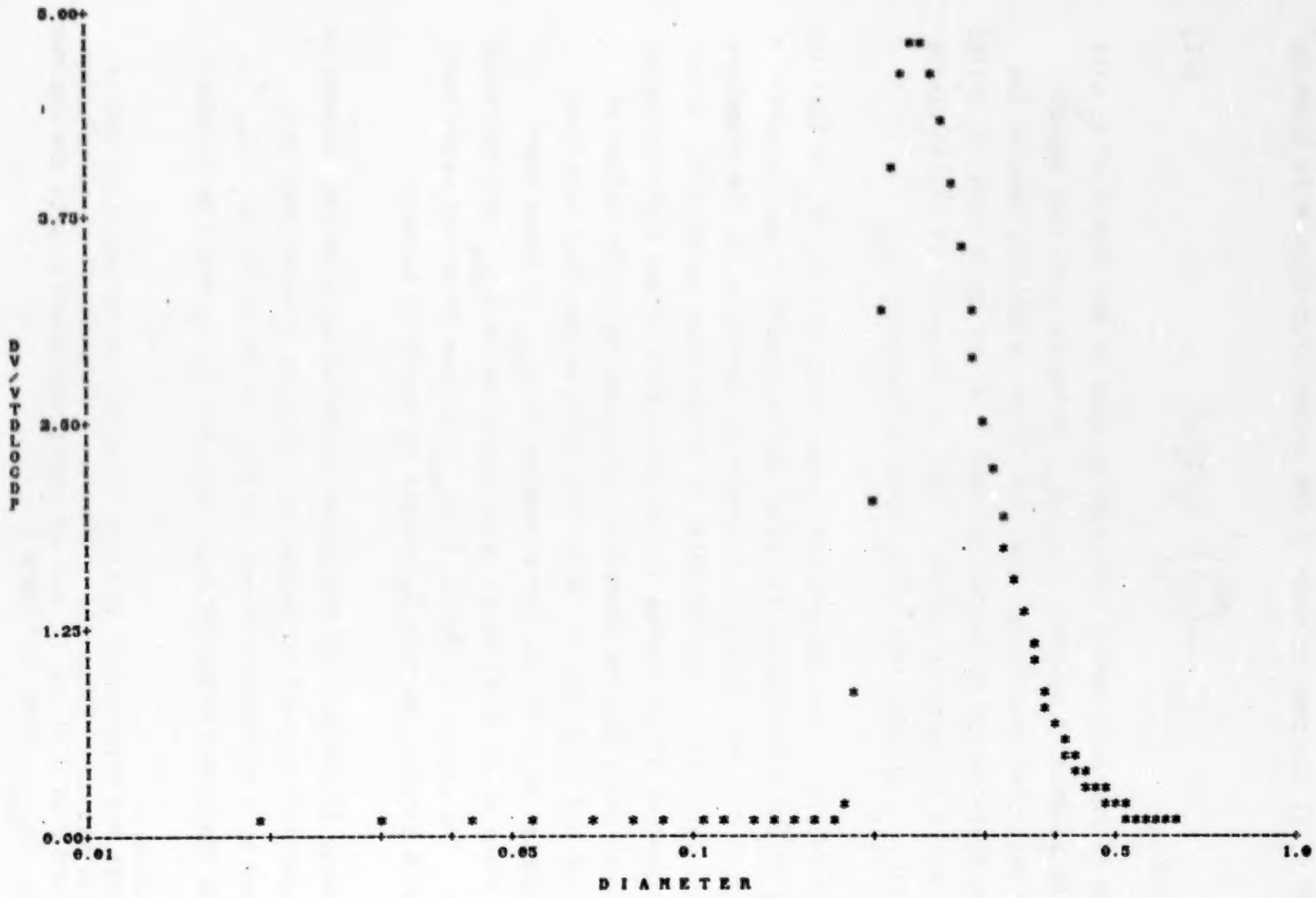

FIGURE 5c. VOLUME DISTRIBUTION AFTER SEVEN HOURS FOR CASE WITH NO PRIMARY AEROSOL AND $n(0.01) = 10^4$

The value of D_p at the peak or mode in the volume distribution is given by[†]

$$D_p^* = -4\left(\frac{\partial \bar{n}_0}{\partial D_p}\right)^{-1} \bar{n}_0(D_p^*,t) \quad . \tag{72}$$

The location of the peak varies with time because of the change of $\bar{n}_0$ with time. In the absence of sources, $|\partial\bar{n}_0/\partial D_p|$ increases with time because the smaller particles grow faster than the larger particles, causing the initial size distribution to become narrower. On the other hand, $\bar{n}_0$ shifts to larger sizes with particle growth. Thus, the behavior of $\partial\bar{n}_0/\partial D_p$ tends to decrease $D_{p_{max}}$, whereas that of $\bar{n}_0$ tends to increase $D_{p_{max}}$.

The net result of the changes that occur in $\bar{n}_0$ and $d\bar{n}_0/dD_p$ is that the peak in the volume distribution increases during growth by gas-to-particle conversion, but does not generally increase as rapidly as do the diameters of individual particles. This behavior is illustrated in Table 10, which lists the diameters of the maxima in the calculated volume distribution at three and seven hours and the diameters corresponding to the values of $D_{p_{max}}$ at three and seven hours. From this table we see that particles having a diameter of 0.192 μm, corresponding to $D_{p_{max}}$ at three hours, grow to a diameter of 0.245 μm at seven hours, while $D_{p_{max}}$ only increases to 0.227 μm. The change in $d\bar{n}_0/dD_p$ at $D_{p_{max}}$ between three and seven hours is less than 4 percent, whereas $\bar{n}_0$ changes by nearly 50 percent.

The change of the peak of the volume distribution with time depends on the gas-to-particle conversion mechanism. Here, we assumed that this growth occurs by a diffusion-limited process, for which $dD_p/dt \sim (D_p)^{-1}$. For a volume reaction-limited process, $dD_p/dt \sim D_p$, $\bar{n}_0$ would be expected

---

[†] D_p^* represents the theoretical diameter at which the volume distribution achieves its maximum. Since the resolution of the numerical calculation is on the order of 0.01 μm, D_p^* may not correspond exactly with the maximum value of $\bar{D}_p$, $D_{p_{max}}$, shown in Figure 5.

TABLE 10. THE GROWTH OF PARTICLES ASSOCIATED WITH $D_{p_{max}}$

Diameter (μm)	Time (hours)	$\bar{n}_0(cm^{-3}\mu m^{-1})$	$\frac{d\bar{n}_0}{dD_p}(cm^{-3}\mu m^{-2})$
0.173	3	2.82×10^5	-4.00×10^6
0.227 ($D_{p_{max}}$)	7	2.96×10^5	-4.41×10^6
0.192 ($D_{p_{max}}$)	3	1.99×10^5	-4.26×10^6
0.245	7	2.09×10^5	-4.70×10^6

to broaden with time. As a result, $\partial\bar{n}_0/\partial D_p$ would be expected to decrease with time, leading to a faster increase in the peak of the volume distribution than in the maximum of the $\bar{n}_0$ distribution.

The rapid rate at which the volume distribution increases at $D_{p_{max}}$ can be attributed to its sensitivity to $\bar{n}_0(D_{p_{max}},t)$. From Eqs. (70) and (72), we note that at $D_{p_{max}}$,

$$\frac{dV}{V_T d\log D_p} \sim \bar{n}_0\left(D_{p_{max}},t\right)^5 \quad . \tag{73}$$

Because of this dependence on $\bar{n}_0$, small variations in $\bar{n}_0$ such as those resulting from coagulation, for example, can have a large effect on the value of the volume distribution at the peak.

b. Case (2)

The effect on the volume distribution of changing the boundary condition at D_p = 0.01 μm from Case (1) to Case (2) is illustrated in Figures 6a and 6b. Because coagulation is not explicitly accounted for in the simulation, the larger source of 0.01 μm particles, as compared to Case (1), gives rise to an additional peak in the volume distribution. The discontinuity in the volume distribution resulting from this flux of particles at

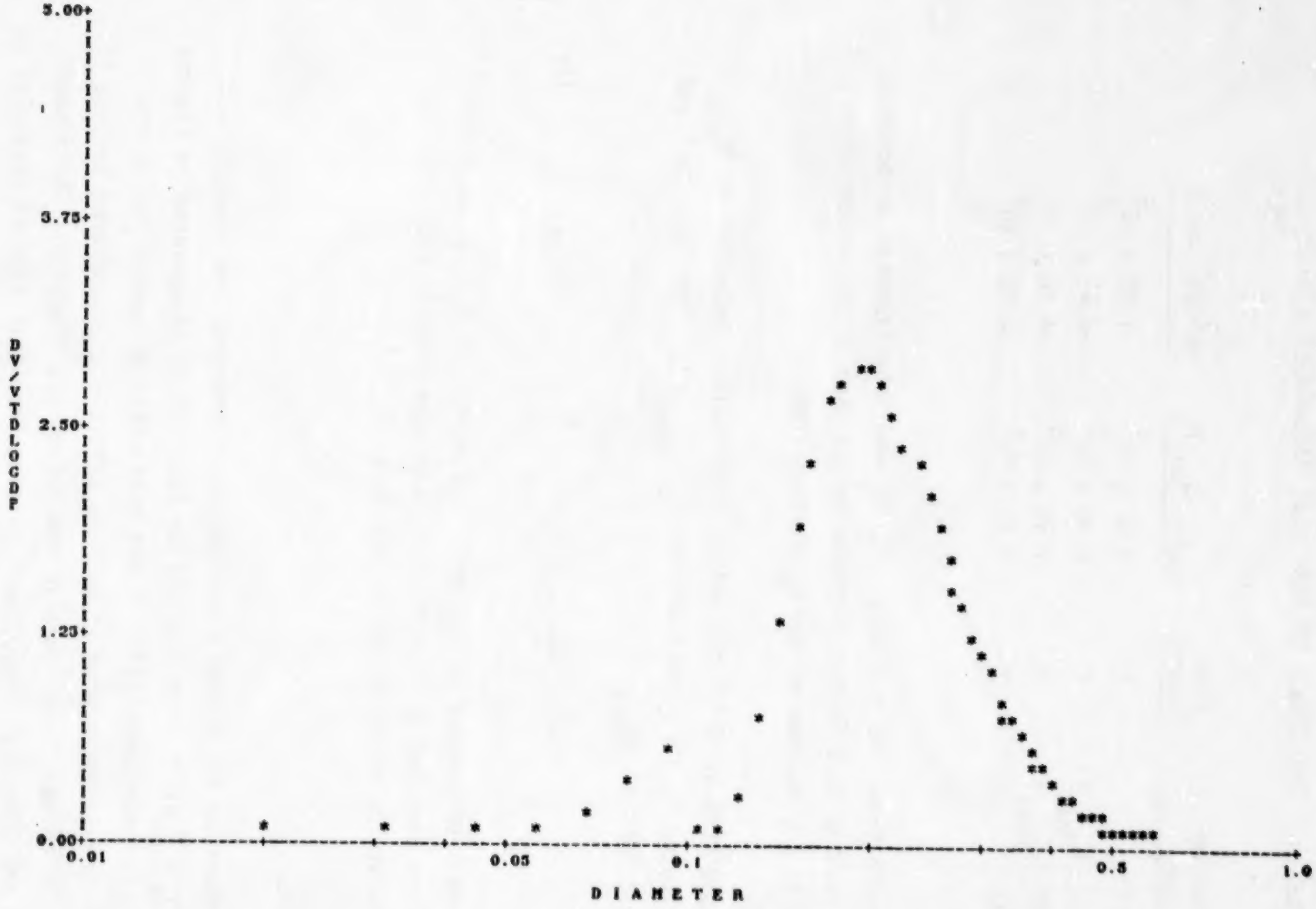

FIGURE 6a. VOLUME DISTRIBUTION AFTER THREE HOURS FOR CASE WITH NO PRIMARY AEROSOL AND n(0.01) = 600/I(0.01)

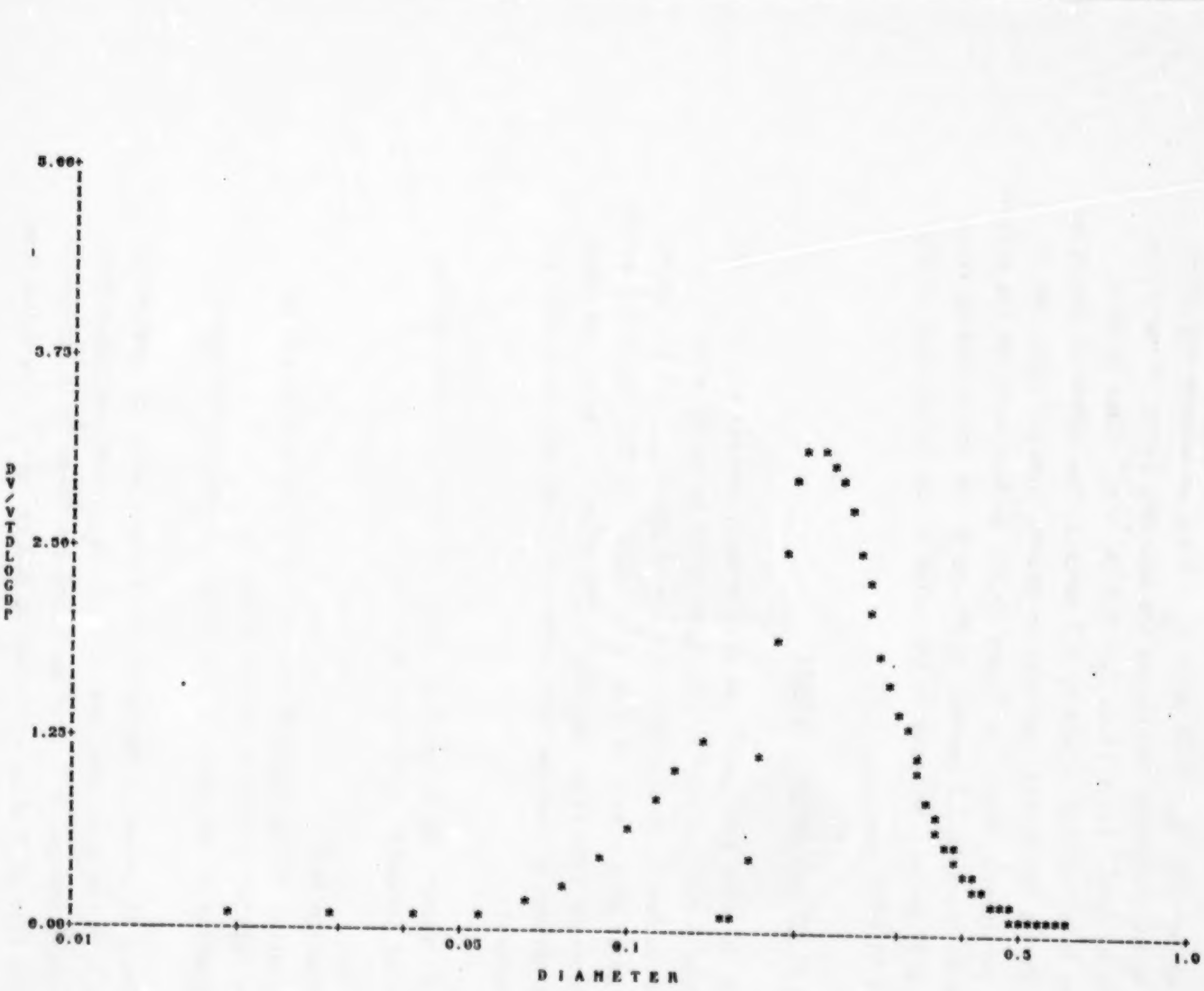

FIGURE 6b. VOLUME DISTRIBUTION AFTER SEVEN HOURS FOR CASE WITH NO PRIMARY AEROSOL AND n(0.01) = 600/I(0.01)

0.01 μm propagates from D_p = 0.09 μm to D_p = 0.132 μm between the third and seventh hours. Although increasing the boundary influx of particles from $S_0 = 100\ cm^{-3}min^{-1}$ (Case 1) to $S_0 = 600\ cm^{-3}min^{-1}$ (Case 2) only increases the total aerosol volume by 0.7 percent, the number of particles is so large that a substantial quantity of gaseous species condenses on these small particles. Hence, in Figure 6b the maximum value of the distribution at seven hours is 3.2 whereas in Figure 5c the corresponding value is 4.8, for a 33 percent decrease in the value at the larger peak in the distribution in Case (2).

2. Effect of Primary Aerosol Sources

We next consider a batch system with primary aerosol sources. The initial volume for these studies was again taken to be 20 $\mu m^3 cm^{-3}$ with a distribution as in Eq. (50) with $\mu = -1.802$ and $\sigma = 0.5$. Again, volume was added at the rate of 0.42 $\mu m^3 cm^{-3} min^{-1}$ so that the total volume after a seven-hour simulation was nearly 200 $\mu m^3 cm^{-3}$. The volume added was divided between primary aerosol (with $\mu = -1.802$ and $\sigma = 0.362$) and secondary aerosol.

Table 11 summarizes the various cases considered in this section. Three types of parameter variations were made:

- Variation in S_0.
- Variation in the ratio of the rate of primary emissions to the rate of secondary aerosol formation.
- Variation in the shape of the primary aerosol distribution.

Run 1 in Table 11 served as the base case against which to compare the other runs. In the base case, one half of the aerosol was added from primary sources and one half from secondary gas-to-particle conversion. The particle flux at 0.01 μm was taken as 600 $cm^{-3}min^{-1}$, the value from

TABLE 11. SIMULATIONS IN A BATCH SYSTEM

Run No.	Percent Primary	Percent Secondary	$S_0(t)$	σ^*	μ^*	Comment
1	50	50	600	0.362	-1.802	Base case
2	50	50	10	0.362	-1.802	Almost no particles at boundary
3	50	50	600,000	0.362	-1.802	Includes contribution from homogeneous nucleation
4	60	40	600	0.362	-1.802	
5	40	60	600	0.362	-1.802	
6	20	80	240	0.362	-1.802	$S_0(t)$ adjusted to correspond to percent primary
7	50	50	600	0.65	-1.802	Width of primary distribution increased
8	50	50	600	0.20	-1.802	Width of primary distribution decreased
9	50	50	600	0.362	-3.19	Mode of primary distribution shifted to the left
10	50	50	600	0.362	-1.11	Mode of primary distribution shifted to the right

---

[*] μ and σ are defined in Eq. (50).

the previous section corresponding to a typical urban flux. Figure 7 shows the normalized volume distribution after one, three, and seven hours of simulation. The initial distribution for this simulation corresponds to the distribution shown in Figure 5a. Because of the symmetric primary source distribution (on the coordinates used), the normalized volume distribution becomes increasingly symmetric as time progresses. We recall that in the absence of primary sources, the volume distribution becomes increasingly skewed to larger particle sizes. The volume distribution for the base case at seven hours is shown in Figure 7c. During the seven-hour period of the simulation the value of $D_{P_{max}}$ remains virtually constant.

Primary aerosol influenced the number and volume distributions directly by adding particles and aerosol volume to the aerosol already present. The rate of particle growth depends on the number of particles added from primary sources as well as the size distribution of the primary aerosol. In many of the simulations, it was found that, to a good approximation, the rate of growth of particles depended only on the total number density,

$$N(t) = \int_0^\infty \bar{n}_0(D_p,t)\, dD_p \quad , \tag{74}$$

and not on the detailed size distribution $\bar{n}_0(D_p,t)$. This is not immediately obvious from the form of the growth law, Eq. (41). The normalizing integral in Eq. (41) can be written as

$$\beta(t) = N(t)\left[\frac{\int_0^\infty \frac{2\pi D_p}{1 + \ell Kn}\bar{n}_0(D_p,t)\, dD_p}{N(t)}\right] \quad . \tag{75}$$

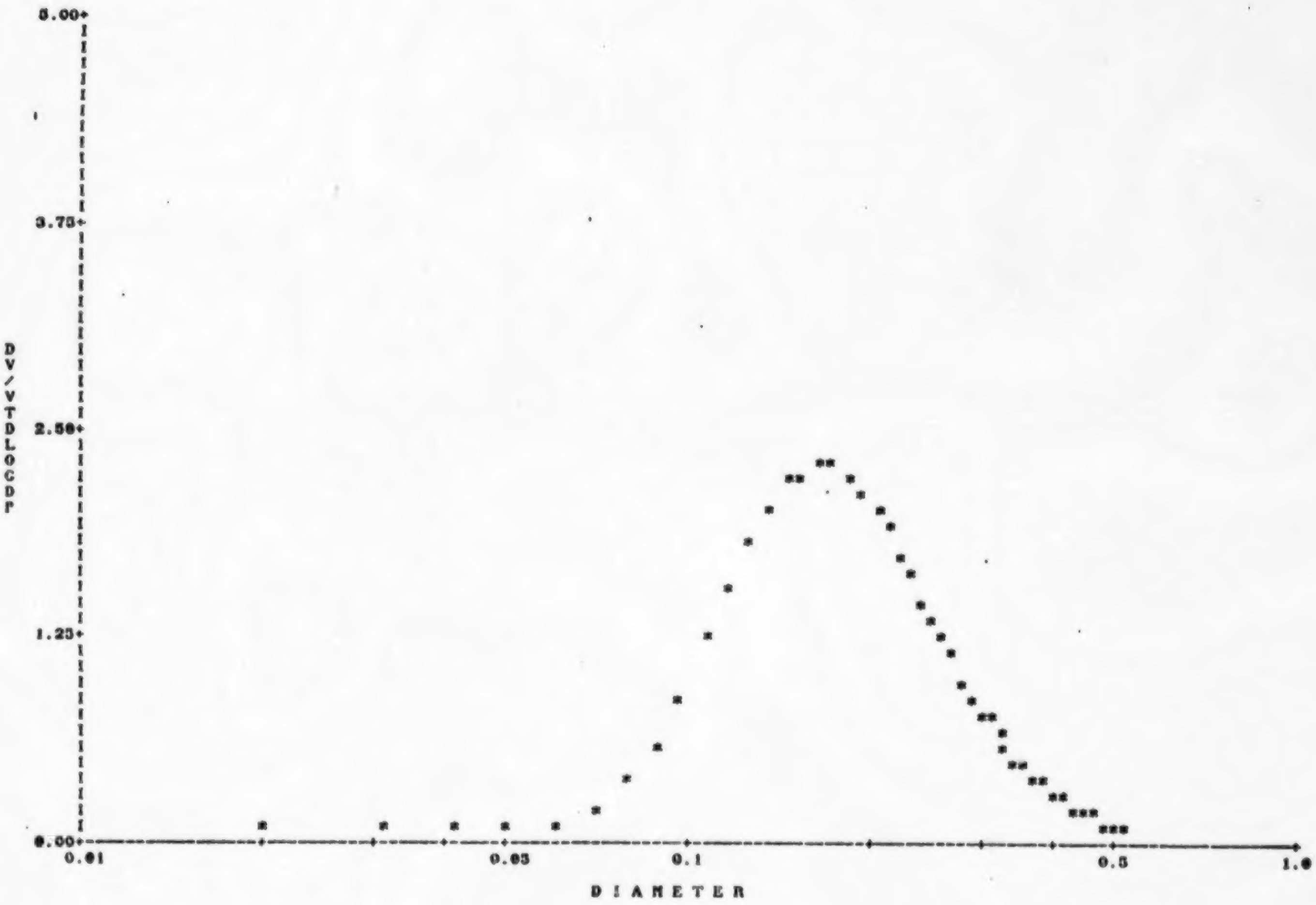

FIGURE 7a. THE VOLUME DISTRIBUTION AFTER ONE HOUR OF SIMULATION IN RUN 1

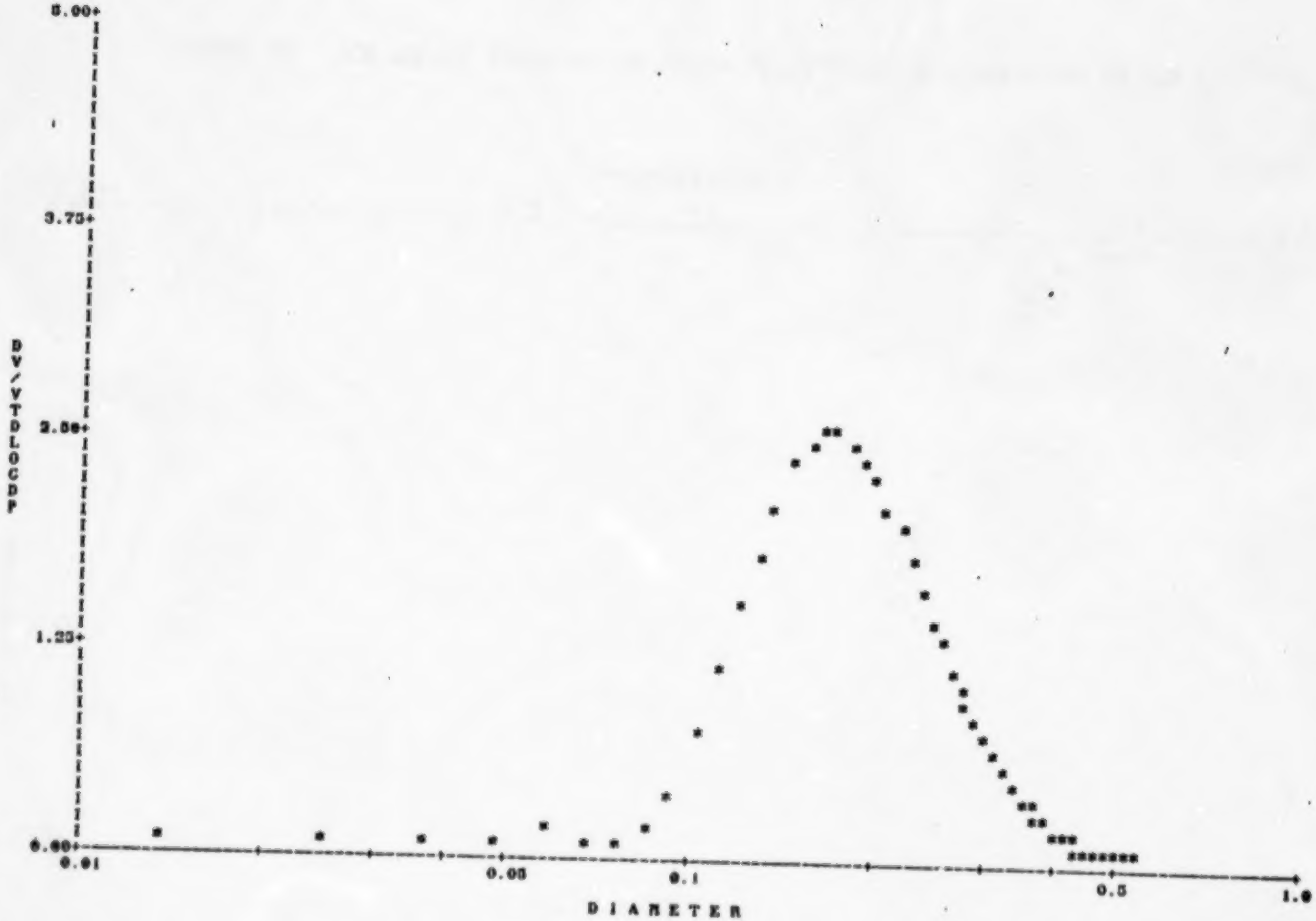

FIGURE 7b. THE VOLUME DISTRIBUTION AFTER THREE HOURS OF SIMULATION IN RUN 1

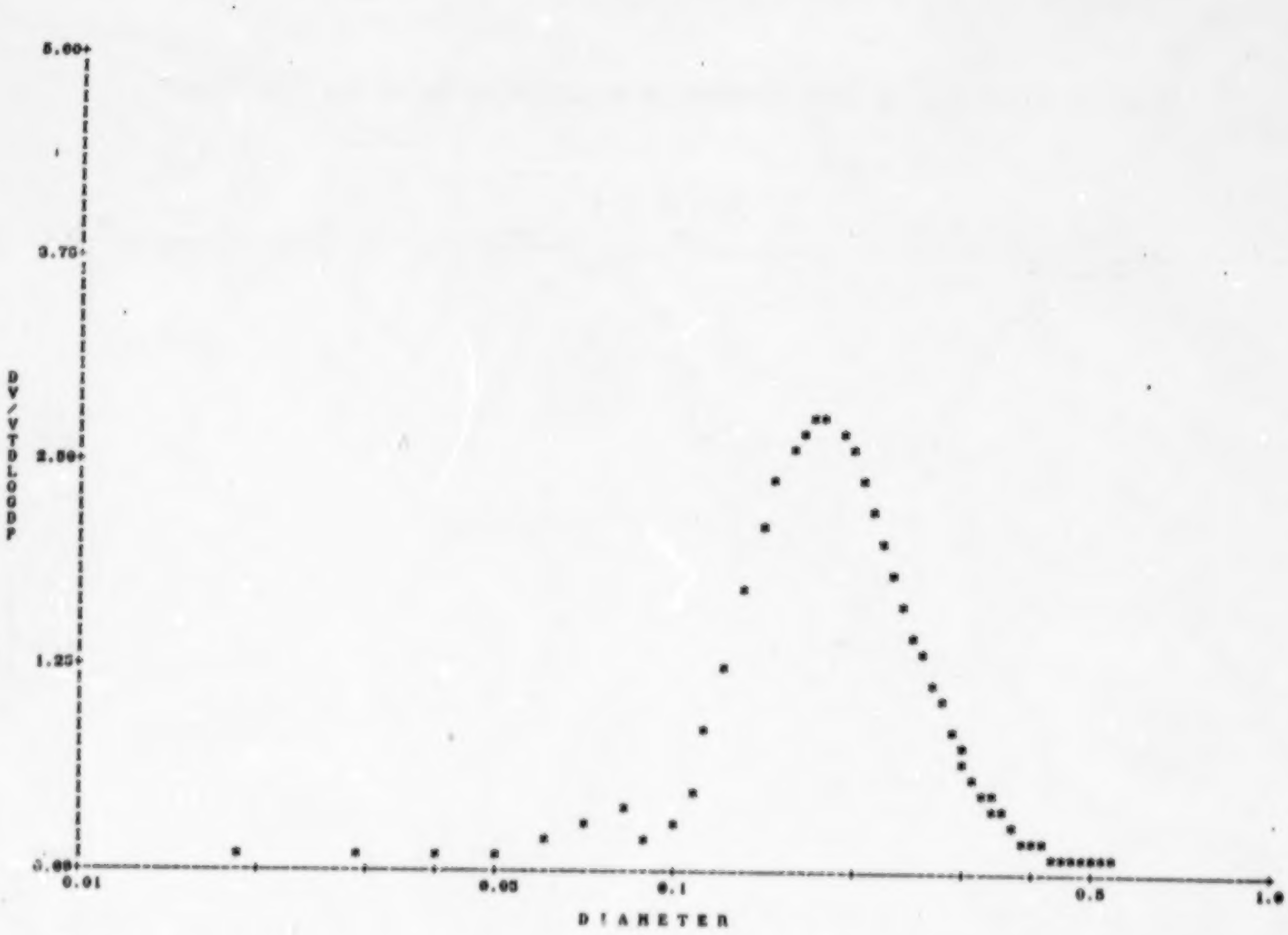

FIGURE 7c. THE VOLUME DISTRIBUTION AFTER SEVEN HOURS OF SIMULATION IN RUN 1

Let us consider the conditions under which the term in brackets might remain constant. From Eq. (24), we note that

$$\ell \mathrm{Kn} = \frac{1.333\mathrm{Kn} + 0.71}{1 + \mathrm{Kn}^{-1}} \quad . \tag{76}$$

A typical value of λ at 300°K and atmospheric pressure is 0.066 μm. Hence, over the particle diameter range 0.01 to 0.5 μm, Kn ranges from 13 to 0.26. When Kn >> 1, ℓKn can be approximated by 1.333 Kn, and we obtain the approximate relation

$$\beta(t)N(t)^{-1} \cong 2\pi(2.666N\lambda)^{-1} \int_0^\infty D_p^2 \bar{n}_0(D_p,t)\, dD_p \quad . \tag{77}$$

The approximate surface area mean diameter of the aerosol is obtained directly from Eq. (77) as

$$(\overline{D_p^2})^{\frac{1}{2}} \cong \left[\frac{2.666\lambda\beta(t)}{2\pi N(t)}\right]^{\frac{1}{2}} \quad . \tag{78}$$

Table 12 shows the approximate surface area mean diameters calculated from Eq. (78) for six seven-hour simulations. With the exception of Run 3 and the simulations discussed previously in which $\bar{n}_0(0.01,t) = 100\ \mathrm{cm}^{-3}\mathrm{min}^{-1}$, the surface area mean diameter is, to a good approximation, constant for all times. Consequently, the rate of particle growth is inversely proportional to N(t). The principal difference between Run 3 and the others in Table 12 is in the magnitude of the flux of 0.01 μm particles into the system. In the other four cases the magnitude of S_0 is such that the influx of 0.01 μm particles maintains the surface area mean diameter nearly constant despite an increase in surface area due to primary sources and gas-to-particle conversion.

TABLE 12. APPROXIMATE SURFACE MEAN DIAMETERS

Elapsed Time (hours)	$\left(D_p^2\right)^{1/2}$ (μm)					
	Run 1	Run 6	Run 9	Run 3	Sub 0.01 μm Particles Only	Growth Only
1	0.070	0.087	0.035	0.013	0.086	0.13
2	0.066	0.088	0.036	0.015	0.083	0.15
3	0.066	0.089	0.036	0.016	0.083	0.17
4	0.065	0.088	0.036	0.017	0.082	0.18
5	0.066	0.088	0.036	0.011	0.082	0.19
6	0.065	0.089	0.036	0.011	0.081	0.20
7	0.066	0.089	0.036	0.011	0.082	0.21

So far, we have focused primarily on the results of the simulation of the base case in Table 11. Runs 2 and 3 were designed to study the effect of the flux of 0.01 μm particles into the system when primary aerosol sources also exist. The base case value of $S_0 = 600\ \mathrm{cm}^{-3}\mathrm{min}^{-1}$ is typical of the rate at which lead particles of size 0.01 μm might be added to an air parcel from automobile exhaust. In Runs 2 and 3, S_0 was taken to be $10\ \mathrm{cm}^{-3}\mathrm{min}^{-1}$ and $6 \times 10^5\ \mathrm{cm}^{-3}\mathrm{min}^{-1}$, respectively. The latter value is typical of the rate of particle formation by homogeneous nucleation at high relative humidity when the existing aerosol number density is low (see Chapter III). (The value of $6 \times 10^5\ \mathrm{cm}^{-3}\mathrm{min}^{-1}$ for S_0 represents an extreme upper limit to the particle flux at 0.01 μm because coagulation has been neglected and ambient number densities are generally high.) For comparison of the overall impact of the three boundary conditions, $S_0 = 10$, 600, and $6 \times 10^5\ \mathrm{cm}^{-3}\mathrm{min}^{-1}$, after seven hours, the total number density and aerosol volume in the three runs are listed below:

Run No.	$S_0(\mathrm{cm}^{-3}\mathrm{min}^{-1})$	$N(\mathrm{cm}^{-3})$	$V(\mu\mathrm{m}^3\mathrm{cm}^{-3})$
1	600	3.7×10^5	197.8
2	10	9.8×10^4	197.6
3	6×10^5	3.2×10^9	353.5

Despite the small change in V that occurs when S_0 is changed from 600 $\mathrm{cm}^{-3}\mathrm{min}^{-1}$ to 10 $\mathrm{cm}^{-3}\mathrm{min}^{-1}$, there is a noticeable change in the volume distribution between the two cases. Figure 8 shows the volume distribution at seven hours for Runs 1 and 2. Note the small shift of the peak to a larger diameter and about a 15 percent increase in the maximum value from Run 1 to Run 2. The increase in the fraction of the total volume in the accumulation range in Run 2 is a consequence of reduced loss of gaseous species to the small particles. Thus, the influx of small particles, while not influencing the total volume substantially, can influence the rate of growth of larger particles through the surface area they provide. (We note again that coagulation was neglected.)

As expected, both the number and volume distributions change substantially from those observed in the base case when S_0 is increased to 6×10^5 $\mathrm{cm}^{-3}\mathrm{min}^{-1}$. In these simulations the particles grow at a more rapid rate than would occur if the Kelvin effect was included. Furthermore, because of the high number density of these particles, coagulation must also be taken into account.

Runs 4 and 5 in Table 11 were designed to study the effect of varying the relative quantities of primary and secondary material. The rate of growth of a particle in the aerosol depends on the number of particles present. Hence, both increasing the rate of production of secondary aerosol and decreasing the number of particles in the aerosol have the effect of increasing the rate of growth of a particle. In Run 1 there is little change in the location of the peak of the volume distribution between zero and seven hours. As the ratio of primary to secondary aerosol

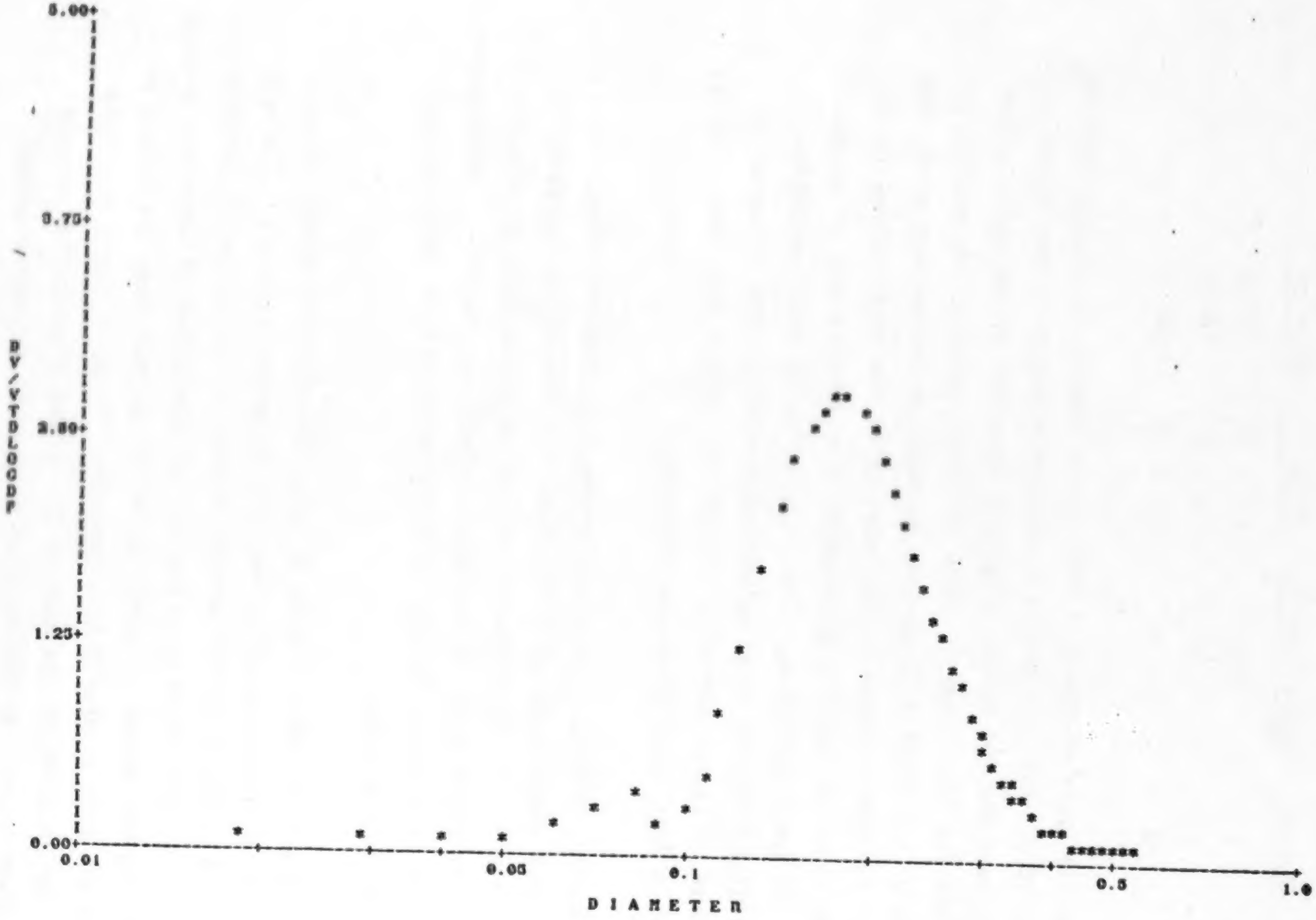

FIGURE 8a. THE VOLUME DISTRIBUTION AFTER SEVEN HOURS OF SIMULATION WITH $S_0 = 600\ cm^{-3}min^{-1}$

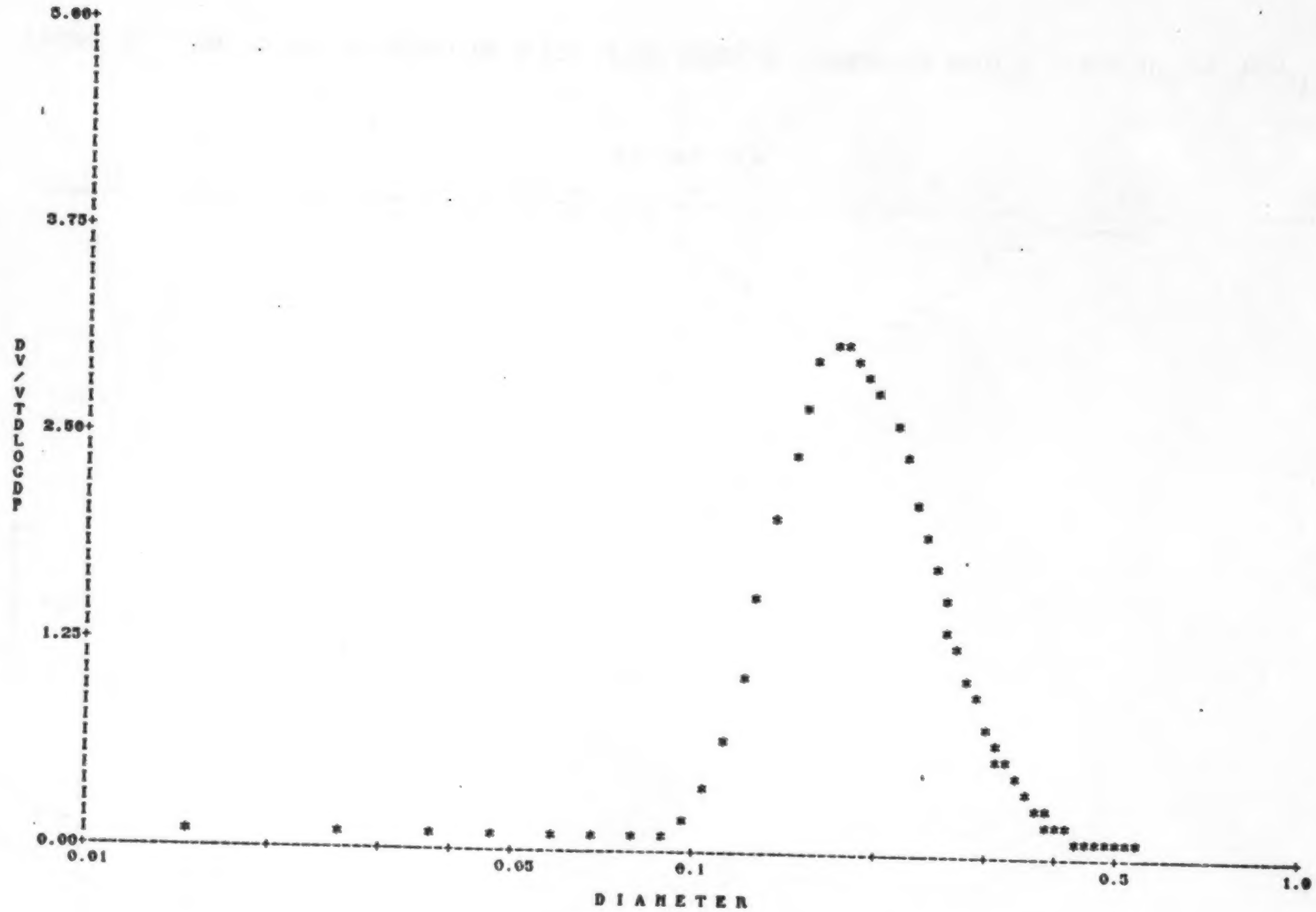

FIGURE 8b. THE VOLUME DISTRIBUTION AFTER SEVEN HOURS OF SIMULATION WITH $S_0 = 10\ cm^{-3}min^{-1}$

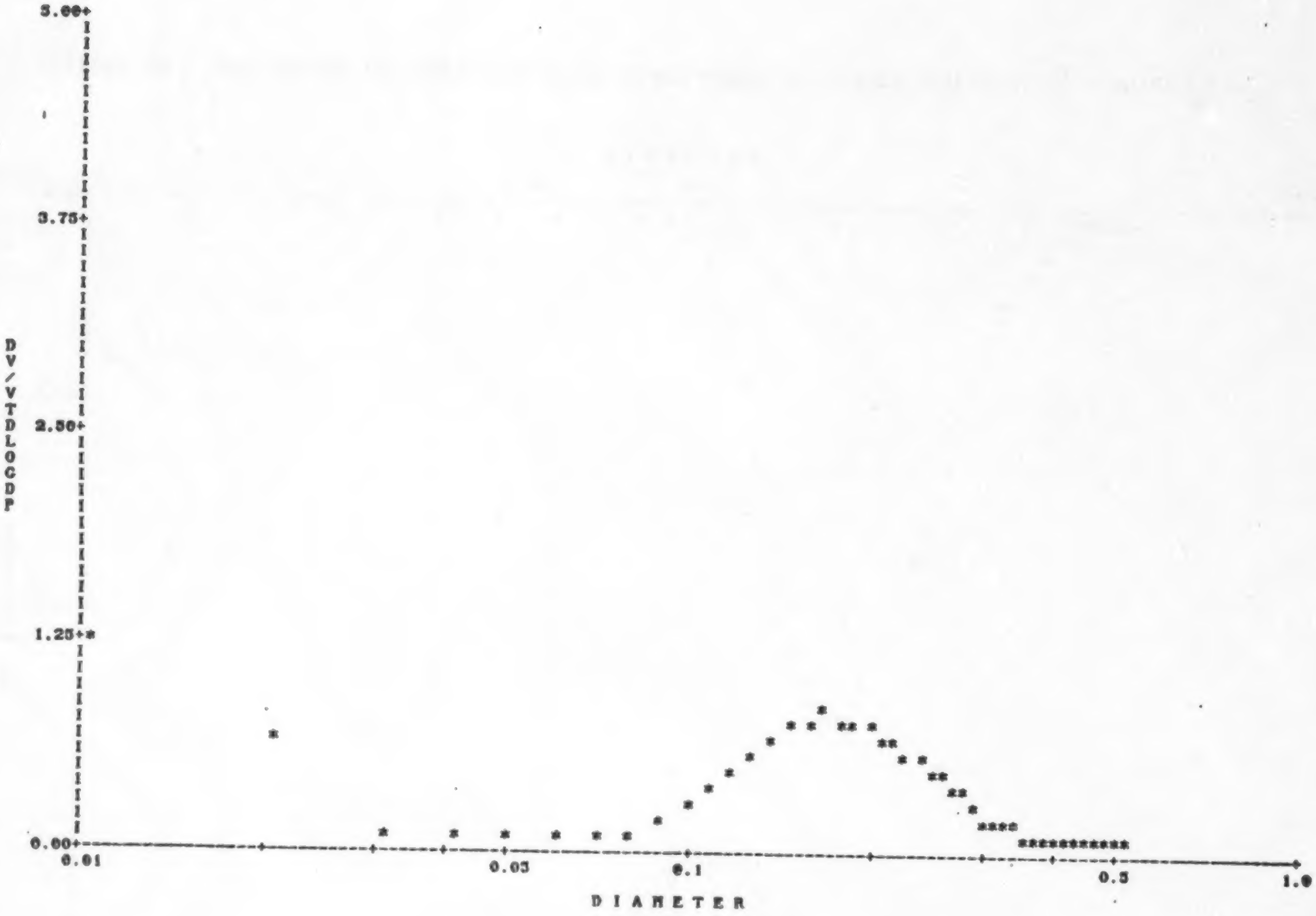

FIGURE 8c. THE VOLUME DISTRIBUTION AFTER SEVEN HOURS OF SIMULATION WITH $S_0 = 6 \times 10^5\ cm^{-3}min^{-1}$

decreases, the increase in the peak of the volume distribution should become more pronounced because of the increased rate of particle growth. The rates of growth of particles of diameter 0.01 μm and 0.16 μm in systems in which the volumes added are 20 and 60 percent primary are shown in Figure 9. In interpreting Figure 9 one should keep in mind that the systems also contain the background aerosol and the small particle source, which reduce the difference between the ratios of growth.

Figures 10a and 10b show the normalized volume distributions at seven hours for two simulations in which primary emissions were 20 percent and 60 percent of the mass added to the system. The peak of the distribution is at a larger particle size in the case in which more of the aerosol volume comes from secondary gas-to-particle conversion (0.19 μm as opposed to 0.165 μm). Furthermore, the peak of the distribution is sharper and is skewed in the system with fewer particles. This evolution of the size distribution is very similar to that observed in the absence of sources of primary particulates.

The remaining three simulations were designed to study the response of the system to changes in the primary source distribution. For this purpose the parameters μ and σ in Eq. (50) were varied as indicated in Table 11. The three normalized volume distributions used for the primary source distribution are shown in Figure 11. As noted above, in each of the three distributions in Figure 11 the total volume is conserved, but the number density is not. As a result, in Runs 6 through 8 the number density of particles after seven hours of simulation is $5.5 \times 10^5 cm^{-3}$, $3.5 \times 10^5 cm^{-3}$, and $4.8 \times 10^6 cm^{-3}$, respectively.

The time variations of several parameters characterizing the aerosol size distribution for Runs 1, 6, 7, and 8 are shown in Table 13. Figures 12 to 14 show the predicted volume distributions at one, three, and seven hours for Runs 6 to 8. Provided that the initial and source distributions

TABLE 13. VARIATIONS WITH TIME OF PARAMETERS CHARACTERIZING THE AEROSOL SIZE DISTRIBUTION

	Source	Simulation Time										
		1 Hour			4 Hours			7 Hours				
Run No.	$D_{p_{peak}}$	$D_{p_{max}}$	$G\left(D_{p_{max}}\right)^*$	$\left(\overline{D_p^{-2}}\right)^{1/2}$	$D_{p_{max}}$	$G\left(D_{p_{max}}\right)^*$	$\left(\overline{D_p^{-2}}\right)^{1/2}$	$D_{p_{max}}$	$G\left(D_{p_{max}}\right)^*$	$\left(\overline{D_p^{-2}}\right)^{1/2}$	N_T (cm^{-3})	V_T ($\mu m^3 cm^{-3}$)
1	0.17 μm	0.16 μm	2.3	0.070 μm	0.17 μm	2.7	0.065 μm	0.17 μm	2.8	0.066	3.7×10^5	198
6	0.17	0.16	1.9	0.062	0.15	1.9	0.059	0.15	1.9	0.060	5.5×10^5	195
7	0.17	0.17	3.0	0.070	0.18	3.8	0.066	0.19	4.0	0.065	3.5×10^5	198
8	0.041	0.047	1.4	0.035	0.048	2.3	0.035	0.052	2.5	0.036	4.8×10^6	198

---

* $G\left(D_{p_{max}}\right) = [dV/V_T d(\log D_p)]_{max}$

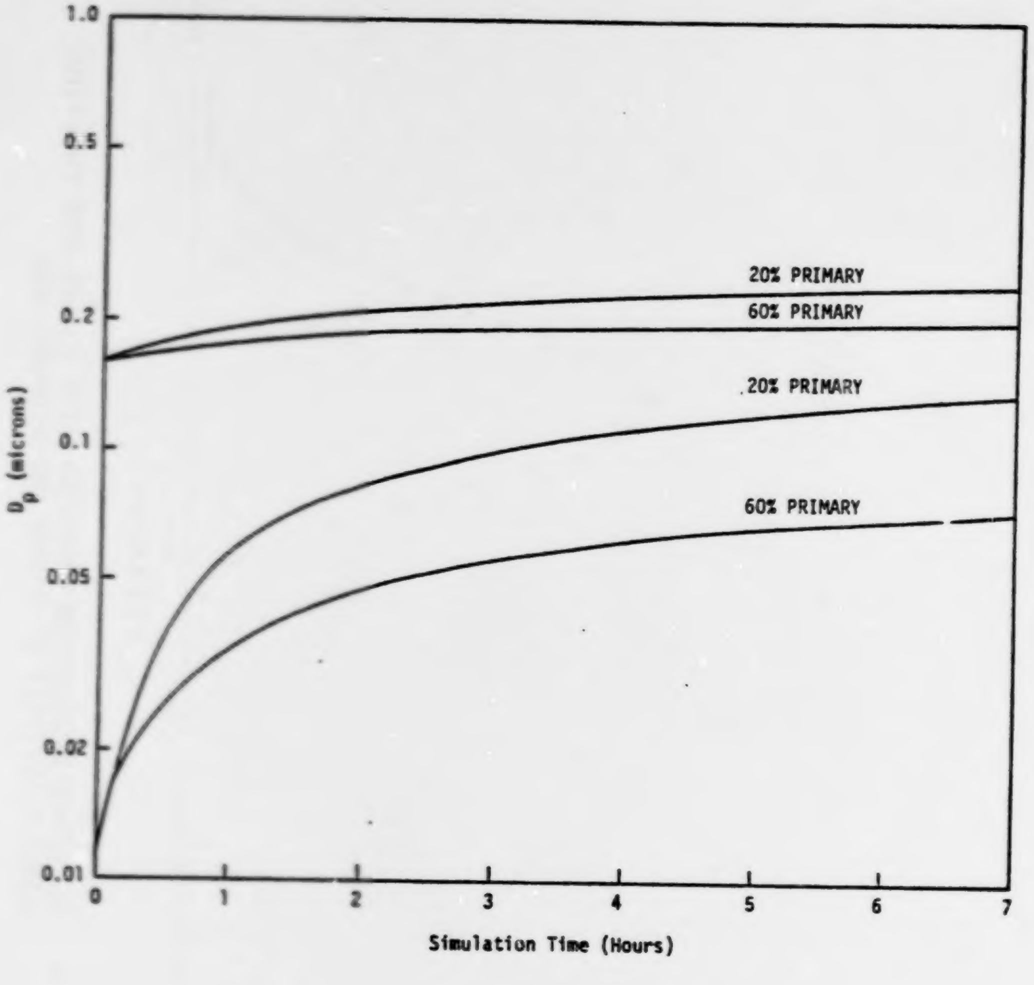

FIGURE 9. THE GROWTH OF PARTICLES IN THE BATCH SYSTEMS OF RUNS 4 AND 6

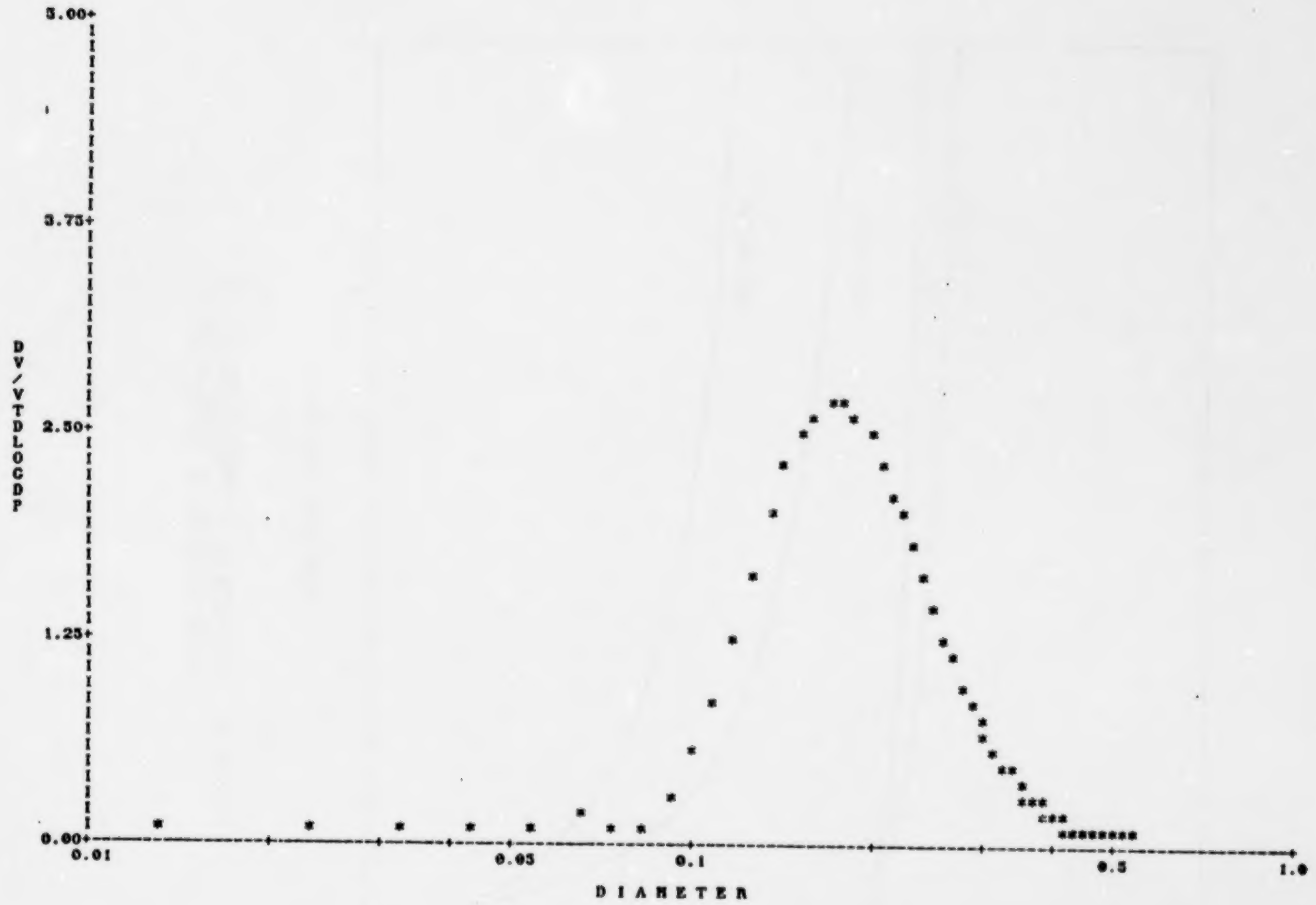

FIGURE 10a. THE VOLUME DISTRIBUTION PREDICTED AFTER A SEVEN-HOUR SIMULATION WITH A 60/40 SPLIT OF PRIMARY AND SECONDARY MASS

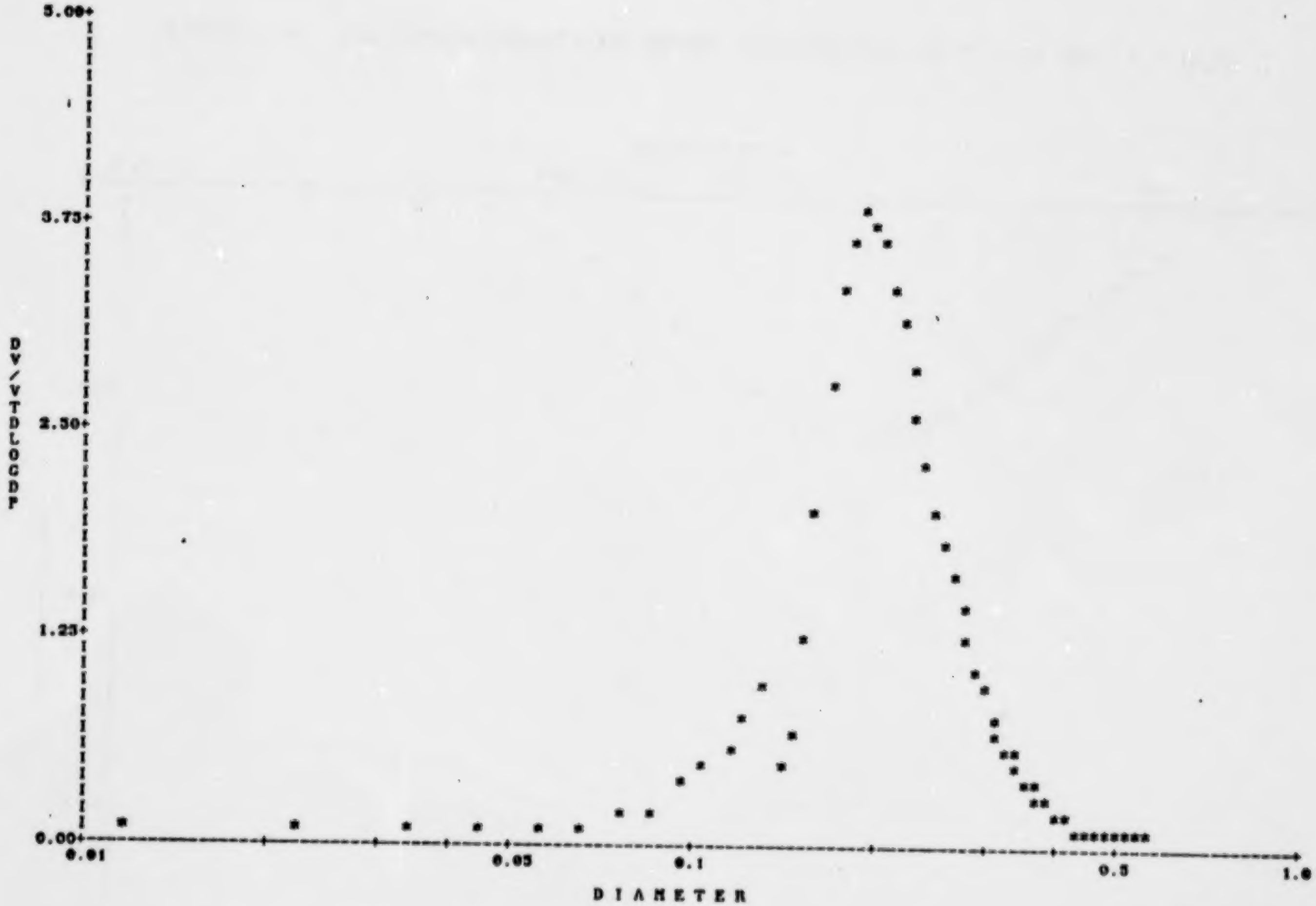

FIGURE 10b. THE VOLUME DISTRIBUTION PREDICTED AFTER A SEVEN-HOUR SIMULATION WITH A 20/80 SPLIT OF PRIMARY AND SECONDARY AEROSOL

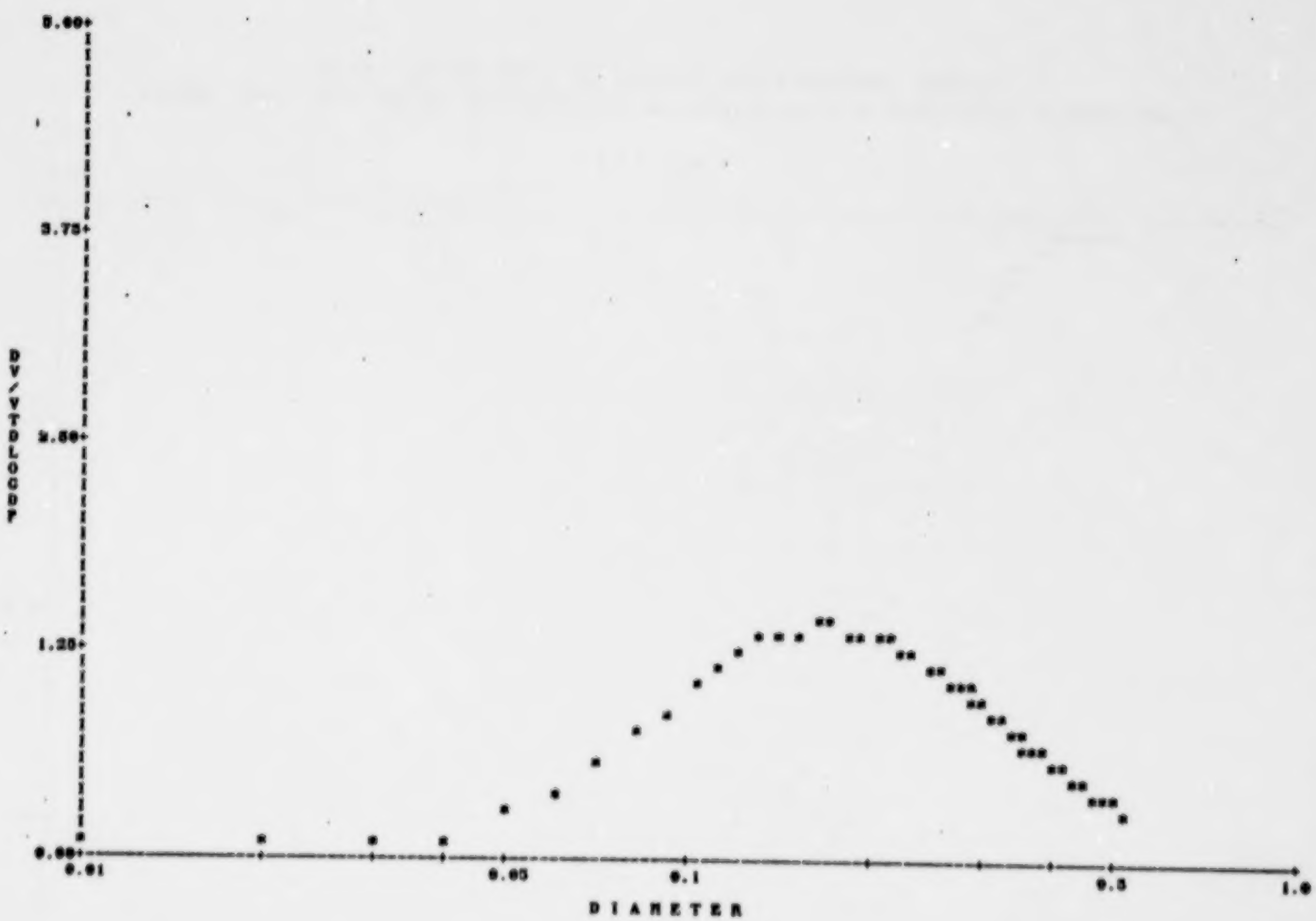

FIGURE 11a. THE SOURCE-NORMALIZED VOLUME DISTRIBUTION FOR $\mu = -1.802$, $\sigma = 0.65$

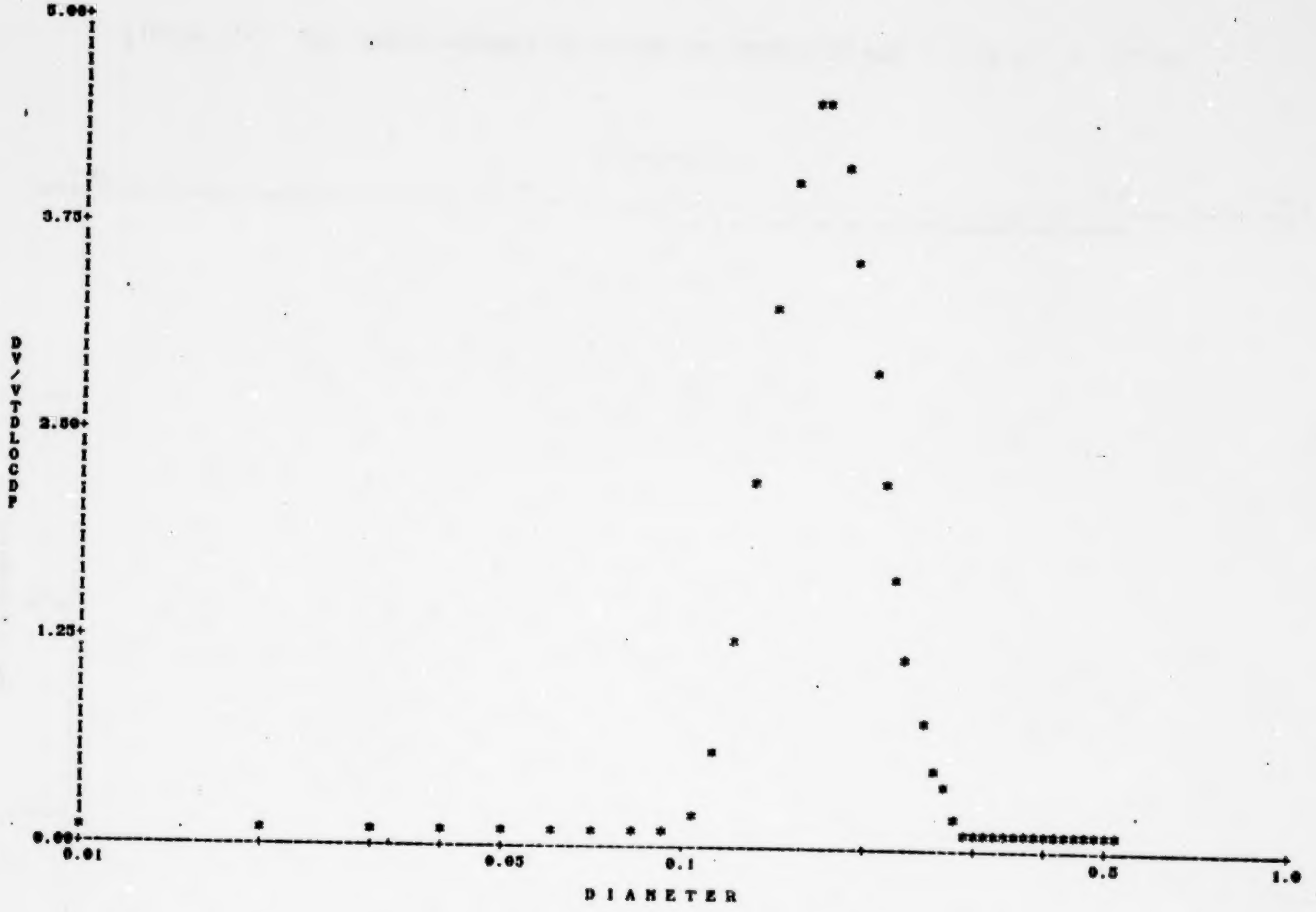

FIGURE 11b. THE SOURCE-NORMALIZED VOLUME DISTRIBUTION FOR μ = -1.802, σ = 0.20

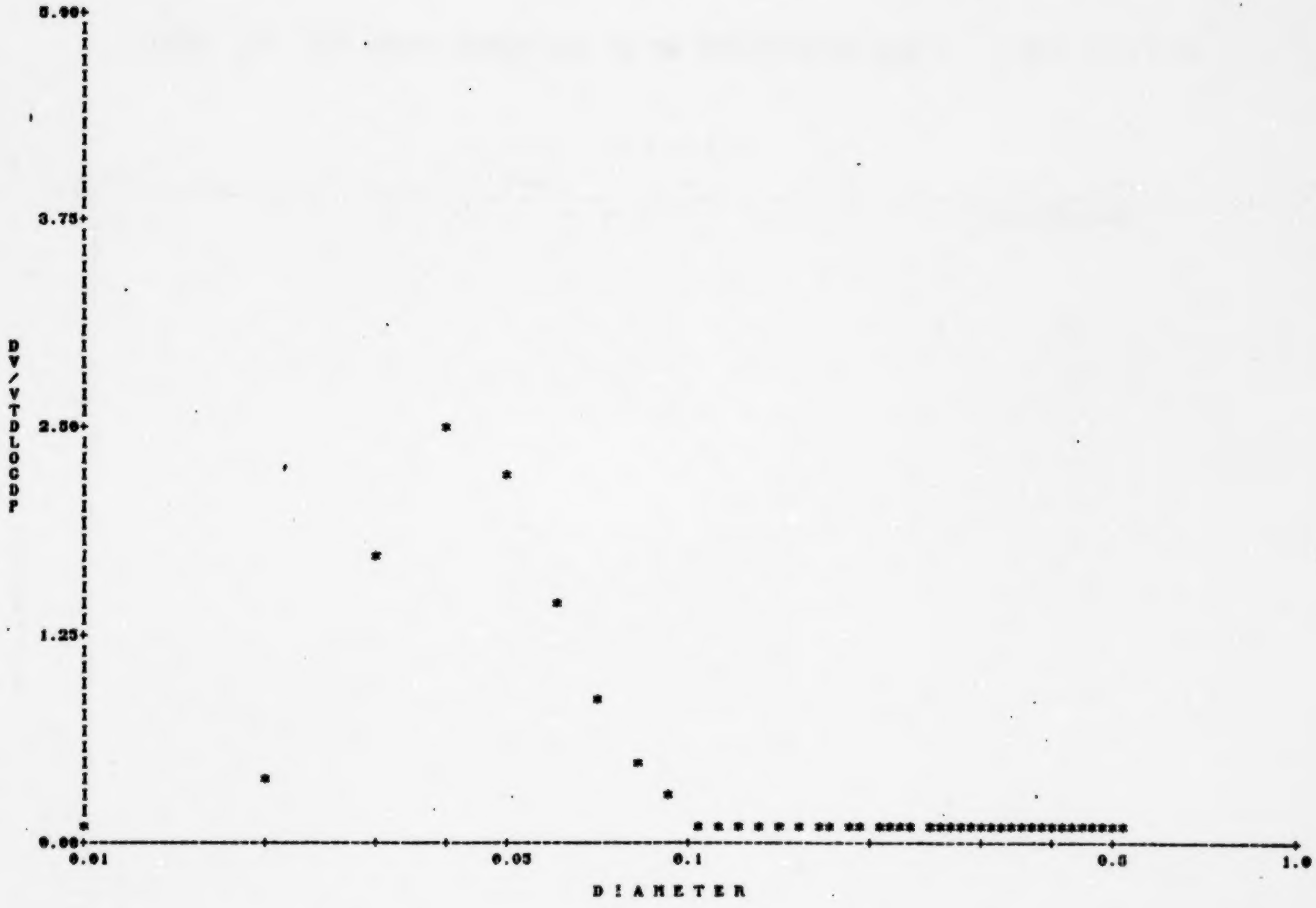

FIGURE 11c. THE SOURCE-NORMALIZED VOLUME DISTRIBUTION FOR μ = -3.19, σ = 0.362

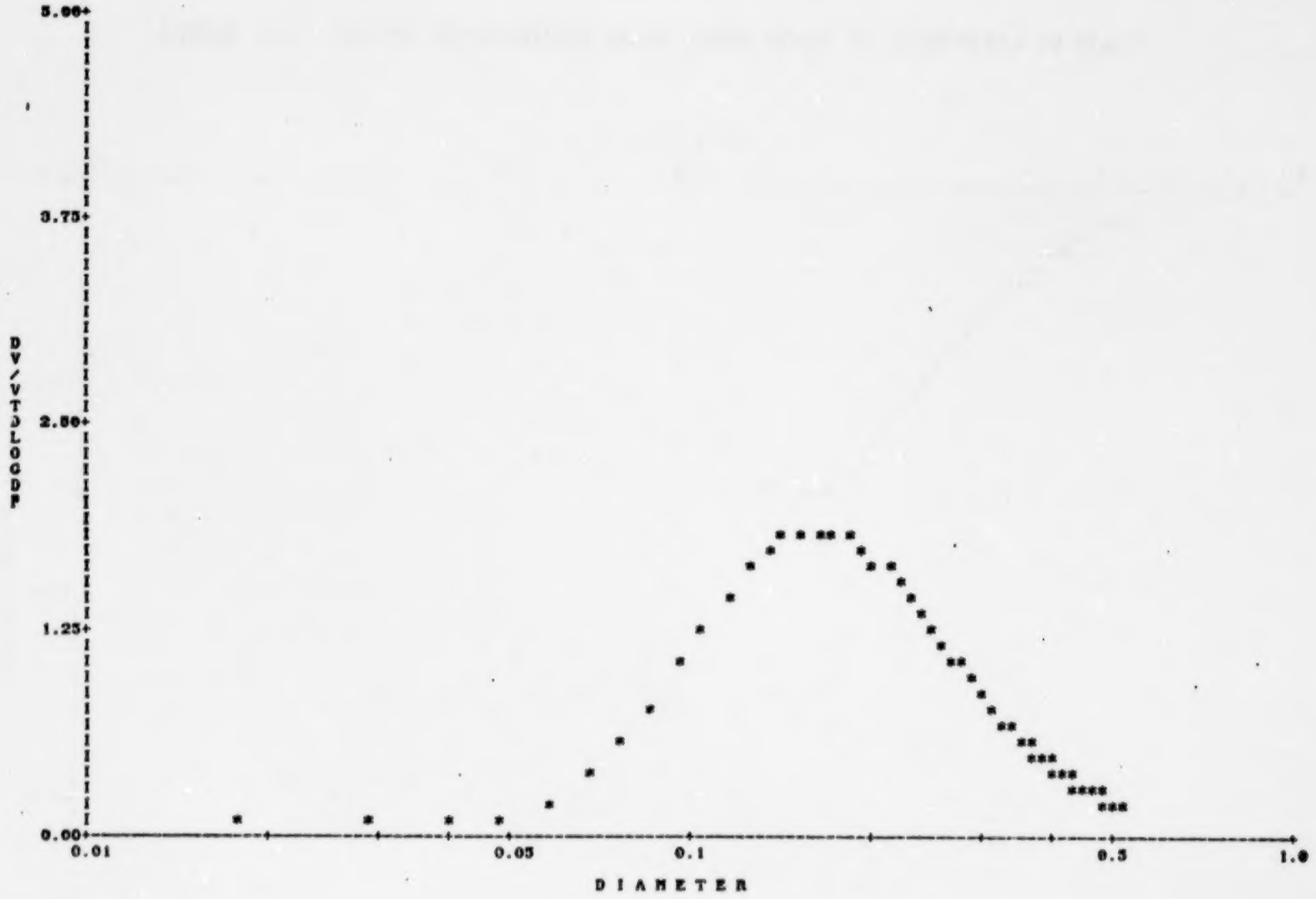

FIGURE 12a. VOLUME DISTRIBUTION AFTER ONE HOUR OF SIMULATION IN RUN 6

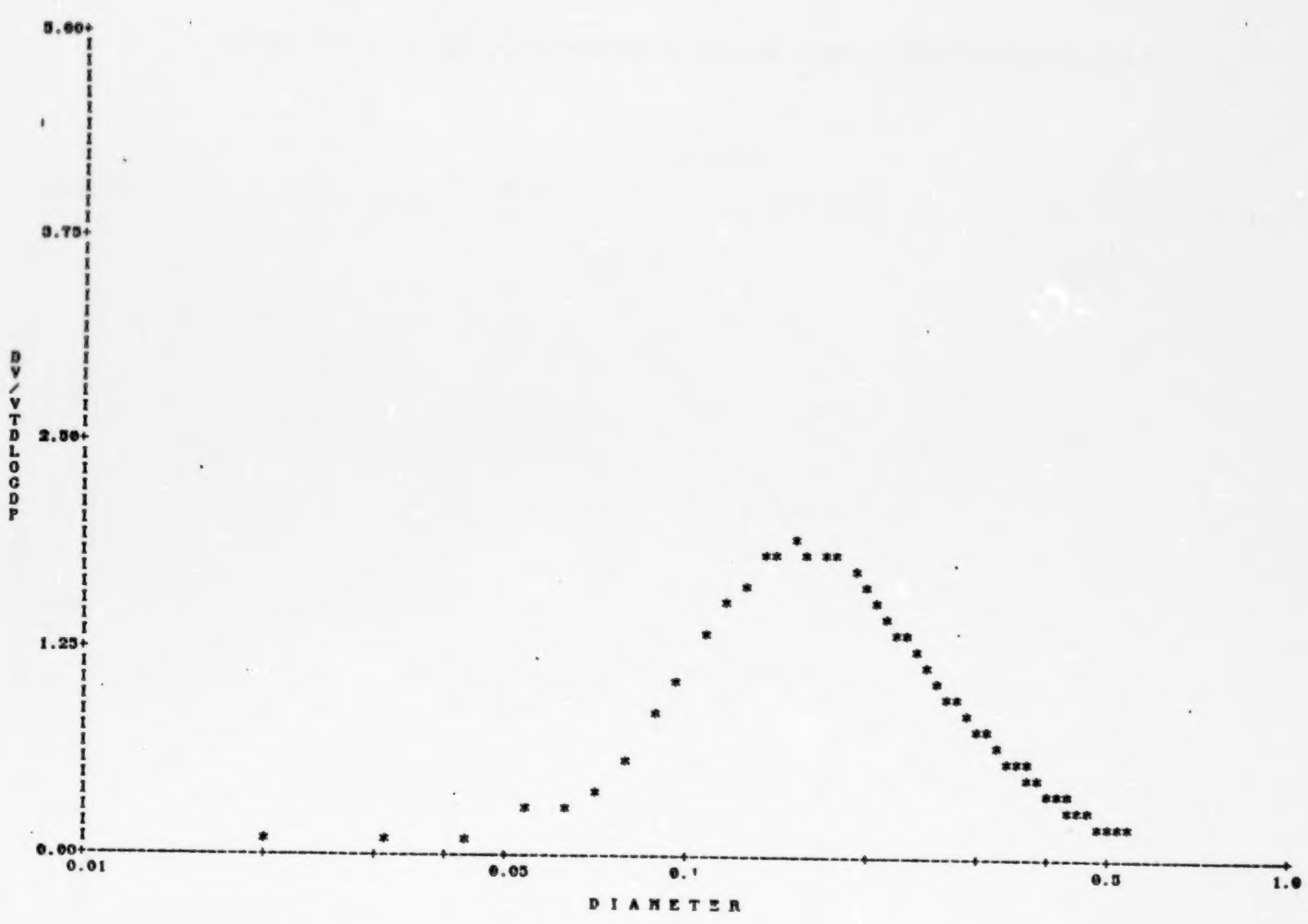

FIGURE 12b. VOLUME DISTRIBUTION AFTER THREE HOURS OF SIMULATION IN RUN 6

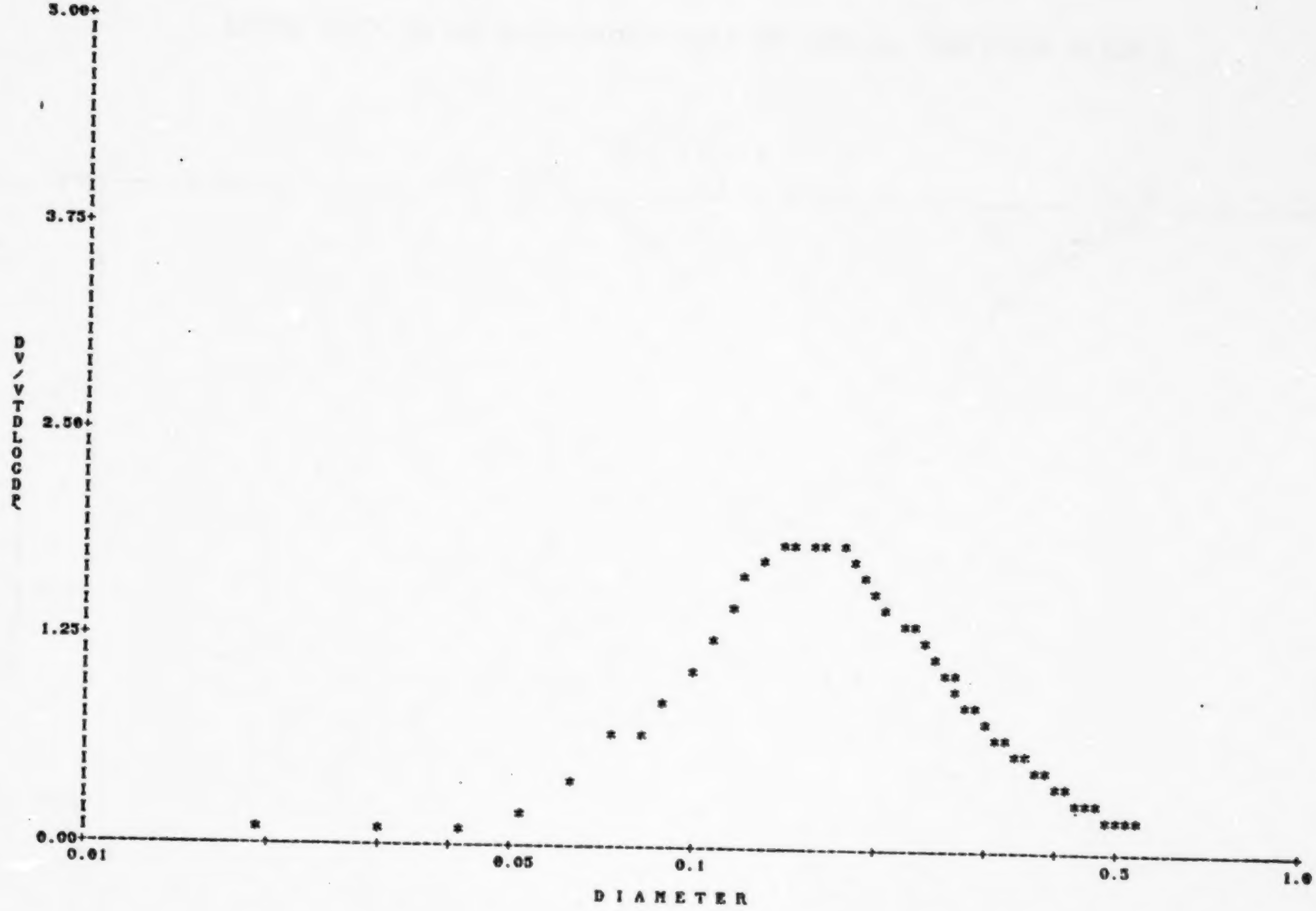

FIGURE 12c. VOLUME DISTRIBUTION AFTER SEVEN HOURS OF SIMULATION IN RUN 6

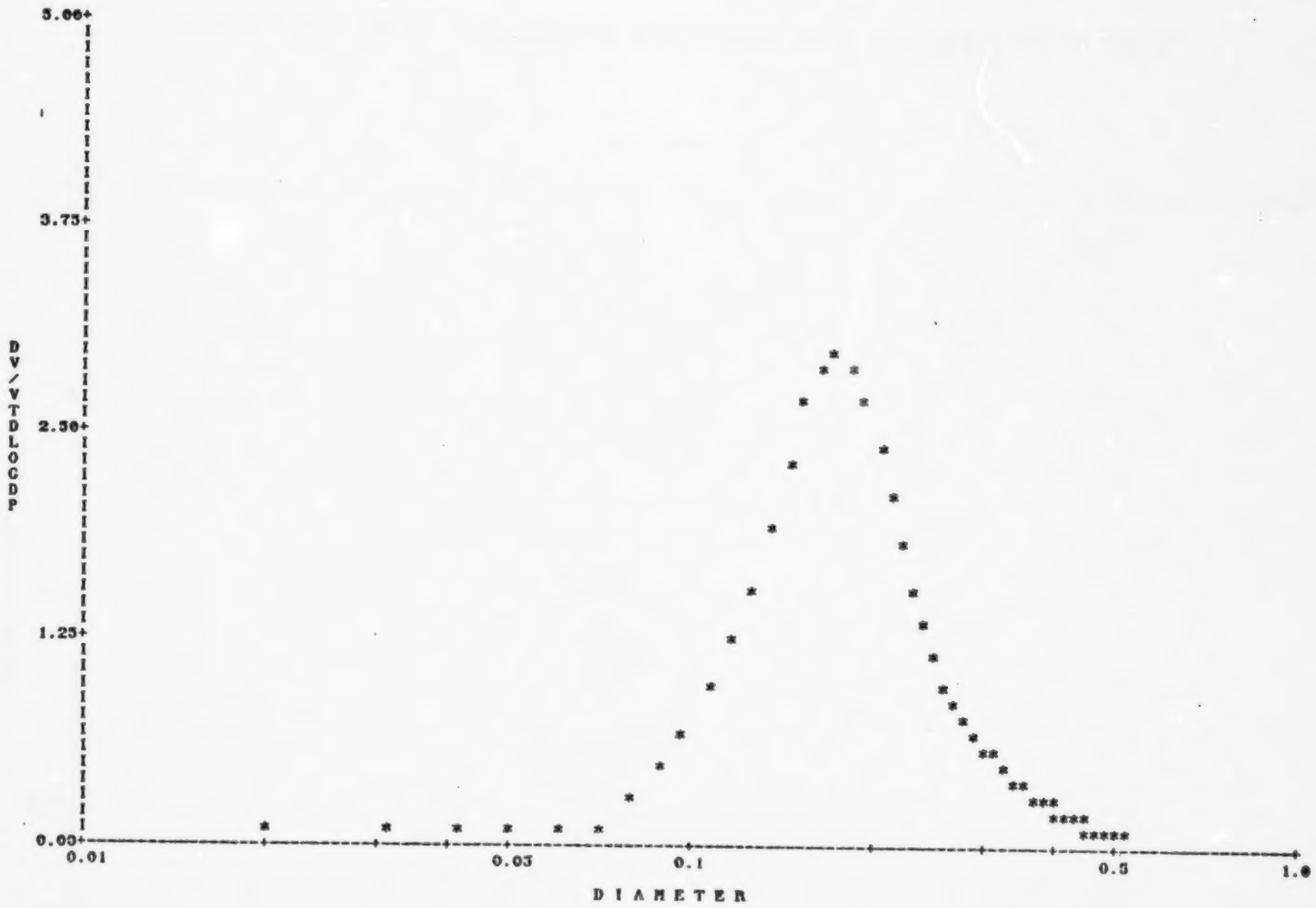

FIGURE 13a. VOLUME DISTRIBUTION AFTER ONE HOUR OF SIMULATION IN RUN 7

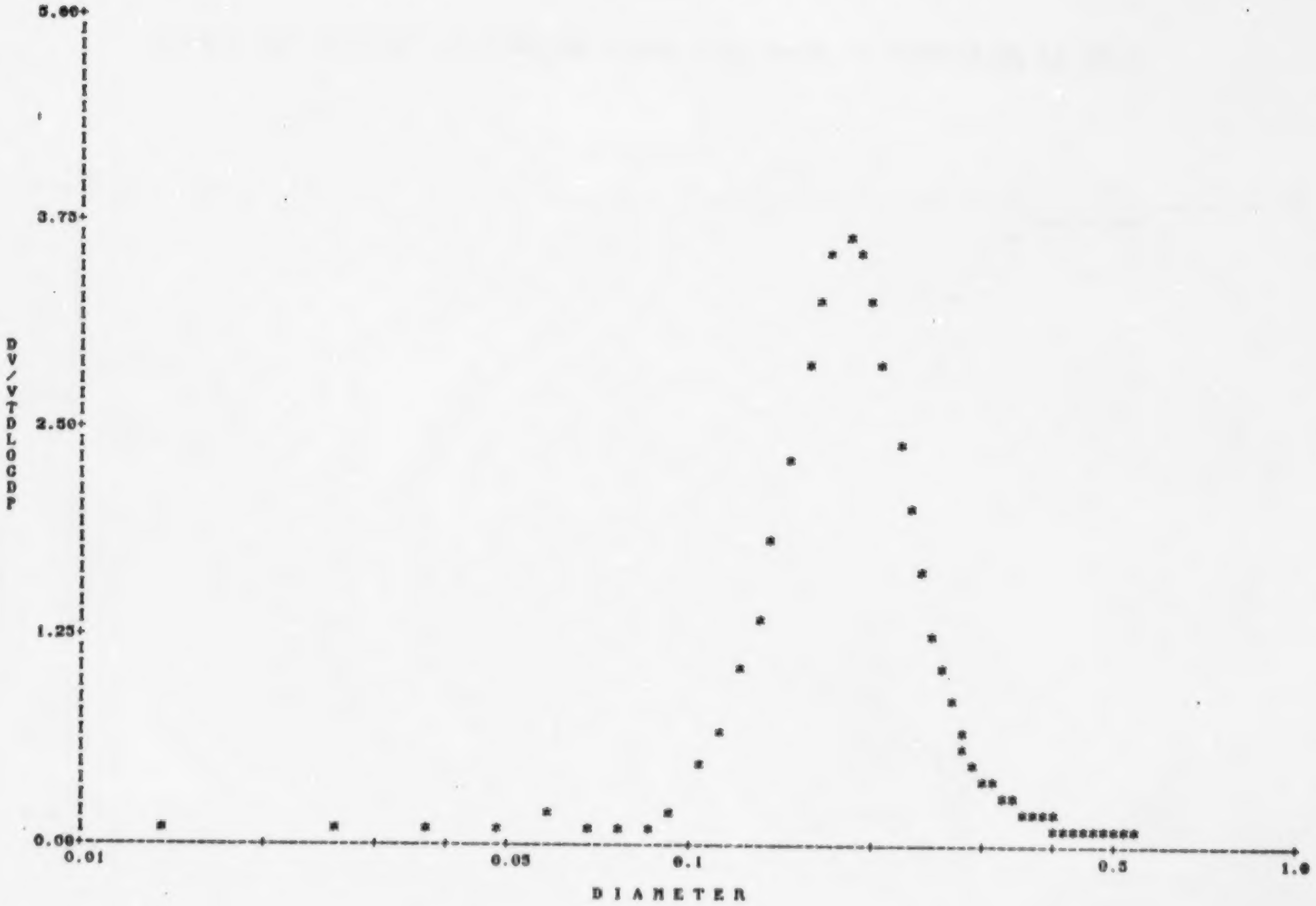

FIGURE 13b. VOLUME DISTRIBUTION AFTER THREE HOURS OF SIMULATION IN RUN 7

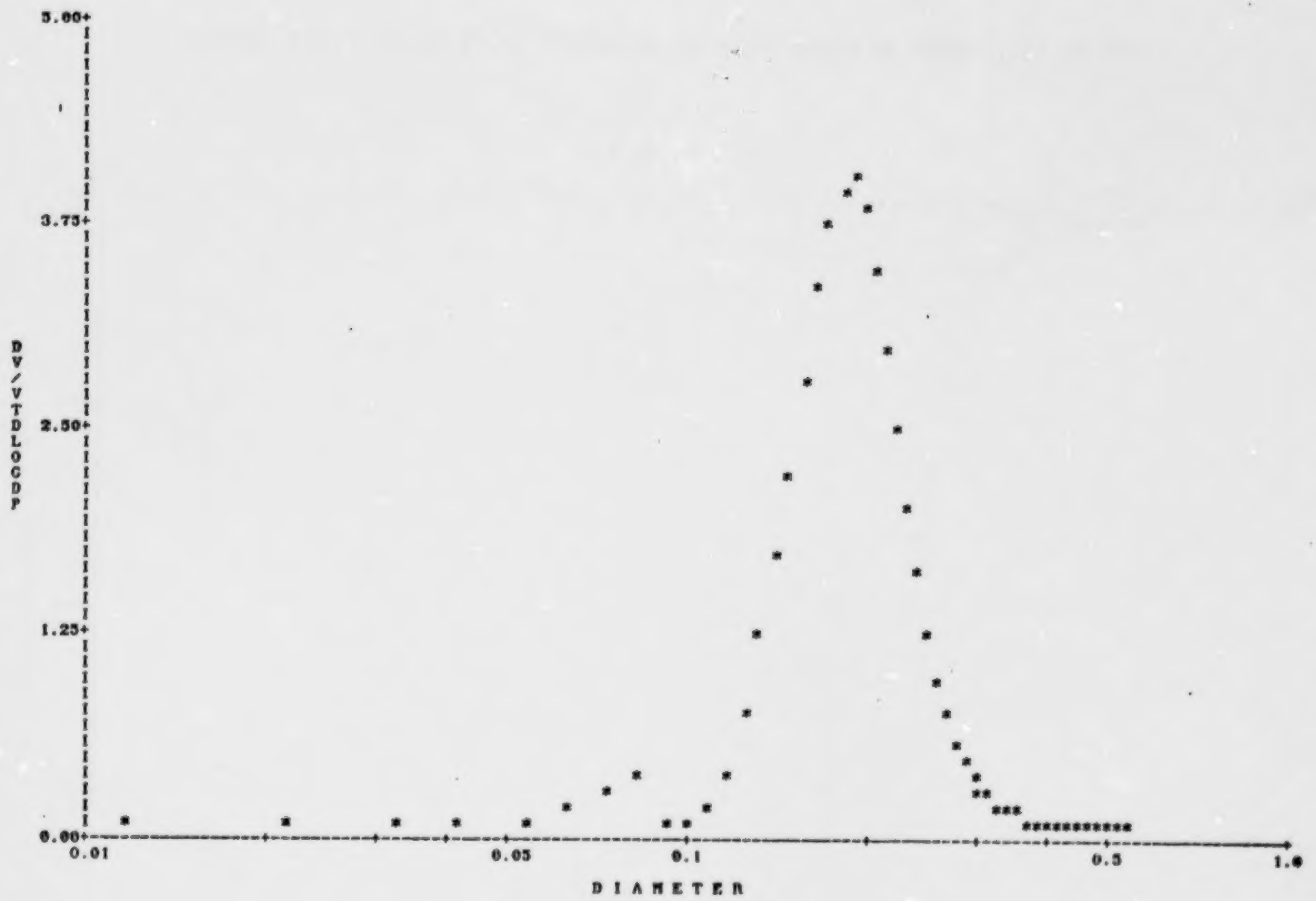

FIGURE 13c. VOLUME DISTRIBUTION AFTER SEVEN HOURS OF SIMULATION IN RUN 7

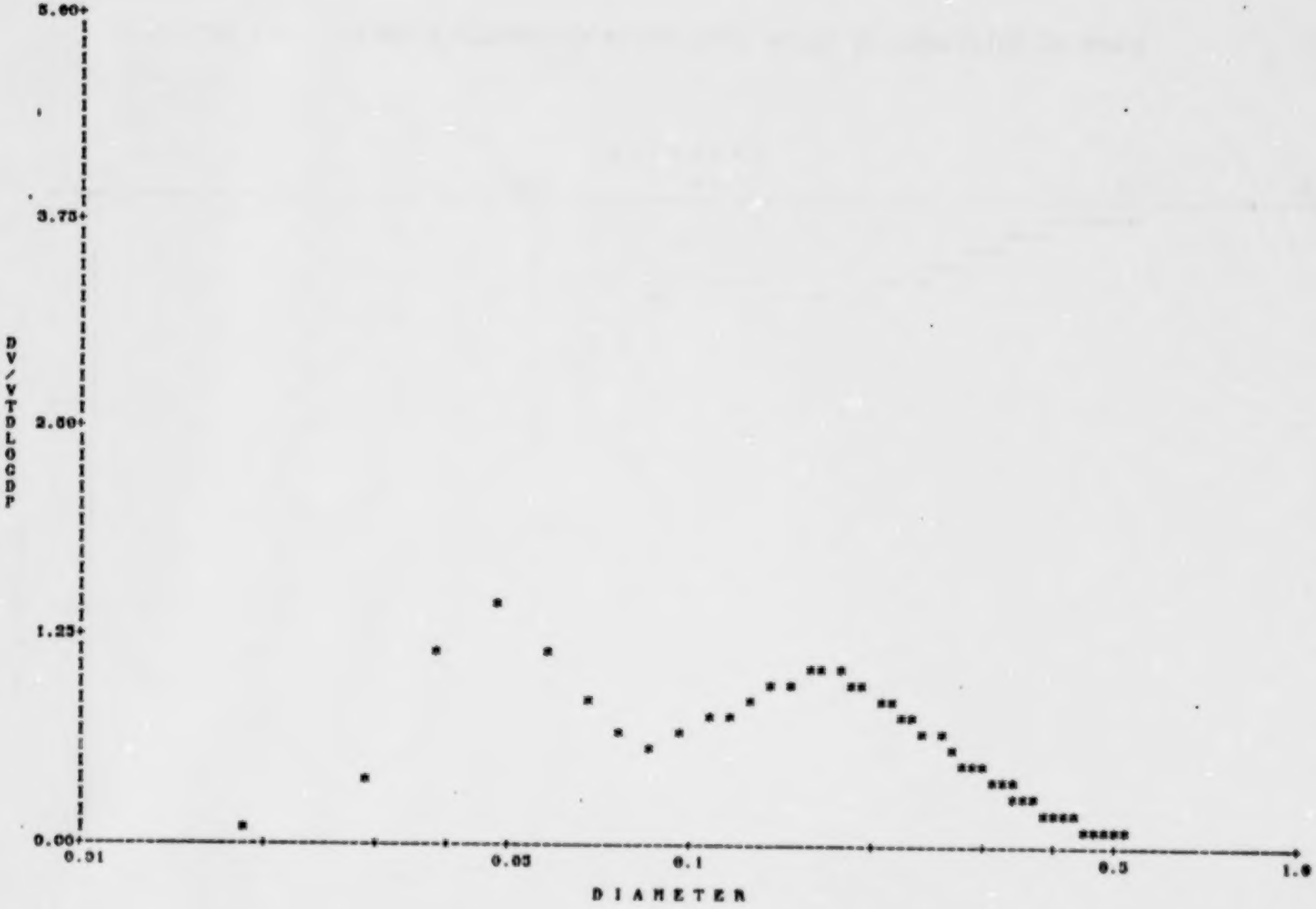

FIGURE 14a. VOLUME DISTRIBUTION AFTER ONE HOUR OF SIMULATION IN RUN 8

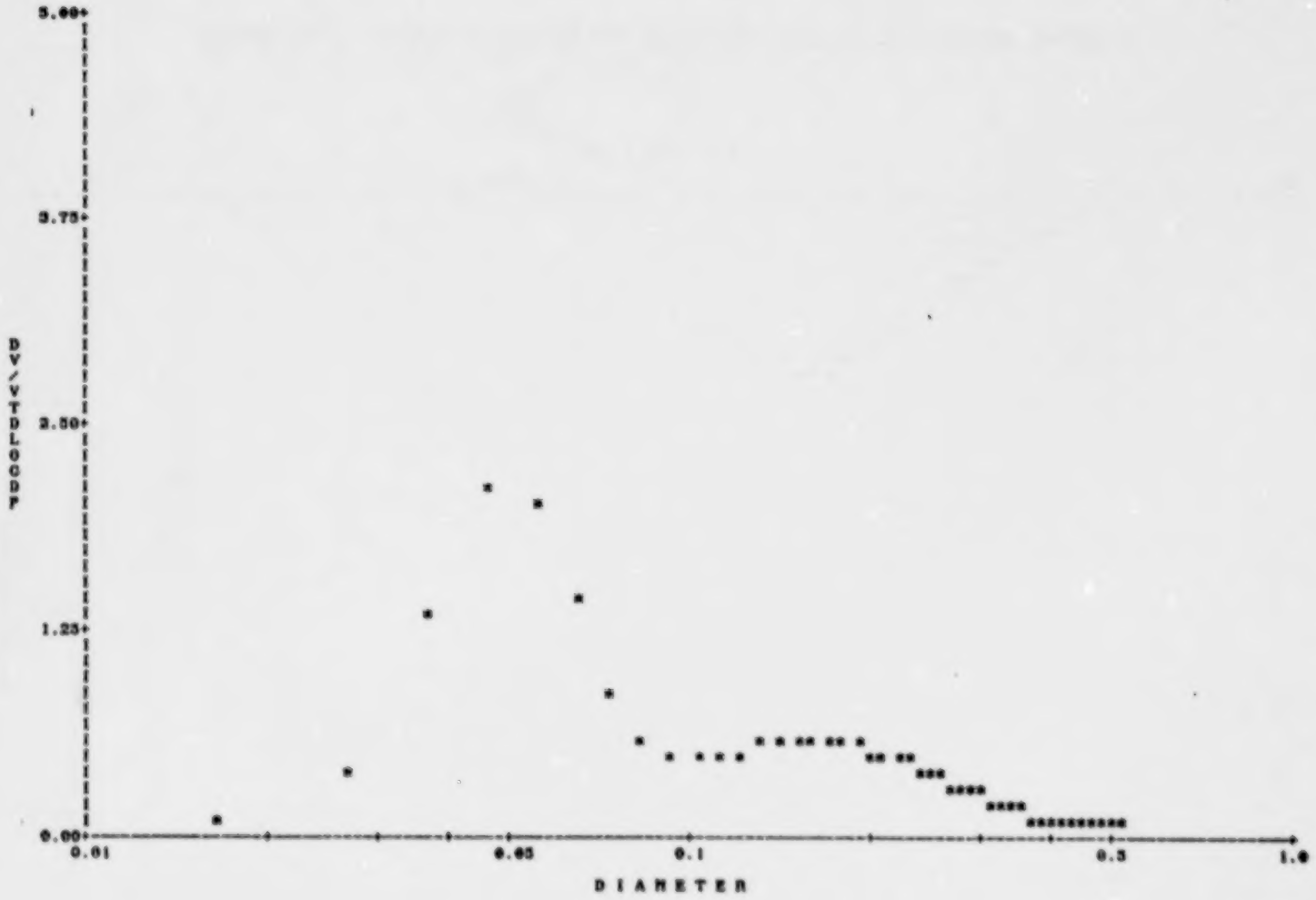

FIGURE 14b. VOLUME DISTRIBUTION AFTER THREE HOURS OF SIMULATION IN RUN 8

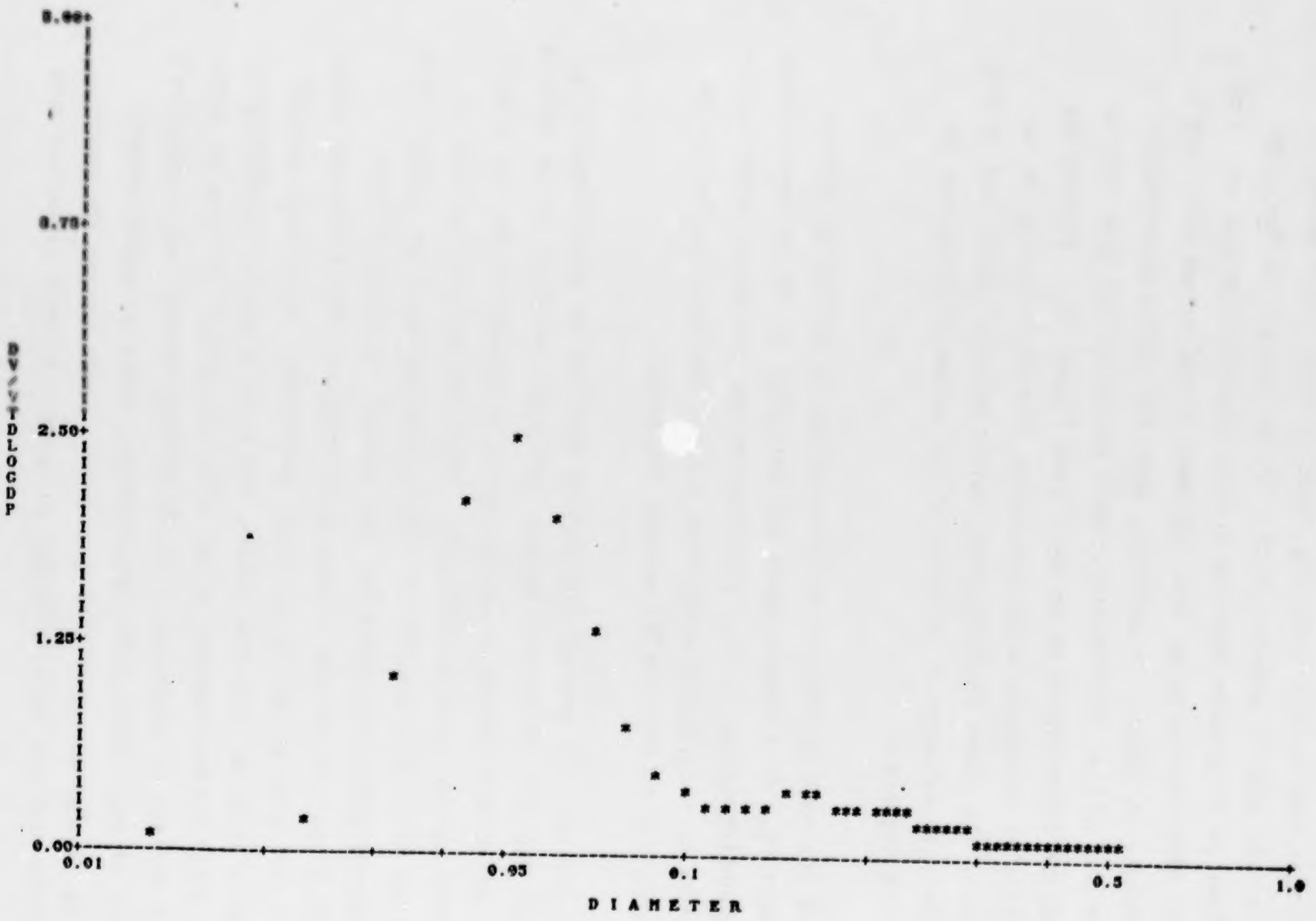

FIGURE 14c. VOLUME DISTRIBUTION AFTER SEVEN HOURS OF SIMULATION IN RUN 8

have the same peak (as in Runs 6 and 7), there is very little change in the location of the peak as growth occurs. In particular, in Run 6 the source distribution is broader than the initial distribution and very little of the initial distribution grows into the peak of the volume distribution as source material is added. In contrast, when the source distribution is narrower than the initial distribution, small particles can grow into or modify the volume distribution as in Run 7 (see Figure 14). Because the number of particles associated with the source size distribution in Run 7 is lower than in the other distributions, particles grow faster and in this simulation there is evidence of shifting of the volume distribution to larger particle diameters.

In Run 8 the peak of the source distribution is shifted to smaller particle diameters. As a result there are two peaks in the volume distribution, corresponding to the initial distribution and the source distribution. As more primary particulate is added from sources the contribution to the volume distribution of the initial aerosol decreases.

Let us consider the general conclusions that can be drawn concerning the effect of the rate of primary aerosol emissions relative to the rate of formulation of aerosol volume by gas-to-particle conversion and the effect of the primary aerosol size distribution. When the rate of increase of aerosol volume by primary sources is roughly equivalent to or greater than that from gas-to-particle conversion, the aerosol size distribution reflects the properties of the primary distribution. Particles that enter the batch system grow by gas-to-particle conversion. As primary aerosol is continually injected into the system, one might expect a broadening of the volume distribution, because at any time the system consists of particles with a variety of histories. If the primary aerosol has a relatively large number of very small particles, however, there is enough aerosol surface area so that all particles grow slowly, even though the overall rate of gas-to-particle conversion may be large. If this situation were to hold generally in the atmosphere, then it might be possible simply to characterize the aerosol size distribution at any point by the source distributions of particles in that air parcel. However, because of the variety of primary sources and their different emission times and rates, it is unlikely that such a simple result will hold in atmospheric applications.

We have shown that the very small particles either formed by homogeneous nucleation or emitted, while contributing very little to the aerosol volume, can substantially change the volume distribution of the aerosol by reducing the amount of secondary aerosol that grows into larger particles. Furthermore, because of their high mobility very small particles have a high rate of coagulation with the particles in the accumulation range. Hence, part of the volume originally lost to these small particles is eventually added to the accumulation range as a result of coagulation.

We have seen that when the ratio of the secondary production rate to the primary aerosol emission rate is very large the volume distribution of particles in the accumulation range may be very narrow and highly packed.*

3. Comparison of Batch System Simulations with Smog Chamber Data

The ultimate purpose for developing aerosol models is to simulate aerosol processes occurring in smog chambers and in the atmosphere. It is necessary, therefore, that predictions be carefully compared with experimental measurements, as, of course, has been done in the large number of studies devoted to gas phase photochemistry (Demerjian et al., 1974; Hecht et al., 1974). Because coagulation and surface removal are not included in the aerosol model, the occurrence of these two processes in smog chambers may make detailed comparisons between predictions and measurements impossible. Nevertheless, we determined in a preliminary way the degree of correspondence between predictions and measurements using data from Kocmond et al. (1975) of Calspan Corp. In the Kocmond et al. study, photochemical smog reactions were carried out in a chamber in the presence of SO_2, and the aerosol number distribution was measured by an electrical aerosol analyzer.

---

*Because the amount of light scattering in the atmosphere is determined by the product of the surface area of the aerosol and the (size-dependent) scattering cross section, any shift of the volume distribution can significantly alter the amount of light scattering.

The variations with time of the total number density and the concentrations of certain gaseous components in two experiments (Calspan Runs 14 and 15) are shown in Figures 15 and 16. In both experiments N first increases rapidly as a result of homogeneous nucleation, then decreases due to coagulation and loss on surfaces. On the other hand, V increases steadily for three or four hours, nearly approaching a constant value. The reduction in the rate of increase of V and the subsequent decrease in V may be the result of limitations in measuring particles with diameters greater than 0.4 μm (Kocmond et al., 1975).

We attempted to simulate these runs. Because we did not explicitly consider coagulation or homogeneous nucleation, we restricted our attention in these two experiments to the time between the occurrence of the maximum in N and the beginning of the reduction in the rate of production of V. During this period, gas-to-particle conversion is the dominant influence on V (although coagulation affects N because of the large value of N). Thus, we consider only 180 minute and 90 minute periods in Runs 14 and 15, respectively.*

The value of N measured shortly after the maximum was used as the initial number density in the simulation. The initial aerosol size

---

*The size distribution data were obtained from Warren Kocmond of Calspan.

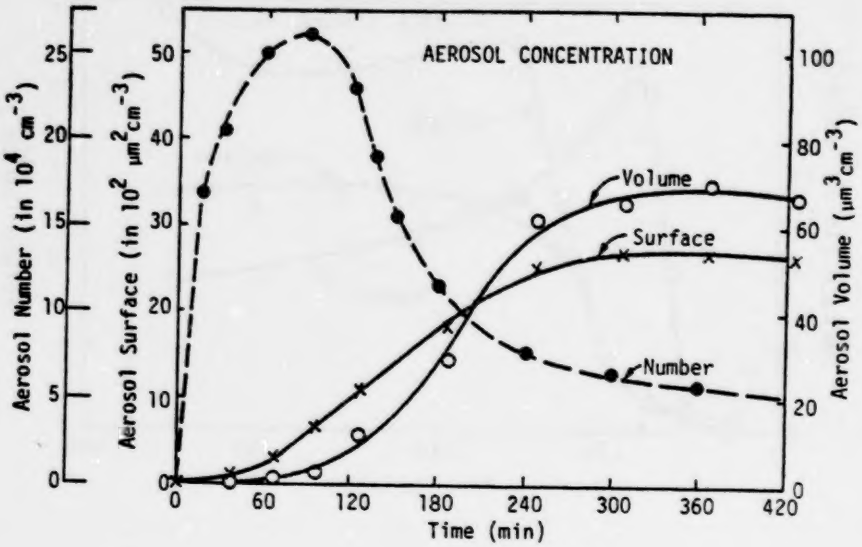

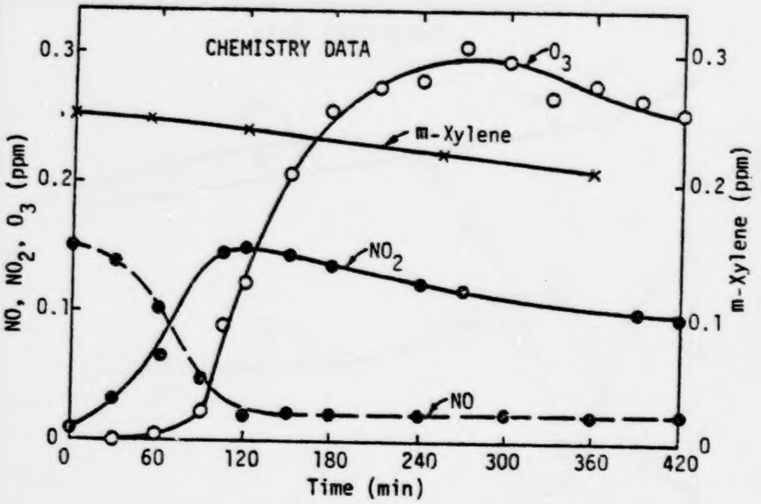

Source: Kocmond et al. (1975)

FIGURE 15. CHEMISTRY AND AEROSOL CONCENTRATION DATA FOR CALSPAN RUN NO. 14. The initial concentrations were 0.34 ppm m-xylene, 0.055 ppm SO_2, 0.150 ppm NO, and 29 percent relative humidity.

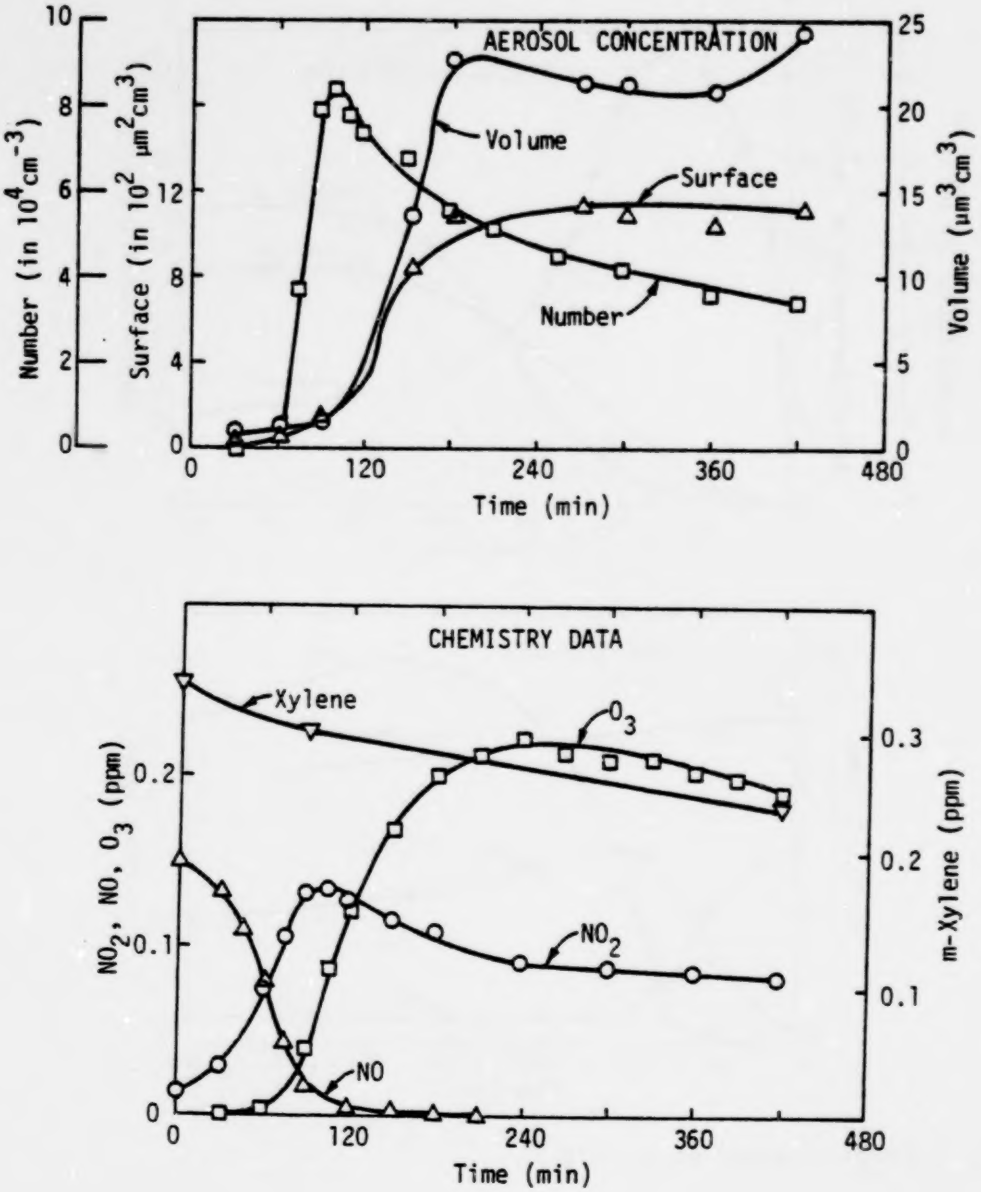

Source: Kocmond et al. (1975)

FIGURE 16. CHEMISTRY AND AEROSOL CONCENTRATION FOR CALSPAN RUN NO. 15, A XYLENE-NO-FILTERED AIR SYSTEM. Initial concentrations were 0.34 ppm m-xylene, 0.150 ppm NO, 0.014 ppm NO_2 and 38 percent relative humidity.

distributions used in the simulations of Calspan Runs 14 and 15 are shown in Figure 17. No particles below a size of 0.01 μm were assumed to be present initially. The predictions at the ends of the simulations and the corresponding measurements are shown in Figures 17 and 18. In these simulations the rate of gas-to-particle conversion was determined from the measured change in the aerosol volume. Thus, we did not attempt to predict the rate of formation of condensable species, such as H_2SO_4, a priori, but rather inferred that rate from the data. Since our objective in this initial study was to ascertain the degree of agreement between measured and predicted size distributions, it was not necessary to compute the rate of formation of condensable species from the gas phase chemistry.

The number distribution predicted after 180 minutes in Calspan Run 14 (Figure 18) was low for particles of $D_p > 0.1$ μm and high for particles of $D_p < 0.1$ μm. This trend in prediction is quite consistent with the neglect of coagulation, which would lead to a transfer of small particles into the larger particle fraction. A similar result was obtained in the simulation of Run 15 (see Figure 19).

4. Reductions in the Resolution of $\bar{n}_0(D_p,t)$

If the aerosol model discussed herein is eventually to be integrated into a grid-type air pollution simulation model, then the number of diameters at which $\bar{n}_0(D_p,t)$ is predicted must be reduced considerably. The greatest obstacle in reducing the resolution of $\bar{n}_0(D_p,t)$ is the wide range of values that this function assumes. Typical size distributions reported for Los Angeles aerosol vary by factors of 10^6 or 10^7 between particle diameters of 0.01 μm and 1.0 μm. The source distributions for aerosols vary over a similar range. Therefore a reduction in the resolution of the model could result in few particles entering a given size range from sources.

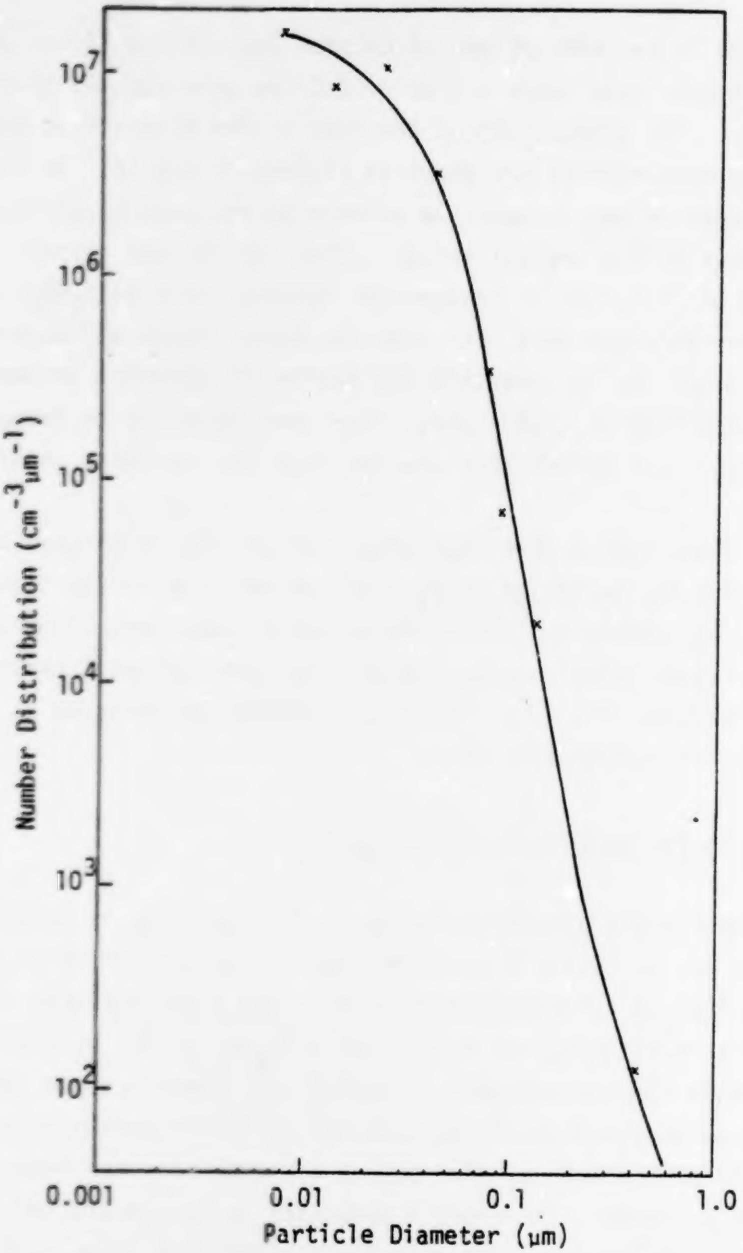

FIGURE 17a. INITIAL NUMBER DISTRIBUTION FOR CALSPAN RUN 14. Calspan data are indicated by X; lines represent the fit to the data.

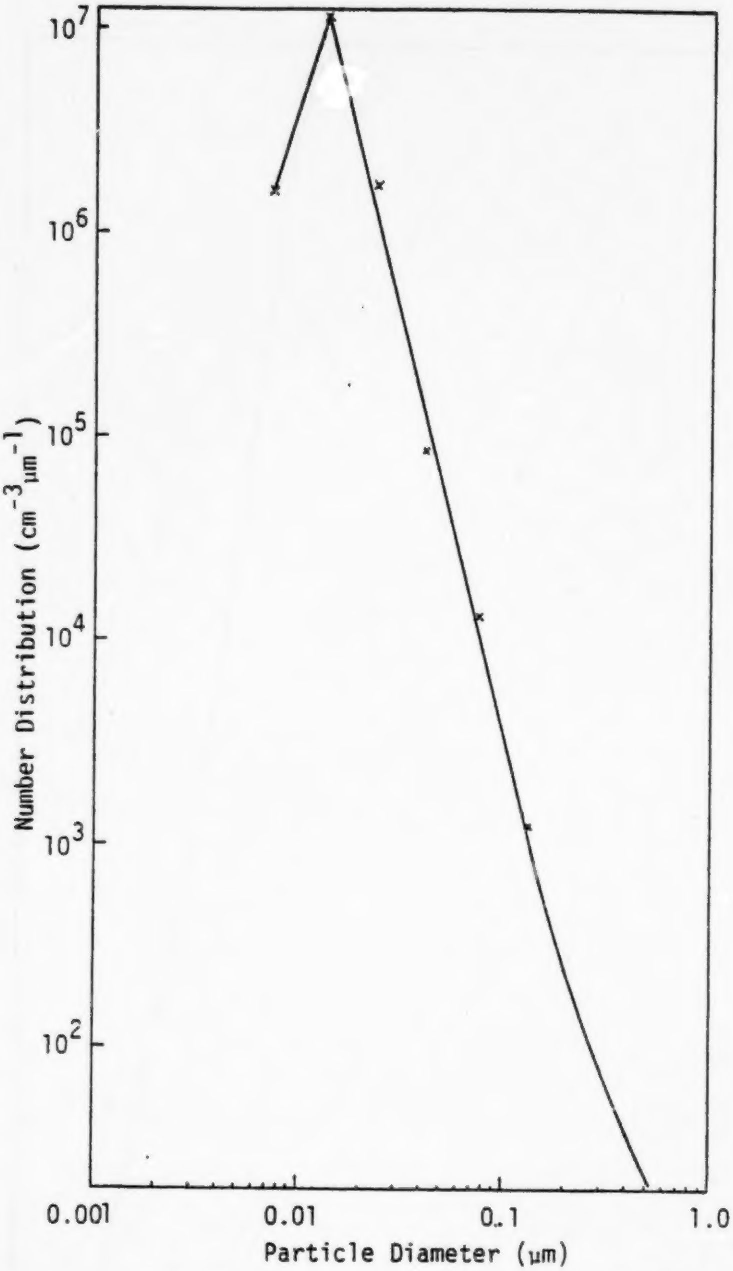

FIGURE 17b. INITIAL NUMBER DISTRIBUTION FOR CALSPAN RUN 15. Calspan data are indicated by X; lines represent fit to the data.

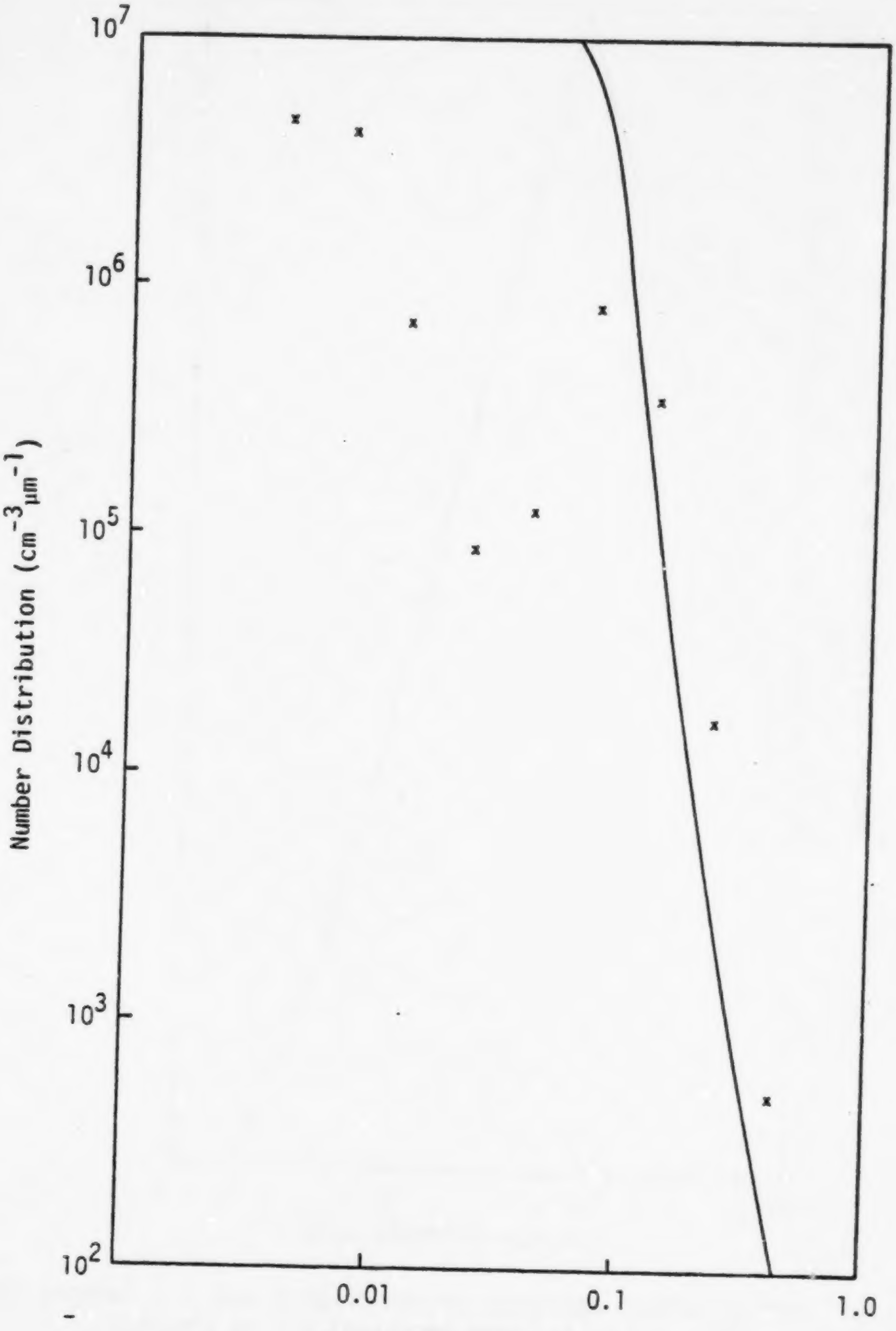

FIGURE 18. PREDICTED AND MEASURED AEROSOL SIZE DISTRIBUTION FOR CALSPAN RUN 14. The solid line indicates predictions, and measurements are indicated by x.

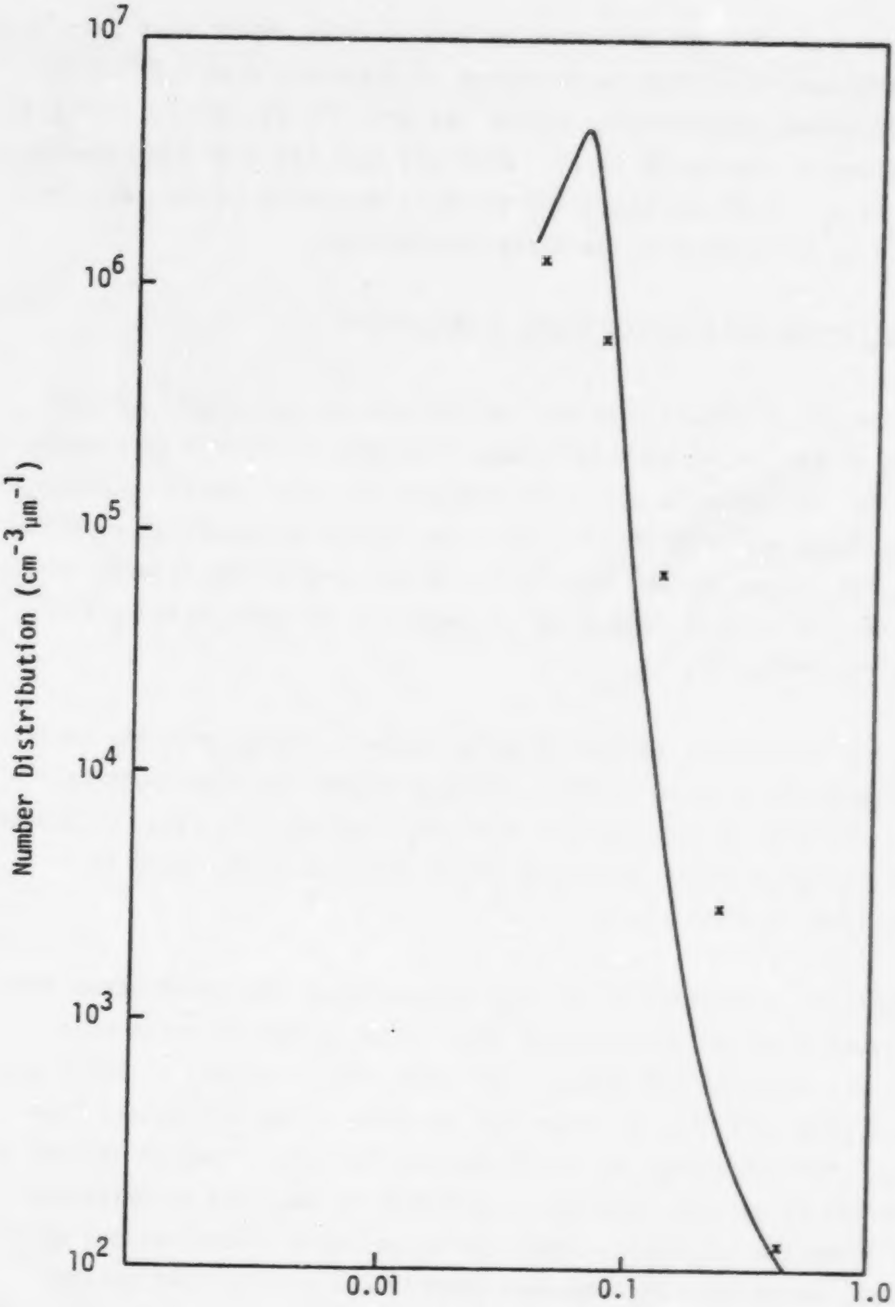

FIGURE 19. PREDICTED AND MEASURED AEROSOL SIZE DISTRIBUTION FOR CALSPAN RUN 15. The solid line indicates predictions, and measurements are indicated by x.

The size distributions presented earlier in this report were calculated for 50 particle sizes in the range of diameters from 0.01 μm to 0.5 μm. The volume distributions calculated with 11, 26, and 50 particle sizes are shown in Figures 20 to 22. Provided that the size distribution is defined at D_p = 0.01 μm, where the boundary condition is applied, there is virtually no difference in the three predictions.

B. SIZE DISTRIBUTION DYNAMICS ALONG A TRAJECTORY

A second set of simulations was carried out to approximate aerosol dynamics in an air parcel advected along a trajectory through an airshed. The air parcel was taken as spatially homogeneous, i.e., vertical concentration gradients were neglected. Thus, the system mathematically resembled the batch system, except that in the trajectory system primary aerosol emissions and the rate of production of secondary aerosol varied with time along the trajectory.

In order to describe aerosol dynamics along a trajectory, the variations in source emission and gas-to-particle conversion rates must be estimated. Primary aerosol sources were estimated as discussed in Chapter III-C, and gas-to-particle conversion rates were estimated based on ambient measured concentrations.

A "typical" trajectory in the Los Angeles Basin was constructed from meteorological data for 30 September 1969. A point at the coast near Long Beach was taken as the starting point of the trajectory at 0800, and hourly wind data were used to trace out the path of the trajectory (see Figure 23). Numbers alongside the trajectory indicate times of arrival of the air parcel at various locations. Air quality data and an emissions inventory along the trajectory were used to estimate concentrations of SO_2, O_3, NO_2, nonmethane hydrocarbons (NMHC), and primary particulate emissions at each point. The data used in the simulation are compiled in Table 14.

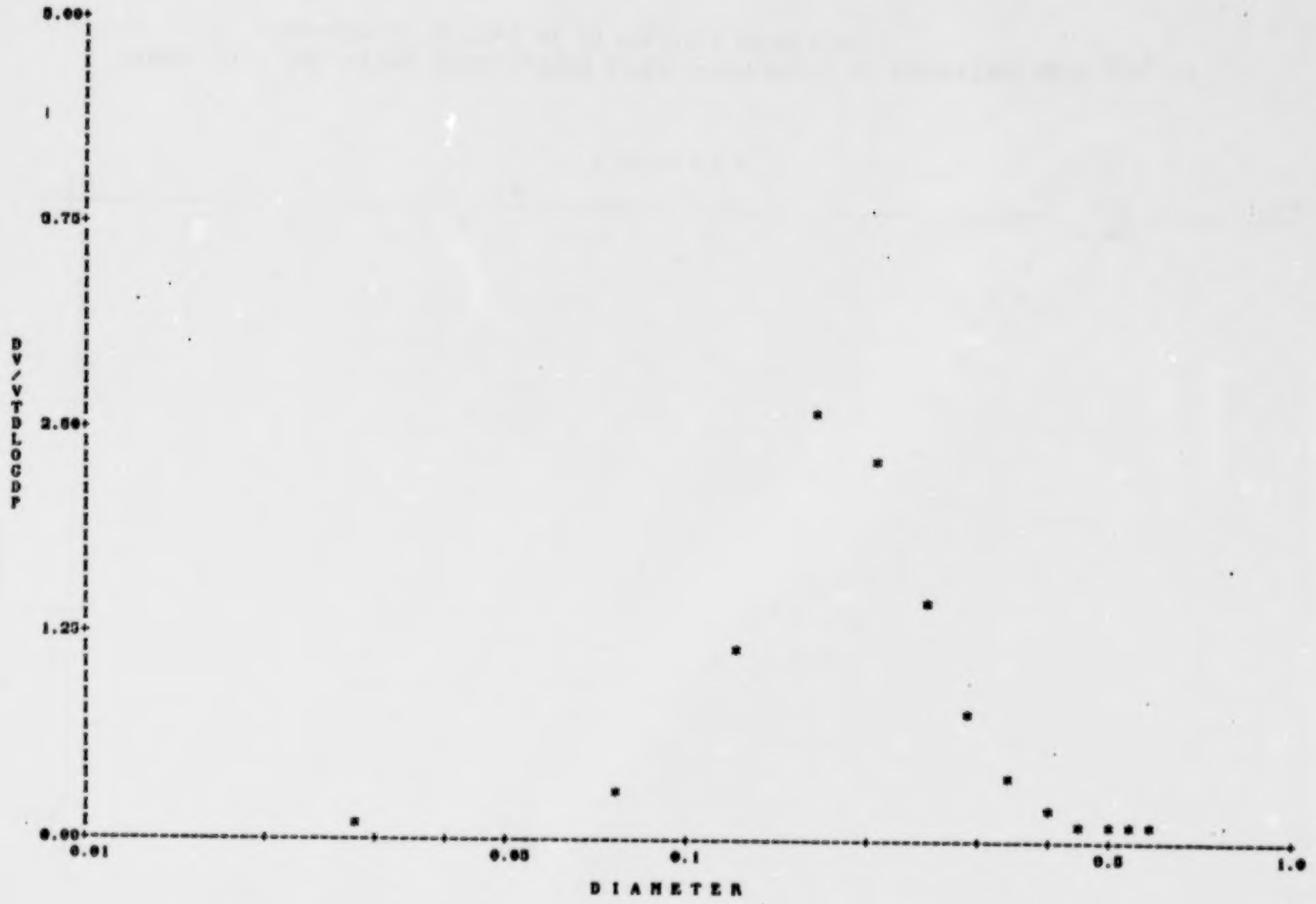

FIGURE 20. THE VOLUME DISTRIBUTION AFTER SEVEN HOURS OF SIMULATION WITH $n(D_p,t)$ ORIGINALLY DEFINED AT 11 PARTICLE DIAMETERS

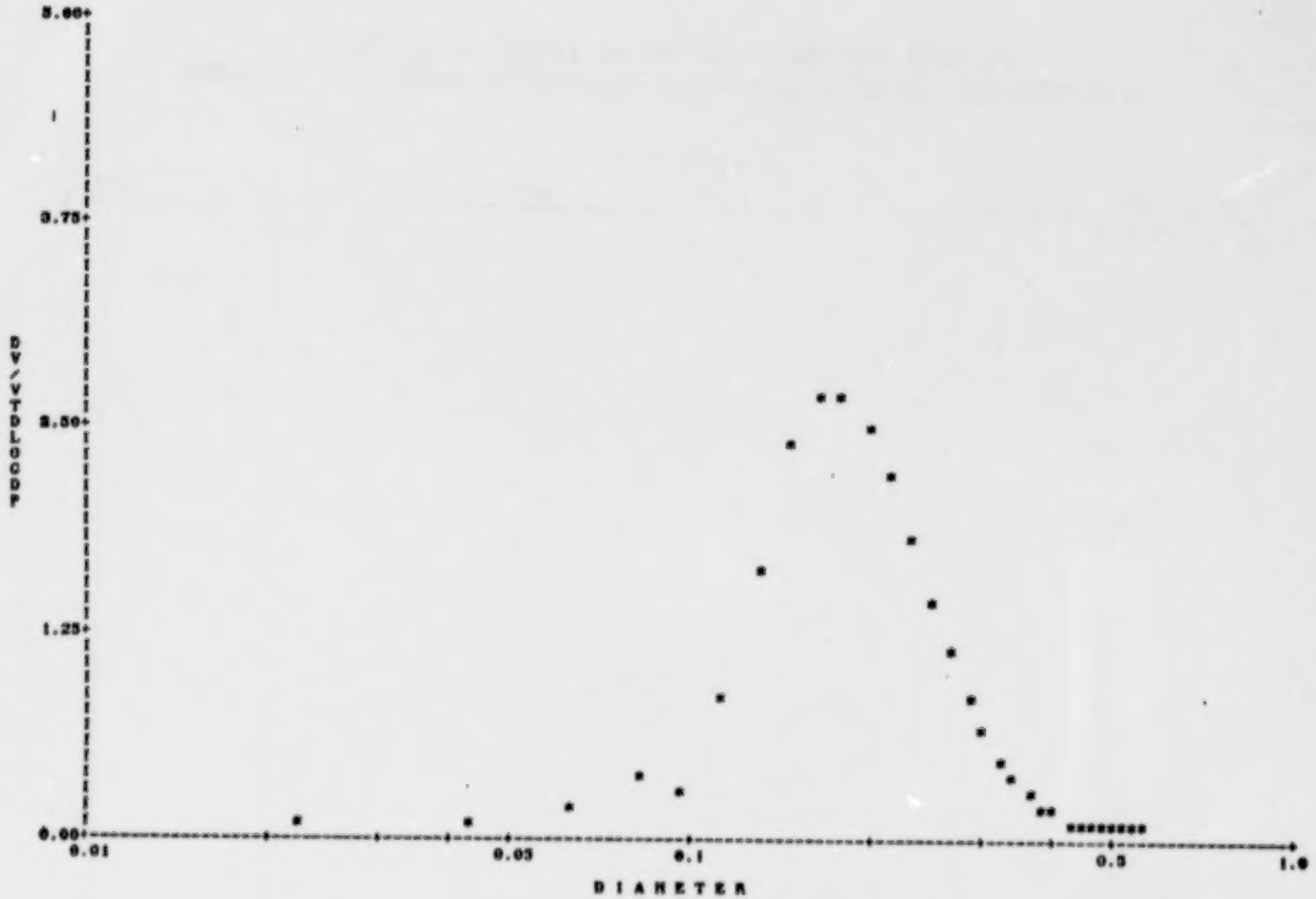

FIGURE 21. THE VOLUME DISTRIBUTION AFTER SEVEN HOURS OF SIMULATION WITH $n(D_p,t)$ ORIGINALLY DEFINED AT 26 PARTICLE DIAMETERS

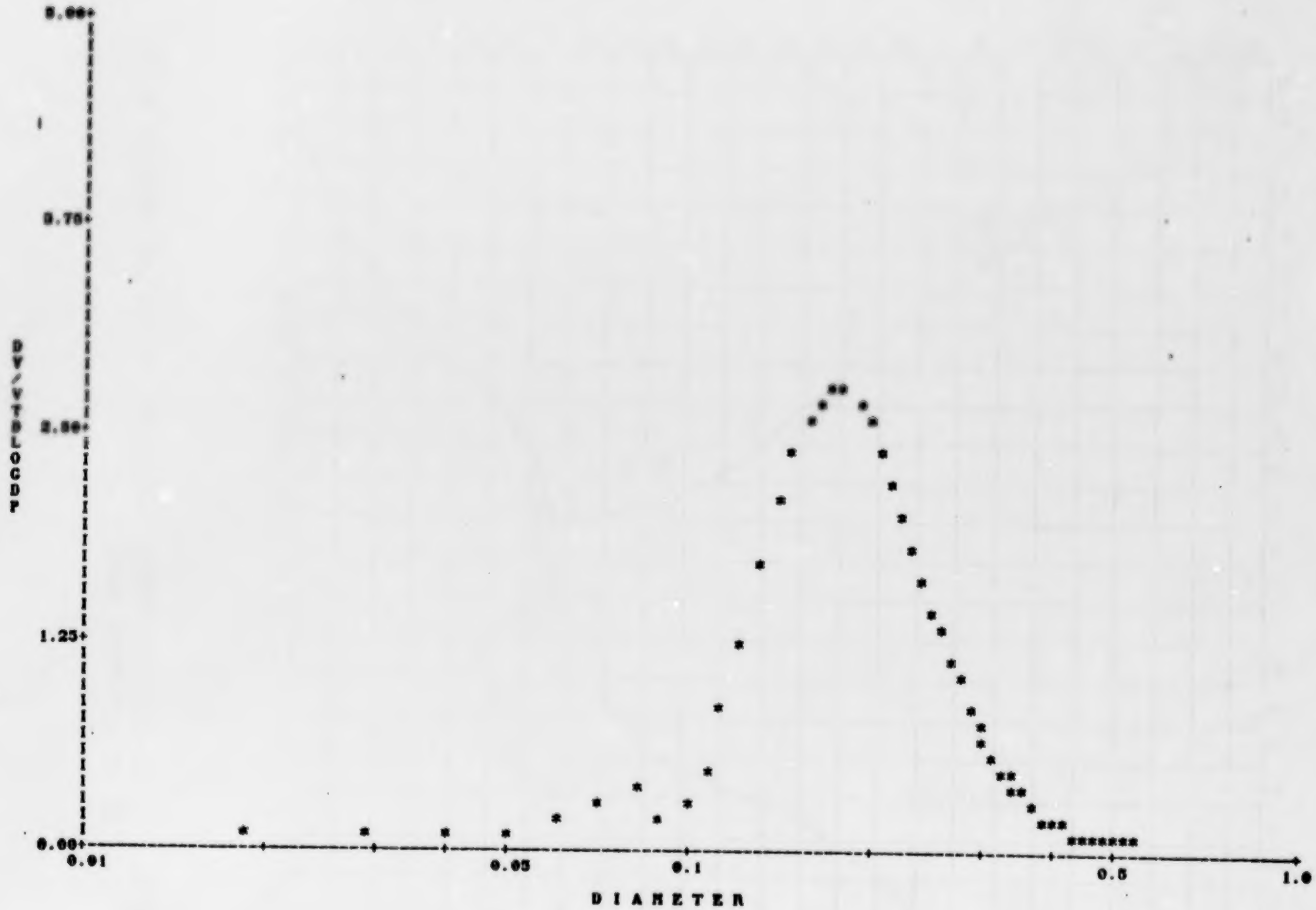

FIGURE 22. THE VOLUME DISTRIBUTION AFTER SEVEN HOURS OF SIMULATION WITH $n(D_p,t)$ ORIGINALLY DEFINED AT 50 PARTICLE DIAMETERS

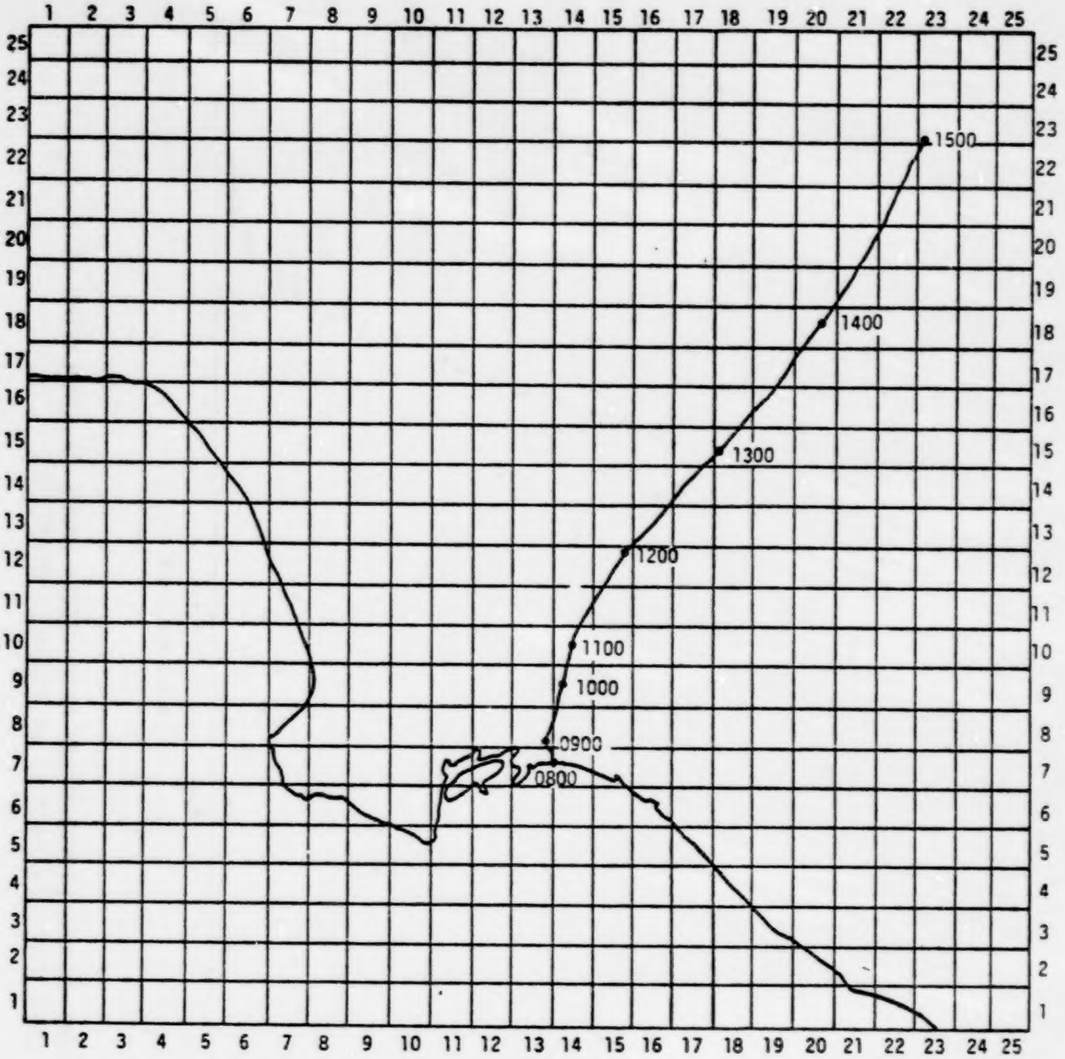
1 2 3 4 5 6 7 8 9 10 11 12 13 14 15 16 17 18 19 20 21 22 23 24 25
0800
0900
1000
1100
1200
1300
1400
1500

FIGURE 23. SEVEN-HOUR AIR PARCEL TRAJECTORY IN THE LOS ANGELES BASIN ON 30 SEPTEMBER 1969

TABLE 14. DATA USED IN TRAJECTORY SIMULATIONS

Time (PDT)	Inversion Height (ft)	Ambient Concentrations (ppm)				Particulate Emissions ($\mu g\ cm^{-3} min^{-1}$)
		SO_2	O_3	NO_2	NMHC	
0800	500	0.03	0.02	0.04	0.1	1.14×10^{-7}
0810	500	0.01	0.02	0.04	0.1	1.42×10^{-7}
0845	600	0.04	0.02	0.06	0.1	2.6×10^{-7}
0920	600	0.03	0.03	0.06	0.1	1.88×10^{-7}
0935	600	0.06	0.02	0.07	0.1	1.82×10^{-7}
1035	700	0.05	0.04	0.07	0.1	1.46×10^{-7}
1115	700	0.02	0.07	0.07	0.2	1.62×10^{-7}
1130	900	0.02	0.09	0.07	0.2	1.30×10^{-7}
1140	1000	0.03	0.09	0.08	0.2	1.06×10^{-7}
1205	1300	0.03	0.10	0.08	0.3	1.36×10^{-7}
1225	1500	0.04	0.11	0.08	0.3	5.00×10^{-8}
1250	1700	0.04	0.13	0.08	0.4	6.20×10^{-8}
1300	1700	0.03	0.13	0.08	0.4	1.44×10^{-8}
1310	1900	0.03	0.15	0.07	0.5	3.00×10^{-8}
1315	2100	0.03	0.15	0.07	0.6	1.86×10^{-8}
1330	2100	0.03	0.17	0.07	0.7	3.40×10^{-8}
1340	2100	0.03	0.18	0.07	0.8	3.00×10^{-8}
1350	2100	0.03	0.20	0.07	1.0	5.60×10^{-8}
1405	2100	0.02	0.16	0.06	1.0	2.60×10^{-8}
1415	2100	0.03	0.19	0.06	1.8	2.60×10^{-8}
1430	2000	0.03	0.16	0.06	0.9	1.04×10^{-9}
1445	2000	0.03	0.16	0.07	0.7	1.78×10^{-10}

The purpose of the trajectory simulations was to illustrate the sensitivity of predictions to changes in the primary aerosol size distribution and the rate of gas-to-particle conversion. In these simulations we were particularly interested in the general features of the size distribution, as opposed to the very small variations discussed for the batch system, since it is unlikely that atmospheric data will be available to validate the model with its current resolution. Furthermore, because the size distributions of the background and the nonautomotive sources have not been characterized, we wanted to examine the impact of variations in these size distributions.

The rate expressions developed in Chapter III for the formation of aerosol precursors were employed to determine sulfate, nitrate, and organic aerosol formation rates based on the measured concentrations of SO_2, NO_2, and NMHC along the trajectory.

For primary aerosol, we classified sources as follows: 1) background aerosol, 2) automobile organic aerosol, 3) automobile lead aerosol, and 4) other aerosol. Following Chu and Seinfeld (1975), we assumed that the mass of particulate emissions from automobiles is equally divided between organic and lead. Huntzicker et al. (1975) estimated that 57 percent of the 18 tons of lead emitted per day by automobiles in 1973 was deposited near the source. Hence, we assumed that only 43 percent by weight of the emitted lead aerosol remains airborne. The size distribution for auto lead was that given by Husar and White (1976) (see Figure 2). The auto organic aerosol size distribution was assumed to follow the form of Eq. (50) with $\mu = -1.802$ and $\sigma = 0.362$. The background and other aerosol were also taken to be of the form of Eq. (50) with μ and σ varied to study the sensitivity of predictions to changes in these parameters. The runs and their associated conditions are listed in Table 15.

TABLE 15. CONDITIONS FOR TRAJECTORY SIMULATIONS

Run No.	0.01 µm Particles ($cm^{-3}\mu m^{-1}$)	σ_{0-}	μ_{0-}	σ_{other}	μ_{other}	Comment
1	10^4	0.362	-1.802	0.362	-1.802	
2	10^6	0.362	-1.802	0.362	-1.802	
3	10^4	0.362	-1.802	0.362	-1.802	No lead
4	10^4	0.362	-1.802	0.50	-1.802	
5	10^4	0.362	-1.802	0.362	-3.00	
6	10^4	0.362	-3.00	0.362	-1.802	
7	10^4	0.362	-3.00	0.362	-2.50	
8	10^4	0.362	-1.802	0.362	-1.802	$\alpha = 5 \times 10^{-3}$
9	10^4	0.362	-1.802	0.362	-1.802	$\alpha = 5 \times 10^{-4}$
10	10^4	0.362	-1.802	0.362	-3.00	48/52 primary/secondary
11	10^4	0.362	-1.802	0.362	-3.00	50/50 auto/other
12	10^4	0.362	-3.00	0.362	-2.50	50/50 auto/other
13	10^4	0.362	-3.22	0.362	-0.916	
14	10^4	0.362	-0.916	0.362	-3.22	
20	10^4	0.523	-1.2	0.362	-1.11	60/40 primary/secondary; 70/30 auto/other
21	10^4	0.523	-1.2	0.362	-2.50	60/40 primary/secondary; 31/69 auto/other
22	10^4	0.523	-1.2	0.362	-1.11	60/40 primary/secondary; 31/69 auto/other
23	10^4	0.523	-1.2	0.362	-2.50	60/40 primary/secondary; 70/30 auto/other
24	10^4	0.523	-1.2	0.362	-2.50	60/40 primary/secondary; 50/50 auto/other
25	10^4	0.523	-1.2	0.362	-1.11	60/40 primary/secondary; 40/60 auto/other
26	10^4	0.523	-1.2	0.60	-1.11	60/40 primary/secondary; 70/30 auto/other
27	10^4	0.523	-1.2	0.50	-1.11	60/40 primary/secondary; 70/30 auto/other

Along the trajectory shown in Figure 23 the ratio of the total volume of primary aerosol emitted during the seven hours of the simulation to the volume of secondary aerosol formed during this period was approximately 30 to 70. Most of the secondary aerosol was condensable organics formed in the last two hours of the simulation. In the simulation the fraction of the primary aerosol that could be attributed to the automobile was only about 31 percent of the total primary mass.

In the batch system we noted that when the primary emissions were from a single source with a single size distribution, the predicted size distribution reflected the distribution of the primary emissions. Furthermore, in the batch system, when the primary and secondary aerosol volumes were nearly the same, there was very little shifting of the peak of the volume distribution to larger particle diameters or increase of the peak value.

In many of the simulations in Table 15 the background aerosol, with an assumed volume of 30 $\mu m^3 cm^{-3}$, was assumed to have the same distribution as the automobile organic distribution [given by Eq. (50) and μ and σ in Table 15]. The purpose of this was to give the maximum sensitivity to the auto organic distribution so as to determine its greatest impact when the other sources were varied. In the other simulations the background aerosol was assumed to have the distribution given by Eq. (50) with $\mu = -1.2$ and $\sigma = 0.523$, which were obtained by fitting the distribution measured for submicron particles at Goldstone on 1 November 1973 (Hidy et al., 1975). In these other simulations the volume of background aerosol was assumed to be 15 $\mu m^3 cm^{-3}$--the remainder was assumed to be in the larger diameter range of the distribution.

For comparison, Table 16 lists the parameters characterizing the aerosol distributions in the first 14 runs listed in Table 15.

TABLE 16. VALUES OF VARIOUS PARAMETERS CHARACTERIZING THE AEROSOL DISTRIBUTION AFTER SEVEN HOURS OF SIMULATION

Run No.	Number Density (cm^{-3})	Aerosol Volume ($\mu m^3 cm^{-3}$)	$\left[dV/V_T d(\log D_p)\right]_{max}$	$\left(D_p^{-2}\right)^{1/2}$ (μm)	$D_{p_{max}}$ (μm)
1	7.1×10^4	142	3.5	0.11	0.20
2	1.6×10^5	140	3.1	0.082	0.20
3	3.3×10^4	141	4.7	0.14	0.21
4	7.7×10^4	140	3.2	0.11	0.19
5	$4,1 \times 10^5$	145	3.1	0.070	0.08
6	8.7×10^5	153	3.7	0.059	0.07
7	9.4×10^5	148	3.5	0.057	0.07
8	7.3×10^4	268	4.0	0.14	0.23
9	7.2×10^4	98	3.2	0.098	0.18
10	7.3×10^5	117	2.3	0.054	0.06
11	3.6×10^5	139	2.8	0.072	0.09
12	9.7×10^5	147	3.5	0.056	0.07
13	1.6×10^6	150	3.7	0.048	0.06
14	7.2×10^6	138	3.4	0.058	0.07

1. Effects of the Boundary Condition $\bar{n}_0(0.01,t)$ and of Very Small Particles on the Volume Distribution

In Chapter III we discussed the specification of the boundary condition at $D_p = 0.01$ μm, the flux of small particles into the system. As noted in Chapter III, the formation and growth of very small particles by homogeneous nucleation and subsequent coagulation are extremely complex, and we have not attempted to describe them in detail. Even the emission of very small particles from primary sources could only be estimated due to the lack of measurement capabilities in the sub-0.01 μm size range. In the trajectory simulations we chose simply to maintain $\bar{n}_0(0.01,t)$ constant at a value that did not significantly influence the total number density. This constant value presumably represents a steady flux of 0.01 μm diameter particles into the system from primary sources and homogeneous nucleation, although the value of $\bar{n}_0(0.01,t)$ has not been derived from the fundamental physics.

Computationally, the boundary condition was handled as follows. The initial size distribution was specified at 50 values of D_p from 0.01 μm to 0.5 μm. At each time step in the solution, particles of $D_p = 0.01$ μm introduced at the previous time step have grown, and it is necessary to introduce $\bar{n}_0(0.01,t)$ to represent the new particles entering the system at $D_p = 0.01$ μm. Rather than introducing new 0.01 μm particles at each time step, which would rapidly increase the number of values of D_p at which $\bar{n}_0(D_p,t)$ is defined, the boundary condition was applied only after particles originally of diameter 0.01 μm had grown to 0.02 μm. In this way, the approximate 0.01 μm resolution in $\bar{n}_0(D_p,t)$ was maintained, and generally not more than a 50 percent increase occurred in the number of values of D_p at which $\bar{n}_0(D_p,t)$ was calculated. Since the rate at which particles exceed 0.02 μm depends on the rate of growth, the impact of the boundary condition on the calculated size distribution depends on the number of particles in the system and the rate of condensation.

The parameters used for the background and source distributions in the trajectory simulations are shown in Table 15. Runs 1 and 2 were performed to study the impact of the boundary condition on the number and volume distributions. Figure 24 shows the number distributions at the end of the seven-hour simulation for the two runs. Due to the increased number density in Run 2, we expect slower growth of particles in this simulation than in Run 1. The volume distributions shown in Figures 25 and 26 reflect the features of the trajectory system that distinguish it from the batch system.

In the first hour the gain in the aerosol volume is almost entirely due to the emission of primary aerosol into the trajectory system. Note that after one hour of simulation the volume distributions in Runs 1 and 2 are virtually identical. There is very little change in the trajectory simulations after the third and fourth hours, although there is a slight shift of the peak in the volume distribution to larger particle diameters in Run 1 as expected from the lower number density.

The formation of secondary aerosol occurs principally during the sixth and seventh hours of the simulation, resulting in considerable narrowing of the volume distribution and a secondary peak at smaller particle diameters. The variation of the emissions rates and secondary aerosol formation rates caused the volume distribution to grow in two stages. In the first stage the rate of emission of primary particulates was high relative to the rate of gas-to-particle conversion, and the growth is very similar to that observed in the batch system with sources. In the second stage of growth, the emission rate of primary aerosol was very low, and the growth is similar to the batch system without sources. This behavior is reflected in $(\overline{D_p^2})^{1/2}$, which is listed for some runs in Table 17.

The secondary peaks in the volume distribution in both systems are due to the small lead particles that entered the systems during the morning

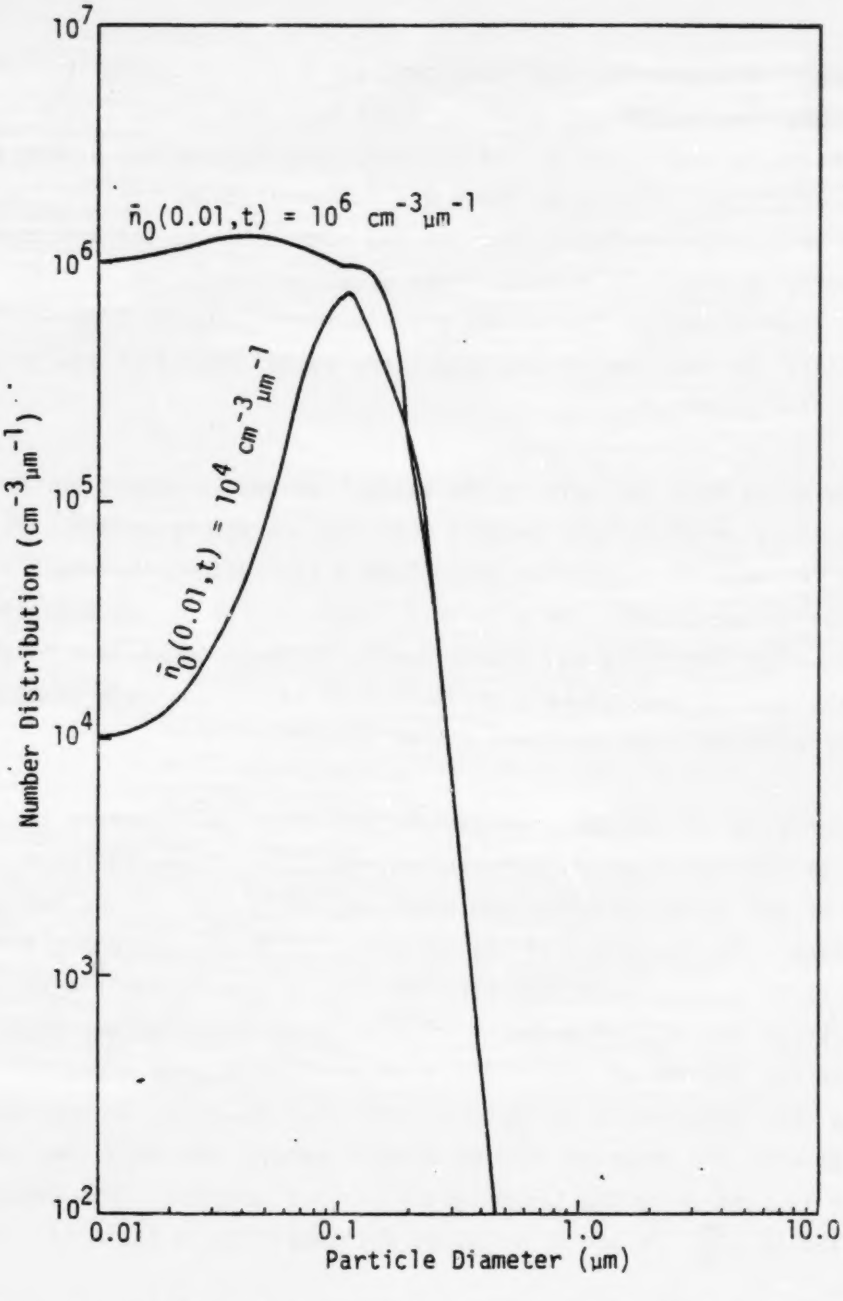

FIGURE 24. THE NUMBER DISTRIBUTIONS AFTER SEVEN HOURS OF SIMULATION WITH $n(0.01) = 10^4$ $cm^{-3}μm^{-1}$ AND $n(0.01) = 10^6$ $cm^{-3}μm^{-1}$

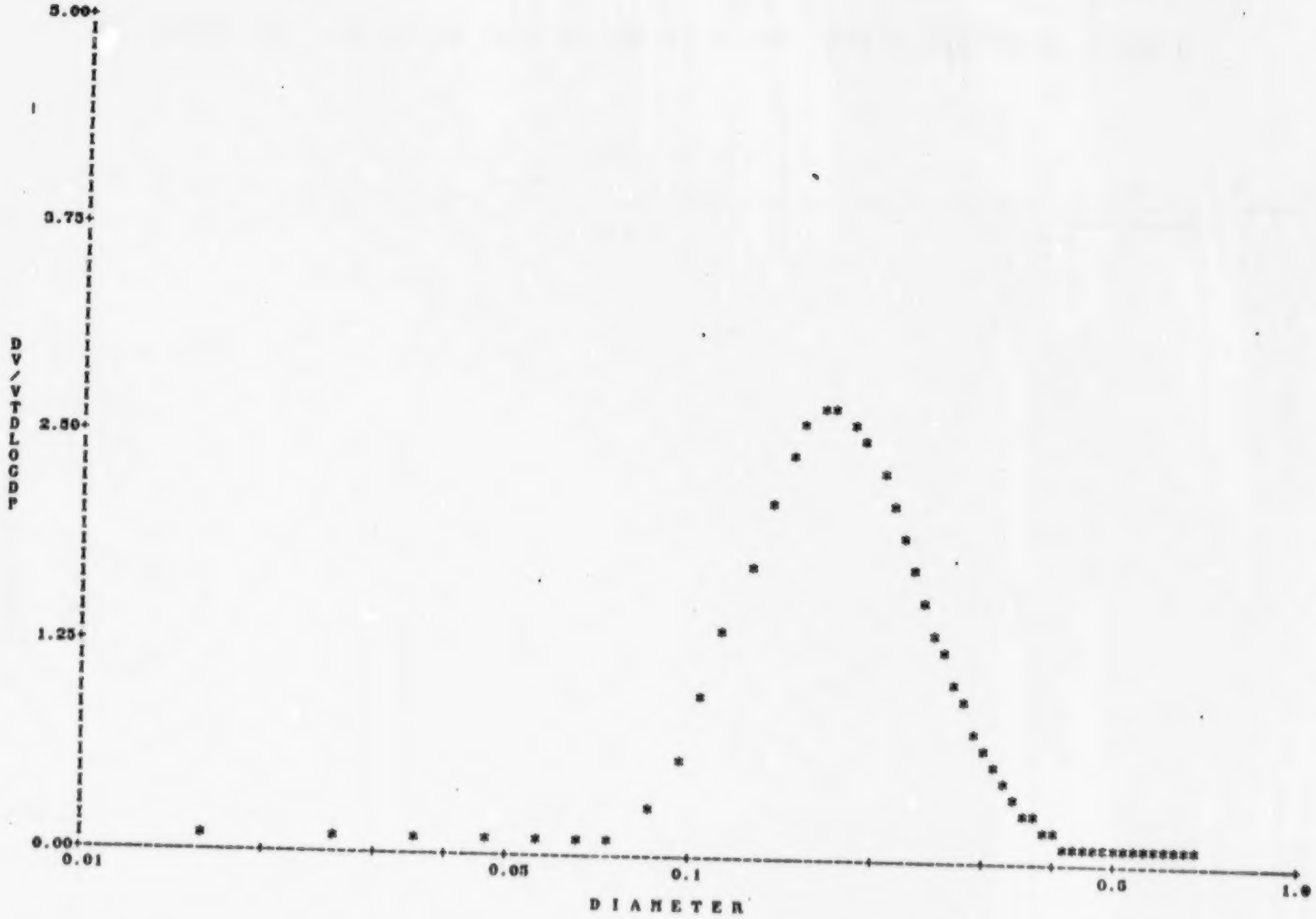

FIGURE 25a. THE VOLUME DISTRIBUTION AFTER ONE HOUR OF SIMULATION IN RUN 1

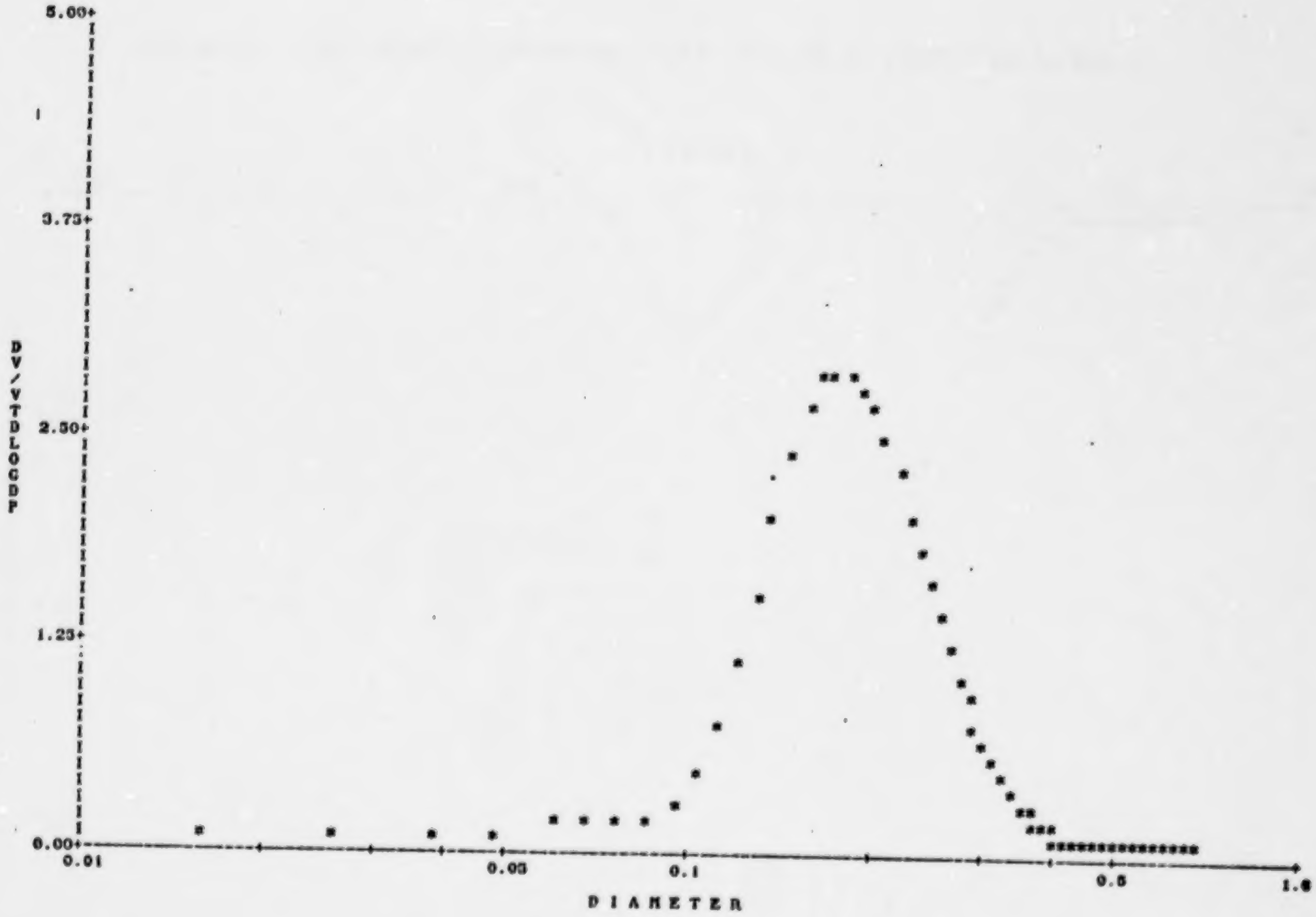

FIGURE 25b. THE VOLUME DISTRIBUTION AFTER FOUR HOURS OF SIMULATION IN RUN 1

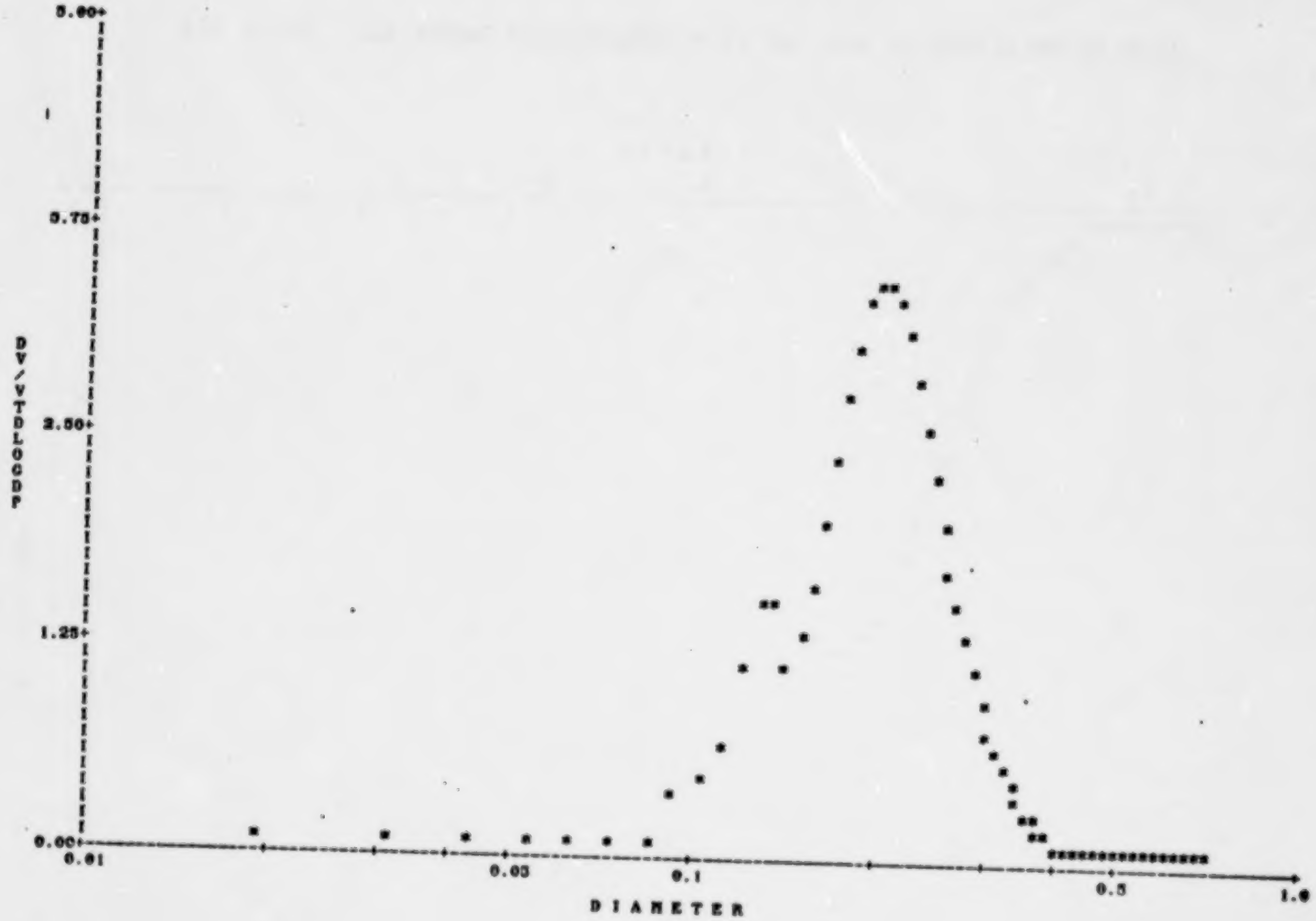

FIGURE 25c. THE VOLUME DISTRIBUTION AFTER SEVEN HOURS OF SIMULATION IN RUN 1

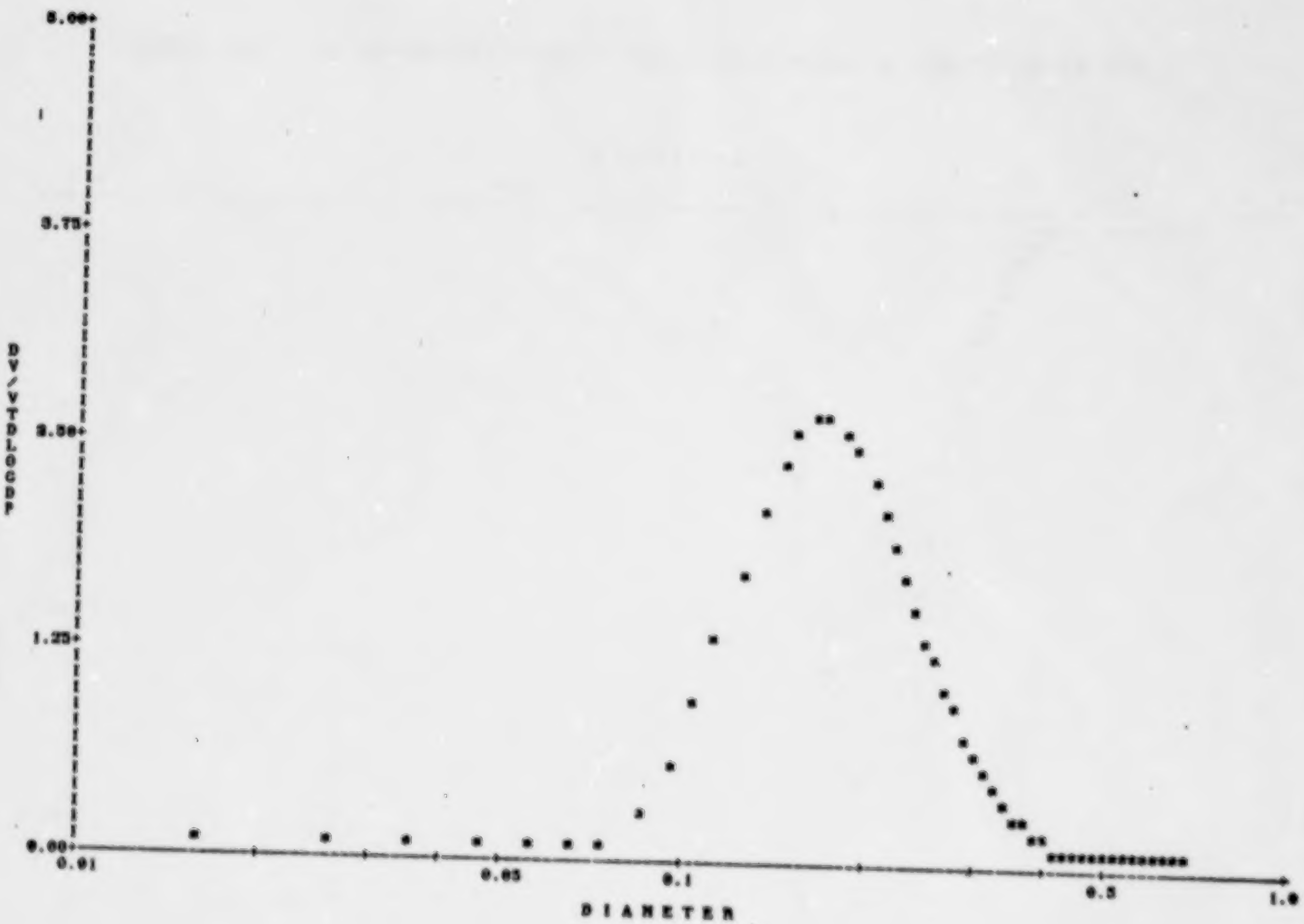

FIGURE 26a. THE VOLUME DISTRIBUTION AFTER ONE HOUR OF SIMULATION IN RUN 2

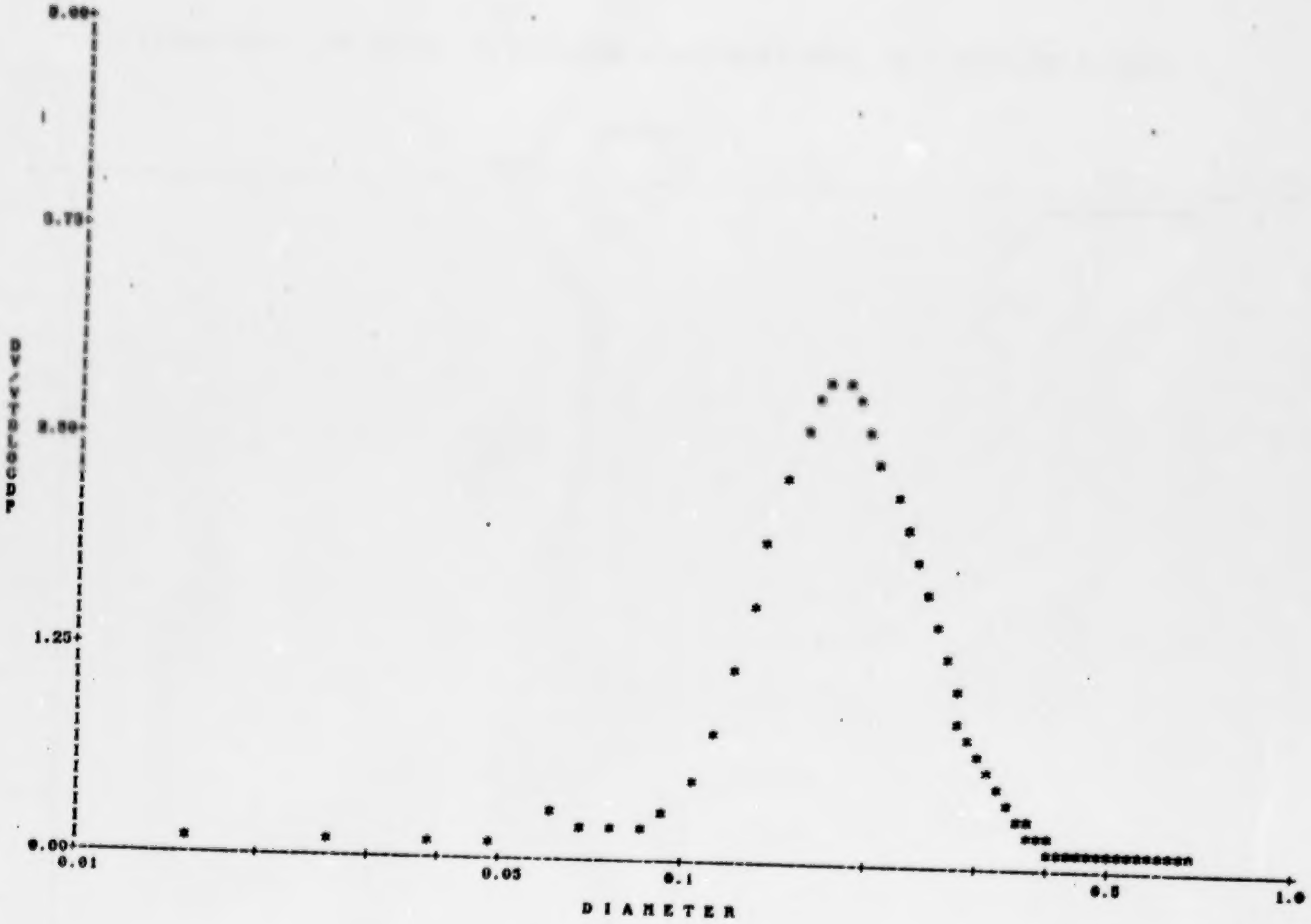

FIGURE 26b. THE VOLUME DISTRIBUTION AFTER FOUR HOURS OF SIMULATION IN RUN 2

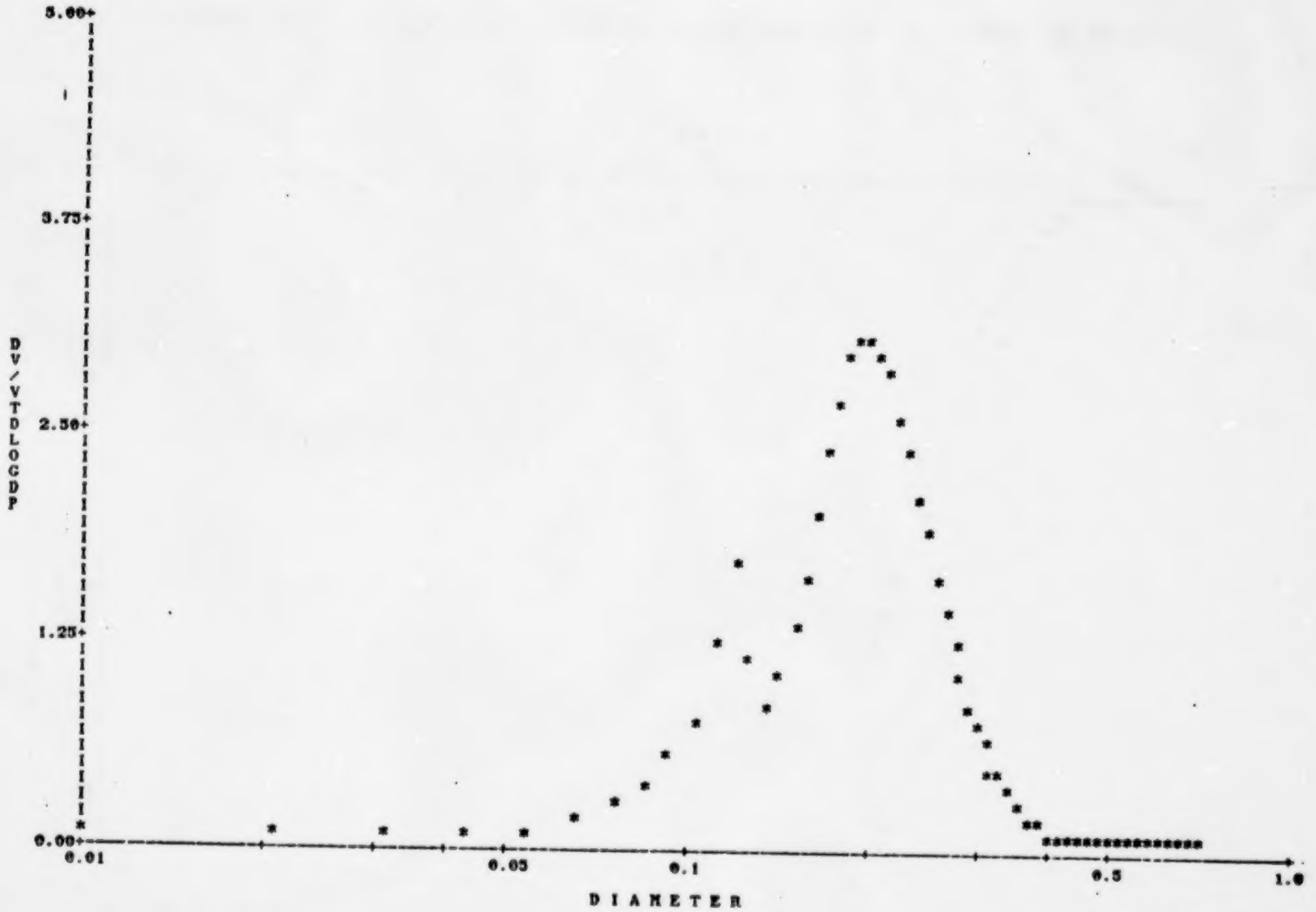

FIGURE 26c. THE VOLUME DISTRIBUTION AFTER SEVEN HOURS OF SIMULATION IN RUN 2

TABLE 17. SURFACE AREA MEAN DIAMETERS CALCULATED FROM EQ. (78)

Hour	Run 1	Run 5	Run 7	Run 10
1	0.077	0.045	0.075	0.074
2	0.075	0.045	0.077	0.072
3	0.075	0.046	0.075	0.074
4	0.074	0.047	0.078	0.074
5	0.082	0.050	0.084	0.082
6	0.098	0.059	0.099	0.098
7	0.11	0.069	0.12	0.12

hours. Unlike the batch system, where the particles were added at a uniform rate, in the trajectory system these particles were emitted at high concentrations over a short period of time, resulting in the observed secondary peak in the distribution. The volume distributions after seven hours of simulation shown in Figures 25c and 26c can be compared with that shown in Figure 27, in which the lead emissions have been removed. In the absence of coagulation the role of the very small particles is to reduce the rate at which volume is added to the accumulation range. We expect this to be true to a lesser extent when coagulation is included because of the high collision rate between very small particles and particles in the accumulation range.

The boundary condition for $\bar{n}_0(D_p,t)$ affects the secondary (small particle) peak and the accumulation range by increasing the number of small particles. The result of this is to increase the rate at which the secondary peak moves to higher particle diameters and to decrease the rate at which volume is added to the accumulation range.

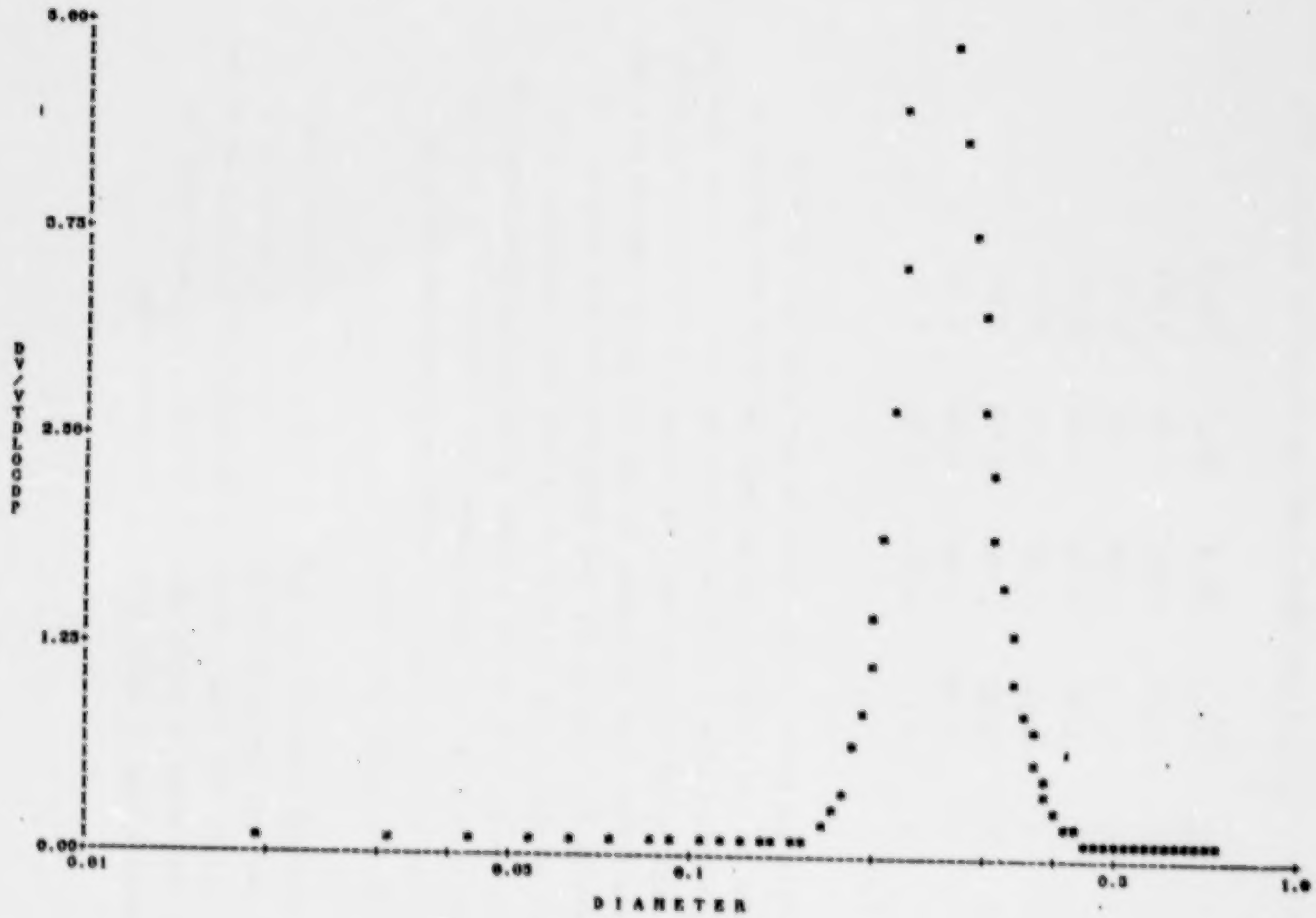

FIGURE 27. THE VOLUME DISTRIBUTION AFTER SEVEN HOURS OF SIMULATION WITHOUT THE LEAD EMISSIONS

2. The Effect of Varying Source and Background Distributions

The purpose of performing Runs 1, 4, 5, and 6 was to study the effect on the predicted volume distribution of a variation in the distribution of either the background or source aerosol with the other aerosol at its original distribution. Shifting the peak of the volume distribution to smaller particle diameters or increasing the variance of the distribution increases the number of particles while maintaining a constant aerosol volume. Because we assumed that the rate of growth of each particle is determined by the number of particles in a unit volume, any change that increases the density of particles in the system slows the growth.

The number distributions after seven hours of simulation in Runs 1, 4, 5, and 6 are compared in Figure 28. [The rapid increase in particle number for the very small particles ($D_p < 0.1$ μm) resulted from the boundary condition of $\bar{n}_0(D_p,t) = 10^4 \mathrm{cm}^{-3} \mu\mathrm{m}^{-1}$ applied at $D_p = 0.01$ μm.] Increasing the variance of the distribution from 0.362 in Run 1 to 0.5 in Run 4 increased the number of sub-0.1 μm particles but only shifted the peak of the volume distribution from 0.20 μm to 0.19 μm and decreased $(\overline{D_p^2})^{1/2}$ slightly. The 10 percent reduction in the peak in the volume distribution at seven hours is attributed to secondary growth occurring on the very small particles instead of on the particles associated with the accumulation range.

In Run 5 the peak of the source distribution was decreased from about 0.16 μm to 0.05 μm. Figure 29 shows the volume distribution after one, three, and seven hours in Run 5. At one hour the original background distribution and the particles added from autos dominate the volume distribution. As the primary sources are added to the aerosol, a second peak associated with this distribution develops. By the third hour there are two distinct peaks in the volume distribution. Continued addition of primary aerosol and secondary growth increase the magnitude of the small particle peak and sharpen it.

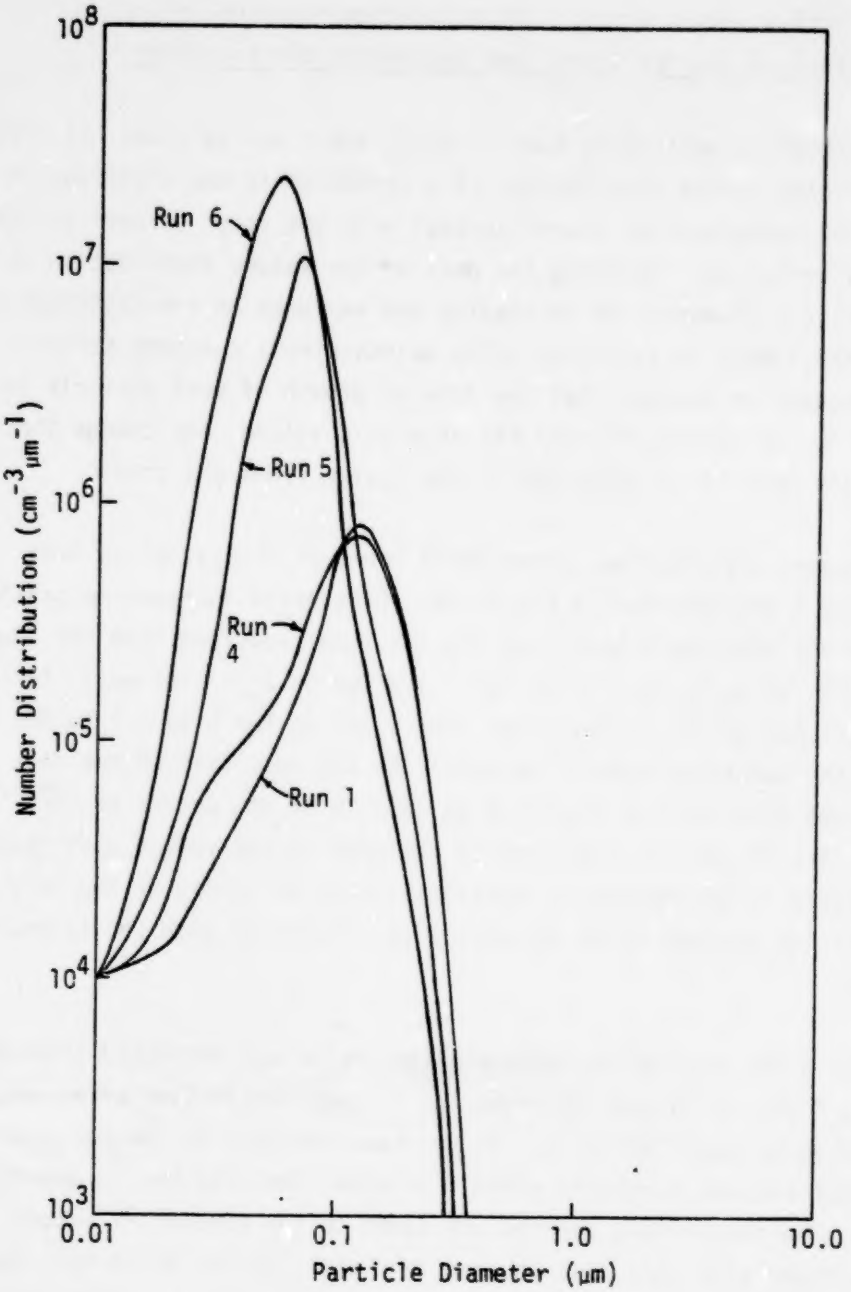

FIGURE 28. THE NUMBER DISTRIBUTIONS AFTER SEVEN HOURS OF SIMULATION IN RUNS 1, 4, 5, AND 6

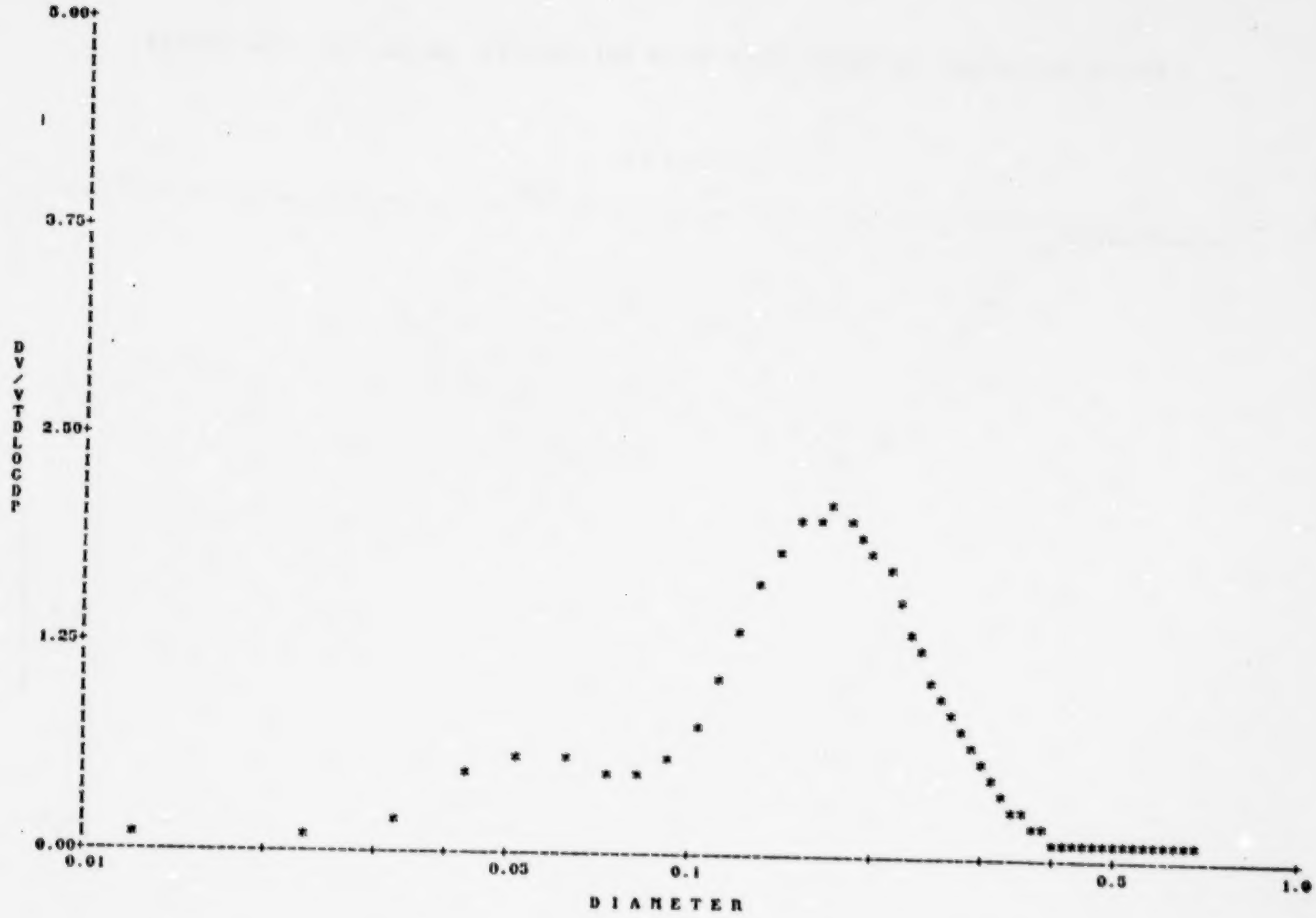

FIGURE 29a. THE VOLUME DISTRIBUTION AFTER ONE HOUR OF SIMULATION IN RUN 5

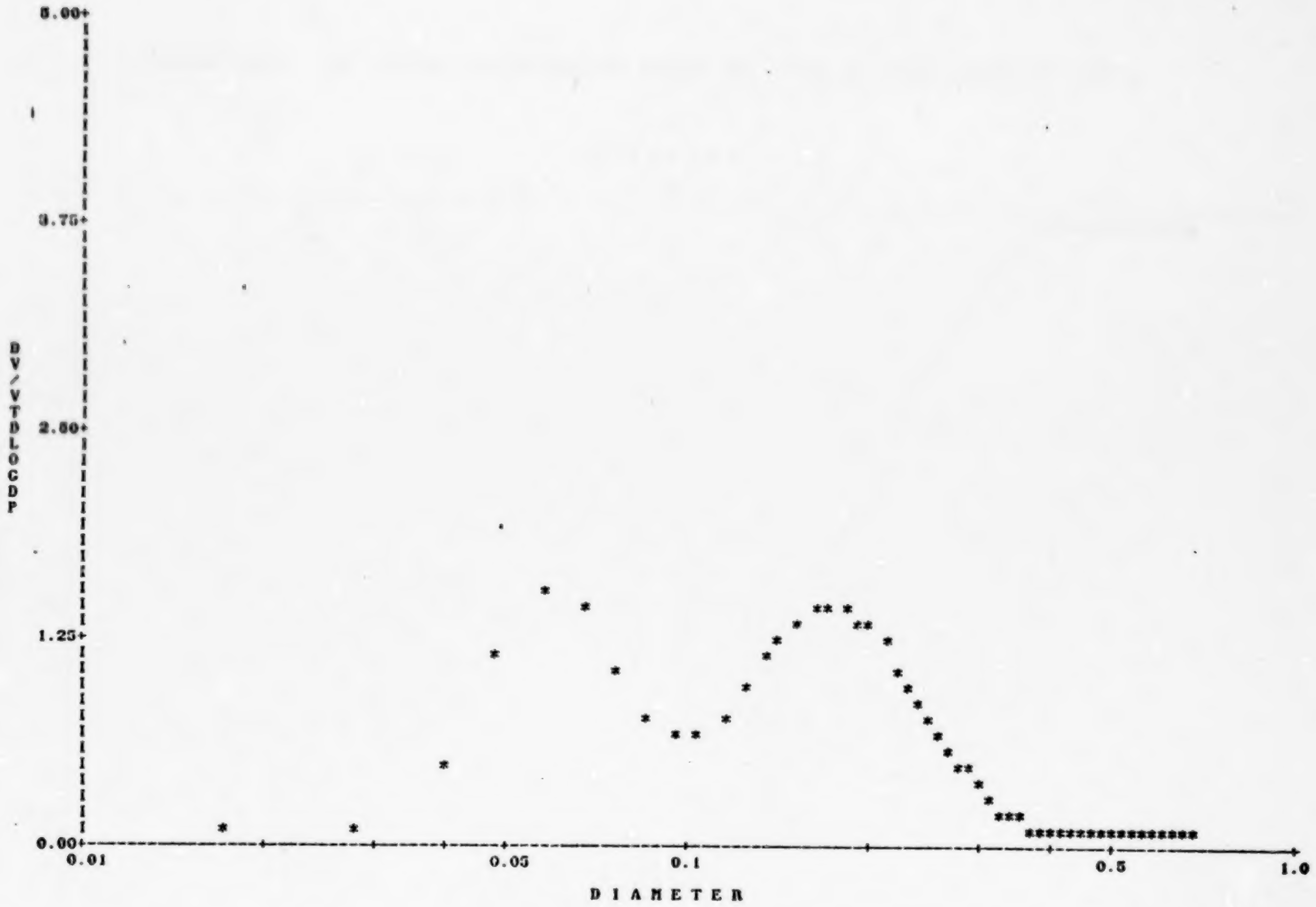

FIGURE 29b. THE VOLUME DISTRIBUTION AFTER THREE HOURS OF SIMULATION IN RUN 5

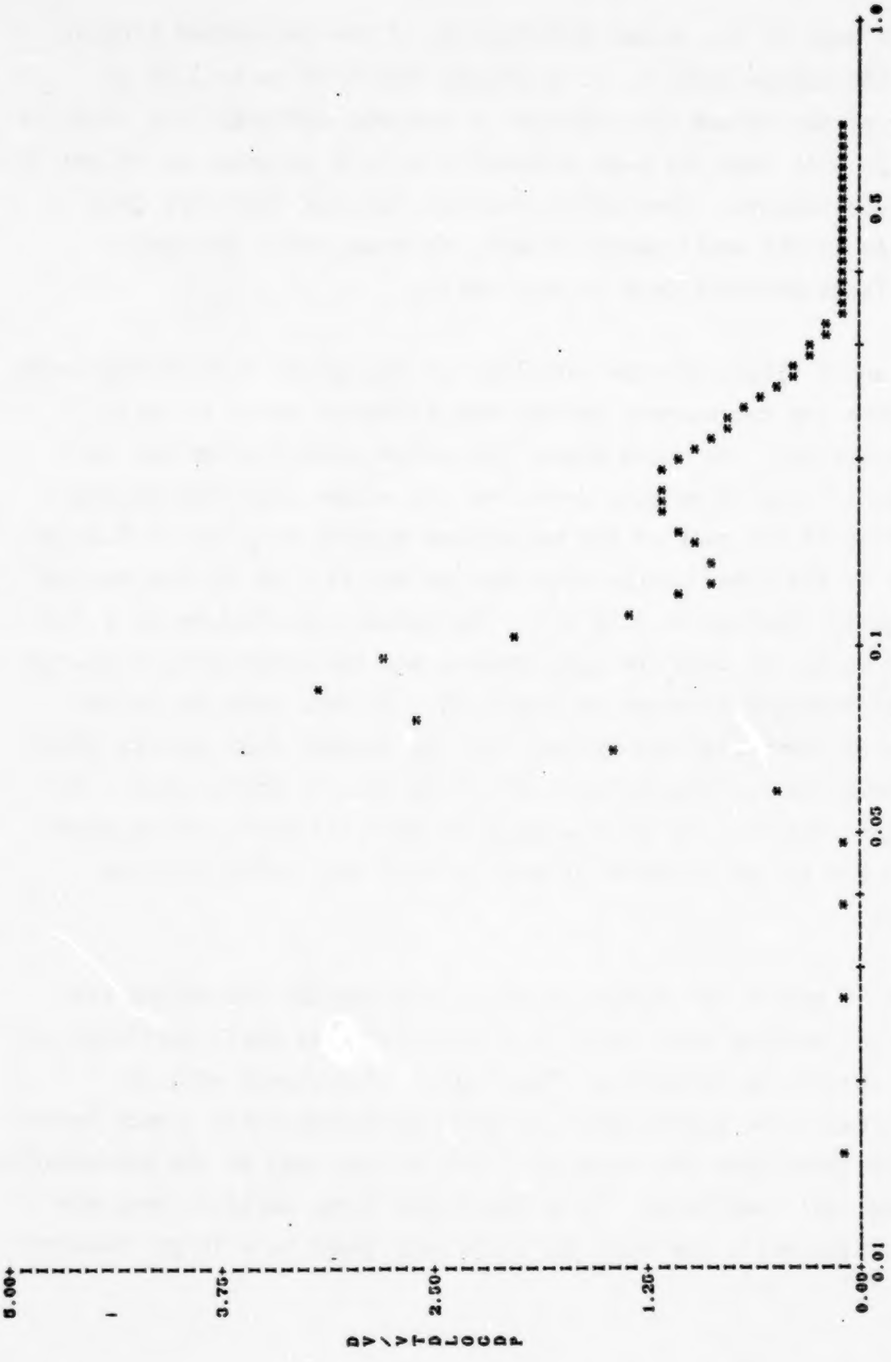

FIGURE 29C. THE VOLUME DISTRIBUTION AFTER SEVEN HOURS OF SIMULATION IN RUN 5

When the peak of the volume distribution of the background aerosol, rather than the source aerosol, is decreased from 0.16 μm to 0.05 μm, the behavior of the volume distribution is somewhat different, as shown in Figure 30. In this case the peak originally at 0.16 μm grows as volume is added from auto exhaust. Eventually, however, because there are many more particles in the small particle peak, it grows until the amplitude of the large particle peak is very small.

Runs 5 and 6 illustrate the variation of the volume distribution with time when there are two sources having very different peaks in their volume distributions. As noted above, the volume distribution has two peaks. In Runs 7 and 12 we considered how the volume distribution might develop in time if the peak of the background distribution was at 0.05 μm and the peak of the other source distribution was at 0.08 μm (the peak of the auto organic remained at 0.16 μm). The volume distribution as a function of time in Run 12 when the auto organic and the other primary sources were of equal strength is shown in Figure 31. In this case the volume distribution of the background aerosol and the aerosol from sources other than the automobile coalesce without any evidence of a double peak. Our results suggest that in the urban atmosphere the size distribution might be broadened due to the presence of many sources with different size distributions.

In Runs 13 and 14 our objective was to examine how the volume distribution might develop when there is a source of very small particles and a source of very large particles. The results (not shown) were as expected: Because the source emitting small particles emits a much larger number of particles than the large particle source, most of the condensation occurs on the small particles. As a result the large particle peak virtually disappears while the small particle peak grows to a larger diameter.

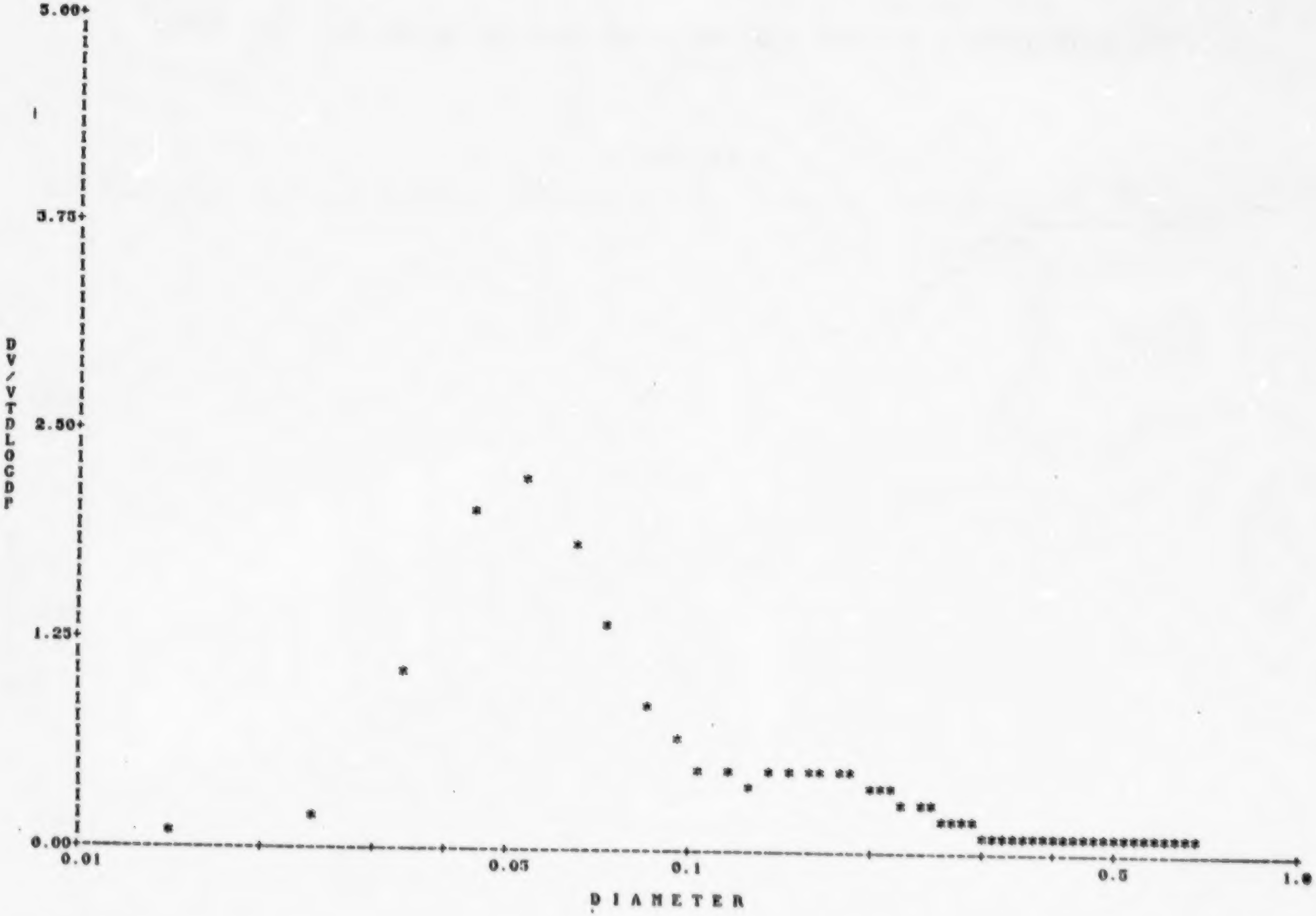

FIGURE 30a. THE VOLUME DISTRUBITION AFTER ONE HOUR OF SIMULATION IN RUN 6

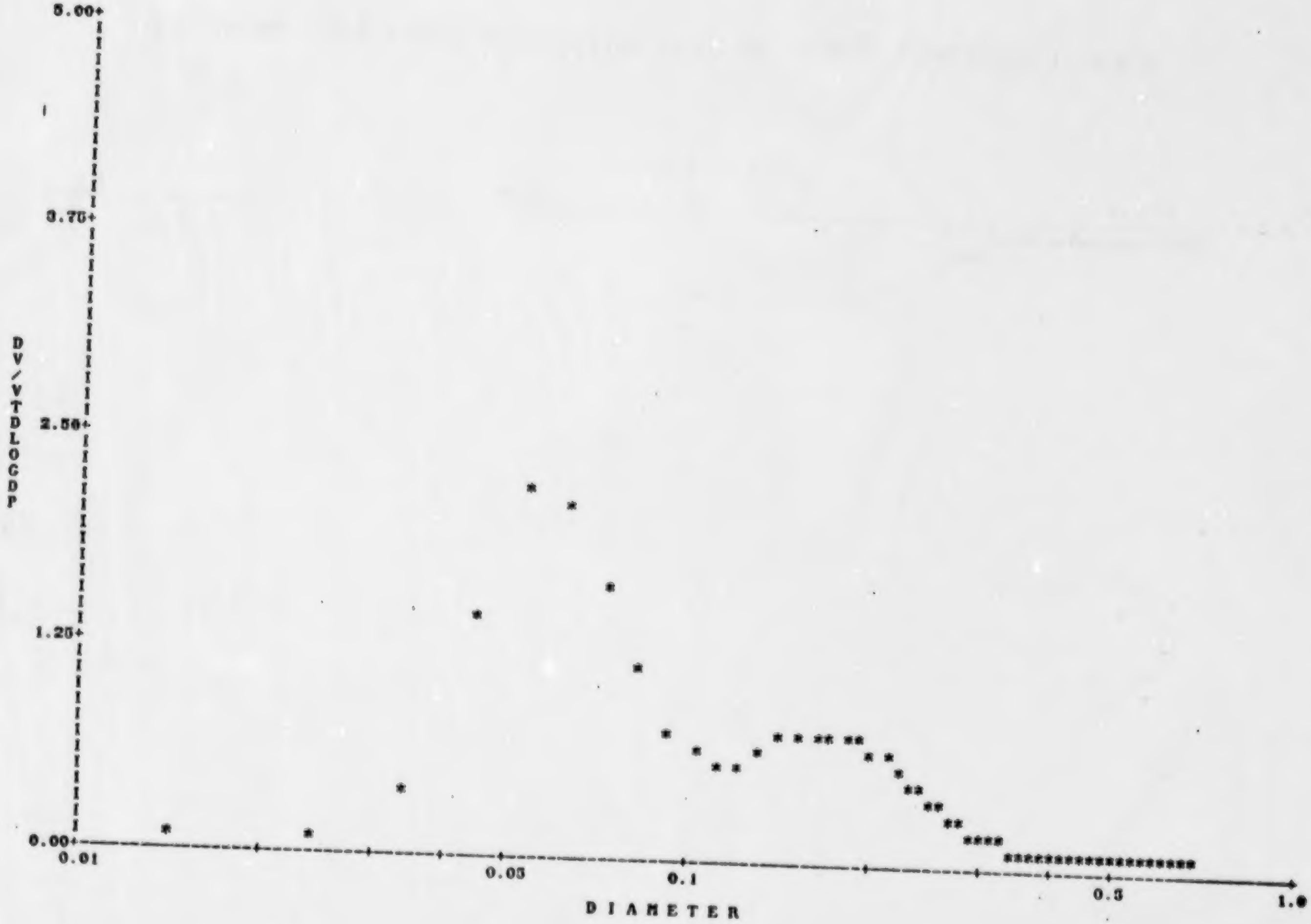

FIGURE 30b. THE VOLUME DISTRIBUTION AFTER THREE HOURS OF SIMULATION IN RUN 6

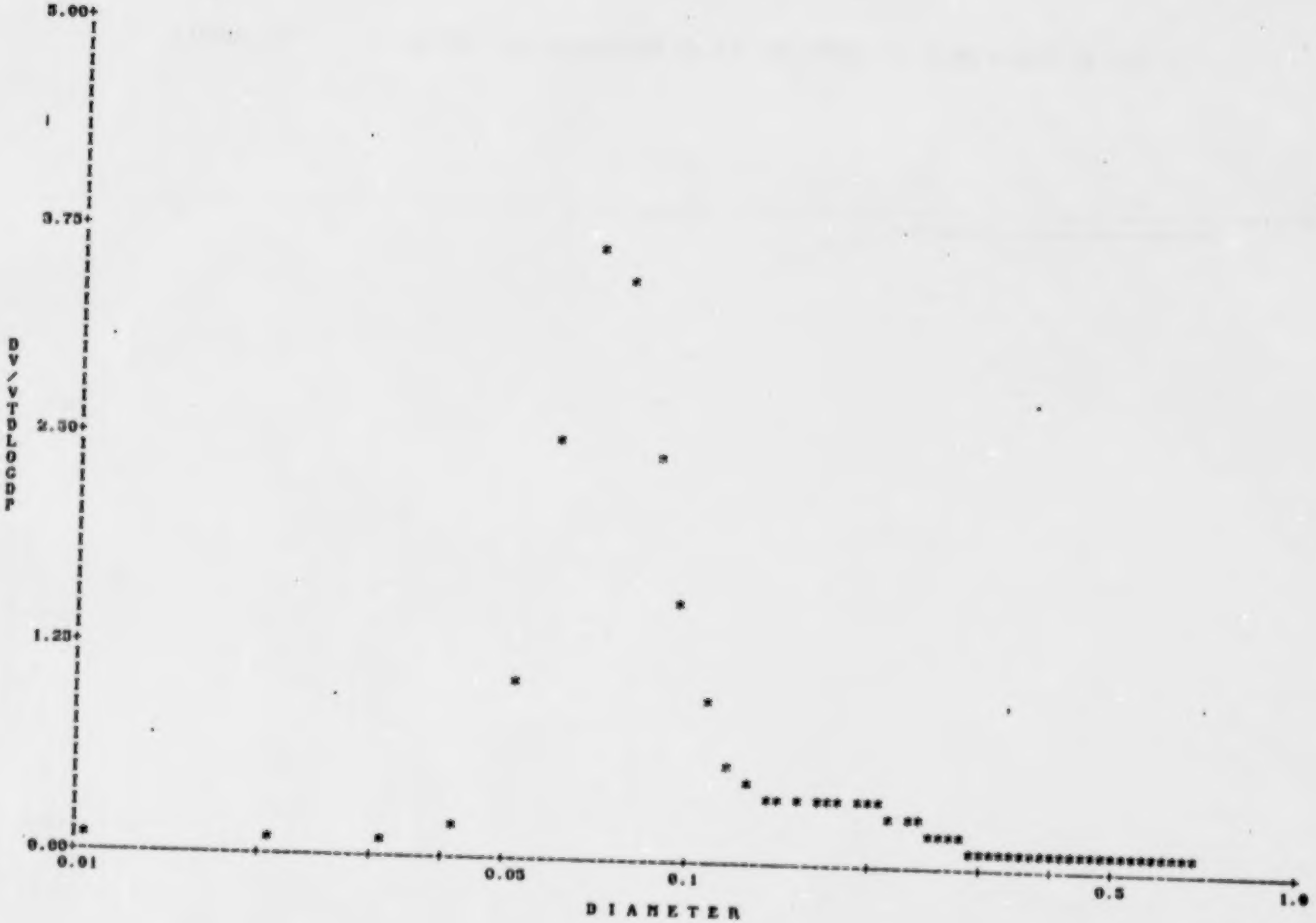

FIGURE 30c. THE VOLUME DISTRIBUTION AFTER SEVEN HOURS OF SIMULATION IN RUN 6

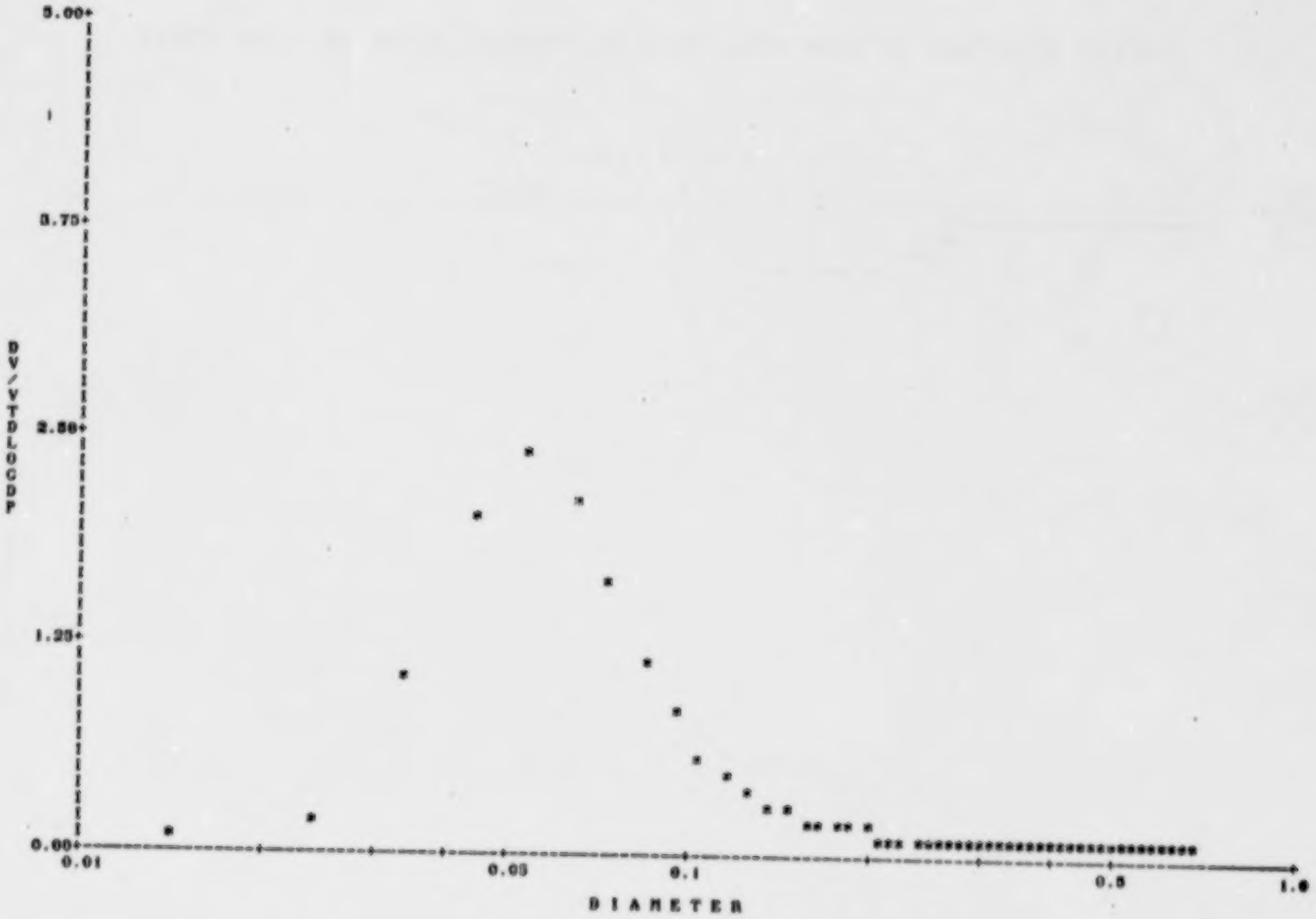

FIGURE 31a. THE VOLUME DISTRIBUTION AFTER ONE HOUR OF SIMULATION IN RUN 12

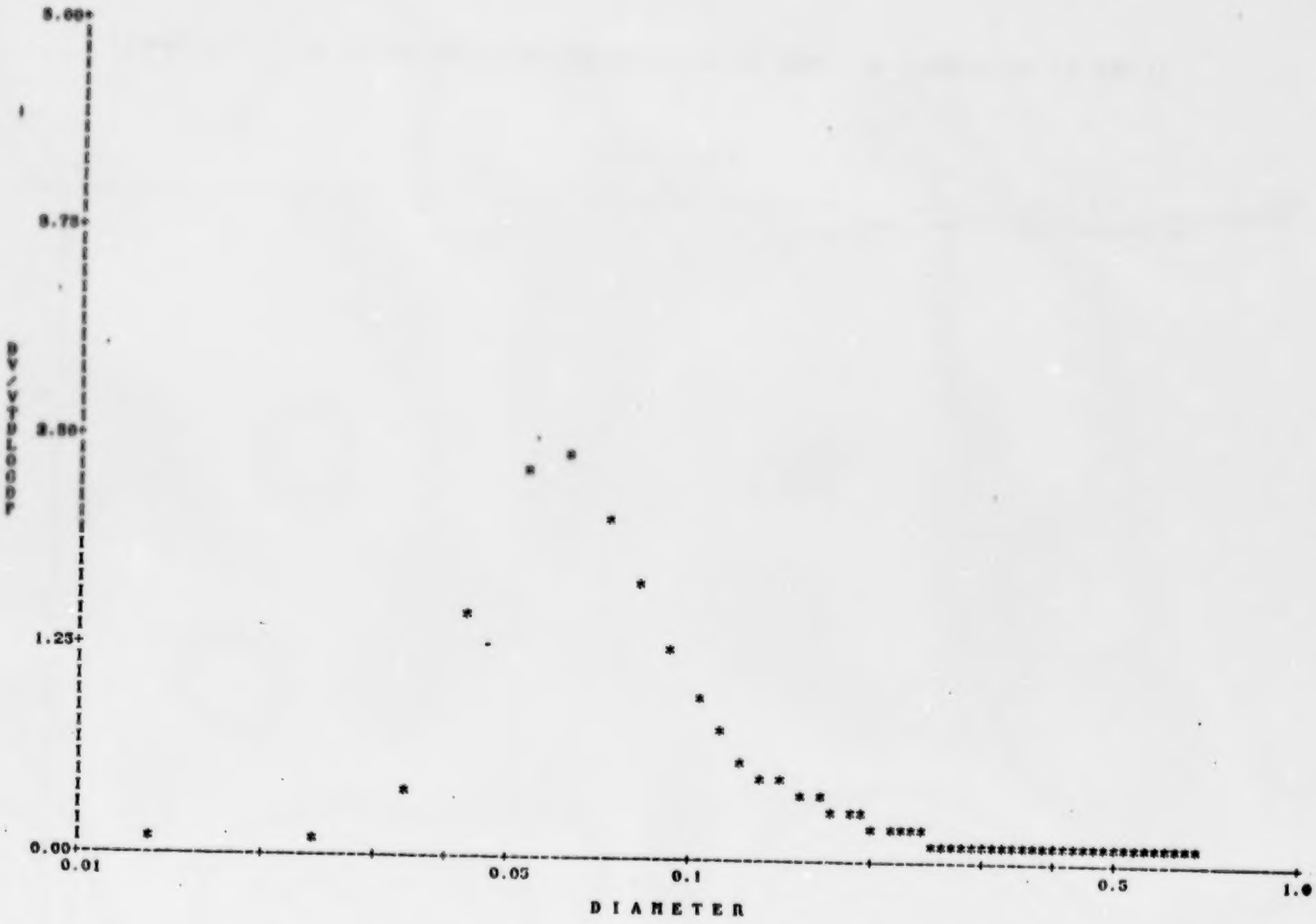

FIGURE 31b. THE VOLUME DISTRIBUTION AFTER THREE HOURS OF SIMULATION IN RUN 12

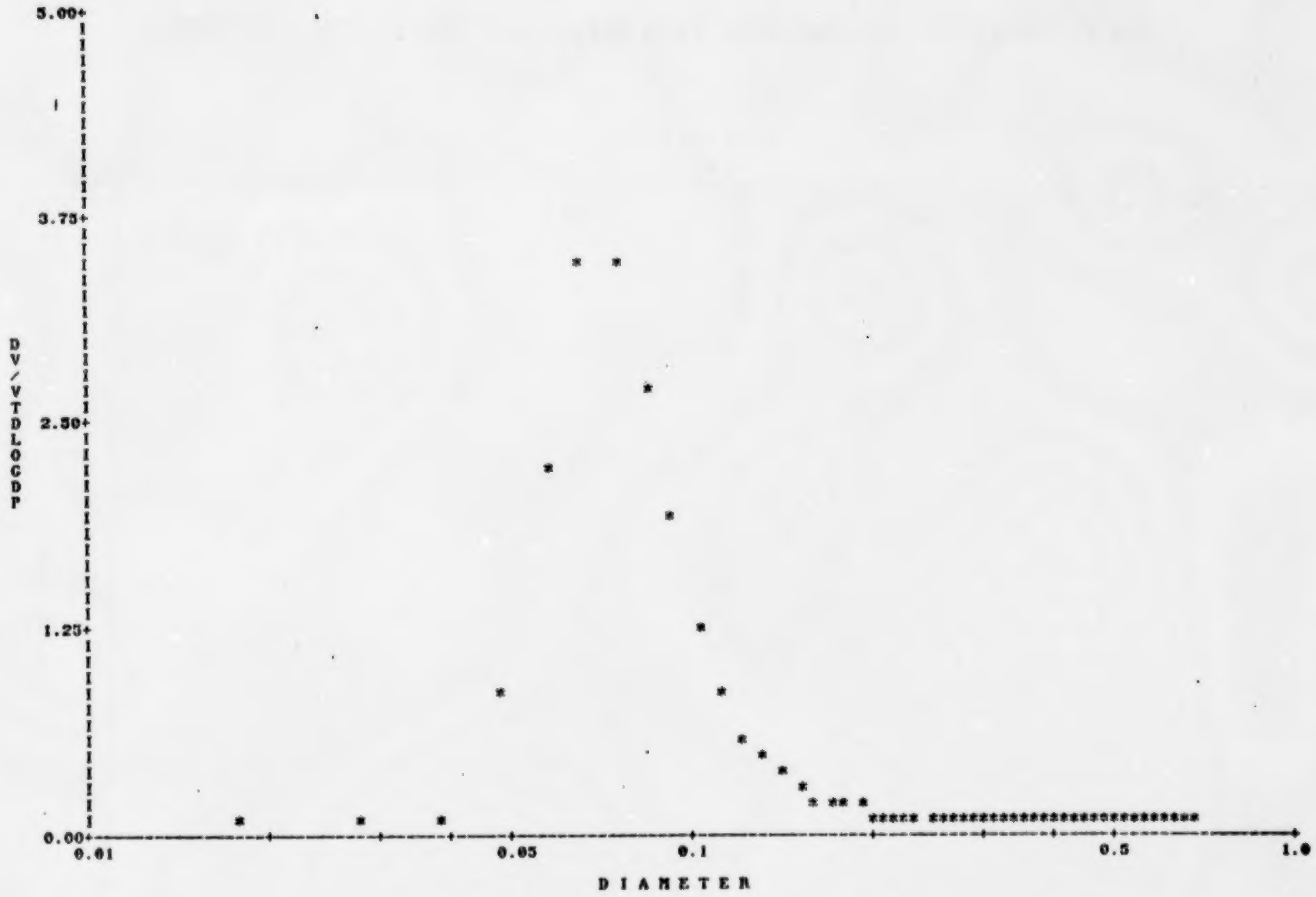

FIGURE 31c. THE VOLUME DISTRIBUTION AFTER SEVEN HOURS OF SIMULATION IN RUN 12

3. The Effect on the Predicted Volume Distribution of Varying The Ratio of Primary to Secondary Volume

Increasing the volume of primary aerosol (while maintaining the same distribution) and decreasing the amount of secondary aerosol volume decreases the rate of growth of the aerosol particles. Runs 5 and 10 in Tables 15 and 16 are similar except that in Run 10 the ratio of primary to secondary aerosol volume was increased from 30/70 to 48/52. Consequently, the number density in Run 10 was approximately 80 percent higher than in Run 5. Because less secondary material must be divided among more particles the rate of growth in Run 10 was considerably slower than in Run 5. In both cases the volume distributions are bimodal, and the mode at smaller particle diameters is associated with nonautomotive sources. The volume distributions after seven hours of simulation are shown in Figure 32. The more rapid rate of growth in Run 5 is apparent in the highly peaked mode of the volume distribution.

We also changed the amount of condensable material available for secondary aerosol by adjusting α, the fraction of the nonmethane hydrocarbons that can react to form condensable material. In the simulations discussed above we set $\alpha = 0.0017$. In Runs 8 and 9 we set $\alpha = 0.095$ and 5×10^{-4}, respectively. In these two runs the aerosol volume densities were 268 $\mu m^3 cm^{-3}$ and 98 $\mu m^3 cm^{-3}$, respectively, compared to an average of about 145 $\mu m^3 cm^{-3}$ in the other simulations. The volume distributions after seven hours of simulation are shown in Figure 33. The distribution in Run 8 reflects the very rapid rate of growth resulting from the added organic material available for condensation. The volume distribution for this run is highly peaked and has two modes, the second attributable to the small particle lead that has grown into the larger particle mode. On the other hand the peak in the volume distribution after seven hours in Run 9 is not as narrow and not as large, reflecting the slower rate of growth. -

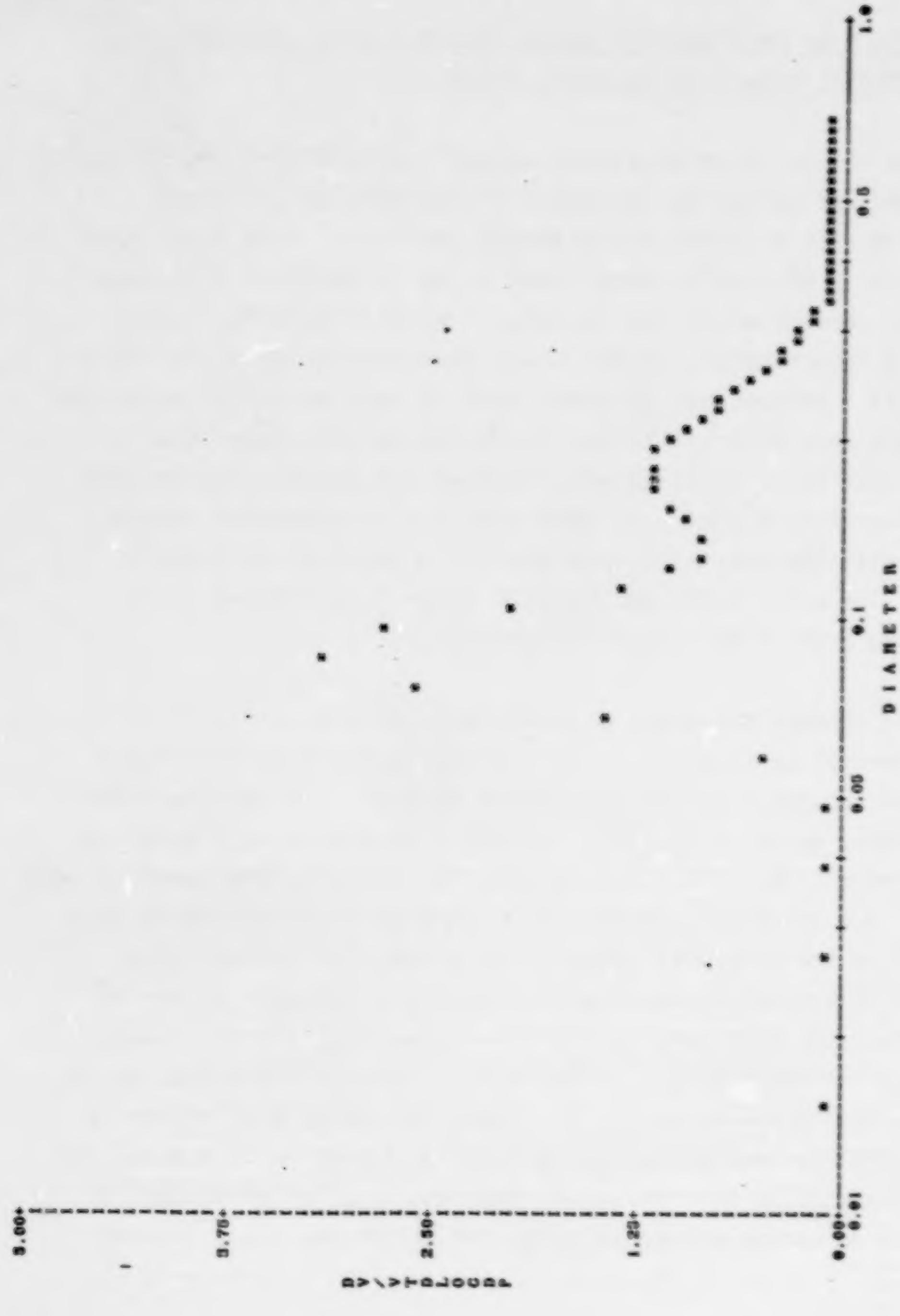

FIGURE 32 a. THE VOLUME DISTRIBUTION AFTER SEVEN HOURS OF SIMULATION IN RUN 5

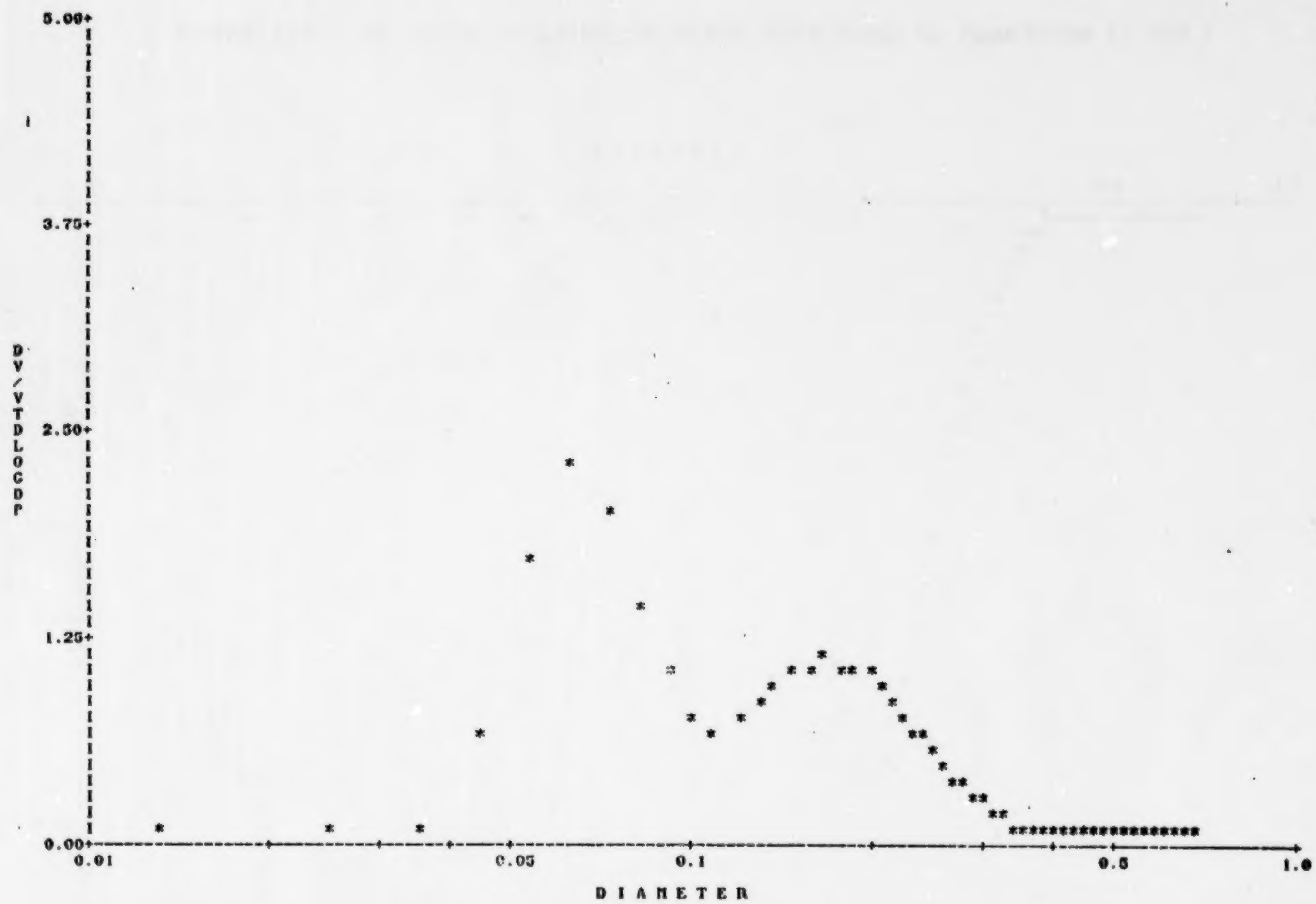

FIGURE 32b. THE VOLUME DISTRIBUTION AFTER SEVEN HOURS OF SIMULATION IN RUN 10

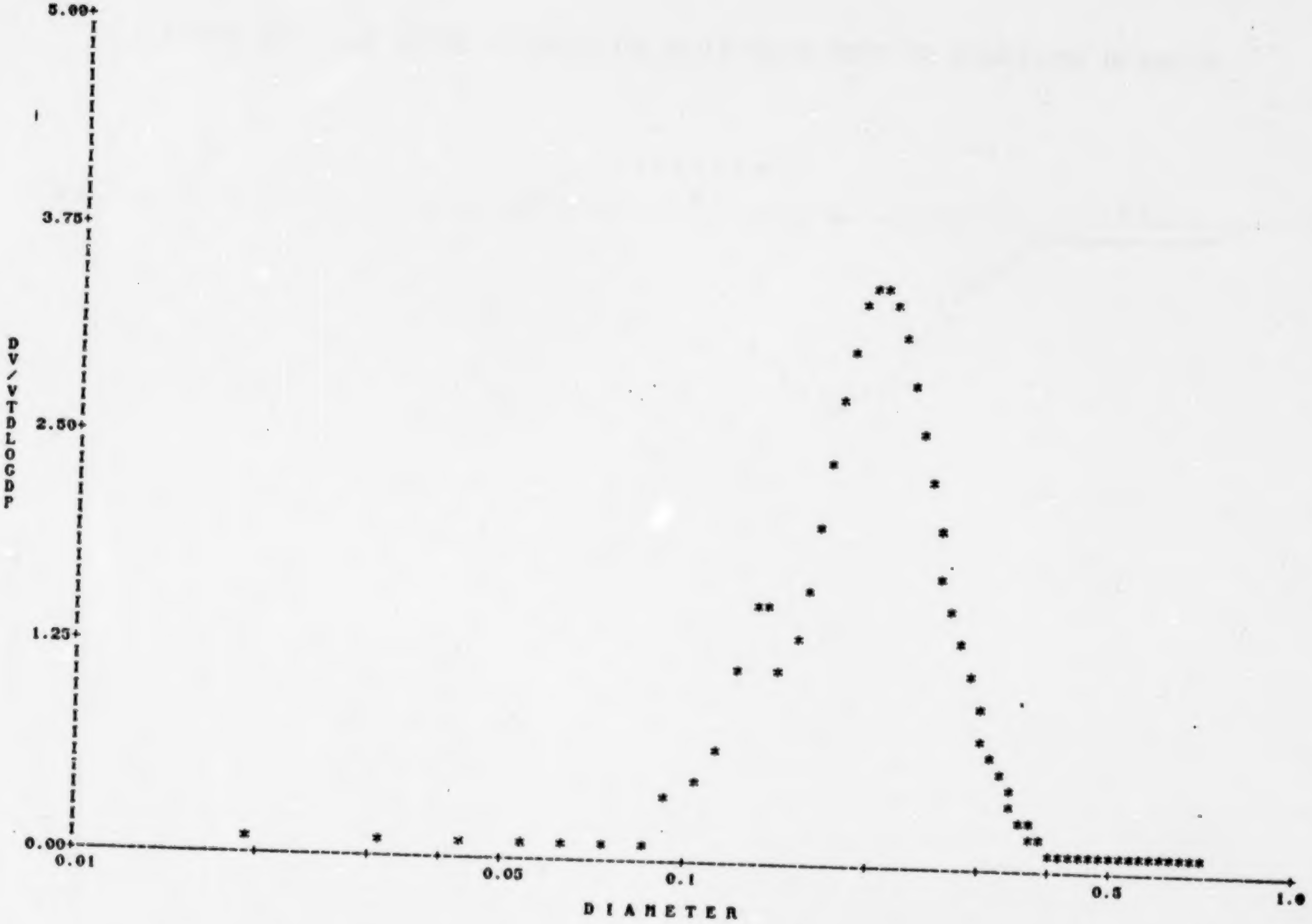

FIGURE 33a. THE VOLUME DISTRIBUTION AFTER SEVEN HOURS OF SIMULATION IN RUN 1

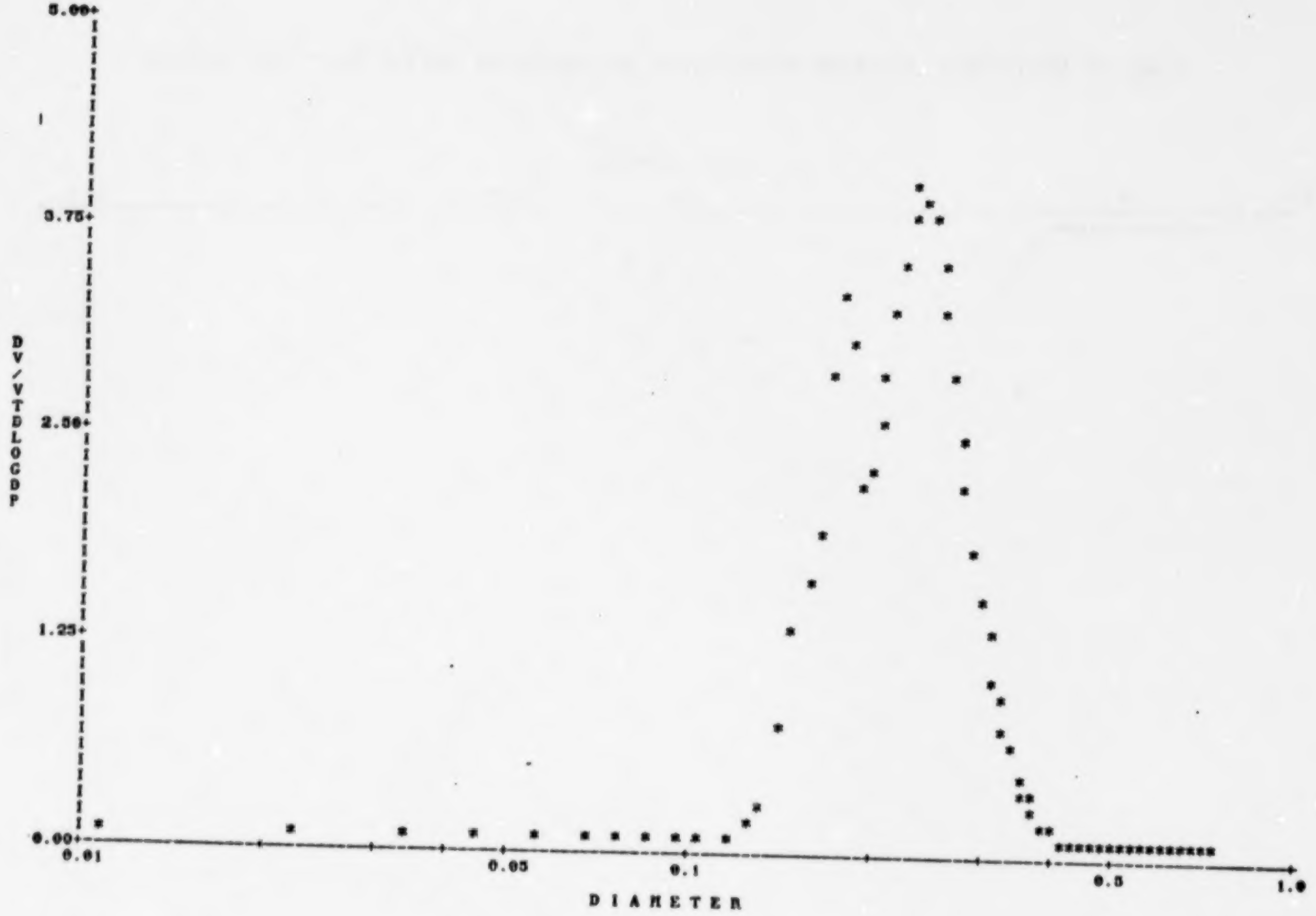

FIGURE 33b. THE VOLUME DISTRIBUTION AFTER SEVEN HOURS OF SIMULATION IN RUN 8

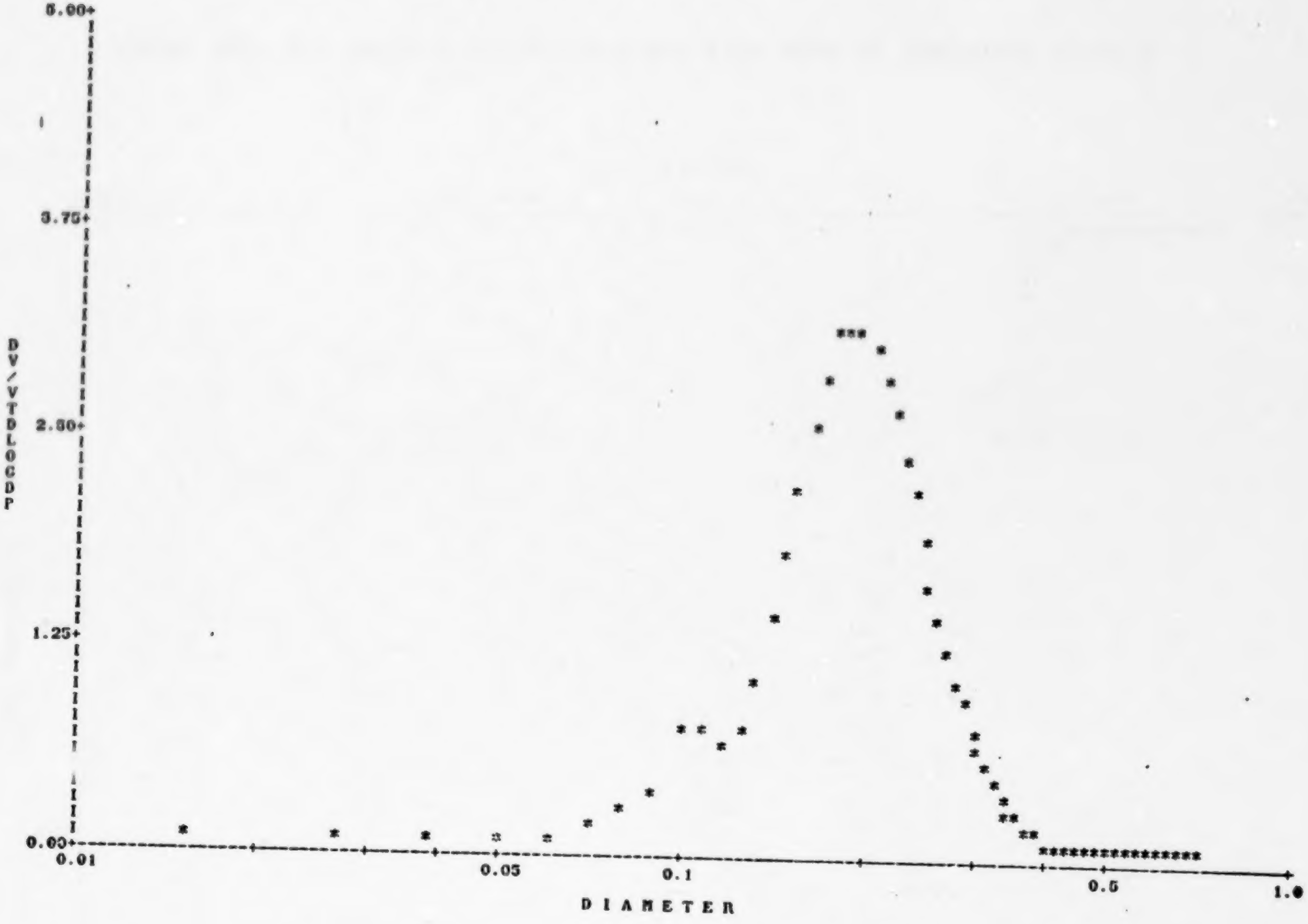

FIGURE 33c. THE VOLUME DISTRIBUTION AFTER SEVEN HOURS OF SIMULATION IN RUN 9

4. The Sensitivity of the Predicted Size Distribution to the Auto Exhaust Distribution

As illustrated earlier, when different sources have volume distributions that overlap, the predicted distribution can be very broad and not have the characteristics of any of the particular source distributions. Our purpose in this phase of the study was to vary the contribution of each source to the total volume. In particular, we wished to ascertain at what point the auto lead and the auto organic distributions would be observed to contribute to the predicted volume distribution. The distributions of the background and the nonautomotive sources that were chosen overlap the auto organic distribution, and the auto organic distribution only becomes apparent when the background and nonautomotive sources become sufficiently small for the auto organic to stand out. In contrast, the lead distribution is composed of very small particles that grow to larger diameters. In general, this distribution can be observed as it moves to larger diameters even when the auto organic is hidden by the other distributions.

The results of this sensitivity study are tabulated in Table 18. The first column gives the ratio of primary volume to secondary volume, the second column gives the ratio of the volume of auto emissions to the volume of other emissions, and the third column lists the aerosol volume density after seven hours. The next six columns list the parameters of each of the distributions, and the final column lists that part of the auto emissions that could be observed.

In all of these simulations the judgment regarding the auto organic distribution was subjective. Even with a 70/30 split (35 percent auto organic), the auto organic was very well hidden by the other distributions.

TABLE 18. SENSITIVITY OF PREDICTED VOLUME DISTRIBUTIONS TO AUTOMOBILE LEAD AND ORGANIC DISTRIBUTION

Primary/ Secondary	Auto/ Other	Total Volume ($\mu m^3 cm^{-3}$)	μ_{other}	σ_{other}	μ_{auto}	σ_{auto}	μ_b	σ_b	Lead, Organic, Both
60/40	31/69	102	-1.11	0.5	-1.802	0.362	-1.2	0.523	lead
60/40	31/69	104	-2.50	0.6	-1.802	0.362	-1.2	0.523	none
60/40	70/30	95	-1.11	0.5	-1.802	0.362	-1.2	0.523	both
60/40	50/50	102	-2.50	0.6	-1.802	0.362	-1.2	0.523	none
60/40	70/30	94	-1.11	0.5	-1.802	0.362	-1.2	0.523	both
60/40	70/30	93	-1.11	0.6	-1.802	0.362	-1.2	0.523	both
60/40	40/60	101	-1.11	0.5	-1.802	0.362	-1.2	0.523	lead
60/40	70/30	94	-2.50	0.6	-1.802	0.362	-1.2	0.523	lead

V NUMERICAL SOLUTION OF THE DYNAMIC EQUATION FOR PARTICULATE SYSTEMS

Thus far we have neglected the influence of coagulation on the size distribution dynamics of the urban aerosol. Coagulation is important in the immediate vicinity of sources, where particle concentrations are high enough for coagulation to proceed at an appreciable rate. Although we do not consider near-source phenomena in this study, the ability to solve coagulation problems will be important in eventual aerosol modeling applications. Thus, we chose to devote a portion of our overall effort to the task of solving the general particulate balance equation, which includes the coagulation process.

A. INTRODUCTION

The state of a spatially and chemically homogeneous particulate system is described by its size distribution density function, $n_v(v,t)$, where $n_v(v,t)\ dv$ is the number of particles per unit volume of fluid having volumes in the range v to v + dv. The dynamics of such a system in which individual particles may grow through accretion of material from the fluid phase (or shrink by loss of material) and in which particles may collide and coagulate are described by the general particulate balance equation (Drake, 1972; Ramabhadran et al., 1976).

$$\begin{aligned}\frac{\partial n_v(v,t)}{\partial t} &= -\frac{\partial}{\partial v}\left[I_v(v,t)n_v(v,t)\right] \\ &+ \int_0^{v/2} \beta_v(v-\tilde{v},\tilde{v})\ n_v(v-\tilde{v},t)n_v(\tilde{v},t)\ d\tilde{v} \\ &- n_v(v,t)\int_0^{\infty} \beta_v(v,\tilde{v})n_v(\tilde{v},t)\ d\tilde{v} \\ &+ S_v[n_v(v,t),v,t] \qquad (79)\end{aligned}$$

where $I_v(v,t) = dv/dt$, the rate of change of the volume of a particle of volume v by transfer of material between the particle and the fluid phase, $\beta v(v,\tilde{v})$ is the coagulation coefficient for particles of volumes v and $\tilde{v}$, and S_v is the net rate of addition of fresh particles into the system. The initial and boundary conditions required for Eq. (79) are generally stated as

$$n_v(v,0) = n_{v_0}(v) \qquad (80)$$

and

$$n_v(0,t) = 0 \qquad (81)$$

respectively. (The latter condition indicates that there are no particles of zero size.)

The first term on the right hand side of Eq. (79) represents the rate of growth of particles by transfer of material to individual particles. The second term represents the rate of accumulation of particles in the size range $(v, v + dv)$ by collision of two particles of volumes $v-\tilde{v}$ and $\tilde{v}$ to form a particle of volume v (assuming conservation of volume during coagulation). The third term represents the rate of loss of particles in the size range $(v, v + dv)$ by collision with all other particles. The last term represents all particle sources and sinks. Equation (79) arises in a wide variety of physical contexts, such as colloid chemistry, atmospheric aerosol dynamics, crystallization kinetics, and biological population dynamics.

Although Eq. (79) is well-suited for analytical solution, because v usually ranges over many orders of magnitude, it is inappropriate for numerical solution. Equation (79) can be written in terms of particle diameter D (assuming spherical particles),

$$\begin{aligned}\frac{\partial n_D(D,t)}{\partial t} &= -\frac{\partial}{\partial D}\left[I_D(D,t)n_D(D,t)\right] \\ &+ D^2\int_0^{D/\sqrt[3]{2}} \beta_D(\psi,\tilde{D})n_D(\psi,t)n_D(\tilde{D},t)\,\frac{d\tilde{D}}{\psi^2} \\ &- n_D(D,t)\int_0^{\infty}\beta_D(D,\tilde{D})n_D(\tilde{D},t)\,d\tilde{D} \\ &+ S_D\left[n_D(D,t),D,t\right]\end{aligned} \qquad (82)$$

where $n_D(D,t) = (\pi D^2/2)n_v(v,t)$, $\psi = (D^3 - \tilde{D}^3)^{1/3}$, and $I_D = dD/dt$. For the description of actual particulate systems Eq. (82) is generally preferable to Eq. (79) because of the reduction in the range of D as compared to v.

In spite of the great importance of Eqs. (79) and (82) to particulate system dynamics, solutions have been difficult to obtain. Analytical solutions are available only for a few simple forms of the initial conditions, $\beta_v(v,\tilde{v})$, $I_v(v,t)$ and $S_v[n(v,t), v,t]$ (Ramabhadran et al., 1976; Golovin, 1963; Scott, 1968; Peterson et al., in press). Numerical solutions have been reported (Hidy, 1965; Twomey, 1966; Mockros et al., 1967; Takahashi and Kasahara, 1968; Suzuki et al., 1969; Cohen and Vaughan, 1971; Gillette, 1972; Berry, 1967; Burgmeier et al., 1973; Singh and Ramkrishna, 1975; Middleton and Brock, 1976) but the optimum method for solving Eq. (79) has not been determined.

In this work we report on a numerical technique developed to solve the general dynamic equation based on orthogonal collocation on finite elements. In Section B we discuss the proper scaling of the equation, in Section C we develop the method, and Section D we describe the results of applying the method to several test problems for which analytical or asymptotic solutions are available. It is our conclusion that from the standpoint of accuracy and efficiency the method presented here represents the most attractive technique for the solution of Eqs. (79) and (82) currently available.

B. SCALING OF THE EQUATIONS

Equations (79) and (82) must be rescaled to a finite domain prior to numerical solution. We select a dimensionless finite particle size domain scaled from zero to one. Let us denote v_a, v_b and D_a,D_b as the chosen lower and upper limits on the volume and diameter, respectively, that will be employed in the numerical solution. Because the range of D is smaller than that of v, we will generally want to solve Eq. (82), rather than Eq. (79), numerically. Two possible transformations to a finite particle size domain (D_a,D_b) are linear and logarithmic:

$$u = \frac{D-D_a}{D_b-D_a} \quad , \tag{83}$$

and

$$w = \frac{\ell n(D/D_a)}{\ell n(D_b/D_a)} \quad . \qquad (84)$$

For the representation of real systems, the logarithmic transformation of Eq. (84) is preferred over the linear transformation of Eq. (83). Generally, the larger number of particles occur in the smallest size range, and Eq. (84) more effectively expands that region. If significant effects occur equally over the entire particle size range, then a linear transformation [Eq. (83)] is preferred. The use of a finite particle size domain introduces errors in that the general dynamic equation is based on an infinite particle size domain. For an actual particulate system, however, there are usually upper and lower bounds on the sizes of the particles that exist. In theory, D_a should be chosen as that of the smallest existing particle. (Although the general equations are written as if there exists a continuous spectrum of sizes down to zero, there is actually a lower cut-off in a real system.) D_b should be chosen large enough to include nearly all the particles in the system, yet small enough so that the region of major dynamic activity is not obscured. We will discuss the choice of D_a and D_b subsequently.

The analytical solutions of Eq. (79) currently available are based on rather idealized forms of the initial conditions, β_v, I_v, and S_v (Ramabhadran et al. 1976; Golovin, 1963; Scott, 1968; Peterson et al., in press). For that reason, these solutions do not correspond directly to realistic physical conditions. Nevertheless, the use of available analytical solutions represents the only unambiguous way to ascertain the accuracy of the numerical solutions. Thus, in this work we will concentrate on obtaining numerical solutions for those cases for which analytical solutions are available.

Using Eq. (84), Eq. (82) becomes

$$\frac{\partial m(w,t)}{\partial t} = - \frac{\partial}{\partial w} [I(w,t)m(w,t)]$$

$$+ \zeta^{3w} \int_{0}^{w-\frac{\ell n2}{3\ell n\zeta}} \beta(x,z)m(x,t)m(z,t) \frac{dz}{\zeta^{3w}-\zeta^{3z}} - m(w,t)\int_{0}^{1} \beta(w,z)m(z,t)\, dz$$

$$+ S[m(w,t),w,t] \quad , \qquad (85)$$

where

$$x = \frac{\ell n(\zeta^{3w}-\zeta^{3z})}{3\ell n\zeta} \quad ,$$

$$\zeta = D_b/D_a \quad , \qquad (86)$$

and

$$m(w,t) = D\ \ell n\, \zeta\, n_D(D,t) \qquad (87)$$

$$S = D_a\ \zeta^w\ \ell n\ \zeta\ S_D \quad . \qquad (88)$$

From Eq. (87), we can relate $m(w,t)$ and $n_v(v,t)$ as follows:

$$n_v(v,t) = \frac{2}{\pi \ell n\zeta D^3} m(w,t) \quad . \qquad (89)$$

C. ORTHOGONAL COLLOCATION ON FINITE ELEMENTS

The most promising class of methods for solving Eq. (85) is that based on the methods of weighted residuals, in which the form of the solution is assumed in terms of a complete set of functions (generally polynomials) and substituted into the governing equation (Finlayson, 1972; Villadsen and Stewart, 1967). To produce equations for the unknown coefficients of the expansion, the equation is multiplied by a weight factor, which is dependent on the method used, and integrated over the domain of interest. Among all the commonly used methods of weighted residuals, such as orthogonal collocation, the Galerkin method and the method of moments, only orthogonal collocation does not require extensive integral evaluations. Therefore, orthogonal collocation emerges as the most attractive method of weighted residuals for Eq. (85).

In the traditional application of orthogonal collocation a finite expansion of order $\bar{M}$ is forced to satisfy the differential equation at $\bar{M}+1$ predetermined collocation points. For $\bar{M}\rightarrow\infty$, the expansion will satisfy the differential equation at an infinite number of points in the region and at an infinite number of points at the boundary. Then the expansion by definition is a representation of the exact solution. However, due to the large variations in magnitude of m(w,t), a single high order polynomial fit is not feasible. Therefore, the finite element technique combined with orthogonal collocation (Martin and Carey, 1973; Carey and Finlayson, 1975) represents a promising approach.

In the method of orthogonal collocation on finite elements the domain of the independent variable is divided into elements within which the dependent variable is represented by a polynomial, often a cubic. At the grid points between elements the distributions and their derivatives are forced to be continuous. Within each element the independent variable is linearly rescaled from 0 to 1 to avoid numerical round off errors, and collocation points are taken as the roots of the shifted Legendre polynomial.

Dividing the distribution, m(w,t) into M elements and using a cubic polynomial in each element results in the following representation of m(w,t) in the _i_th element,

$$m(w,t) = A_{i,1}(t) + A_{i,2}(t)y_i + A_{i,3}(t)y_i^2 + A_{i,4}(t)y_i^3$$

$$i = 1,2,\ldots, M \,, \qquad (90)$$

where $A_{i,j}$ is the $\underline{j}$th coefficient of the $\underline{i}$th element, and $y_i = (w-w_{i-1})/(w_i-w_{i-1})$ for $w_{i-1} < w \leq w_i$. Imposing the condition of continuity of m(w,t) and its first derivative at the grid points gives

$$A_{i,1} + A_{i,2} + A_{i,3} + A_{i,4} = A_{i+1,1} \tag{91}$$

$$A_{i,2} + 2A_{i,3} + 3A_{i,4} = \frac{(w_i-w_{i-1})}{(w_{i+1}-w_i)} A_{i+1,2} \quad . \tag{92}$$

At each collocation point η within each element we have

$$\frac{dA_{i,1}}{dt} + \eta \frac{dA_{i,2}}{dt} + \eta^2 \frac{dA_{i,3}}{dt} + \eta^3 \frac{dA_{i,4}}{dt} = B_{i,k} \tag{93}$$

and where $B_{i,k}$ represents the right hand side of Eq. (85) for the $\underline{k}$th collocation point in the $\underline{i}$th element and $w = \eta(w_i - w_{i-1}) + w_{i-1}$. Using Eqs. (91) and (92) we can derive the following set of 2M+2 linear algebraic equations for the unknown coefficients,

$$(1 - 3\eta_k^2 + 2\eta_k^3) \frac{dA_{i,1}}{dt} + (\eta_k - 2\eta_k^2 + \eta_k^3) \frac{dA_{i,2}}{dt} + (3\eta_k^2 - 2\eta_k^3) \frac{dA_{i+1,1}}{dt}$$

$$\frac{(w_i-w_{i-1})}{(w_{i+1}-w_i)} (\eta_k^3 - \eta_k^2) \frac{dA_{i+1,2}}{dt} = B_{i,k} \tag{94}$$

$$i = 2,\dots, M-1; \qquad k = 1,2$$

$$i = 1; \quad k = 1,2,3 \quad ,$$

and

$$\frac{dA_{M,1}}{dt} + \eta_k \frac{dA_{M,2}}{dt} + \eta_k^2 \frac{dA_{M,3}}{dt} + \eta_k^3 \frac{dA_{M,4}}{dt} = B_{M,k}$$

$$k = 1,2,3 \quad . \tag{95}$$

When placed in conventional matrix form, Eqs. (94) and (95) lead to a banded matrix of bandwidth 7 that can be inverted easily. Since the elements of the matrix are time independent, elimination need only be carried out once. To obtain initial conditions for the coefficients $A_{i,j}$, Eqs. (94) and (95) are solved using the initial distribution $m(w,0)$ at the corresponding collocation points for $B_{i,k}$, and $dA_{i,j}/dt$ is replaced by $A_{i,j}$. If $I(w,t)$ is nonzero for $t > 0$, $A_{1,1}$ is fixed at $m(0,t)$, and the first row and column of the matrix is deleted.

Usually when applying orthogonal collocation to differential equations it is not the expansion coefficients that are solved for, but the dependent variable at the collocation points (Finlayson, 1972). For Eq. (85) it is not convenient to implement the method in this manner. For example, if collocation points are taken at w_j, $j = 1, \ldots, 2M+2$, it is not possible to solve directly for all $m(w_j,t)$ in terms of $m(w_k,t)$, $K = 1, \ldots, 2M+2$. Using any common quadrature technique the integrand of the first integral in Eq. (85) contains $m(w_j,t)$ and $m(x_k,t)$. However, x_k will not necessarily be one of the collocation points w_k, leading to an unclosed set of ordinary differential equations for the values of $m(w_j,t)$. To circumvent this problem two approaches have been taken. In Middleton and Brock (1976) a cubic spline interpolation was used, requiring curve fitting at each time step. In this work the coefficients of the expansion are obtained directly. In the applications, the differential equations for the $A_{i,j}$ were solved with a Runge-Kutta-Gill-Adams-Moulton predictor corrector routine. Integrals were evaluated using a 40-point Gauss-Legendre quadrature.

The final consideration is the location of the finite elements. In Carey and Finlayson (1975) it is suggested that the elements be located to minimize the residual. Although this is an excellent criterion, it would require a costly iterative procedure in the present application. Without any prior knowledge of the behavior of $m(w,t)$, the elements were equally spaced in w, or in terms of a dimensionless diameter.

D. NUMERICAL IMPLEMENTATION

We will consider the exponential initial volume distribution.

$$n_{v_0}(v) = \frac{N_0}{\nu_0} e^{-\bar{v}} \qquad (96)$$

where N_0 is the total initial number of particles, ν_0 is the mean initial volume, and $\bar{v} = v/\nu_0$.

Because the mechanism of coagulation poses the greatest numerical difficulty, we will first consider the solution of Eq. (85) in the absence of growth and sources. In this case we will consider two different collision mechanisms, $\beta_v = \beta_0$ and $\beta_v = \beta_1(v + \bar{v})$. Then, the effect of simultaneous coagulation and growth will be studied. As mentioned previously, in actual particulate systems an upper limit to the particle size exists because of removal mechanisms, such as sedimentation or deposition. Therefore, the effects on the distribution of a first order removal mechanism will be studied. Finally, the numerical solution will be compared to an asymptotic solution for a system undergoing simultaneous coagulation and removal with a constant particle source. The cases considered are summarized in Table 19.

Particulate size distributions can be represented in a variety of ways. When the predominant number of particles occurs in the small size regime, we select a representation that expands the lower end of the spectrum. In such a case the distribution is usually represented versus a logarithmic size coordinate, e.g. Eq. (84). When representing the analytical solutions to the cases listed in Table 19, however, it is most convenient to use, as the independent variable, $\bar{D}$ and, as dependent variable, $\bar{n}_{\bar{D}}(\bar{D},t)/N_0$, where $\bar{D} = D/D_0$, $D_0 = (6\ \nu_0/\pi)^{1/3}$ and $\bar{n}_{\bar{D}}(\bar{D},t) = D_0\ n_D(D,t)$..

All solutions will be expressed in terms of dimensionless groups, defined for each case in Table 20. Since all cases include coagulation, other mechanisms such as growth, removal, and sources will be expressed in terms of dimensionless groups scaled to coagulation. Although the definition of the dimensionless time τ varies depending on the coagulation mechanism, for comparison purposes the same values of τ will be used in each case for which we present solutions. For convenience Λ, θ, and Ω will always be

TABLE 19. SUMMARY OF CASES CONSIDERED OF THE GENERAL DYNAMIC EQUATION FOR PARTICULATE SYSTEMS*

$$\frac{\partial n_v}{\partial t} = - \frac{\partial}{\partial v}\left[I_v n_v\right] + \int_0^{v/2} \beta_v(v-\tilde{v},\tilde{v}) n_v(v-\tilde{v},t) n_v(\tilde{v},t)\, d\tilde{v}$$

$$- n_v(v,t) \int_0^{\infty} \beta_v(v,\tilde{v}) n(\tilde{v},t)\, d\tilde{v} + S_v(n_v,v,t)$$

Case	$\beta_v(v,v)$	$I_v(v,t)$	$S_v(n_v,v,t)$	Analytical Solutions
1	β_0	0	0	Scott (1968)
2	$\beta_1(v+\tilde{v})$	0	0	Golovin (1963) Scott (1968)
3	β_0	σv	0	Ramabhadran et al.(1976)
4	$\beta_1(v+\tilde{v})$	0	$-R_0 n_v$	Peterson et al.(in press)
5	β_0	0	$\frac{S_0 e^{-v/v^*}}{v^*} - R_0 n_v$	Peterson et al. (in press)

---

* R_0, S_0, and σ are constant.

TABLE 20. DIMENSIONLESS GROUPS ASSOCIATED WITH THE GENERAL DYNAMIC EQUATION FOR PARTICULATE SYSTEMS

Group		Interpretation
$\tau = N_o \beta_o t$	(Cases 1,3,5)	Dimensionless time
$= N_o \nu_o \beta_1 t$	(Cases 2,4)	
$\Lambda = \sigma / N_o \beta_o$	(Case 3)	$\frac{\text{Condensation rate}}{\text{Coagulation rate}}$
$\theta = R_o / N_o \nu_o \beta_1$	(Case 4)	$\frac{\text{Removal rate}}{\text{Coagulation rate}}$
$= R_o / N_o \beta_o$	(Case 5)	
$\Omega = S_o / N_o^2 \beta_o$	(Case 5)	$\frac{\text{Source rate}}{\text{Coagulation rate}}$

assumed to be unity. All analytical solutions will be shown as solid lines, and all numerical solutions will be represented by discrete points. The analytical solutions are given in Table 21.

1. Finite Domain Error

A major consideration in numerically solving an equation described over an infinite domain is the error incurred by the solution on a finite domain. To evaluate this so-called "finite-domain error," the fractions of the total number and volume of particles contained in the finite computational domain can be determined based on the analytical solutions. Thus,

$$M_0(t) = \frac{\int_{v_a}^{v_b} n_v(v,t)dv}{\int_0^{\infty} n_v(v,t)dv} , \tag{97}$$

and

$$M_1(t) = \frac{\int_{v_a}^{v_b} vn_v(v,t)dv}{\int_0^{\infty} vn_v(v,t)dv} . \tag{98}$$

TABLE 21. ANALYTICAL SOLUTIONS TO EQ. (79) FOR INITIAL DISTRIBUTION EQ. (96)

Case	β_v	I_v	S_v	$n_v(v,t)$	Reference
1	β_0	0	0	$\frac{4N_0}{\nu_0(\tau+2)} \exp\left[-\frac{2\bar{v}}{\tau+2}\right]$	Scott (1968)
2*	$\beta_1(v+\tilde{v})$	0	0	$\frac{N_0(1-T)}{v\sqrt{T}} \exp\left[-(1+T)\bar{v}\right] I_1(2\bar{v}\sqrt{T})$	Golovin (1963) Scott (1968)
3	β_0	σv	0	$\frac{4N_0}{\nu_0(\tau+2)^2} \exp\left[-\frac{2\bar{v}\tau}{\tau+2} \exp(-\Lambda\tau) - \Lambda\tau\right]$	Ramabhadran et al. (1976)
4†	$\beta_1(v+v)$	0	$-R_0 n_v$	$\frac{N_0\tilde{T} \exp\left(\frac{\tilde{T}-1}{\theta}\right)}{\nu_0 \sqrt{g}\, \bar{v}} \exp\left[-(1+g)\bar{v}\right] I_1(2\sqrt{g}\, \bar{v})$	Peterson et al. (In press)

---

* $T = 1-e^{-\tau}$, I_1 is the modified Bessel function of the first kind of order one.

† $g(\tilde{T}) = 1 - \exp\left[\frac{\tilde{T}-1}{\theta}\right]$
$\tilde{T} = \exp(-\theta\tau)$

represent these two fractions. Obviously, we desire to select v_a and v_b such that M_0 and M_1 do not differ appreciably from unity but not so close to 0 and ∞, respectively, that the computational requirements are excessive. It is important to note that Eqs. (97) and (98) are evaluated based on the exact solution and therefore represent only the theoretical errors committed through the use of a finite computational domain. It is also important to distinguish the finite domain errors from errors usually associated with numerical solutions, in that regardless of the numerical method or its accuracy, there will be an error incurred merely because the computation is carried out on a finite rather than an infinite domain. Due to the nature of Eq. (79), particles within any finite computational domain interact with particles outside the computational domain. Hence, as more particles form outside the computational domain, unavoidable errors are introduced into the distribution within the computational domain. Therefore, all mechanisms which form particles rapidly at the upper end of the size spectrum can lead to errors within the computational domain. For the cases given in Table 21 the analytical expressions for M_0 and M_1 are given in Table 22. Table 23 lists the finite domain errors for Cases 1 through 4.

2. Numerical Results

The numerical and analytical results in Case 1 are shown in Figure 34. Using 15 equally spaced elements in $\tilde{D}$, Eq. (85) was solved numerically by the method of Section C. Excellent agreement between the numerical and exact solutions was obtained. From Table 23 we see that for the times considered in Figure 34 the finite domain errors are negligible. In fact, up to $\tau = 10$, no significant finite domain errors can be anticipated.

Figure 35 shows exact and numerical solutions for Case 2. Consistent with Table 23, we see that as τ increases the deviation between the two solutions increases. The finite domain error is considerably more serious in Case 2 than in Case 1 because in Case 2, β_v increases as the size of either

TABLE 22. ANALYTICAL EXPRESSIONS FOR THE FINITE DOMAIN ERRORS*

Case	$M_o(t)$	$M_1(t)$
1	$\exp - \frac{2\bar{v}}{\tau+2}$	$\exp\left[- \frac{2\bar{v}}{\tau+2} \quad \frac{2\bar{v}}{\tau+2} + 1\right]$
2	$\sum_{k=o}^{\infty} \frac{(2k)!T^k}{k!(k+1)!} e^{-(1+T)\bar{v}} \sum_{r=o}^{2k} \frac{\bar{v}^{2k-r}}{(2k-r)!(1+T)^{r+1}}$	$(1-T) \sum_{k=o}^{\infty} \frac{(2k+1)!T^k}{k!(k+1)!} e^{-(1+T)\bar{v}} \sum_{r=o}^{2k+1} \frac{\bar{v}^{2k+1-r}}{(2k+1-r)!(1+T)^{r+1}}$
3	$\exp\left[- \frac{2\bar{v}}{\tau+2} \exp(-\Lambda\tau)\right]$	$\exp\left[- \frac{2\bar{v}}{\tau+2} \exp(-\Lambda\tau)\right]\left[\frac{\bar{v}}{\tau+2} \exp(-\Lambda\tau) + 1\right]$
4	$\sum_{k=o}^{\infty} \frac{(2k)!g^k}{k!(k+1)!} \exp[-\bar{v}(1+g)] \sum_{r=o}^{2k} \frac{\bar{v}^{2k-r}}{(2k-r)!(1+g)^{r+1}}$	$\exp\left[\frac{\tilde{T}-1}{\theta}\right] \sum_{k=o}^{\infty} \frac{(2k+1)!g^k}{k!(k+1)!} \exp\left[- \bar{v}(1+g)\right] \sum_{r=o}^{2k+1} \frac{\bar{v}^{2k+1-r}}{(2k+1-r)!(1+g)^{r+1}}$

---

* Each expression is to be evaluated at $\bar{v}_a$ minus its value at $\bar{v}_b$. Subsequently $\bar{v}_a$ and $\bar{v}_b$ are taken as 10^{-9} and 27.0, respectively.

TABLE 23. FINITE DOMAIN ERRORS FOR CASES 1-4

Case	τ	M_0	M_1
1	1.0	1.00	1.00
	3.0	1.00	1.00
	5.0	1.00	0.996
	7.0	0.998	0.983
	10.0	0.989	0.939
2	0.5	0.999	0.988
	1.0	0.983	0.776
	1.5	0.950	0.483
	2.0	0.921	0.283
	3.0	0.887	0.0979
3	1.0	0.999	0.990
	1.5	0.968	0.858
	2.0	0.839	0.545
	2.5	0.627	0.259
	3.0	0.416	0.102
4	1.0	0.998	0.959
	2.0	0.990	0.856
	3.0	0.986	0.806
	5.0	0.983	0.780
	7.0	0.983	0.776
	10.0	0.983	0.776

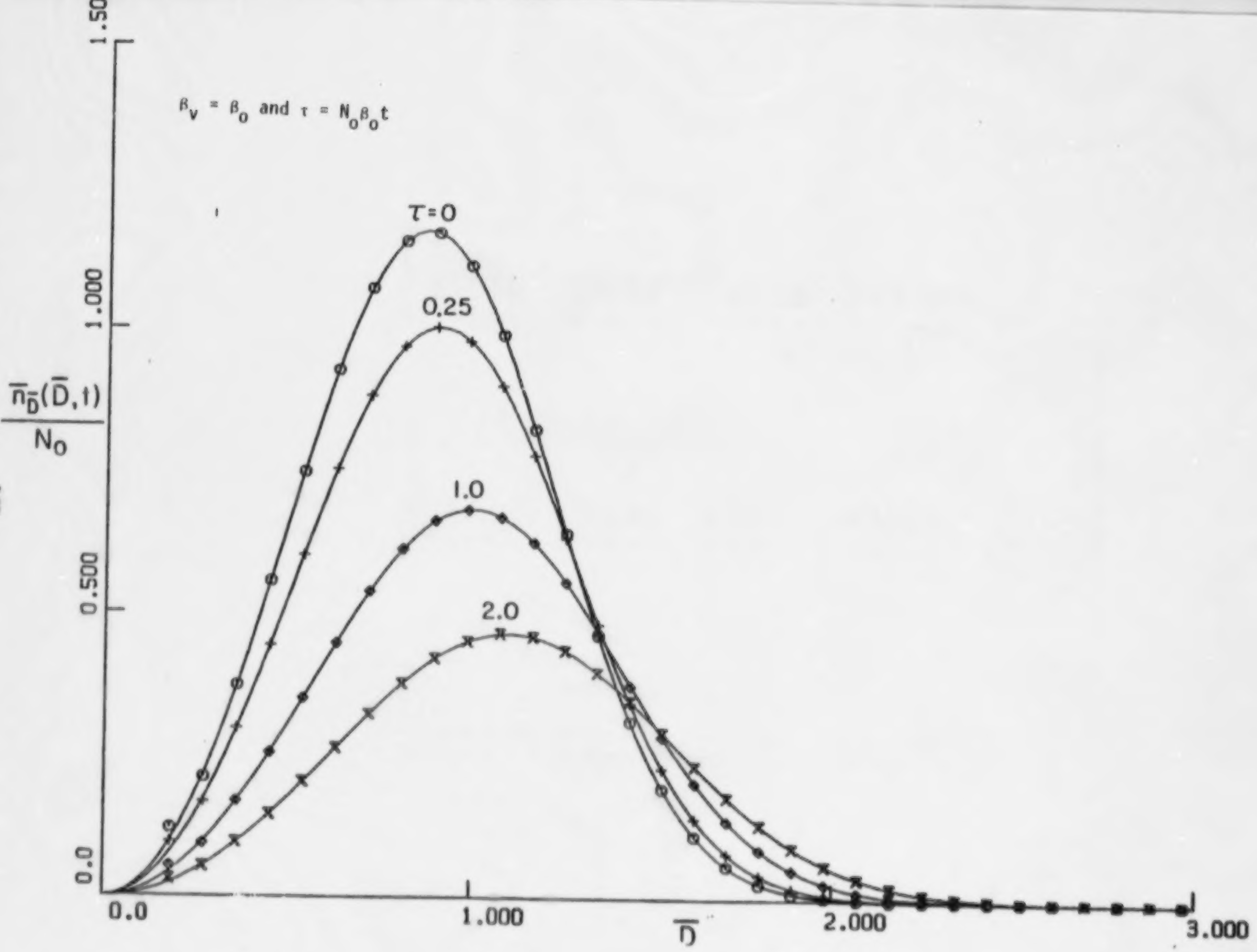

FIGURE 34. COMPARISON OF NUMERICAL AND ANALYTICAL SOLUTIONS FOR CASE 1

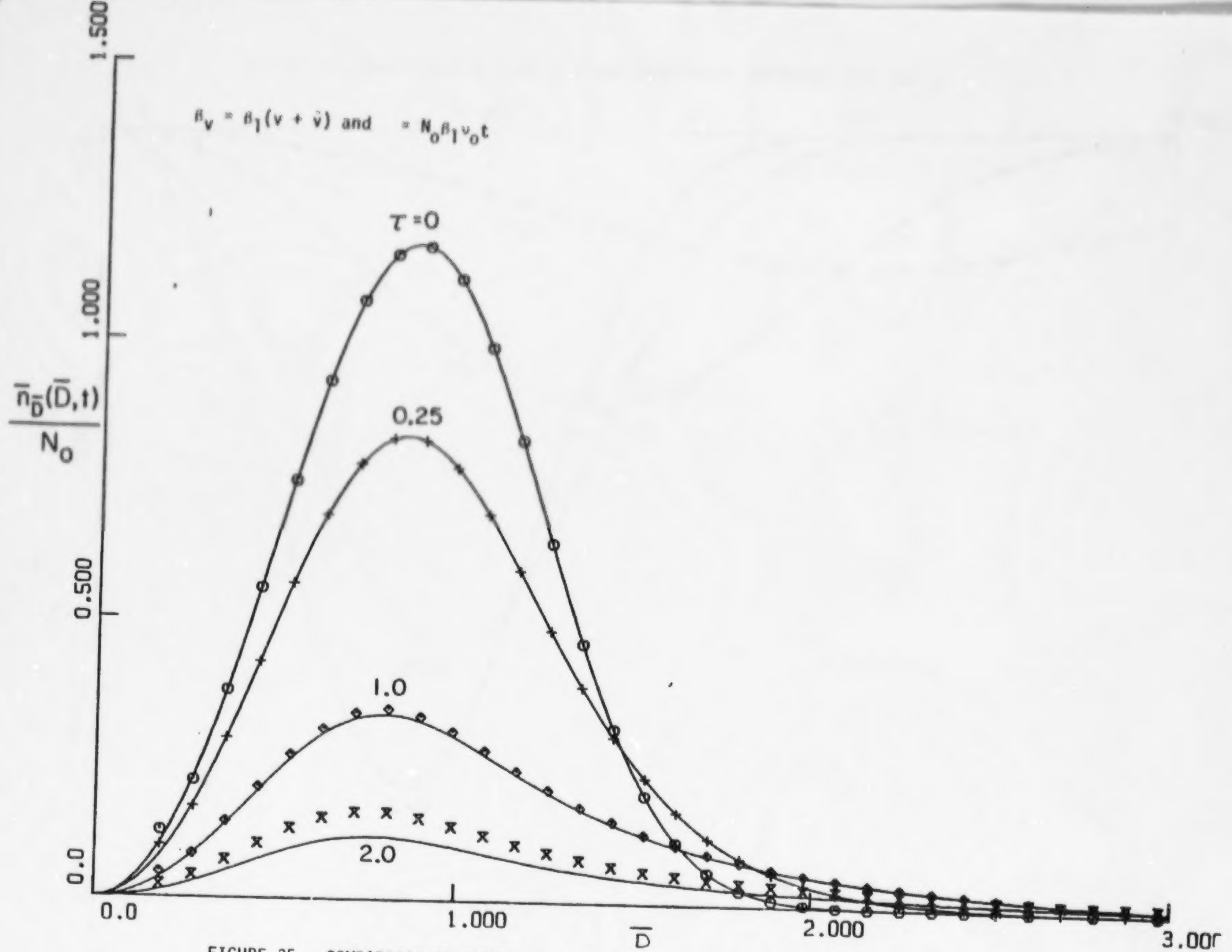

FIGURE 35. COMPARISON OF NUMERICAL AND ANALYTICAL SOLUTIONS FOR CASE 2

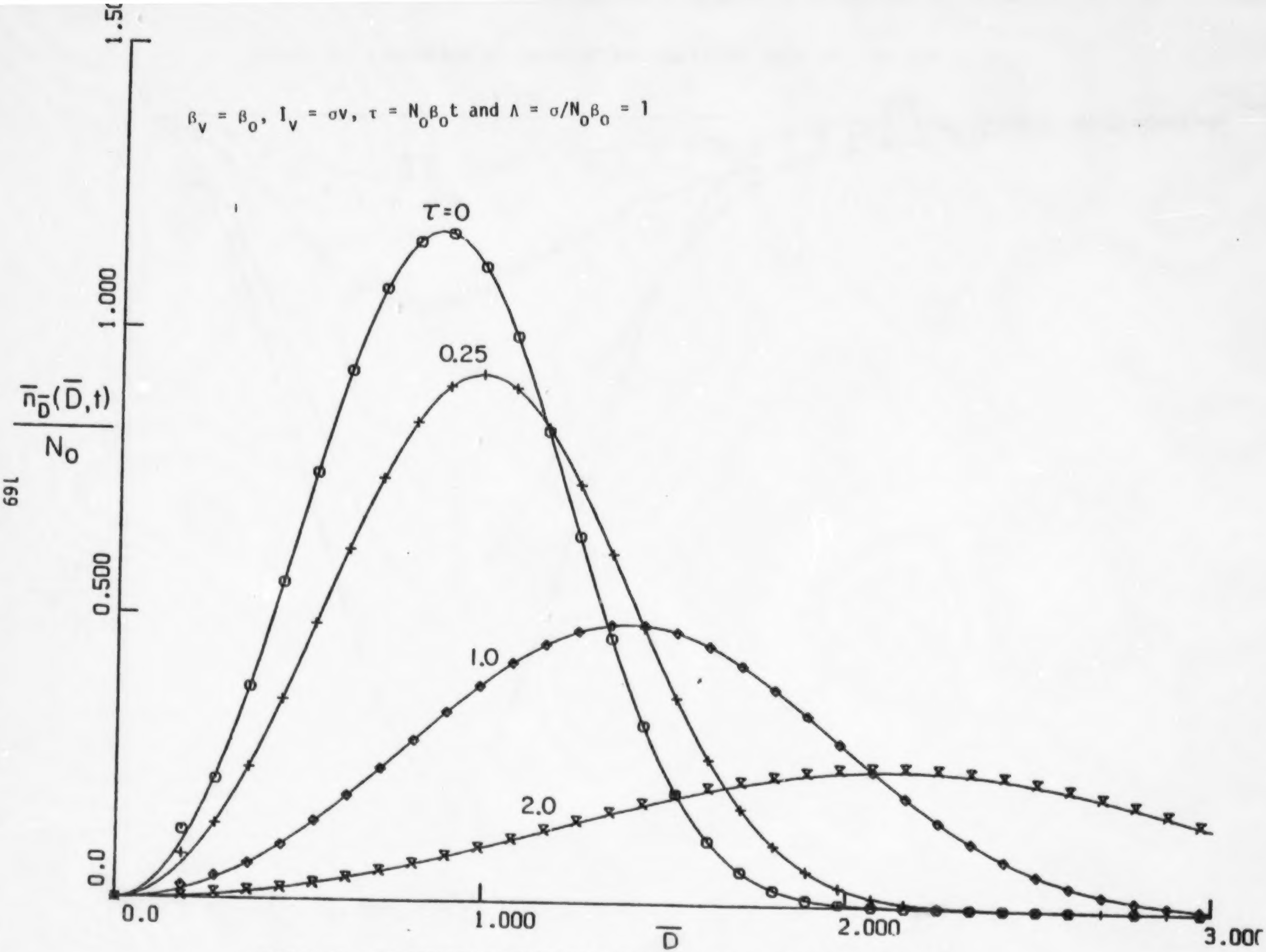

FIGURE 36. COMPARISON OF NUMERICAL AND ANALYTICAL SOLUTIONS FOR CASE 3

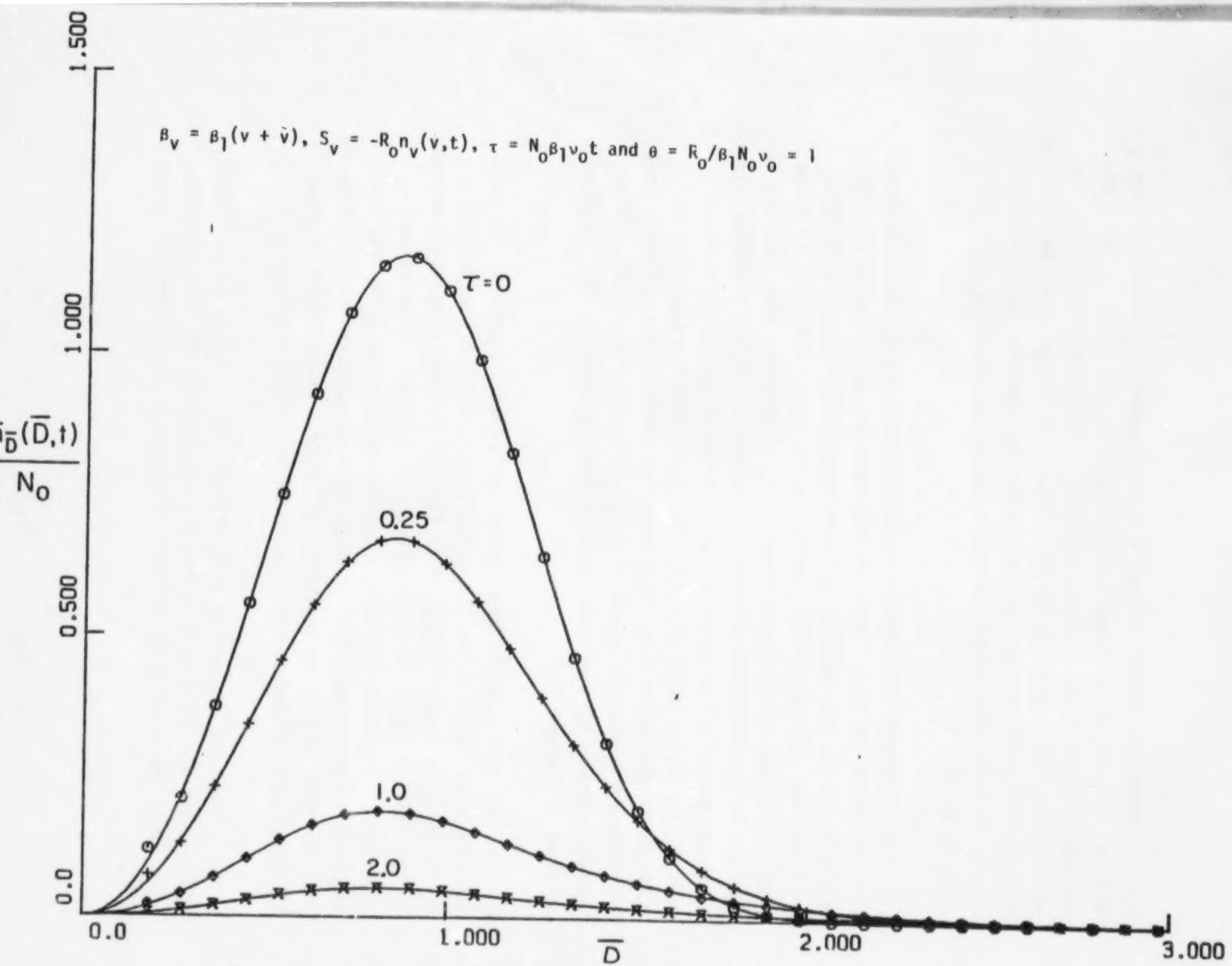

FIGURE 37. COMPARISON OF NUMERICAL AND ANALYTICAL SOLUTIONS FOR CASE 4

particle increases, whereas in Case 1, β_v is constant. Consequently, the shift of the spectrum to larger particle sizes is more rapid in Case 2 at comparable values of the dimensionless time τ. At short times, $\tau < 1$, the numerical and exact solutions are very close. For longer times the numerical solution lies above the exact solution since the numerical solution does not account for collisions between particles inside the domain $[\bar{v}_a, \bar{v}_b]$ with those larger than $\bar{v}_b$.

Case 3 includes both coagulation and particle growth. Particle growth does not change the total number of particles; however, since only a finite domain is used in the numerical solution, particles will be artificially lost when they grow beyond the computational domain. From Table 23 we see that even greater finite domain errors in $M_0(t)$ exist for this case than for Case 2. We see that particle growth is responsible for the additional error. Since the growth is independent of the distribution at any point in the domain, even for an infinite domain, the finite-domain errors shown in Table 23 do not lead to significant errors in the numerical solution. Thus, even though a substantial number of particles has been excluded, excellent agreement between the numerical and analytical solutions is still obtained, as shown in Figure 36.

In most particulate systems removal mechanisms are present. To study the effect of removal on the finite domain error in Case 4 we consider $\beta_v = \beta_1(v+\bar{v})$, $S_v = -R_0\, n_v(v,t)$. From Table 23 we see a substantial decrease in the finite domain error with the addition of a first order removal mechanism. Since there are fewer particles greater than $\bar{v}_b$ in Case 4 as compared to Case 2, the effect of coagulation of particles within the domain with particles outside the domain is negligible. Hence, Figure 37 shows excellent agreement between the analytical and numerical solutions.

In Case 5, $\beta_v = \beta_0$ and $S_v = (S_0/v^*)\exp(-v/v^*) - R_0 n_v$. For initial distribution Eq. (96) only an asymptotic solution for the large particle size end of the spectrum is available (Peterson et al., in press). Since the exact solution is not available, only the total number and volume of particles can be calculated for an infinite domain. Integrating Eq. (79) over v from 0 to ∞ leads to the following equation for N(t), the ratio of the number of particles present at time t to the initial number of particles,

$$\frac{dN}{d\tau} = -\frac{1}{2}N^2 - \theta N + \Omega \quad , \tag{99}$$

where

$$N(t) = \frac{1}{N_o}\int_0^\infty n_v(v,t)\, dv \quad . \tag{100}$$

Similarly, the ratio V of the total volume of particles at any time t to the initial volume of particles is described by

$$\frac{dV}{d\tau} = -\theta V + \Delta\Omega \quad , \tag{101}$$

where $\Delta = v^*/\nu_o$ and

$$V(t) = \frac{1}{N_o \nu_o}\int_0^\infty v n_v(v,t)\, dv \quad . \tag{102}$$

Solving Eqs. (35) and (37) yields

$$N(t) = \frac{r_1 - r_2\left(\frac{1 - r_1}{1 - r_2}\right)\exp\left[\frac{(r_2 - r_1)\tau}{2}\right]}{1 - \left(\frac{1 - r_1}{1 - r_2}\right)\exp\left[\frac{(r_2 - r_1)\tau}{2}\right]} \tag{103}$$

and

$$V(t) = \left[\frac{\theta - \Delta\Omega}{\theta}\right]\exp\,(-\theta\tau) + \frac{\Delta\Omega}{\theta} \quad , \tag{104}$$

where $r_1 = -\theta + \sqrt{\theta^2 + 2\Omega}$ and $r_2 = -\theta - \sqrt{\theta^2 + 2\Omega}$.

The numerical and asymptotic analytical solutions are shown in Figure 38 for $\Delta = 0.01$, $\theta = 1.0$, and $\Omega = 1.0$. In this case only, 15 equally spaced elements in w, not $\bar{D}$, were used because of the large number of particles generated in the small size range. The solutions deviate in this range because the asymptotic solution does not hold. N(t) and V(t) were computed from Eqs. (103) and (104) and compared to the numerically computed values of N and V. The results are given in Table 24, where we see that, for the time considered, there is little finite domain error.

TABLE 24. FINITE DOMAIN ERROR FOR CASE 5. $\beta_v = \beta_o$, $S_v = \frac{S_o}{v^*} e^{v/v^*} - R_o n_v$†

τ**	$\frac{N_{analytic}}{N_{numerical}}$	$\frac{V_{analytic}}{V_{numerical}}$
0.25	1.00	0.994
1.0	1.00	0.992
2.0	1.00	0.986

** $= N_o \beta_o t$.

† $\Omega = S_o/N_o^2\beta_o = 1.0$, $\theta = R_o/N_o\beta_o = 1.0$, and $\Delta = v^*/v_o = 0.01$.

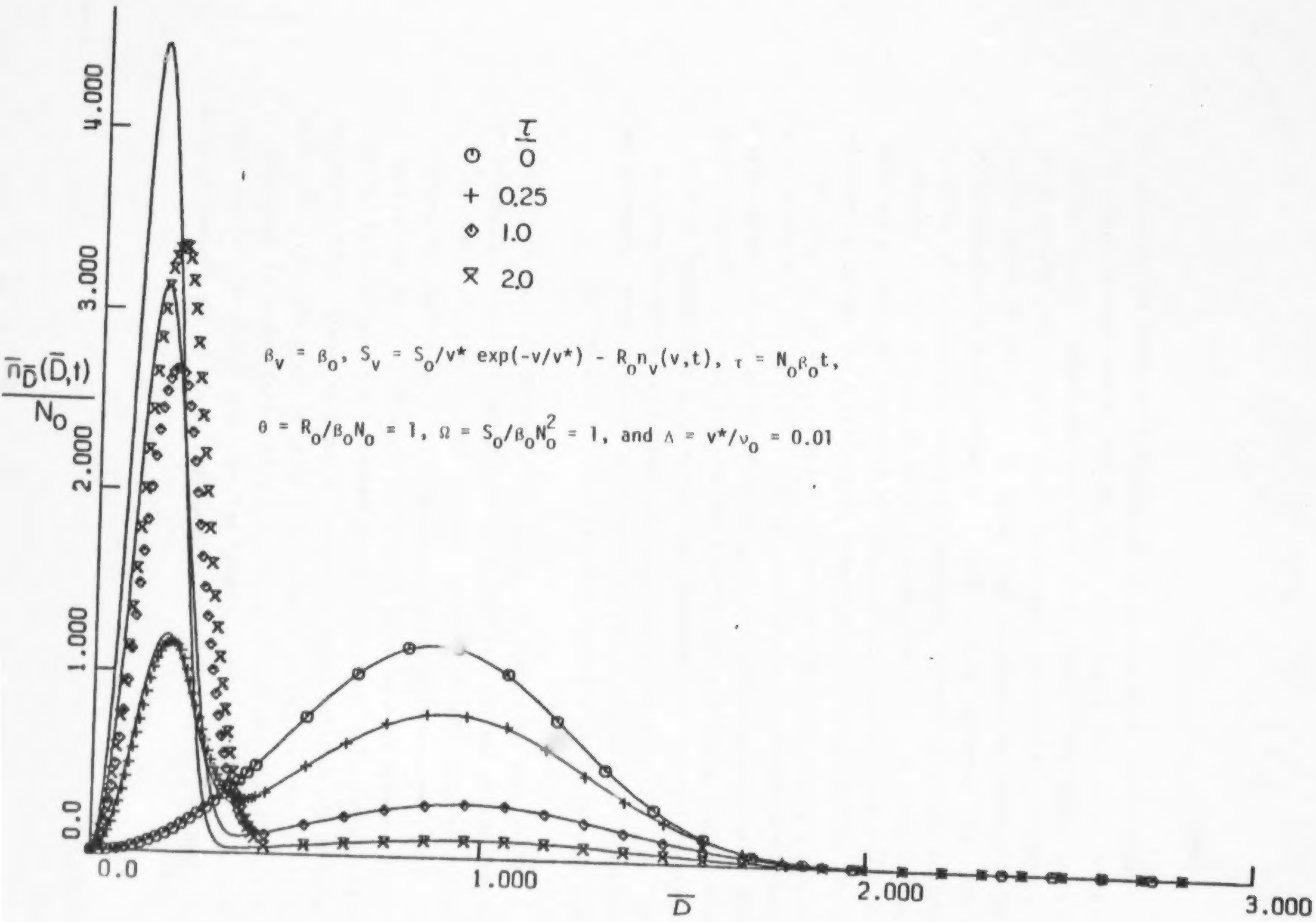

FIGURE 38. COMPARISON OF ANALYTICAL AND NUMERICAL DATA FOR CASE 5

E. SUMMARY

The principal alternatives to the method of weighted residuals for the solution of Eq. (79) either rely on assumptions on the expected shape of the solution (Cohen and Vaughan, 1971; Singh and Ramkrishna, 1975) or employ discretization of particle sizes (Hidy, 1965; Twomey, 1966; Mockros et al., 1967; Takahashi and Kasahara, 1968; Suzuki et al., 1969; Gillette, 1972; Berrg, 1967; Burgmeier et al., 1973). The former class of methods, while computationally attractive, requires some prior knowledge of the solution. For a discrete or finite-difference solution to account for all possible particle sizes, the mesh spacing must, in principle, be equal to the size of the smallest particle. The number of particle sizes needed to represent exactly a distribution between particle volumes v_a and v_b is v_b/v_a; for atmospheric aerosols this ratio can be 10^{10}. Clearly, for a discrete solution to be computationally feasible, the mesh spacing must be several orders of magnitude larger than the size of the smallest particle. In such a case substantial errors are committed when representing the integral terms in Eq. (79). For problems of the type considered here methods of weighted residuals, such as orthogonal collocation on finite elements, appear to be more attractive and efficient than finite-difference methods.

Minimizing the number of ordinary differential equations is crucial in determining the computational requirements for orthogonal collocation on finite elements. For M elements, 2M+2 (or 2M+1 if particle growth is included), ordinary differential equations need to be solved. To begin, enough elements must be taken to obtain a reasonable fit to the initial distribution. The lower limit to the number of elements required can be based on the expected shape of m(w,t). A cubic polynomial can be expected to fit a curve varying by a factor of 3 to 4, or for simplicity, $\sqrt{10}$. Thus 10 elements are required if m(w,t) varies over five orders of magnitude. If m(w,t) is expected to be bimodal and vary over five orders of magnitude, 20 elements (i.e., 42 differential equations) would be the minimum required.

The major source of error in solving Eq. (79) by orthogonal collocation on finite elements is the use of a finite computational domain. The cases considered here represent a severe test of the so-called finite domain error because the distributions for those cases for which analytical solutions can be obtained tend to have uncharacteristically large numbers of particles at the upper end of the size spectrum when compared with most actual particulate systems. For most actual particulate systems the range of particle sizes is finite, and the finite domain error can be expected to be considerably less than that for cases such as those considered here.

VI CONCLUSIONS AND RECOMMENDATIONS

Urban air pollution consists of gaseous and particulate components. Over the last several years considerable effort has been devoted to experimental studies of the chemistry and physics of air pollutants and to the development of mathematical models of gaseous air pollutants. As a result, our understanding of the gas-phase chemistry of urban air pollutants and of turbulent diffusion in the lower atmosphere has been advanced. Until very recently, however, mathematical modeling of the behavior of the particulate component of air pollution was not considered, except for inert particles, which behave essentially as inert gases. The lack of understanding of the gas-phase chemistry and the lack of laboratory and field data on aerosol behavior were primarily responsible for this lack of attention. The realization that adverse health effects are probably associated with ambient aerosols immediately increased the importance of aerosol modeling.

Since gas-to-particle conversion is an important factor in aerosol behavior, one must understand to a large extent the gaseous processes as a prerequisite to understanding aerosol processes. Aerosols are influenced not only by the same advection-diffusion processes that influence gases, but also by such complex processes as diffusion of gaseous species to surfaces, chemical reactions within particles, and coagulation. Modeling aerosols is thus more complicated than modeling gaseous pollutants. Just to characterize an aerosol requires, in principle, the distribution of particles by size,composition, location, and time, which is indicative of the complexity of aerosol modeling.

The chemical and physical data necessary for detailed modeling of the size and composition of an urban aerosol do not exist at present. Nevertheless, it is important that modeling be considered now so that the types of data needed for modeling can be elucidated. This report represents the first phase of an effort to develop mathematical models for urban aerosols. We developed much of the theoretical basis that will ultimately be required for aerosol modeling. However, we adopted a somewhat limited objective--to develop a model capable of predicting the overall submicron aerosol size distribution (and therefore the total aerosol volume and surface area). The model was formulated in such a way that it could be included within a gas-phase model.

Although the chemical composition of a particle influences its rate of growth by vapor condensation, and the chemical composition changes with time, explicitly including particle chemical composition in a model cannot be justified at this time. As a first approximation, we assumed that the transfer of vapor species to the aerosol occurs independently of the particle composition. In spite of the neglect of particle composition, the integration of the aerosol model into the Systems Applications, Inc. (SAI) gas-phase model will not be a straightforward task because of the new independent variable, particle diameter. With only ten particle diameters characterizing the aerosol size distribution, which spans two orders of magnitude, an additional 6.25K of storage would be required to include the aerosol model into the SAI gas-phase model with a 25 x 25 grid and no vertical resolution. Furthermore, in a simulation of a seven-hour period the current aerosol model would add roughly 10 minutes of CPU time (CDC 7600 computer) to the computing time, which represents approximately a 100 percent increase over the current execution time for the SAI gas-phase model alone.*

---

* Note that, since the aerosol formed is not assumed to influence the incident radiation, the aerosol model need not be executed simultaneously with the gas-phase model. This assumption is not actually valid but not invoking it would add an unjustified degree of complexity to the model.

The aerosol model developed in this study is capable of predicting the dynamics of the size distribution, and its inclusion in the SAI gas-phase model would represent a justifiable effort. The portion of the aerosol model that predicts the rate of secondary aerosol formation has been incorporated into the SAI model to predict the total aerosol mass concentration as a function of location and time. This aspect is discussed within another volume of this report.

The major question to be considered at this point is the direction of further research. We could add complexity to the aerosol model by explicitly including particle chemical composition and by developing microscale source-oriented models that consider coagulation. Another path would be to integrate the current model into the SAI gas-phase model and thoroughly test it with pertinent available data. Thus, the second path would not center on further model development but would focus on application and use of the current aerosol model. It is the recommendation of this report that future work follow the second path.

We recommend that the following studies be carried out in conjunction with the continued development of an urban aerosol model:

1. The total mass concentration aerosol model, currently integrated into the SAI airshed model, should be tested on available data for Los Angeles and St. Louis. Sensitivity studies should be carried out with respect to gas-to-particle conversion rates.
2. The aerosol model developed in this study should be integrated into the SAI airshed model. The model should then be tested on available data for Los Angeles and St. Louis. Sensitivity studies should be carried out with respect

to primary source emission rates and particle size distributions, background aerosol, and gas-to-particle conversion rates.

This approach will serve the purpose of providing a usable urban aerosol model in the minimum period of time.

REFERENCES

Abramowitz, M., and I. A. Stegun (1972), Handbook of Mathematical Functions (Dover Publications, Inc., New York, New York).

Appel, B. R., P. Colodny, and J. J. Wesolowski (1976), "Analysis of Carbonaceous Materials in Southern California Atmospheric Aerosols," Environ. Sci. Technol., Vol. 10, pp. 359-363.

Berry, E. X. (1967), "Cloud Droplet Growth by Collection," J. Atmos. Sci., Vol. 24, pp. 688-701.

Birckos, J. N. (1974), "1974 Profile of Air Pollution Control," County of Los Angeles Air Pollution Control District, Los Angeles, California.

Bufalini, J. J. (1971), Environ. Sci. Technol., Vol. 5, p. 685.

Burgmeier, J. W., I. H. Blifford, and D. A. Gillette (1973), "A Reinforced Coagulation Sedimentation Aerosol Model," Water, Air and Soil Pollution, Vol. 2, pp. 97-104.

Byers, H. R. (1965), Elements of Cloud Physics (University of Chicago Press, Chicago, Illinois), 191 pp.

Cadle, R. D. (1975), The Measurement of Airborne Particles, pp. 311-312 (John Wiley and Sons, New York, New York).

Cahill, T. A., and P. J. Feeney (1974), "Contribution of Freeway Traffic to Airborne Particulate Matter," U.C. Davis Crocker Nuclear Laboratory, ARB R 502 7406.

Calvert, J. G. (1974), "Modes of Formation of the Salts of Sulfur and Nitrogen in an NO_x-SO_2-Hydrocarbon-Polluted Atmosphere," paper presented at the Conference of Atmospheric Salts and Gases of Sulfur and Nitrogen in Association with Photochemical Oxidant, University of California, Irvine, California (January 1974).

Carey, G. F., and B. A. Finlayson (1975), "Orthogonal Collocation on Finite Elements," Chem. Eng. Sci., Vol. 30, pp. 587-596.

Castlemen, A. W., Jr. (1974), "Nucleation Processes and Aerosol Chemistry," Space Sci. Rev., Vol. 15, pp. 547-589.

Charlson, R. J., N. C. Ahlquist, and H. Horvath (1968), "On the Generality of Correlation of Atmospheric Aerosol Mass Concentration and Light Scatter," Atmos. Environ., Vol. 2, pp. 455-464.

Chu, K. J., and J. H. Seinfeld (1975), "Formulation and Initial Application of a Dynamic Model for Urban Aerosols," Atmos. Environ., Vol. 9, pp. 375-402.

Ciacco, L. L., R. L. Rubino, and J. Flores (1974), "Composition of Organic Constituents in Breathable Airborne Particulate Matter Near a Highway," Environ. Sci. Technol., Vol. 8, pp. 935-942.

Clark, W. E., D. A. Landis, and A. B. Harker (1976), "Measurement of the Photochemical Production of Aerosols in Ambient Air Near a Freeway for a Range of SO_2 Concentrations," Atmos. Environ., Vol. 10, pp. 637-644.

Cohen, E. R., and E. U. Vaughan (1971), "Approximate Solution of the Equations for Aerosol Agglomeration," J. Colloid Interf. Sci., Vol. 35, pp. 612-623.

Courant, R., and D. Hilbert (1953), Methods of Mathematical Physics, Vol. 1, p. 65 (Interscience Publishers, New York, New York).

Cox, R. A., and S. A. Penkett (1972), "Aerosol Formation from Sulfur Dioxide in the Presence of Ozone and Olefinic Hydrocarbons," J. Chem. Soc., Vol. 68, p. 1735.

__________ (1971), "Oxidation of Atmospheric SO_2 by Products of the Ozone-Olefin Reaction," Nature, Vol. 230, p. 321.

__________ (1970), "The Photo-Oxidation of Sulfur Dioxide in Sunlight," Atmos. Environ., Vol. 4, p. 425.

Cukor, P., et al. (1972), "Some Chemical and Physical Characteristics of Organic Fractions in Airborne Particulate Matter," Environ. Sci. Technol., Vol. 6, pp. 633-637.

Davies, C. N. (1974), "Size Distribution of Atmospheric Particles," J. Aerosol Sci., Vol. 5, pp. 293-300.

Demerjian, K. L. (1976), private communication.

Demerjian, K. L., J. A. Kerr, and J. G. Calvert (1974), Advances in Environmental Sciences and Technology, J. N. Pitts and R. L. Metcalf, eds., Vol. 4, pp. 1-262 (John Wiley and Sons, New York).

Doyle, G. J. (1961), "Self-Nucleation in the Sulfuric Acid-Water System," J. Chem. Phys., Vol. 35, pp. 795-799.

Drake, R. L. (1972), Topics in Current Aerosol Research, G. Hidy and J. Brock, eds. (Pergamon Press, Oxford).

Dreisbach, R. R., ed. (1959), "Physical Properties of Chemical Compounds, II," Adv. in Chem., Vol. 22, pp. 110-217.

Finlayson, B. (1972), The Method of Weighted Residuals and Variational Principles (Academic Press, New York, New York).

Fletcher, N. H. (1958), "Size Effect in Heterogeneous Nucleation," J. Chem. Phys., Vol. 29, pp. 572-576.

Friedlander, S. K. (1961), "Theoretical Considerations for the Particle Size Spectrum of the Stratospheric Aerosol," J. Meteor., Vol. 18, pp. 753-759.

Fuchs, N. A. (1964), The Mechanics of Aerosols (Pergamon Press, New York, New York).

Gangley, J. T., and G. S. Springer (1974), Environ. Sci. Technol., Vol. 8, pp. 340-347.

Gartrell, G., and S. K. Friedlander (1975), "Relating Particulate Pollution to Sources: The 1972 California Aerosol Characterization Study," Atmos. Environ., Vol. 9, pp. 279-299.

Gatz, D. P. (1974), "St. Louis Air Pollution: Estimates of Aerosol Source Coefficients and Elemental Emission Rates," Proc. Symposium on Atmos. Diffusion and Air Pollution, Santa Barbara, California, pp. 109-114.

Gerhard, E. R., and H. F. Johnston (1955), "Photochemical Oxidation of Sulfur Dioxide in Air," Ind. Eng. Chem., Vol. 47, p. 972.

Gillette, D. A. (1972), "A Numerical Model Simulating Coagulation and Sedimentation of a Leaded Aerosol in the Presence of an Unleaded Background Aerosol," Atmos. Environ., Vol. 6, pp. 451-462.

Golovin, A. M. (1963), Sov. Phys. Doklady, Vol. 8, p. 191

Groblicki, P. J. (1976), "General Motors Sulfate Dispersion Experiment: Aerosol Sizing Measurements," Report EV #28, Research Laboratories, General Motors Corporation, Warren, Michigan.

Grosjean, D. (1975), "Solvent Extraction and Organic Carbon Determination in Atmospheric Particulate Matter: The Organic Extraction-Organic Carbon Analyzer (OE-OCA) Technique," Anal. Chem., Vol. 47, pp. 797-805.

Grosjean, D., and S. K. Friedlander (1975), "Gas-Particle Distribution Factors for Organic and Other Pollutants in the Los Angeles Atmosphere," J. Air. Poll. Control Assoc., Vol. 25, pp. 1038-1044.

Grosjean, D. (1977), "Aerosols," Chapter 3 in Ozone and Other Photochemical Oxidants (National Research Council/National Academy of Sciences).

Hall, T. C., Jr. (1953), Ph.D. Thesis, University of California, Los Angeles, California.

Hamill, P. (1975), "The Time-Dependent Growth of H_2O-H_2SO_4 Aerosols by Heteromolecular Condensation," J. Environ. Sci., Vol. 6, p. 1. .

Hamill, P., C. S. Kiang, and R. D. Cadle (1975), "The Nucleation of H_2SO_4-H_2O Solution Aerosol Particles in the Stratosphere," unpublished manuscript.

Hecht, T. A., J. H. Seinfeld, and M. C. Dodge (1974), "Growth Mechanisms for Urban Aerosol Particles," California Institute of Technology, Pasadena, California.

Heisler, S. L. (1975), Ph.D. Thesis, California Institute of Technology, Pasadena, California.

Heisler, S. L., and S. K. Friedlander (1977), "Gas-to-Particle Conversion in Photochemical Smog: Aerosol Growth Laws and Mechanisms for Organics, Atmos. Environ., Vol. 11, pp. 157-168.

Hidy, G. M. (1965), "On the Theory of the Coagulation of Noninteracting Particles in Brownian Motion," J. Colloid Sci., Vol. 20, pp. 123-144.

Hidy, G. M., and J. Brock (1970), The Dynamics of Aerocolloidal Systems, pp. 337-339 (Pergammon Press, New York, New York).

Hidy, G. M., et al. (1975), "Characterization of Aerosols in California (ACHEX)," Final Report, Air Resources Board, State of California.

__________ (1972), "Characterization of Aerosols in California (ACHEX)," Interim Report for Phase I, Air Resources Board, State of California.

Hirschler, D. A., et al., (1957), Ind. Eng. Chem., Vol. 49, p. 1131.

Huntzicker, J. J., S. K. Friedlander, and C. I. Davidson (1975), "Material Balance for Automobile-Emitted Lead in Los Angeles Basin," Environ. Sci. Technol., Vol. 9, pp. 448-457.

Husar, R. B. (1971), "Coagulation of Knudsen Aerosols," Ph.D. Thesis, Department of Mechanical Engineering, University of Minnesota.

Husar, R. B., W. H. White, and D. L. Blumenthal (1976), "Direct Evidence of Heterogeneous Aerosol Formation in Los Angeles Smog," Environ. Sci. Technol., Vol. 10, pp. 490-491.

Husar, R. B., K. T. Whitby, and B.Y.H. Liu (1972), "Physical Mechanisms Governing the Dynamics of Los Angeles Smog Aerosol," in Aerosols and Atmospheric Chemistry, G. M. Hidy, ed., pp. 271-284 (Academic Press, New York, New York).

Japar, S. M., C. H. Wu, and H. Niki (1974), "The Rate Constants for the Reaction of Ozone with Olefins in the Gas Phase," J. Phys. Chem., Vol. 78, p. 2318.

Jerskey, T. N., and J. H. Seinfeld (1976), "Continued Research in Mesoscale Air Pollution Simulation Modeling: Volume IV--Examination of the Feasibility of Modeling Photochemical Aerosol Dynamics," EPA-600/4-76-016d, U. S. Environmental Protection Agency, Research Triangle Park, North Carolina.

Junge, C. (1963), Air Chemistry and Radioactivity (Academic Press, New York, New York).

Katz, M., and S. B. Gale (1970), "Mechanism of Photooxidation of Sulfur Dioxide in the Atmosphere," Proc. Second IUAPPA Clean Air Congress, pp. 336-343 (Academic Press, New York, New York).

Kiang, C. S., and D. Stauffer (1973), "Chemical Nucleation Theory for Several Humidities and Pollutants," Faraday Sym., Vol. 7, pp. 26-33.

Kocmond, W. C., et al. (1975), "Study of Aerosol Formation in Photochemical Air Pollution," Calspan Corporation, Buffalo, New York.

Köhler, H. (1926), Zur Thermodynamik der Kondensation un Hygroskopischen Kernen und Hemerkungen über des Zusammenfliessen der Tropfen," Meddn St. Met.-Hydrogr. Anst. 3, No. 8.

Lanczos, C. (1938), "Trigonometric Interpolation of Empirical and Analytical Functions," J. Math. Phys., Vol. 17, pp. 123-199.

Lapidus, L. (1962), Digital Computation for Chemical Engineers (McGraw-Hill, New York, New York).

Lapidus, L., and J. H. Seinfeld (1971), Numerical Solution of Ordinary Differential Equations (Academic Press, New York, New York).

Liepeles, M., et al. (1973), "Mechanisms of Formation and Composition of Photochemical Aerosols," EPA-R3-73-036, U.S. Environmental Protection Agency.

Liu, B.Y.H., and D.Y.H. Pui (1975), "On the Performance of the Electrical Aerosol Analyzer," J. Aerosol Sci., Vol. 6, p. 249.

Ludwig, F. L. (1968), "Behavior of a Numerical Analog to a Cascade Impactor," Environ. Sci. Technol., Vol. 2, pp. 547-550.

Martin, H. C., and G. F. Carey (1973), *Introduction to Finite Element Analysis* (McGraw-Hill, New York, New York).

McMurry, P. H. (1977), "On the Relationship Between Aerosol Dynamics and the Rate of Gas-to-Particle Conversion," Ph.D. Thesis, California Institute of Technology.

Mason, B. J. (1971), *The Physics of Clouds*, 2nd Ed. (Clarendon Press, Oxford, England), 671 pp.

Middleton, P., and J. Brock (1976), "Simulation of Aerosol Kinetics," *J. Colloid Interf. Sci*., Vol. 54, pp. 249-264.

Middleton, P., G. K. Yue, and C. S. Kiang (1976), "Kinetic Model for Sulfate Aerosol," National Center for Atmospheric Research, Boulder, Colorado.

Miller, D. G., and A. Levy (1976), "Exhaust Hydrocarbon Relationships with Photochemical Aerosol Formation," *J. Air Poll. Control Assoc*., Vol. 26, pp. 778-782.

Miller, D. F., et al (1976), "Combustion and Photochemical Aerosols Attributable to Automobiles," *J. Air Poll. Control Assoc*., Vol. 26, p. 576-581.

Miller, M. S., S. K. Friedlander, and G. M. Hidy (1972), "A Chemical Element Balance for the Pasadena Aerosol," in *Aerosols and Atmospheric Chemistry*, G. M. Hidy, ed., pp. 301-311 (Academic Press, New York, New York).

Mirabel, P., and J. L. Katz (1974), "Binary Homogeneous Nucleation as a Mechanism for the Formation of Aerosols," *J. Chem. Phys*., Vol. 60, pp. 1138-1144.

Mockros, L. F., J. E. Quon, and A. T. Hjelmfelt (1967), "Coagulation of a Continuously Reinforced Aerosol," *J. Colloid Interf. Sci*., Vol. 23, pp. 90-98.

Nair, P.V.N., and K. G. Vohra (1975), "Growth of Aqueous Sulfuric Acid Droplets as a Function of Relative Humidity," *J. Aerosol Sci*., Vol. 6, p. 265.

Novakov, T., et al. (1976), "Chemical Characterization of Aerosol Species Produced in Heterogeneous Gas-Particle Reactions," Paper 76-20.4, Annual Meeting of the Air Pollution Control Association, Portland, Oregon.

O'Brien, R. J., J. R. Holmes, and A. H. Bockian (1975a), "Organic Photochemical Aerosol I. Environmental Chamber Experiments," unpublished manuscript.

O'Brien, R. J., et al. (1975b), "Formation of Photochemical Aerosol from Hydrocarbon Atmospheric Analysis," Environ. Sci. Technol., Vol. 9, pp. 577-582.

Peterson, T. W., F. Gelbard, and J. H. Seinfeld (1978), J. Colloid and Interface Science, Vol. 63, pp. 426-445.

Phillips, W. F. (1975), "Drag on a Small Sphere Moving Through a Gas," Phys. Fluids, Vol. 18, p. 1089.

Ramabhadran, T. E., T. W. Peterson, and J. H. Seinfeld (1976), AICHE J., Vol. 22, p. 840.

Reif, F. (1965), Fundamentals of Statistical and Thermal Physics (McGraw Hill, New York, New York).

Reiss, H. (1950, "The Kinetics of Phase Transitions in Binary Systems," J. Chem. Phys., Vol. 18, pp. 840-848.

Roberts, P. T., and S. K. Friedlander (1975), "Conversion of SO_2 to Sulfur Particulates in the Los Angeles Atmosphere," Environmental Health Perspectives, Vol. 10, pp. 103-108.

Sander, S., and J. H. Seinfeld (1976), "Chemical Kinetics of Homogeneous Atmospheric Oxidation of Sulfur Dioxide," Environ. Sci. Technol., Vol. 10, pp. 1114-1123.

Schuetzle, D., A. L. Crittendon, and R. J. Charlson (1973), "Application of Computer Controlled High Resolution Mass Spectrometry to the Analysis of Air Pollutants," J. Air Pollut. Control Assoc., Vol. 23, pp. 704-709.

Schuetzle, D., et al. (1975), "Molecular Composition of Secondary Aerosol and Its Possible Origin," Environ. Sci. Technol., Vol. 9, pp. 838-845.

Scott, W. T. (1968), "Analytical Studies of Cloud Droplet Coalescence," J. Atmos. Sci., Vol. 25, pp. 54-65.

Seinfeld, J. H., and T. E. Ramabhadran (1975), "Atmospheric Aerosol Growth by Heterogeneous Condensation," Atmos. Environ., Vol. 9, pp. 1091-1097.

Sem, G. J., and J. A. Borgos (1973), "State of the Art: 1971 Instrumentation for Measurement of Particulate Emissions from Combustion Sources, Volume IV," Environmental Protection Technology Series, U.S. Environmental Protection Agency, Washington, D.C.

Shannon, L. J., P. G. Gorman, and W. Park (1974), "Feasibility of Emission Standards Based on Particle Size," Office of Research and Development, U.S. Environmental Protection Agency, Washington, D.C.

Singh, P. N., and D. Ramkrishna (1975), "Transient Solution of the Brownian Coagulation Equation by Problem-Specific Polynomials," J. Colloid Interf. Sci., Vol. 53, pp. 214-223.

Smith, J. E., and M. L. Jordan (1964), "Mathematical and Graphical Interpretation of the Log-Normal Law for Particle Size Distribution Analysis," J. Colloid Sci., Vol. 19, pp. 549-559.

Stauffer, D., V. A. Mohnen, and C. S. Kiang (1973), "Heteromolecular Condensation Theory Applied to Gas-to-Particle Conversion," J. Aerosol Sci., Vol. 4, pp. 461-471.

Suzuki, A., N.F.H. Ho, and W. I. Higuchi (1969), "Prediction of the Particle Size Distribution Changes in the Emulsions and Suspensions by Digital Computations," J. Colloid Interf. Sci., Vol. 29, pp. 552-564.

Takahashi, K., and M. Kasahara (1968), "A Theoretical Study of the Equilibrium Particle Size Distribution of Aerosols," Atmos. Environ., Vol. 2, pp. 441-453.

Takahashi, K., M. Kasahara, and M. Itoh (1975), "A Kinetic Model of Sulfuric Acid Aerosol Formation from Photochemical Oxidation of Sulfur Dioxide Vapor," J. Aerosol Sci., Vol. 6, pp. 45-55.

Ter Haar, G. L. (1972), "Composition, Size, and Control of Automobile Exhaust Particulates," J. Air Poll. Contr. Assoc., Vol. 22, p. 39.

Ter Haar, G. L., and R. E. Stephens (1971), "The Effects of Automobile Exhaust Particulates on Visibility," 12th Conference on Methods in Air Pollution and Industrial Hygiene Studies, Los Angeles, California, April 1971.

Twomey, S. (1966), "Computation of Rain Formation by Coalescence," J. Atmos. Sci., Vol. 23, pp. 405-411.

Urone, P., et al. (1971), Proc. of the Second International Clean Air Congress, H. M. Englund and W. T. Berry, eds., pp. 370-372 (Academic Press, New York, New York).

__________ (1968), "Static Studies of Sulfur Dioxide Reactions in Air," Environ. Sci. Technol., Vol. 2, p. 611.

Urone, P., and W. H. Schroeder (1969), "SO_2 in the Atmosphere: A Wealth of Monitoring Data but Few Reaction Rate Studies," Environ. Sci. Technol., Vol. 3, pp. 436-445.

Villadsen, J. V., and W. E. Stewart (1967), "Solution of Boundary Value Problems by Orthogonal Collocation," Chem. Engineer. Sci., Vol. 22, pp. 1483-1501.

Whitby, K. T., and B. Cantrell (1975), "Atmospheric Aerosols--Characteristics and Measurement," Mechanical Engineering Dept., University of Minnesota, Minneapolis, Minnesota 55455.

Whitby, K. T., R. B. Husar, and B.Y.H. Liu (1972), "The Aerosol Size Distribution of Los Angeles Smog," J. Colloid Interf. Sci., Vol. 39, pp. 177-204.

Whitby, K. T., et al. (1969), "Generation and Decay of Small Ions," Particle Laboratory Publication No. 137, Department of Mechanical Engineering, University of Minnesota.

White, W. H., and R. B. Husar (1976), "A Lagrangian Model of the Los Angeles Smog Aerosol," J. Air Poll. Control Assoc., Vol. 26, pp. 32-35.

Willeke, K., and K. T. Whitby (1975), "Physical Characteristics of Denver-Area Aerosols," J. Air Poll. Control Assoc., Vol. 25, p. 529.

Willeke, K., et al. (1974), "Size Distributions of Denver Aerosols--A Comparison of Two Sites," Atmos. Environ., Vol. 8, pp. 609-634.

Woodcock, A. H. (1953), "Salt Nuclei in Marine Air as a Function of Altitude and Wind Force," J. Meteorology, Vol. 10, pp. 362-371.